Hybrid Solar Thermo-Electric Systems for Combined Heat and Power

RAMADAN MAWI YAHIA KAZUZ

Cardiff School of Engineering

Cardiff University

Thesis submitted in candidature for the degree of Doctor of Philosophy

at

Cardiff University

September 2014

TABLE OF CONTENTS

TABLE OF CONTENTS ii

TABLE OF FIGURES vi

TABLE OF TABLES xi

DECLARATION AND STATEMENTS xii

ACKNOWLEDGMENT xiii

ABSTRACT xv

NOMENCLATURE xvii

1 Chapter One: Introduction 1

1.1 INTRODUCTION 1

1.2 STATISTICS AND BENEFITS OF SOLAR ENERGY 1

1.3 SOLAR HOT WATER TECHNOLOGY 4

1.4 COMBINED HEAT AND POWER TECHNOLOGY 5

1.5 PHOTOVOLTAIC AND THERMOELECTRIC SOLAR SYSTEMS 6

1.6 MOTIVATION 7

1.7 AIMS AND OBJECTIVES 8

1.8 THESIS OUTLINE 9

2 Chapter Two: Literature review 14

2.1 INTRODUCTION 14

2.2 SOLAR THERMAL SYSTEMS CLASSIFICATION 14

2.3 CONCENTRATOR COLLECTORS 18

2.3.1 PARABOLIC TROUGH SYSTEMS 20

2.3.2 SOLAR POWER TOWER 22

2.3.3 DISH-STIRLING SYSTEM 24

2.3.4 LINEAR FRESNEL SYSTEMS 26

2.4 STATIONARY COLLECTORS 27

2.4.1 EVACUATED TUBE SYSTEMS 32

2.4.2 FLAT PLATE COLLECTORS 33
2.5 THERMOELECTRIC DEVICES 38
2.5.1 INTRODUCTION 38
2.5.2 PRINCIPLES OF THERMOELECTRIC DEVICES 40
2.5.2.1 Power generation based on the Seebec effect: 40
2.5.2.2 Peltier effect 41
2.5.2.3 Influence of the Thomson effect 42
2.6 THE THEORY OF HEAT AND ELECTRIC POWER OF THE TEG 43
2.7 RECENT DEVELOPMENTS IN THE SOLAR THERMOELECTRIC SYSTEMS 45

3 Chapter 3: Research methodology 50
3.1 INTRODUCTION 50
3.2 EXPERIMENTAL SYSTEM DESCRIPTION 50
3.3 DEFINITION OF THE SYSTEM CONVERSION EFFICIENCIES 52
3.4 DETERMINE THE HEAT ABSORBED BY THE ABSORBER 54
3.5 DETERMINE THE HEAT LOST FROM THE ABSORBER 56
3.5.1 SLOPE TECHNIQUE BASED ON TEMPERATURE PROFILE 57
3.5.2 CALCULATION FROM CONVECTION AND RADIATION 58
3.6 DETERMINING HEAT ABSORBED BY THE WATER 59
3.7 DETERMINE THE ELECTRICAL POWER OUTPUT 61
3.8 THEORETICAL MODEL 64
3.9 CONCLUSIONS 65

4 Chapter 4: Effect of TEG geometry on Solar Thermoelectric System 67
4.1 INTRODUCTION 67
4.2 DESCRIPTION OF EXPERIMENTS 67
4.3 VALIDATING THE SLOPE TECHNIQUE 68
4.4 SELECTION OF TEGS FOR EXPERIMENTS 72

4.5 EFFECT OF TEG ON SOLAR HOT WATER SYSTEM 74

4.6 DETERMINE THE OPTIMAL TEG GEOMETRY FOR OBTAINING MAXIMUM HEAT AND ELECTRICAL POWER OUTPUTS 80

4.6.1 DETERMINATION OF THERMAL POWER TRANSFERRED INTO HOT WATER 80

4.6.2 DETERMINATION OF ELECTRICAL POWER OUTPUT 83

4.6.3 DETERMINING THE OPTIMUM TEG GEOMETRY FOR HEAT AND POWER PRODUCTION 87

4.7 CONCLUSION 92

5 Chapter 5: Design and construction of an improved solar thermoelectric system with vacuum enclosure 94

5.1 INTRODUCTION 94

5.2 EXPERIMENTAL SETUP 96

5.2.1 THE LIGHT SOURCE 99

5.2.2 THE GLASS 100

5.2.3 THE VACUUM CHAMBER 104

5.2.4 THE SOLAR ABSORBER 106

5.2.5 THE HEAT SINK 107

5.2.6 THE WATER CONTAINER 108

6 Chapter 6: Results and discussion 110

6.1 INTRODUCTION 110

6.2 DETERMINATION OF THE LIGHT INTENSITY ON THE ABSORBER 110

6.3 DETERMINATION OF THERMAL POWER 111

6.4 DETERMINATION OF THE ELECTRICAL POWER OUTPUT 124

6.5 OPTIMAL TEG SIZE FOR MAXIMUM THERMAL AND ELECTRICAL POWER 129

6.6 DETERMINATION OF SYSTEM EFFICIENCIES 130

6.6.1 THE EFFICIENCIES OF THE SYSTEMS UNDER CONDITION 1 131

6.6.2 THE EFFICIENCIES OF ALL SYSTEMS UNDER CONDITION 2 131

6.6.3THE EFFICIENCIES OF ALL SYSTEMS UNDER CONDITION 3 132

6.6.4 THE EFFICIENCIES OF ALL SYSTEMS UNDER CONDITION 4: 133

6.6.6 THE EFFICIENCIES OF ALL SYSTEMS UNDER CONDITION 5 133

6.7 THERMAL AND ELECTRICAL POWER OUTPUT FROM A REALISTIC SYSTEM .. 136

6.8 CONCLUSION 139

7 Chapter 7: Conclusions and Future Work 140

7.1 CONCLUSIONS 140

7.2 FURTHER WORK 143

8 References 145

9 Bibliography 156

10 Appendix 160

TABLE OF FIGURES

Figure 1.1 Estimated average solar energy in Libya, in kWh/m2 per annum, Mohamed et al. (2013). 3
Figure 1.2 Average daily solar radiation in Sabha, Ghadames and Tripoli, Libya, Ahwidea et al. (2013). 3
Figure 2.1 Concentrating solar thermal power global capacity, 1984-2012 ,REN21, (2013). 17
Figure 2.2 A typical Parabolic CSP System (Chu. Yinghao, 2011). 19
Figure 2.3 Solar collectors based on parabolic trough system (Xu Li et al., 2013). 21
Figure 2.4 Solar power tower surrounded by large number of heliostats, (Sargent & Lundy LL Consulting Group, 2003). 23
Figure 2.5 Two types of solar towers: (a) external receiver and (b) cavity receiver (Bateson ,1981). 24
Figure 2.6 A dish collector and its mounted receiver (Camacho et al., 2012). 25
Figure 2.7 Compact linear Fresnel reflector type (Lina et al., 2013). 26
Figure 2.8 An active SWH system in closed loop (a) solar collector; (b) gap between the pipes and the tank; (c) water tank; (d) water storage tank; (e) water pump (Rittidech. et al., 2009). 29
Figure 2.9 A passive thermosiphon SWH system (International Committee of the Red Cross; 2012). 30
Figure 2.10 Types of stationary collectors (Ayompea et al., 2011). 31
Figure 2.11 Schematic of glazed flat-plate solar collector (modified from : www.georgesworkshop.blogspot.co.uk). 33
Figure 2.12 Heat transfer through a Flat Plate collector. 37
Figure 2.13 Thermoelectric figure of merit as a function of temperature for a number of established thermoelectric materials (Brown et al., 2006). 39
Figure 2.14 Seebeck effect: The voltage resulting from temperature difference. 40
Figure 2.15 Thermoelectric refrigeration based on the Peltier effect. 42
Figure 2.16 Heat absorption in conductor due to the Thomson effect when a temperature difference and electric current are applied (Min, 2010). 43
Figure 2.17 Schematic of thermoelectric device. 44
Figure 2.18 Schematic diagram of the STEG system based on evacuated-tube collector presented by Wei He et al, (2012). 47

Figure 2.19 Schematic diagram of the concentrated solar thermoelectric system using a parabolic collector with an evacuated tubular absorber (Miljkovic and Wang, 2011). 48
Figure 2.20 Evacuated STEG with Flat-Panel solar absorber (Kraemer et al, 2011). 49
Figure 3.1 Schematic of the experimental setup, which represents a laboratory-scale solar thermoelectric system using a flat-panel collector for combined heat and power generation. 51
Figure 3.2 Schematic diagram of energy flow in the experimental system of Figure 3.1. 52
Figure 3.3 Classic heating curve of a solar absorber. The inset represents the temperature change of the absorber during the initial period of irradiation, which shows a linear relation between ΔT & Δt. 56
Figure 3.4 The net heat produced and retained in the absorber as a function time (estimated using the slope method). 57
Figure 3.5 Heat loss determined using the slope technique, compared with that calculated based on heat transfer theory. 59
Figure 3.6 Measuring the TEG's internal resistance, which achieves the maximum power. 61
Figure 3.7 Maximum power as a function of load resistance of TEG. 62
Figure 4.1 The absorber temperatures as a function of time for three different lighting power (Intensities). 69
Figure 4.2 The absorber temperatures during the first 12 seconds under three different lighting power. 69
Figure 4.3 Readings obtained from measurements using the Pyranmeter at 5 different locations on solar absorber plane. 70
Figure 4.4 Three tests of the absorber temperature profile to show good repeatability of the experiments. 72
Figure 4.5 Determination of the internal resistance (1.8 Ω) of the TEG with an aspect ratio of 0.136. 74
Figure 4.6 The absorber and water temperature of the system, without a TEG, as a function of time. The model here represents a solar hot water system. The inset shows the water temperature change during the initial period. A linear relationship between ΔT and Δt is evident. 77

Figure 4.7 The temperature profiles of the absorber and the water of the system with the TEG that has an aspect ratio of 0.68. The inset is the temperature profile of the water during the initial period. A linear relationship between ΔT and Δt is evident. 78
Figure 4.8 The absorber and water temperature of the other model sizes, plotted as a function of time. 81
Figure 4.9 The electrical power and temperature difference of all system sizes, as functions of time. 84
Figure 4.10 The electrical power output of the TEG with an aspect ratio of 0.536 as a function of temperature difference ΔT. 85
Figure 4.11 Two measurements (M1 and M2) of the electrical power output to demonstrate the reproducibility of electrical power measurements. The measurements were carried out using the TEG that has an aspect ratio of 0.536. 86
Figure 4.12 The temperature difference across a TEG (ΔT) as a function of TEG size (aspect ratio). The squares represent experimental results and the dashed line represents the theoretical calculation. 88
Figure 4.13 The experimental and the calculated electrical power output as a function of the TEG size. 90
Figure 4.14 The measured and calculated heat power, as a function of TEG geometrical size. 91
Figure 5.1 The calculated electrical power outputs of the solar thermoelectric system operated in ordinary ambient atmosphere and in vacuum. 95
Figure 5.2 Photograph of the complete experimental setup in a safety metal box. The solar absorber and the TEG are sealed in an aluminium vacuum chamber from top by a special glass and from button by metal heat sink block. 97
Figure 5.3 The experiment set-up in further detail. 98
Figure 5.4 The cross section of the experimental kit. 98
Figure 5.5 The spectral irradiance of Xenon (green), halogen (blue) and mercury (red) light bulbs compared with the spectral irradiance from the sun (purple) (D Alan, 2007). 99
Figure 5.6 Light transmission of Robax glass with a thickness of 5mm(www.schott.com). 103
Figure 5.7 UV transmission of Robax glass (www.schott.com). 104
Figure 5.8 The vacuum chamber. 105

Figure 5.9 Home-made feed through using a blank cover, which can be attached to the standard KF flange. 106
Figure 5.10 The backside (left) and front side of the solar absorber. 107
Figure 5.11 The photograph of the fabricated heat sink (left) and its design drawing (right). 108
Figure 5.12 Photograph of the fabricated water container (left) and its design drawing (right). 109
Figure 6.1 The hot side temperatures of the TEG as a function of time for 5 different TEG modules under 5 different environmental conditions. 114
Figure 6.2 The steady state hot side temperatures (Th) as functions of the environmental conditions. 115
Figure 6.3 The TEG cold side temperatures, as functions of time, under the different conditions. 116
Figure 6.4 The temperature differences (ΔT) across the TEGs at the steady state as a function of operating environments for 5 different TEGs. 117
Figure 6.5 Thermal powers transferred into hot water of the solar thermoelectric system at the steady state, calculated using the conduction method (QTEG), displayed as a function of the aspect ratio of the TEG. 120
Figure 6.6 Thermal power transferred into hot water in a steady state as a function of operating environmental conditions for the systems of different aspect ratios. The results were calculated using the conduction method (QTEG). 120
Figure 6.7 Thermal power determined using the slope technique, plotted as a function of the aspect ratio of the TEGs for different operating environmental conditions. 121
Figure 6.8 Thermal power determined using the conduction method during the period of the first 8 minutes as a function of the aspect ratio of the TEGs for different operating environmental conditions. 122
Figure 6.9 The electrical powers generated by the TEGS as a function of time for different operating environmental conditions. 125
Figure 6.10 The electrical power of as a function of the operating environmental conditions for 5 different TEGs. 128
Figure 6.11 The electrical power outputs as a function of the aspect ratio of the TEGs for different environmental conditions. 128

Figure 6.12 Calculated thermal and electrical power as a function of the ratio of the area to length of the thermo element in a TEG. 137
Figure 6.13 The optimal ratio of area to length for the thermo elements in a TEG to obtain maximum electrical power output indicated by both the experimental and calculated results. 138

TABLE OF TABLES

Table 2.1 Solar collectors classification (Kalogirou, 2004, p. 24 Table 2. 24) 16
Table 2.2 The electricity generated by CSP technology in megawatt, REN21(2013). 17
Table 2.3 Performance data for various CSP technologies. (Pitz-Paal et al -2013a, p. 311). 20
Table 2.4 Advantages and disadvantages of various absorber types (Deutsche Gesellschaft Für Sonnenenergie (D G S)-German Solar Energy Society, 2010,p.22). 35
Table 2.6 Evacuated tube vs. flat plate (Yang & Yu, 2011). 36
Table 4.1 Comparison of the heat power determined from the slope technique and the power in the light irradiation measured using Pyranmeter. 71
Table 4.2 The geometrical parameters of TEGs selected for this study 73
Table 4.3 The heat power delivered by the solar TEG modules, using two alternative methods in the same time period. 82
Table 4.4 The measured TEG, Tc, ΔT and the Tc assumed values in the previously established theory. 87
Table 4.5 Comparison between measured and estimated electrical power in addition to the thermal power and total heat and power from the system at the steady state condition for each TEG size. 92
Table 6.1 The dimension, aspect ratio, internal resistance and the cost of the TEG devices employed in this experiment 113
Table 6.2 Comparison of ΔT between Condition 5 and Condition 1 in the steady state. 118
Table 6.3 The efficiency results of all system sizes under Condition 1. 131
Table 6.4 The efficiency results for all system sizes under Condition 2. 132
Table 6.5 The efficiency results for all system sizes under Condition 3. 132
Table 6.6 The efficiency results of all system sizes under Condition 4. 133
Table 6.7 The efficiency results of all system sizes under Condition 5 134

DECLARATION AND STATEMENTS

DECLARATION

This work has not previously been accepted in substance for any degree and is not concurrently submitted in candidature for any degree.
Signed……(Ramadan .M.Yahia Kazuz) Date…….

STATEMENT 1

This thesis is being submitted in partial fulfilment of the requirements for the degree of Doctor of Philosophy (PhD).
Signed …… (Ramadan .M.Yahia Kazuz) Date…….

STATEMENT 2

This thesis is the result of my own independent work/investigations, except where otherwise stated. Other sources are acknowledged by explicit references.
Signed …….. (Ramadan .M.Yahia Kazuz) Date…….

STATEMENT 3

I hereby give consent for my thesis, if accepted, to be available for photocopying and for inter-library loan, and for the title and summary to be made available to outside organisations.
Signed …… (Ramadan .M.Yahia Kazuz) Date……..

ACKNOWLEDGMENT

إهداء

لجميع افراد العائلة

شكراً

In reaching the end of a very long and winding road for this research, I highly appreciate all the assistance, support and motivation I have received from everyone throughout the research period. Without this support, I would not have been able to reach this stage. First, I would appreciate the hardship I received from Cardiff school of Engineering during the last 4 months of my experimental work period, which was the most difficult period for me.

I am extremely grateful for the guidance and support I have had from my Supervisor, Dr. Gao Min. I also appreciate the assistance and comments I have received from Dr. John Bomphrey, as well as Dr. Jorge Garcia-Cañadas and all the colleagues in the Thermoelectric Laboratory. My sincere thanks go to all the technicians who have been involved, starting with Mr. Andrew Rankmore and the entire mechanical workshop group for their kind assistance and their much appreciated patience during the design process period. I would also like to thank Mr. Steve Mead, Mr. Paul Malpas, Mr. Malcolm Seaborne and Mr. Paul Farrugia.

My deepest appreciation goes to my beloved family, mother, sisters, brothers, nieces and nephews, especially the Sweet Hadeel and the helpful Abdualwahab. Simply, this work would have been impossible without your support. My high appreciation is extended to my friends: Dr. Khaled Aljaeel, Hisham Hilally and Hassan Elatta, for their company during this period.

I present this thesis as a gift to my dear sons: Elyas and Awab (Awabey and Elyasoo), who gave me the strength and motivation to continue until the end.

ABSTRACT

Solar energy has been extensively used in the renewable technology field, especially for domestic applications, either for heating, electrical generation or for a combination of heat and power (CHP) in one system. For CHP system solar photoelectric/thermal (PV/T) is the most commonly used technology for roof top applications. However, combination between solar hot water and thermoelectric generators has become an attractive for CHP system, this is due to its simplicity of construction and its high reliability. Moreover, this technology does not rely simply on sunlight and it can work with any other heat source, such as waste heat. However, its main drawback is its low efficiency. Recent publications by Kraemer et al (2011) and Arturo (2013) have shown that the efficiency of solar thermoelectric systems has improved dramatically, especially when combined with a solar concentrator system, as well as within a vacuum environment. The project recorded in this thesis focused on the design, construction and investigation of an experimental solar thermoelectric system based on a flat plate solar absorber. The aim was to study the technical feasibility and economical viability of generating heat and electric power using a solar thermoelectric hot water system.

The design procedure involved on determining the heat absorbed and emitted, as well as the electrical power that was generated by the system. It began by obtaining the efficiency of the solar absorber, including selecting its paint, this was done through an experimental technique to determine the heat absorbed by the absorber, and the results obtained were verified by direct measurements of the light intensity.

An intensity meter was used, and results from both the experimental and theoretical models showed good agreement. The process also included calculating the heat from the system that was gained, lost and generated, as well as the electrical power provided. This was done to provide the system optimal size optimization to obtain the best and most economical system.

Further improvement was made to the system by assembling a vacuum cavity, to improve the system's efficiency. Although the maximum electrical efficiency obtained was relatively low (0.9%), compared to results recorded in the literature (Kraemer et al ,2011 and Arturo, 2013). However, the results of the electrical power output, under a vacuum level of 5 x 10-2mbar, increased approximately three times compared to the results obtained under normal (atmospheric) conditions. Additionally, the thermal power increased by 37% at this level of vacuum. The process involved determining the best thermoelectric geometries to achieve the optimum power outcome under different environmental conditions. The results showed that the system, which included the Thermoelectric device (TEG) with a larger geometric size, produced the best thermal power among other sizes. It was concluded that the system with the smallest TEG geometric size provided the best electrical power output.

NOMENCLATURE

Q_{in}	The incident light radiation upon the absorber [W].
Q_u	The useful heat flux flow through the system [W].
Q_a	The amount of heat absorbed by the solar absorber [W].
Q_l	The heat lost by the absorber to the surrounding environment [W].
Q_r	The incident light reflected back from the absorber [W].
Q_{con}	Heat convection [W].
Q_{TEG}	The heat transferred through the thermoelectric generator [W].
M	The absorber and the water mass [kg].
Cp	Specific heat capacity [J $kg^{-1}.K^{-1}$].
$\Delta T/\Delta t$	The rate of temperature change in response to time [K /s].
Ac	The absorber area [m^2].
σ	Stefan and Boltzmann Constant [$\sigma = 5.6 \times 10^{-8}$ W/($m^2 x K^4$)].
E	Emissivity.
T_h	Absorber temperature; Hot side temperature of TEG [K].
T_c	Cold side temperature of TEG [K].
Ta	Ambient temperature - room temperature [K].
h	Convection coefficient [$Wm^{-2}K^{-1}$].
STEG	Solar thermoelectric generator.
TEG	Thermoelectric generator.
A_{TEG}	TEG area [m^2].
L	Thermoelement length [m].

K	Thermal conductivity of TEG material [$Wm^{-1}.K^{-1}$].
N	Number of the thermoelements in TEG.
α	Seeback coefficient [μVK^{-1}].
ρ	Electrical resistivity of the TEG material [Ω.m].
lc	Thickness of contact layer [mm].
r	The ratio of thermal contact to bulk resistivity.
n	The ratio of electrical contact to bulk resistivity [mm].
R_{TEG}	The TEG's internal resistance [Ω].
V	The voltage drop across the TEG [V].
η_a	The absorber's efficiency in converting solar radiation into heat.
η_E	The TEG power generation conversion efficiency.
η_H	The efficiency of thermal power production.
η	The overall system efficiency (heat and electrical power production).

CHAPTER ONE: INTRODUCTION

1.1 INTRODUCTION

A number of topics concerning solar thermoelectric (TEG) systems for heat and electric power production are presented in this introductory chapter. Starting with a historical background of people who have harnessed solar energy, this is followed by an overview of solar hot water systems (SHW). Additionally, the harnessing of solar energy, taking Libya as an example of an oil depending country, is briefly discussed. Given the fact that the focus of the present study is Combined Heat and Power (CHP), based on solar hot water (SHW) collector, photovoltaic (PV) cells and thermoelectric devices attached to SHW collectors are also discussed in this section. The aims and objectives of the present study are highlighted in this chapter and, lastly, the thesis's structure is outlined.

1.2 STATISTICS AND BENEFITS OF SOLAR ENERGY

Since ancient times through to the industrial revolution and the space age, solar energy has been exploited as a source of useful energy (Walker, 2012). For millennia humans have harnessed solar energy by capturing light and heat from the sun's rays. The ability to do so was first discovered when people used magnifying glasses, around the 7th century BC, to make fire and burn ants (US Department of Energy, 2013). Later, in the 3rd century BC, the Greeks and Romans used mirrors to concentrate the sun's rays and create light torches (Ngô & Natowitz, 2009). It was rumoured that during the Romans' siege of Syracuse in 211 B.C.,

Archimedes set fire to the Roman's wooden ships by focusing sunlight on them, using shields made of bronze as mirrors (Ngô & Natowitz, 2009). This achievement may only be a myth, but there are various reports of solar energy being used to heat homes, bath houses, and public buildings (US Department of Energy, 2013). In the 1830s, the world's first solar collector was built by a Swiss scientist for cooking food (Boinpally, 2010). Into the latter half of the 19^{th} century and the 20^{th} century, more ways of harnessing solar energy were discovered, devolved and implemented (see US Department of Energy, 2013, for further details).The amount of solar radiation impinging on the earth is measured at 1.368 kW/m² (Al-Karaghouli, 2007), which indicates that the total solar energy reaching the surface of the earth is 173,000 terawatt (TW) (Goldenberg & Johansson, 2004; Abbasi & Abbasi, 2010). Furthermore, solar thermal energy is also reported to be the most abundant source of all the renewable sources of energy. It is available in both direct and indirect forms, and the energy emitted by the sun is about $3.8x10^{23}$ kW while the energy received by the earth is around $1.08x10^{14}$ kW (Thirugnanasambandam et al., 2010). This seemingly unlimited energy from sunlight, in the form of heat and light, can be harnessed by using various different technologies. Examples include solar for water heating and for electrical power production, or as a combination of both technologies. However, despite the enormous amount of solar energy the earth receives, it's still a fairly unexplored subject. This is because the power generated by traditional sources, such as coal, oil and natural gas, is easily accessible. These common methods represent approximately 80% of the world's current energy consumption (Kumara et al., 2010). Cost challenges are also a factor.

According to data provided by the German Aerospace Centre (DLR) in 2007, Libya is a country rich in solar energy. An average estimation of annual, direct and normal solar irradiance in Libya, in $kWhm^{-2}$ per year, is between 1,200 and 3,000 (as illustrated in Figure

1.1). This demonstrates that high solar energy can be converted into heat, electrical power, or a combination of both (Mohamed et al., 2013). Solar energy can be applied almost all year round (Figure 1.2) (Ahwidea et al. 2013).

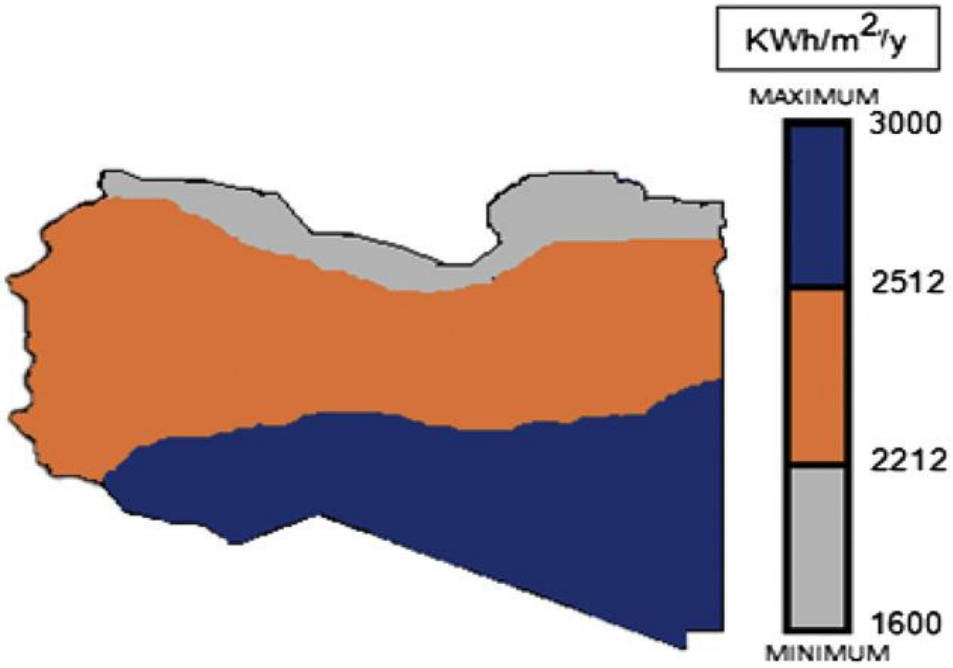

Figure 1.1 Estimated average solar energy in Libya, in kWh/m2 per annum, Mohamed et al. (2013).

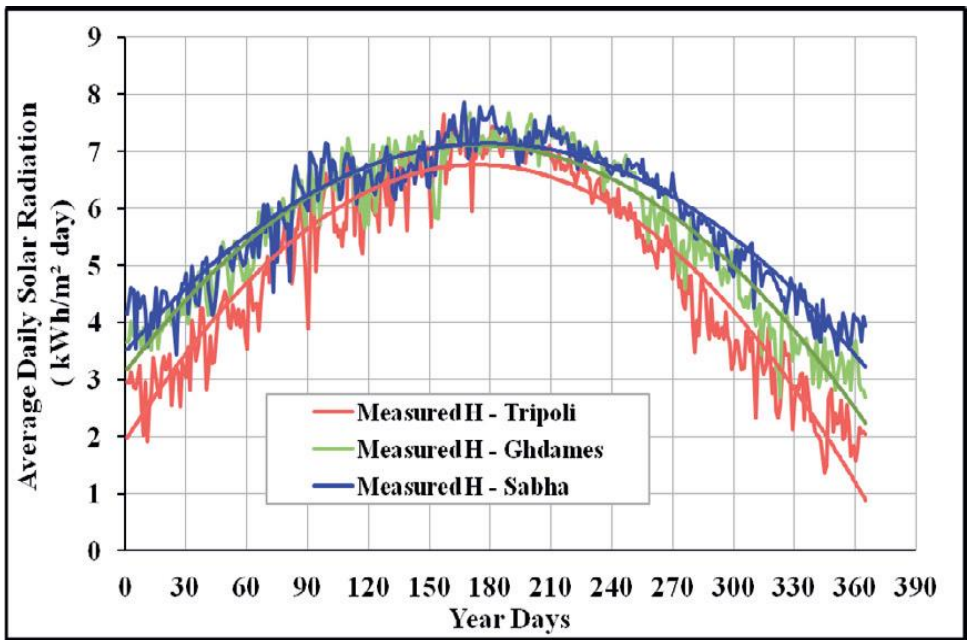

Figure 1.2 Average daily solar radiation in Sabha, Ghadames and Tripoli, Libya, Ahwidea et al. (2013).

1.3 SOLAR HOT WATER TECHNOLOGY

A solar hot water system (SHW) is a conversion tool, which transforms sunlight into heat to produce hot water. Such technology is extremely cost efficient and can generate hot water in any climate (Mills, 2004). Recently, SHWs have been more commonly implemented to provide useful power. In 2010 SHW implementation capacity increased worldwide by an estimated 25 giga watts-thermal, compared to 2009 (Renewables 2012, Global Status Report, Ren21 Map). This increase is mainly due to the system's long-term performance, which requires relatively little maintenance, and low set-up cost compared to other solar conversion systems. For example, in Britain approximately 55 % of the total energy is consumed by domestic heating, mostly for space and water heating (Barker, 2011).

Results from a field study run by the Energy Saving Trust in early 2011 demonstrated that installing a solar hot water system can save between £55-£80, per year, compared to heating water based on gas and electricity (The Energy Saving Trust, 2011). Currently, more than 2.7 million buildings have been fitted with SHW systems in the US and Japan, while Israel, Greece and Australia are embarking on the widespread use of solar hot water systems. However, the opportunity to harness the solar power delivered by sunlight is still great, and we are yet to take full advantage of solar energy systems (Homola, 2009).

1.4 COMBINED HEAT AND POWER TECHNOLOGY

Combined heat and power (CHP) is when the two are combined to generate thermal and electrical energy from a single component. It can be used in small-scale units in residential buildings, or large-scale units specifically designed for substantial applications. The existing CHPs' have proven their effectiveness and success. As a result of increasing demand for both thermal and electrical energy, wide scale use of CHP technologies is anticipated. This is of particular interest to energy intensive industries and in the small to medium enterprises' energy related sectors (Alamiri. A, 2013). Due to proven benefits, the deployment of CHP systems, based on solar technology, is highly feasible in countries with a wealth of sunshine. Nevertheless, these technologies have not been widely applied in such countries. In the USA, according to Chittum (2013), only a few US electric utilities have deployed or encouraged new CHP systems in their service areas.

In general, there are two different ways of generating electricity from a solar hot water system. One could concentrate sunlight to produce steam, which in turns drives a conventional generator. Such technologies are mainly employed in large scale plants where mega-watt capacity of electricity is produced. Another approach is to incorporate photovoltaic solar cells (PV) or thermoelectric generators (TEG) into the solar hot water system, which is usually suitable for small-scale domestic applications.

1.5 PHOTOVOLTAIC AND THERMOELECTRIC SOLAR SYSTEMS

The CHP system that combines PV cells with solar water heating is usually referred to as the Solar Photovoltaic/Thermal (PV/T) system. They are well suited for applications where there is a demand for both heat and electrical power and the available roof spaces are limited. A CHP system based on PV/T has the potential to drastically minimise energy wastage (Pearce, 2009). However, there are some disadvantages in using PV cells - especially those made of silicon. For instance, they are expensive, and requiring significant amounts of energy to make, starts from the taking out the raw materials from the sand, followed by separation and purification stages and ends with manufacturing of the PV components, and only functional during daylight hours. Furthermore, the operation temperature of the PV/T collectors needs to be low (usually less than 50ºC), as the efficiency of PV cells decreases significantly with increasing temperature (Mahtani et al., 2007). This limitation affects the hot water temperature of the hybrid system, preventing it from reaching a hygienic temperature (Watts, 2000). A common problem in deploying photovoltaic power generation in hot countries, such as Libya, is the tremendous decrease in efficiency of the photovoltaic cells when they are operated at higher temperatures (Goetzberger et al., 2002).

Solar thermoelectric generator is another promising solar power technology that is worth of studying (Yonghua Cai et al., 2011). The thermoelectric phenomenon is related to the production of electricity potential from temperature difference. Thermoelectric devices have advantages of easy to fabricate, easy to control and highly reliable. They have no moving parts and are therefore noiseless and maintenance-free. The thermoelectric generator has the

potential to dramatically improve with more efficient material (Fleurial et al., 1999), and it shows the capability to operate for longer life. The conversion efficiency of a thermoelectric generator increases with increase temperature difference. The higher the applied temperature is, the better the performance of the thermoelectric generator (Patyk, 2013). This facilitates the production of hot water of temperatures over 50 ^{o}C without comprising the conversion efficiency. In addition, it would perform better in countries with hot climates, such as Libya. These characteristics make TEG more attractive than the PV cell. The disadvantages of current thermoelectric generators are relatively high cost and low conversion efficiency. Nevertheless, recent studies of Solar thermoelectric generation (STEG) demonstrate that the efficiency of solar thermoelectric systems has increased up to 5% (Kraemer et al, 2011; Arturo et al, 2013). This result indicates that solar thermoelectric generator is a promising alternative for solar energy conversion, particularly in the area of combined heat and power generation.

1.6 MOTIVATION

In the United Kingdom, solar hot water systems are widely deployed and currently there is more than 100,000 nationwide, with a higher number of systems which combine heat and power for small scale applications, (Greening & Azapagic, 2014). However, most of these products are based on PV/T, the systems are rarely combined with TEG. Despite the increasing interest in solar TEG technology, the low conversion efficiency remains the main barrier in implementing the system, especially when it is compared to PV technology. But the use of thermoelectric devices has a native advantage as it can use the radiation emitted by the sun, while PV utilizes only the visible light (Arvizu et al., 2011). A large number of previous

studies have focused on how to improve the electrical power of the system, (Amatya et al., 2010; Tritt et al. ,2008; Gou et al., 2010; Kubo et al., 2005; Champier et al., 2009; Kraemer et al., 2011; Hsiao et al., 2010), while others focused on optimizing the TEG geometries to gain the most advantageous conversion efficiency (Min & Rowe, 1995; Rowe & Min, 1998; Han et al., 2010; Hodes, 2010). Furthermore, only a small part of the literature has considered the heating power alongside the electrical power (Edgar & Vorobiev, 2013; Lei et al., 2013). Investigating solar thermoelectric systems for their combined heat and power, with the aim of improving the systems' efficiency, is the primary focus of this research, aiming to improve the system's total efficiency and to add the knowledge into this particular research field.

1.7 AIMS AND OBJECTIVES

The main aim of the present project is to develop a laboratory-scale STEG system for experimental investigation of the performances and characteristics of heat and electricity production. The basic configuration of the proposed solar thermoelectric system is essentially a thermoelectric device sandwiched between a solar absorber and a hot water channel. In addition to generate electricity, the thermoelectric device also serves as heat exchanger to transfer the thermal energy from the absorber to hot water. The aspect ratio of the thermoelectric module has significant influence on the efficiencies of heating water and generating electricity. A key objective of this PhD project is to study the effects of size and geometry of thermoelectric device on the performances of the solar thermoelectric system. The knowledge and understanding gained from this work provide important insights and guidelines for the design of optimal geometry of solar thermoelectric system.

The surrounding atmosphere of the solar thermoelectric system can have a significant

effect on the operating temperature of the solar absorber and heat transfer effectiveness of the system. The second objective of the present project is to construct an improved solar thermoelectric system, in which the vacuum level can be controlled, for studying the effect of convective heat losses on the performance of the solar thermoelectric system. The experimental investigation aims to understand the influence of relationship among the system efficiency in heat production and electricity generation. Three different vacuum levels were applied to the system to investigate any improvement in the system's efficiency (the working temperature), where the heat convection lost to the surrounding ambience is minimized or eliminated. The next stage was to identify the optimal TEG geometries required to attain the maximum heat and power under a vacuum. To achieve this, a number of objectives were identified:

1. Design and construct a basic measurement through which to investigate the heat absorbed by the system. (This would determine the absorber's efficiency, through application of heat to the absorber alone).
2. Identify the heat and electrical power efficiency of an unglazed system, by designing and testing small scale unglazed solar thermoelectric system. Then testing the efficiency of the same system when different vacuum levels applied.
3. Identify the optimal TEG size (ratio) to achieve maximum heat and power, both with and without a vacuum.

1.8 THESIS OUTLINE

Chapter One: This section provides a brief introduction to the background of this study.

The history of solar energy harnessing and the amount of useful energy that the earth receives. It highlights the benefits that rise from the implementation of solar hot water for home use, and some of the present statistics regarding system implementation are shown. Additionally, the benefits of harnessing the solar energy that Libya receives is presented. The combined heat and power system, in particular a system based on solar powered hot water technology, is defined and reviewed. A comparison between solar photovoltaic (PV) and solar thermoelectricity technology is also shown, highlighting the most suitable system for implementation in the Libyan climate. The problems and reasons that have resulted in the creation of this study are also addressed, and this is followed by the thesis' aims, objectives and outline.

Chapter Two (Literature Review): This discusses the literature related to solar hot water (SHW) systems, including a detailed review of the advantages and statistics and the types of SHW systems (based on their collectors). There is also a brief explanation of the influence of selective coating on the absorber, together with a review of how the heat flows through the flat plate solar collectors. Literature related to thermoelectric generators are reviewed and discussed in terms of their history, working principles and effects. It also explores the recent development of TEG efficiency. And, lastly, the literature related to the Seebeck effect, and the recent improvements of solar thermoelectricity have been reviewed.

Chapter Three (Experimental Techniques): This section begins with an introduction, followed by a brief description of the experimental system using simple diagrams. Heat absorbed by the absorber is described in relation to the principles of the techniques, including the experimental setup. The results obtained from the experimental techniques (in relation to

the heat absorption in the transient and steady state) are discussed, as well as the heat that is lost from the system. Methods to obtain the electrical power generated from the system, with respect to the module geometries, are also described, with measurements and estimated calculations. Determining the TEGs' internal resistance, through which the maximum electrical power is achieved, is explained. Lastly, the system's total efficiency is determined and clarified, in relation to determining the absorber's efficiency, the system's thermal efficiency and the TEGs' conversion efficiency.

Chapter Four: This starts with a summary of the last chapter and an introduction, and explains how it will focus on investigating the effect of TEG geometry on the solar thermoelectric system's performance. The experimental technique was implemented and measured based on the method provided on last chapter. The results related to the heat absorption of the solar absorber at the transient state (slope technique), were analyzed and compared to the results obtained by direct measurements using the intensity meter. The results highlight the amount of thermal power generated by the system, in both the transient and steady states (slope and conduction method), also the results of the electrical power generated by the system, obtained by experiments and calculations, and the results of determine the TEG internal resistance were analysed and discussed. Following this, the optimum heat and electrical power as a function of the TEG geometries (ratio) were analysed, discussed and presented. Finally, a summary of the chapter's results were presented.

Chapter Five: This particular chapter focuses on designing and constructing a solar thermoelectric system, based on a flat-panel in vacuum enclosure. The content describes the design and construction of the vacuum experiment system, starting with an introduction that

explains the motivation behind implementing such experiments. This was followed by a description of the set-up, and each part of the experimental module is clearly explained. A detailed description of the chosen heat source is presented, followed by an explanation of the calculation implemented to choose the glass used (mechanical load and heat influences were considered). The vacuum chamber is explored in detail, as well as the heat sink and water container.

Chapter Six (Results and discussion): This is concerned with the analysis and discussion of the results obtained from the system with a built-in vacuum chamber. The chapter starts with an introduction, where a brief summary showing how the results were obtained and presented. These begin by determining the heat absorption of the solar absorber (slope method) employed in the experiments, followed by the thermal power generated by all modules, in five different environmental conditions. The thermal power results presented were obtained in transient (slope method) and steady (conduction method) state conditions. The results are compared, analyzed and discussed. The electrical power generated in the steady state by each module size, under each environmental condition, was experimentally determined. Following this, the right module size was determined to generate the best electrical power with the environmental conditions applied. Accordingly, the best module size was decided, which would achieve the optimal heat and power, in the steady state condition, under the environmental conditions. Consequently, the system's efficiencies, under each environmental condition, could be recorded. Based on the results obtained, suggestions regarding the right system, depending on the application required, are provided. The chapter is concluded with a summary of the data presented and discussed.

Chapter Seven: Conclusions of the main study results are drawn up and recommendations are suggested.

CHAPTER TWO: LITERATURE REVIEW

2.1 INTRODUCTION

Two major methods of capturing solar energy for human benefit currently in use include solar photovoltaic and solar thermal processes (Lewis et al., 2005; Luque & Hegedus, 2003; Green, 2003; Mills, 2004; Roeb and Muller-Steinhagen, 2010; Kraemer, 2011; Solanki, 2013; Weinstein et al., 2013). Photovoltaic cells in which generate electricity can be used as on flat panel roof application, such on houses, buildings and in solar farms. While solar thermal technology can be harnessed for two distinctive applications; electricity is generated by steam mechanical engines, which usually used in large power plants, or providing hot water, which generally demonstrate in domestic application (Kraemer et al., 2011; Solanki, 2013). An overview of solar PV technology is presented in Chapter One. The focus of this chapter is on solar thermal energy, in which a mechanism referred to as solar collectors is used to convert solar radiation into heat energy.

2.2 SOLAR THERMAL SYSTEMS CLASSIFICATION

Solar collectors are special type of heat exchangers, which transform solar radiation energy into thermal energy (Kalogirou, 2004; Zambolin, 2011; Tian & Zhao, 2013). It is a key element of a solar thermal system, where the incoming solar radiation is absorbed and transformed into useful heat (Kalogirou, 2004). The useful heat is convey from the absorber

to circulating fluid, where the hot water can be generated. The hot water can be used either straightaway or to be stored in storage tank, where it can be used at night and/or cloudy days (Tian & Zhao, 2013; Kalogirou, 2004). The solar collectors and thermal energy storage are the two essential parts in a solar thermal system. The solar collectors should have excellent optical performance; that is, absorbing as much as possible and release the heat at the needed speed, and excellent long–term durability (De Winter, 1991; Zalba et al., 2003; Sharma et al., 2009; Tian & Zhao, 2013). There are basically two types of solar collectors: stationary (non-concentrating) and concentrating collectors (De Winter 1991; Tian & Zhao, 2013), the stationary collectors can heat the water up to 100°C, concentrator collectors usually used to heat water to above than 100°C . The stationary collector has the same area for intercepting and absorbing solar radiation. It has a simple structure and does not need a tracking device. However the energy density of stationary collector is relatively low and will not be able to reach very high temperatures.

The concentrating solar collector usually has concave reflecting surfaces to capture and directs the solar beam radiation onto a smaller receiving area, thus increasing the radiation flux (Kalogirou, 2004). It can have relatively high energy density and reach much high temperature. However, the concentrating solar collector involves complicated structure and need accurate tracking system. Table 2.1 shows a number of solar thermal collectors available in the market. One of the key applications of concentrated solar power (CSP) is to generate electricity from thermal energy (steam) (Solanki, 2013). The CSP market has been growing rapidly over the past a few year with the total global capacity of thermal power of 269.3 GWth (Mauthner.F and Weiss.W 2014), and 2,550 MW of electric power (see Table.2.2, Figure 2.2) (REN, 2013),while only 139 GW of electricity globally generated by Solar PV (European Photovoltaic Industry Association–EPIA-,2014.). Table 2.2 shows that

the capacity of CSP installed in Spain in 2012 doubled relative to 2011, while Figure 2.1 shows that the total world solar thermal capacity in 2012 increased by around 80% compared to 2007 (REN21, 2013).

Table 2.1 Solar collectors classification (Kalogirou, 2004, p. 24 Table 2. 24)

Motion	**Collector type**	**Absorber type**	**Concentration ratio***	**Indicative temperature range (°C)**
Stationary				
	Flat plate collector (FPC)	Flat	1	30-80
	Evacuated tube collector (ETC)	Flat	1	50-200
Concentrator				
Single-axis tracking	Linear Fresnel reflector (LFR)	Tubular	5-15	60-30
	Parabolic trough collector (PTC)	Tubular	10-40	60-250
	Cylindrical trough collector (CTC)	Tubular	15-45	60-300
Two-axes tracking				
	Parabolic dish reflector (PDR)	Point	100-1000	100-500
	Heliostat field collector (HFC)	Point	100-1500	150-200

Table 2.2 The electricity generated by CSP technology in megawatt, REN21(2013).

Country	**Total Capacity End-2011**(MW)	**Added in 2012**(MW)	**Total End-2-12**(MW)
Spain	999	951	1,950
United States	507	0	507
Algeria	25	0	25
Egypt	20	0	20
Morocco	20	0	20
Australia	3	9	12
Chile	0	10	10
Thailand	5	0	5
World Total	**1,580**	**970**	**2,550**

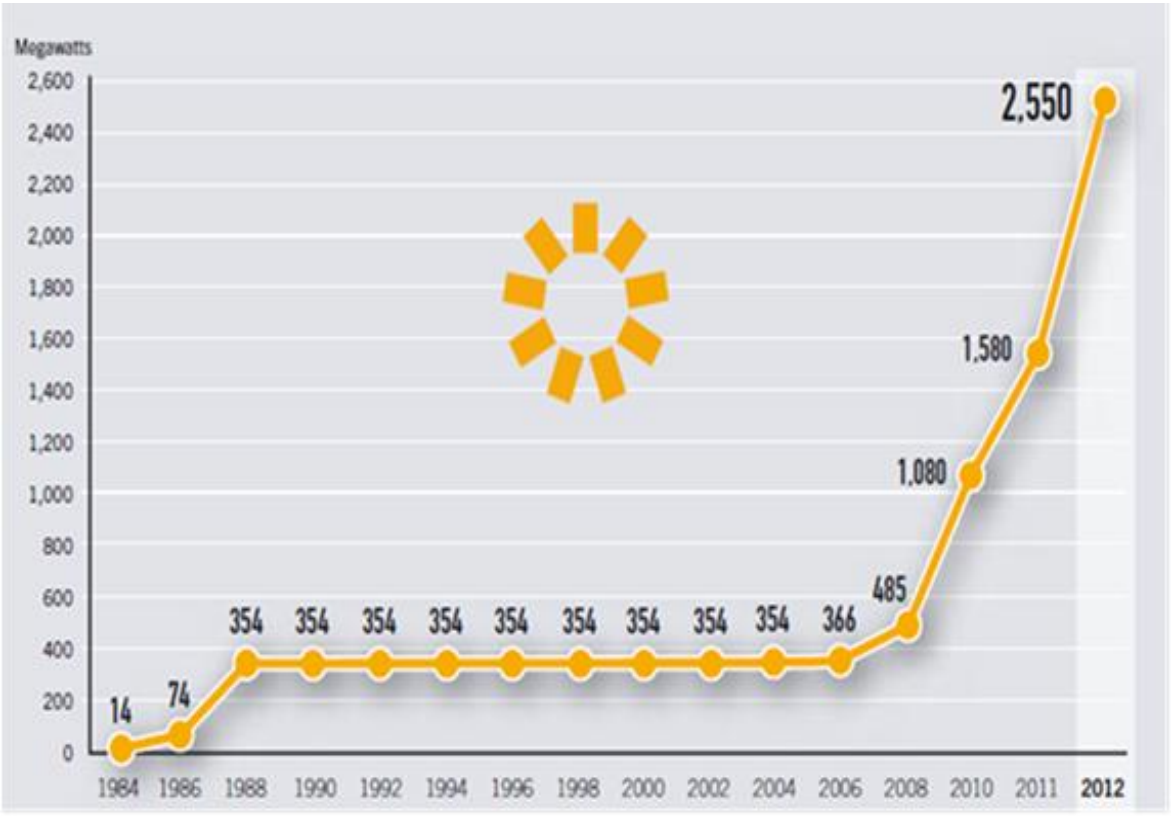

Figure 2.1 Concentrating solar thermal power global capacity, 1984-2012, REN21, (2013).

One of the key applications of concentrator solar thermal energy is to generate electricity by the technology referred to as concentrator solar power (CSP) technology (Solanki, 2013). The principle of power generation is that the steam is generated through solar radiation, and that the steam generated is used to operate turbines that rotate electricity generators so as to generate electricity. The sun light is captured by a variety of solar collectors which provide heat that is then used for several applications, including heating water for domestic uses (Solanki, 2013). Water is heated to between 50° and 60°C; nonetheless, for applications that need higher temperatures, such as higher than 100°C, a special type of solar collectors, concentrator collectors are used (Solanki, 2013).

2.3 CONCENTRATOR COLLECTORS

In contrast to the photovoltaic solar cells, solar concentrator converting the energy from sunlight to electricity by concentrating sunlight by collector (usually use mirrors) and reflect the light energy into receivers that convert it into heat, circulated fluid in the receiver catch the heat and become steam to rotate engine, rather than the photovoltaic which effect that directly transfers photon energy into electricity energy (Chu. Y, 2011). While Viebahn et al. (2008) indicate that concentrator solar system generate steam which be able to produce electricity by rotating various types of turbines, including steam gas turbines or Stirling engines (Viebahn et al. 2008). Concentrator collectors collect light from a large area and concentrate it in a small area; hence, because of this concentration higher temperatures, from some hundreds up to 1000°C, are attained. Concentrator collectors are mainly used at large power stations, where steam is generated to drive engine turbines as illustrated in Figure 2.2 (Chu. Y, 2011).

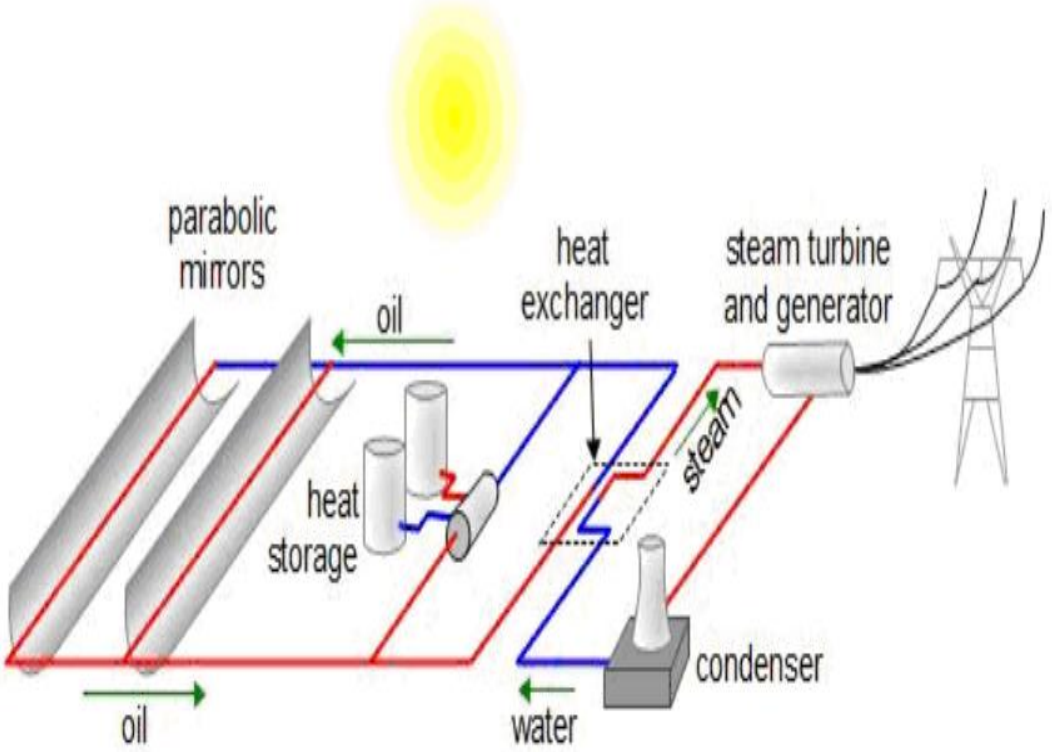

Figure 2.2 A typical Parabolic CSP System (Chu. Yinghao, 2011).

From an engineering perspective, Concentrating collectors can present problem, as they need to be oriented to 'track' the sun in order that beam radiation is directed onto the absorbing surface, hence, there are needs for maintenance, especially in regard to retaining the quality of optical systems for long periods in the presence of dirt, weather, and oxidising or other corrosive atmospheric components (Duffie & Beckman, 2013). The four main types of solar thermal power plants are: Parabolic trough; Linear Fresnel systems; Power tower or solar tower; and Dish-Stirling systems. The performance data for these four concentrating solar power technologies are summarised in Table 2.3. The parabolic trough is the most mature technology and it continues to dominate the market, representing around 95% of the facilities that were in operation at the end of 2011, and 75% of plants under construction by mid-2012 (REN, 2013). Towers/central receivers are becoming more common and comprise

around 18% of plants under construction by mid-2012. These are followed by Fresnel (6%) and parabolic dish technologies which are under development (REN, 2013).

Table 2.3 Performance data for various CSP technologies. (Pitz-Paal et al -2013a, p. 311).

Type	**Capacity (MW_{el})**	**Concentration**	**Peak system efficiency (%)**	**Annual system efficiency (%)**
Trough	10-200	70-100	21	10-16
Fresnel	10-200	25-100	20	9-13
Power Tower	10-200	300-1000	23	8-23
Stirling Dish	0.01-0.4	1000-3000	29	18-23

2.3.1 PARABOLIC TROUGH SYSTEMS

Parabolic trough systems have so far been the dominant technology that is commercially available (Baker and Parker, 2009, p428). Parabolic collectors have the ability of concentrate and reflecting the sun radiation to the absorber within wide limits, the geometry of the mirrors ensures that all the travelling light from all directions is directed to the absorber, which greatly improves the income of solar energy in less light conditions(Viebahn et al., 2008). Parabolic trough systems usually consist of trough solar collector arrays and a conventional power block with steam turbine and generator (Viebahn et al., 2008). Figure 2.3 shows a typical parabolic trough collector installed in a solar farm (Xu Li et al., 2013).

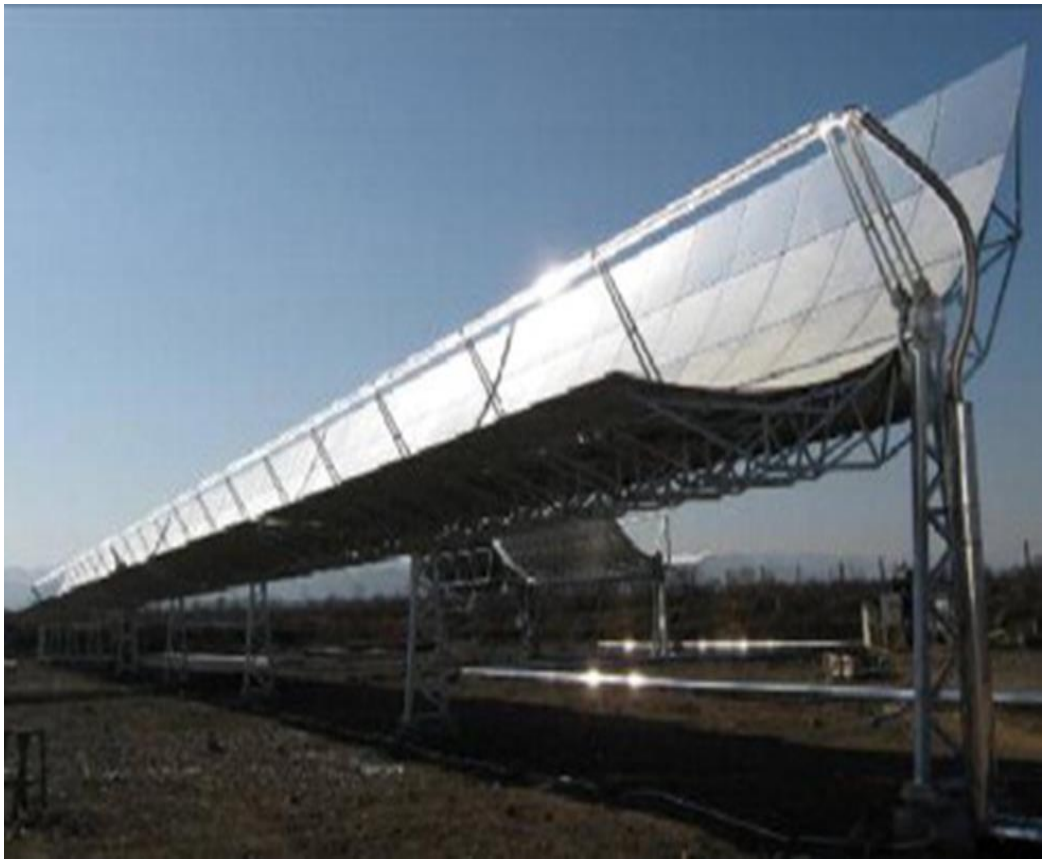

Figure 2.3 Solar collectors based on parabolic trough system (Xu Li et al., 2013).

The basic elements of parabolic trough systems include the receiver tubes, curved mirror assemblies (concentrators) and heat transfer fluid (HTF) (Kulichenko & Wirth, 2012). The receiver is the element in which solar energy is converted to thermal energy in the form of sensible or latent heat of the fluid which circulates through it (Kulichenko & Wirth, 2012, p. 86). The absorber - receiver is an essential part of solar power plant that has significant influence on its performances. Solar radiation is captured by curved mirror that reflect the sunlight and concentrate it onto absorber tube, the absorber tube located at the mirror focus line, it's absorbs the incoming heat and transfer it to the circulated fluid. The absorber can be made by transparent material such as elastic (usually used in lower temperatures) or glass, however Electro-chemically deposited black chrome is generally widely used due to the high performance and the ability to resist high temperatures (Dey, C.J. 2004). To minimise heat

losses, vacuum level is applied within the absorber tube. At the present, the vacuum is employed by all parabolic trough power plants (Kulichenko and Wirth, 2012). The purpose of the curved concentrator mirrors is to focus solar radiation on the receiver, which is located in the line of focus. The parabolic geometry and optical reflectivity of the curved mirrors are highly important given that they are the essential properties which make it possible to efficiently concentrate the solar energy (Kulichenko & Wirth, 2012). Accordingly, the mirrors usually have a support structure, a metal, glass or plastic plate, to provide them with the firmness they need, and on which there is a film of a highly reflective material (usually silver or aluminium). A glass substrate mirror with silver deposition is the most commonly used collector reflector, having a maximum reflectivity of about 93.5% (Kulichenko & Wirth, 2012).

2.3.2 SOLAR POWER TOWER

Solar power towers generate electricity from solar radiation via focusing concentrated solar radiation onto a tower-mounted receiver (heat exchanger) (Sargent & Lundy LL Consulting Group, 2003). The solar power tower system consists of a receiver, also referred to as the Heliostat Field Collector (Tian & Zhao, 2013), mounted on a tower and a field of hundreds to thousands of heliostats (large two-axis sun tracking individual mirrors) which concentrate incident solar radiation onto the central receiver (absorber) at the top of a tower (Figure 2.4). The solar receiver (absorber) on solar power tower system usually in shape of tube, the absorber tube is mainly made from metallic alloy material coated with an absorbing paint. The transported fluid at the absorber is heated by exposing the absorber to the

concentrated and reflected solar flux; the fluid temperature usually reaches 700 ^{o}K (Boubault.A et al 2013).

Figure 2.4 Solar power tower surrounded by large number of heliostats, (Sargent & Lundy LL Consulting Group, 2003).

Solar power towers are of two types: external type (Figure 2.5a) and cavity type (Figure 2.5b) (Tian & Zhao, 2013). The external receiver, used at the Solar One in California, located at the top of the central tower, consists of 24 panels; six for heating water and eighteen for generating steam, and HTF includes water/steam, synthetic oils, liquid sodium and molten salts (Tian and Zhao, 2013). In a cavity receiver, the flux from the heliostat field is reflected via an aperture onto absorbing surfaces forming the walls of the cavity.

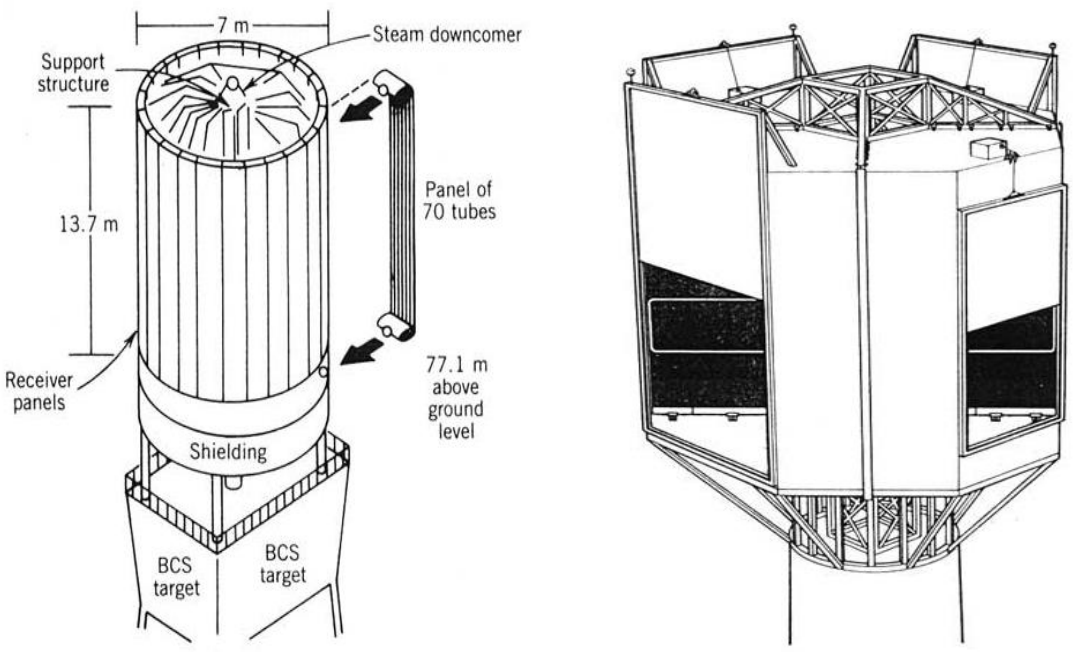

Figure 2.5 Two types of solar towers: (a) external receiver and (b) cavity receiver (Bateson ,1981).

2.3.3 DISH-STIRLING SYSTEM

Dish systems are often referred to as Dish-Stirling systems as they are often used to operate Stirling engine turbines. In contrast to trough and tower power plants, which are only economically viable in large-scale applications of many megawatts, Dish-Stirling systems can be used in smaller units, such as supplying remote villages or towns (Quaschning, 2010). Dish-Stirling systems use concentrators comprised of many reflective mirrors which approximate a parabolic dish (Masters, 2013), which focus the solar radiation onto a dish-mounted receiver at its focal point (EUREC Agency, 2011) as shown in Figure 2.6. A Stirling engine is also located at the focus point to convert heat from the thermal receiver into electricity (Mancini et al., 1994; Kaddour & Benyoucef, 2013). Since the thermal receiver

plays the role of transferring the solar heat to the engine, and heat losses from the thermal receiver can considerably reduce the efficiency and consequently the cost effectiveness of the system. It is important to assess, and subsequently to improve the thermal performance of the thermal receiver (Stine, 1993; Stine & Diver, 1994; Kaddour & Benyoucef, 2013).

Figure 2.6 A dish collector and its mounted receiver (Camacho et al., 2012).

The heat absorber consist of a motor head and a heat exchanger, and it's made as a cavity shaped to transfer the flow of heat coming solar radiation to the head (combustion heat engines), which consisted of one or more pistons moved by the expansion of the heated fluid. The fluid then flow through the heat exchanger, which usually made by a number of fins with good thermal conductivity, in which the working fluid cooled to be return to start the cycle again (Abate,S et al 2012).

2.3.4 LINEAR FRESNEL SYSTEMS

Linear Fresnel power plants (Figure 2.7) comprise a number of Linear Fresnel reflectors mirrors, absorber tube, heat transfer fluid (HTF), a steam generation system, a Rankine steam turbine/generator cycle as well as optional thermal storage and/or fossil-fired back up system (Kulichenko & Wirth, 2012).

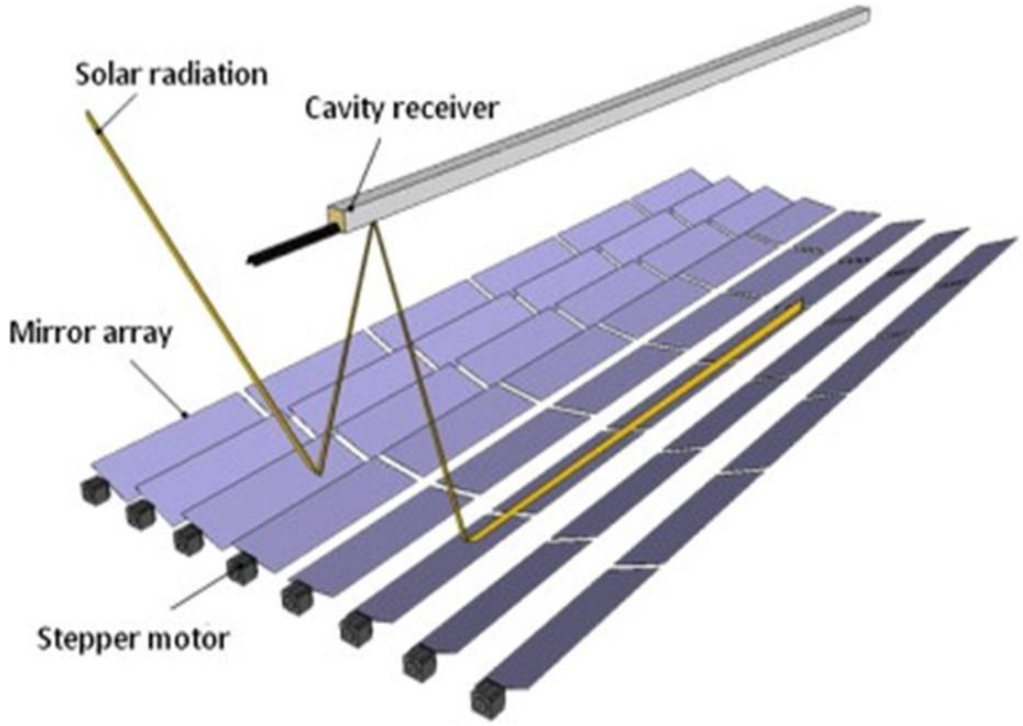

Figure 2.7 Compact linear Fresnel reflector type (Lina et al., 2013).

Figure 2.7 shows sample of linear Fresnel collector, the running fluid will be turning to steam, as the absorber tubes (usually evacuated glass) absorbed the reflected solar energy from the mirrors situated below it (Sahoo.S, et al 2012). At present, Linear Fresnel system operate with saturated steams parameters of up to 55 bar/270°C, though in the medium- and

long-term, superheated steam generation is suggested. They can also operate using molten salt or synthetic oil as the heat transfer fluid (Verdier.F, 2011).

2.4 STATIONARY COLLECTORS

Solar energy collectors also distinguished by their motion in addition to their working temperatures. Some collectors are stationary while the others are moving (tracking the sun). Stationery collectors are permanently fixed in one position and do not track the sun. The stationary collectors are the main element of Solar Water Heating (SWH) systems for domestic applications (Kalogirou,2004). SWH systems used for domestic applications are reported to be the most extensively utilised application of low temperature solar heat, in which conventional collectors use mainly either flat-plate or evacuated tube technologies (Global Energy Assessment, 2012). Adopting SWH has recently become more attractive due to the environmental and economic benefit. By the end of 2010, the SWH collectors installed correspond to a total area of around 280 million square meters (Weiss & Mauthner, 2010). This figure represents more than twice of 132 million square meters installed in 2003. By the end of 2011, there was another surge in installing SWH systems, reaching a total of 335.1 million square metres (Mauther & Weiss, 2013). The greater majority of the total capacity in operation was installed in China (152.2 GWth) and Europe (39.3 GWth); together they represented 81.6% of the total thermal power installed (Mauther & Weiss, 2013). The remaining installed capacity in GWth was shared by the USA and Canada (16.7), Asia not including China (9.6), Latin America (6.3), Australia and New Zealand (4.9), Israel, Jordan, Lebanon, Morocco and Tunisia (4.7), and in some of the Sub-Saharan African countries of Mozambique, Namibia, South Africa and Zimbabwe (0.9) (Mauther & Weiss, 2013).

SWH depends largely on the geographical location, as it works better in areas with abundant sun light. Nonetheless, SWH systems also have the potential to work well in countries with less sunlight. A study carried out by the Energy Saving Trust, based on field trials in the United Kingdom and Ireland covering around 100 sites across both countries, shows that SHWs can perform well when the system is used correctly (Bradford et al., 2011). The households who participated in those trials were satisfied with their SWH systems (84% were 'satisfied' and more than half were 'very satisfied'). The performance of the system can vary from one system to another, depending on application and location. Based on the shape of the collectors, these systems can be classified into two categories: 1) the flat plate system and 2) the evacuated tube system. They can also be classified according to their system application: 1) for heating only; and 2) for combined heat and electricity. The photovoltaic and thermal (PV/T) system is the most common form for combined electricity and hot water production using solar energy, which is already commercially available (Axaopoulos & Fylladitakis, 2013). SWH system is basically a device which transforms solar radiation into domestic hot water. Most SWH systems consist of solar collectors and storage tanks and it can be one of two types: an active or a passive system. Active SWH systems use a circulating pump, occasionally powered by a small solar electric panel in order to pump the fluid around the heating system (Figure 2.8) (Rumlow & Nusz, 2010; Global Energy Assessment, 2012). The active solar system uses a pump that circulates the heated fluid within the system, and it can be either an open or closed loop. Figure 2.8 illustrate an active SWH system in closed loop, the heated fluid at the glass tube collector (a) moves into a heat exchanger (d), then the heat is transferred inside the heat exchanger with the household water, the hot water is moved out to be used, while the cold water back to the collector by the pump (e) in closed circuit (Rittidech. et al., 2009).

Figure 2.8 An active SWH system in closed loop (a) solar collector; (b) gap between the pipes and the tank; (c) water tank; (d) water storage tank; (e) water pump (Rittidech. et al., 2009).

The Passive systems, on the other hand, depend on water pressure, the buoyancy of warm liquids and gravity to circulate the heat transfer fluid through the system. Figure 2.9 demonstrated close loop system where the fluid is circulated at close circle (Global Energy Assessment, 2012). Passive SWHs circulate either domestic water or heated fluid through the system without utilising pumps, and usually have little, if any, moving components and do not need external energy to operate. Due to their simplicity, they tend to be highly reliable and easy to maintain, as well as being the least expensive system to choose (Ramlow & Nusz, 2010). Passive systems involve the integration of a number of subsystems, including Flat Plate collectors (the key component that is unique to passive systems), heat-storage

containers, fluid transport and distribution systems, and control systems (Amrutkar et al., 2012). Flat Plate collectors are discussed later in this chapter (Section 2.4.2).

Figure 2.9 A passive thermosiphon SWH system (International Committee of the Red Cross; 2012).

Generally, the thermal performance of SWH system relies on a number of factors including: the type of collector, its position and surrounding temperature, as well as the solar irradiance, the inlet water temperature and relative humidity (Kishor, 2010). The solar collectors play a significant role in the efficiency of the system. The report by Global Energy Assessment (2012) indicates that SWH technologies have enhanced significantly during the last 20 years. Nonetheless, they also indicate that there is opportunity for further improvement in cost reduction by employing low cost polymer material, and combining the system with other water heating technology in the building. Stationary collectors are

demonstrated on Flat plate and an evacuated tube collectors, as shown in Figure 2.10. Their major component is the solar absorber, as the absorbers and its emitters are critical elements, high solar absorbance and low thermal emittance are required in order to obtain high efficiency SHW system (Blundell, 2006).

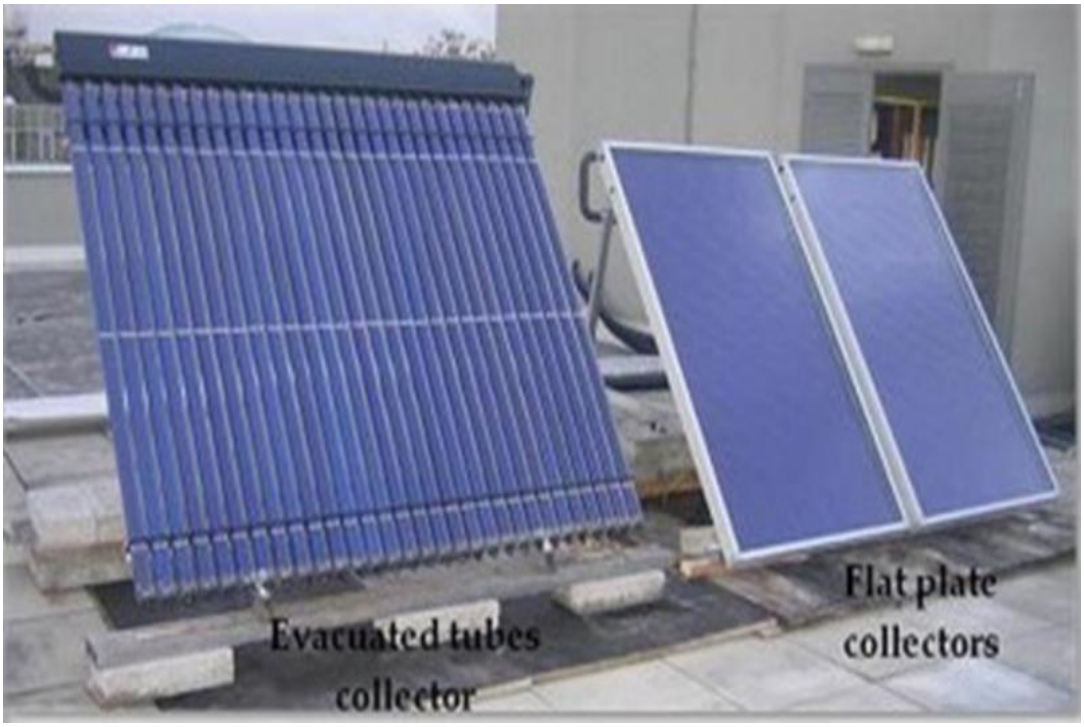

Figure 2.10 Types of stationary collectors (Ayompea et al., 2011).

Materials such as aluminium, copper and stainless steel are mainly used as solar absorber, due to their high thermal conductivity, furthermore, these metals have a high infrared reflectance. However, their disadvantage is the corrosion, therefore, antireflection and metallic corrosion coating is used for the protecting reasons, as well as to improve the solar radiation converting efficiency, the black colour coating is widely used, since black coating have high absorption and less heat emission in addition to protecting the metal (Gelin,et al 2004). A solar collector has to gather as much solar energy as possible at the lowest possible cost. In order to construct a low cost collector, several points should be taken

into account by the designer: the potential corrosion and blockage caused by acidity, the obscurity of the heat transfer, water freezing and the negative effect of the dust or humidity and thermal expansion on the glazing of the flat plate type collectors. To collect more solar radiation, the collectors should be positioned directly towards the equator. In the northern side of the plant it will face south, while it should be pointed north if its located in the southern part of it, with a sloping angle that equals the latitude of the location with an angle variation of around 10–15° (Kalogirou, 2004). Types of stationary collectors can be described further as follows:

2.4.1 EVACUATED TUBE SYSTEMS

The evacuated tube collector consists of many separate inner tubes filled with fluid and covered by outer tubes, the sun radiation passes through the highly transparent outer tubes into the highly absorbent inner tubes, heating the fluid and converting it to thermal energy. Solar evacuated tubes are more efficient in converting sunlight into heat than the flat plate collectors. However, care has to be taken when installing evacuated tubes that the collector should not be large (oversized) (Sharmaa. A et al., 2009). Unlike the Flat Plate collectors, the advantage of using evacuated tubes is that they can operate during the cloudy winter months (Mills, 2001). The vacuum level applied within the tube significantly reduces convection and conduction heat loss, therefore, good efficiency than flat-plate collectors, especially in colder conditions can be achieved).

2.4.2 *FLAT PLATE COLLECTORS*

Flat plate collectors are very simple, comprising a glazed cover, absorber plates, insulation layers, recuperating tubes (usually copper pipes) filled with heat transfer fluids, and they are attached to the absorber plates (Figure 2.11).

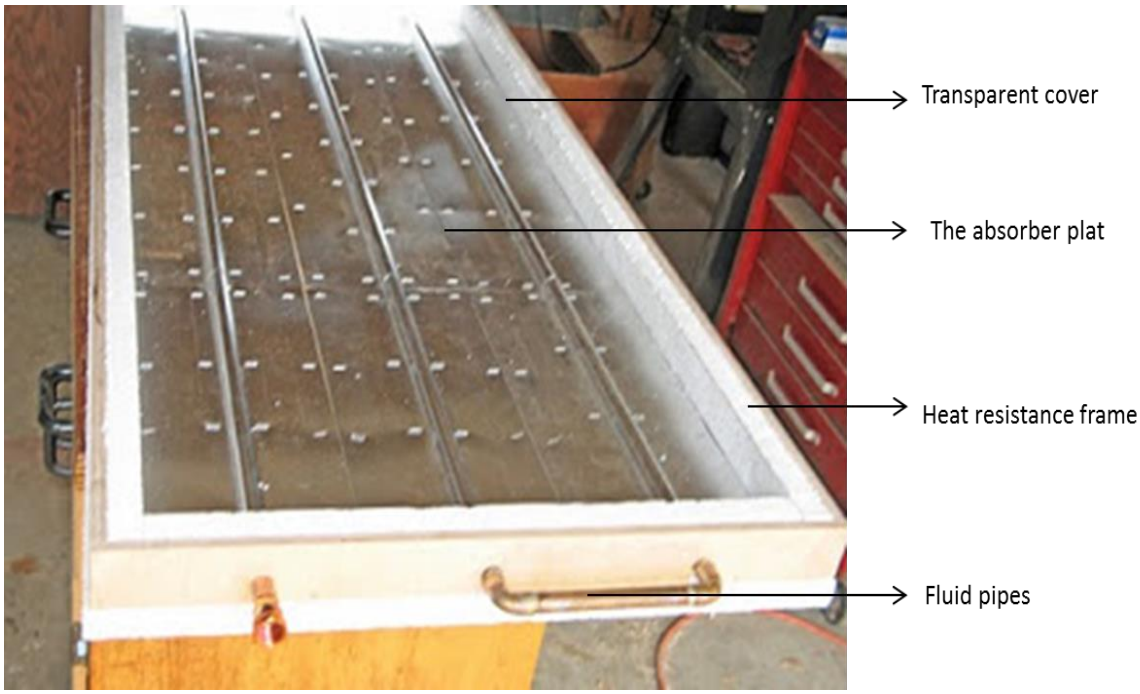

Figure 2.11 Schematic of glazed flat-plate solar collector (modified from : www.georgesworkshop.blogspot.co.uk).

Figure 2.11 demonstrate glazed flat-plate collector, the circulated fluid get heated when the sun light pass through the transparent glass, as the light converted into heat at the absorber and metal pipes, then the circulated fluid inside the pipes is heated and can be used for any thermal application. Flat plate collectors are often permanently fixed in position; hence, they need to be oriented correctly (Tian & Zhao, 2013). Morrison (2001, p145) characterises the key features of flat-plate collectors as follows: a high transmission cover; an absorber plate coated with a high solar absorbency and low emittance layer; a high

conductivity absorber plate with fin and tube construction, or a low conductivity plate with short heat conduction paths through the absorber; heat removal fluid passageways in good thermal contact with the absorber plate; and weatherproof casing with insulation behind the absorber plate. Flat-plate collectors can be designed for applications requiring energy delivery at moderate temperatures, up to perhaps 100°C above the ambient temperature. They use both beam and diffuse solar radiation, do not require the tracking of the sun, and require little maintenance (Amruktar et al., 2013; Duffie & Beckman, 2013), as well as being mechanically simpler than concentrating collectors (Duffie & Beckman, 2013). The major applications of these units are in solar water heating, building heating, air conditioning, and industrial process heating (Amruktar et al., 2013; Duffie & Beckman, 2013). Passively heated buildings can be viewed as special cases for flat plate collectors with the room or storage walls as the absorber (Duffie & Beckman, 2013; Xinjian et al., 2008) have identified some of the technical difficulties of flat-plate collectors, including the problem of scaling in the plate tube, particularly in hard water quality areas, where the major components of the scale are calcium carbonate, calcium sulphate, magnesium sulphate, and magnesium oxide, and when scaling occurs heat transfer performance declines and even close the tube. The technical difficulty of using solar water heaters in tall buildings and the heat loss of flat-plate collectors include that the radiation loss and convection loss are higher than in the evacuated tube collector.

Flat plate collectors are either glazed or unglazed. Glazed collectors consist of a metal absorber, and it is thermally insulated on the back and edges, with a transparent cover on the upper surface in addition to fluid pipes (usually water), as illustrated in Figure 2.11. The absorber is the main part of the collector, which is made of a heat conducting metal sheet, such as copper or aluminium, covered with a dark coating on the heat facing side, and water

pipes from the other side (usually made of copper). There are several types of absorbers. The advantages and disadvantages of these various absorbers are summarised in Table 2.4.

Table 2.4 Advantages and disadvantages of various absorber types (Deutsche Gesellschaft Für Sonnenenergie (D G S)-German Solar Energy Society, 2010,p.22).

Type	**Advantage**	**Disadvantage**
Roll-bonded absorber	Good thermal properties, no mixed materials: simplifies subsequent recycling	Subject to corrosion of aluminium in connection with copper tube
Absorber strips with pressed in copper tube	High flexibility in size; cheap because of greater volume of production	Many solder points
Absorber with tube system pressed in between metal sheets	No mixed materials: simplifies subsequent recycling	High production cost as connection possible only on plain metal sheet
Absorber with soldered-on tube system	Very flexible in size and flow rate	Heat transfer not optimal
Full flow-through stainless steel absorber	Good heat transfer to liquid	High weight, thermal inertia
Serpentine absorber	Only two solder points in tube system	Higher pressure loss than tube register
Tube register (full-surface absorber)	Lower pressure loss than serpentine absorbance	Many solder points in tube; expensive

Unglazed flat plate collectors, on the other hand, represent the simplest types of solar collectors. Since they are not glazed or have no insulated collector box, they comprise only of an absorber (German Solar Energy Society, 2010). For the same sunlight intensity, unglazed collector will achieve a lower temperature than the glazed. due to their higher heat losses and hence, they are usually used in low temperature applications. Because of their simple

structure that has no glass and require no seal, the unglazed flat plate collectors cost less and can be installed and replaced easily on the rooftop. However, it has some disadvantages, such as higher heat loss, which limits the working temperature; also it requires more surface area due to its limited performance. (German Solar Energy Society, (2013, p. 19). Zhang and Li have compared between Flat plate and the evacuated tube collectors, they summarised that evacuated tube collectors are fragile, expensive and needs higher maintenance, but is more efficient compare to flat plate collectors (Zhang & Li, 2008). Yang and Yu have distinguished between the evacuated tube and the flat plate collectors as summarised in Table 2.5.

Table 2.5 Evacuated tube vs. flat plate (Yang & Yu, 2011).

Evacuated Tube Collectors	**Flat-Plate Collectors**
Vacuum between concentric tubes to reduce heat loss	A network of piping through which water is circulated
Adaptable to a wide range of ambient temperatures; anti-freezing, high efficiency in cold areas	High efficiency of heating process in full sunshine conditions
Aside from solar heating, can also be used for solar space heating and cooling	High absorber plate area to gross area ratio. Long lifetime.

In spite of the advantages of evacuated tube collectors, specially, in terms of the efficiency, the performance of the flat plate can be improved, one key element to enhance the flat plate's efficiency is by choosing the best absorber plate, as the solar absorber should have a high solar absorption and a low thermal emittance, copper material coated in black paint has been reported with high absorption (98%) and a low reflective loss (0.02%) at 100°C

(Kennedy, 2002, p. 11). Minimising heat loss from the collector to the surrounding is also another key element of improving the collector efficiency, as heat losses within the collector are mainly attributable to the convection effect between the absorber and the surrounding environment; adding a transparent cover to the collector in addition to applying vacuum level can reduce the heat loss. In addition, there is heat losses from the back side of the absorber, and this loss can be reduced by increasing the conduction heat transfer between the absorber and the pipes- circulated water (Ojike,2011). The figure below describes the main heat losses from the flat plate collector.

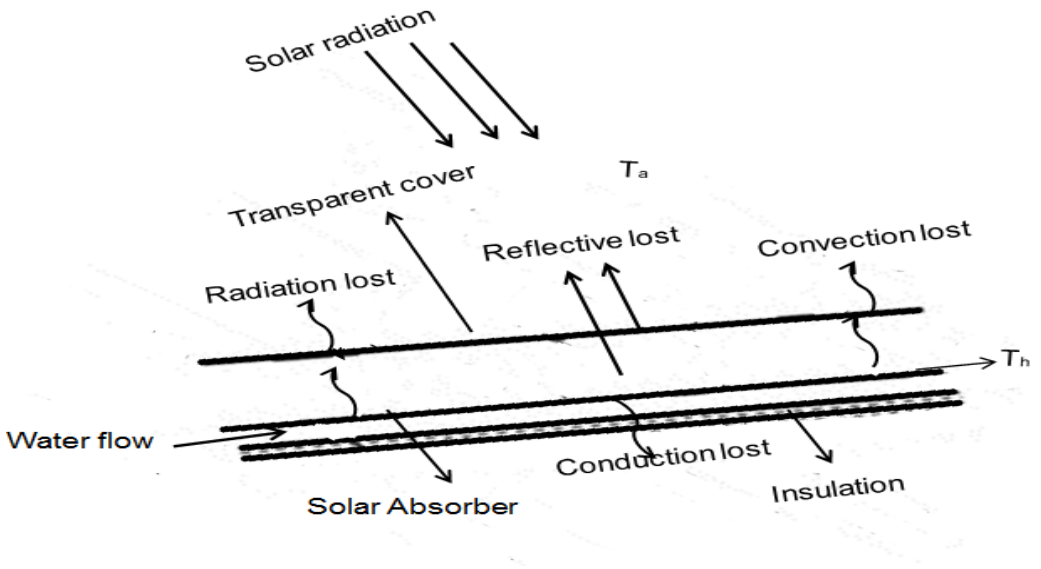

Figure 2.12 Heat transfer through a Flat Plate collector.

The heat transfer due to conduction from the absorber into water may be employed for electricity generation using a thermoelectric generator by sandwiching the thermoelectric generator between the absorber and the water. TEGs represent a proposing technique of utilising solar thermal energy for combined heat and power production, especially on a smaller scale (Amatya & Ram, 2010; Zhang et al., 2010) due to its solid-state nature of the thermoelectric device based on the Seebeck effect. A detailed description of the TEG is given in following Section.

2.5 THERMOELECTRIC DEVICES

2.5.1 INTRODUCTION

A thermoelectric (TE) power generation occurs when a voltage is generated from a temperature difference across two different semiconductor materials. This phenomenon is called the Seebeck effect. Conversely, when a voltage is applied to a circuit formed by two semiconductors, a temperature difference will be created across these two junctions. This is known as the Peltier effect. Furthermore, when electric current flows through a single conducting material and when this single material already has a temperature difference across it, heat energy will be either absorbed or dissipate throughout the material, this effect is known as the Thomson effect. The thermoelectric device is an energy converter based on these effects, which can be used for power generation or refrigeration. In regards to power generation, the efficiency of a thermoelectric device, which called figure of merit (Z), is depends on the three material parameters: the Seebeck-coefficient (α), electrical conductivity (σ) and thermal conductivity (k), this will be explained further in section 2.6. Such requirements can be summarised by the so-called thermoelectric figure of merit, Z (Hendricks.T, 2006):

$$Z = \alpha 2\sigma / k \qquad (2.1)$$

Great efforts have been made to develop high efficiency TE modules mainly by searching for semiconductor materials that have high Z values. Traditionally, there are three types of materials that are the most used as thermoelectric materials, bismuth telluride (Bi2Te3), lead telluride (PbTe) and silicon germanium (SiGe) (Rowe, 2006). Each of those materials has a high performance at a different temperature. At room temperature, bismuth telluride has the best performance, while at a temperature of 1300 ^{o}K, silicon germanium has the highest performance. Lead telluride has the best performance in the temperature range 400-900 ^{o}K (Tripathi & Bhandari, 2005). Figure 2.13 shows the figure of merit as a function of temperature for a number of established thermoelectric materials.

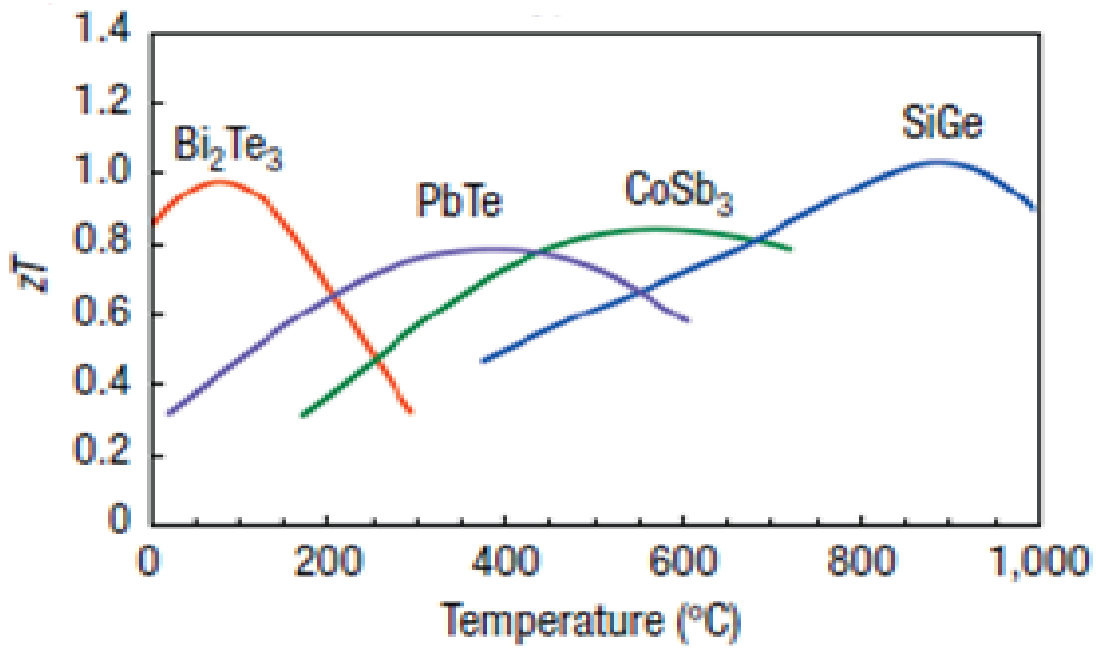

Figure 2.13 Thermoelectric figure of merit as a function of temperature for a number of established thermoelectric materials (Brown et al., 2006).

Even though TE devices have some advantages, such as their simple construction, they are easy to control, high reliability, easy to replace, operate with almost no noise and no moving parts and hence need less maintenance (Azarbayjani & Anderson, 2008). However,

there are a few drawbacks, the major problem is their relatively low conversion efficiency (Rowe, 1999). However, in the solar field, it has the potential to improve further, due to their capability for longer life operation, and independence from sunlight or particular position as a main source. These characters make them attractive and competitive to PV cells (Riffat & Ma, 2003).

2.5.2 PRINCIPLES OF THERMOELECTRIC DEVICES

2.5.2.1 POWER GENERATION BASED ON THE SEEBEC EFFECT:

Figure 2.14 shows the phenomenon of the Seebeck effect in a thermoelectric device, where heat is converted into electrical power by a "thermocouple" consisting of two different types of semiconductor materials.

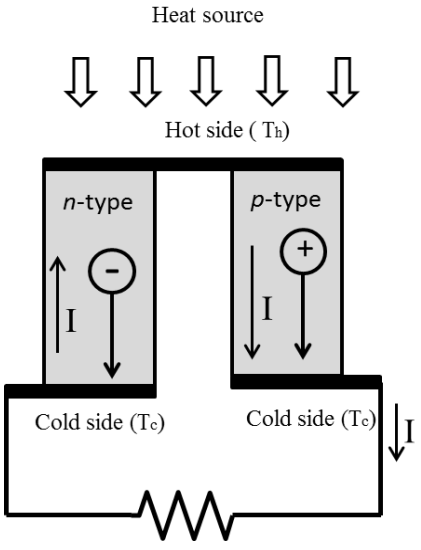

Figure 2.14 Seebeck effect: The voltage resulting from temperature difference.

The electric power (P_c) can be calculated when the voltage (V_c) and load resistance (R_{load}) are measured :

$$P_C = \frac{{V_c}^2}{R_{LOAD}} \qquad (2.2)$$

Electric power in open circuit (P_o) can be calculated too, P_o mathematically driven from equation (2.2), the steps will explain in details on the methodology chapter (3.7). The open circuit method will be used by using the following equation:

$$P_o = \frac{{V_o}^2}{4R_{TEG}} \quad (\text{min}, 2010) \qquad (2.3)$$

Even though, the calculated value of the electrical power that results from a closed circuit is more accurate than the power calculated from an open circuit, however, there are advantages of using open circuit measurement, such as simplicity and accuracy of the measured temperature difference, Peltier Effect is contributed at close circuit condition, which can effect the measurement of the temperature difference of the TEG (this will be explained further in the methodology chapter).

2.5.2.2 ***PELTIER EFFECT***

As shown in Figure 2.15, when the electrical current flows around the circuit (formed by two different semiconductor materials), heat energy is absorbed at one junction and rejected at the other junction. Consequently, the heat is pumped from one end to the other as a result

of the electrical current flow. The amount of heat removed per unit time from one junction to another junction is given by (Min 2010):

$$Q = \pi . I \qquad (2.4)$$

I is the electrical current in the circuit and π is referred to as the Peltier coefficient (W A^{-1}), which is equivalent to volts (Rowe & Min, 1997).

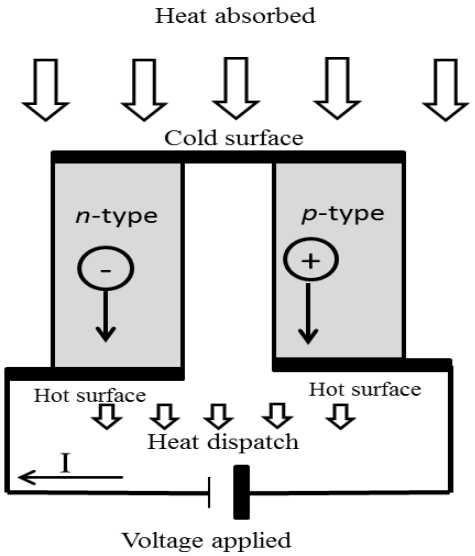

Figure 2.15 Thermoelectric refrigeration based on the Peltier effect.

2.5.2.3 INFLUENCE OF THE THOMSON EFFECT

Additional heat absorption or dissipation will take place in a thermoelectric device regardless whether it operates as a generator or refrigerator due to the existence of the Thomson effect. It is to be noted that the heat absorbed or rejected occurs along the material

as shown in Figure 2.16. It is different from the Peltier effect, where the heat occurs at the junctions. The unit of the Thomson effect is $V.K^{-1}$.

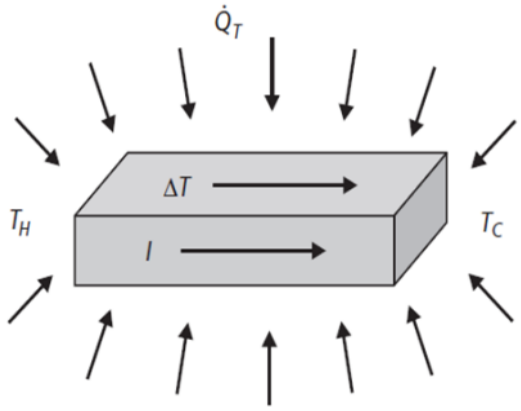

Figure 2.16 Heat absorption in conductor due to the Thomson effect when a temperature difference and electric current are applied (Min, 2010).

2.6 THE THEORY OF HEAT AND ELECTRIC POWER OF THE TEG

A diagram of a TEG module, demonstrated before in (Figure 2.14), shows where the heat power flows through the module mainly due to conduction (through the legs), convection and radiation (in the space between the legs) effects. More than 70% of the heat transferred through the TEG module is caused by the conduction effect (Suter et al. 2011). To calculate the magnitude of the heat power generated from the TEG (Q_{TEG}), the radiation and convection effect are neglected because of their small contribution if compared to the conducted effect (around 30% or less). The heat power generated by the module will therefore be calculated as follows:

$$Q_{TEG} = \frac{(k.A)_{TEG}(T_h - T_c)}{L} \qquad (2.5)$$

where k is material thermal conductivity. A and L are the thermoelements area and legs.

TEG able to convert heat energy to electrical power, this includes heat energy generated by waste heat or solar energy, this conversion based on the Seebeck effect. As illustrated on equation 2.1, the TEG figure of merit (Z) depend on TEG material properties, as the energy conversion required materials with high electrical conductivity, high Seebeck coefficient and low thermal conductivity k. Most efforts to increase Z have cantered about finding a way to decrease the thermal conductivity. Semiconductors have been the materials of choice for further development of thermoelectric devices (Bitschi.A 2009). Alloying remains an active research area. Bismuth telluride (Bi2Te3) alloys have Z values around 1, and have been commercially used within room temperature. Figure 2.17 represents the thermoelectric module, which is equivalent to figure 2.14.

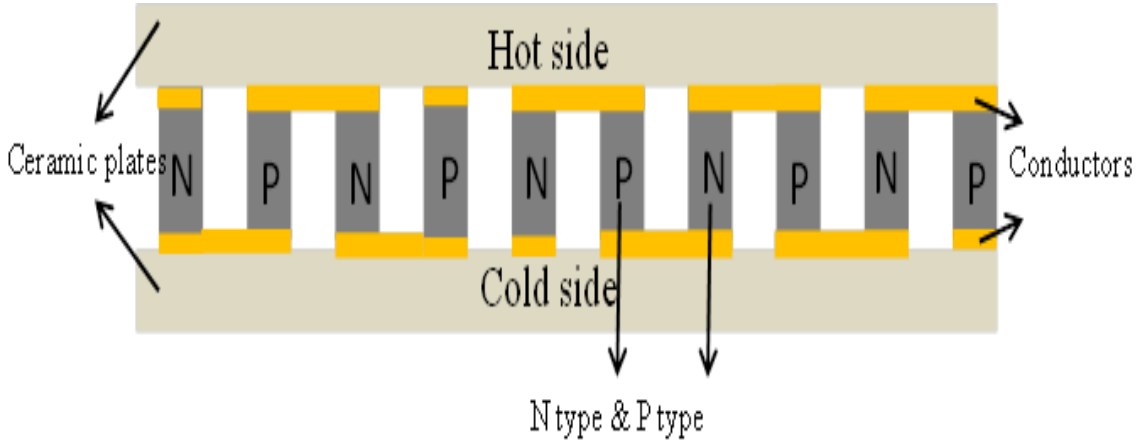

Figure 2.17 Schematic of thermoelectric device.

TEG devices typically consist of two ceramic plates that connected by electrical conductor to semiconductors legs (p and n type), thermoelectric generator consist number of legs (N & P types), every pair legs forms a thermoelectric couples. Heating one side of a thermoelectric material causes the electrons to move away from the hot end toward the cold end, consequently, an electrical current is occur. Usually, the Seebeck coefficient for the off-shelf materials available on the market is in the range of 150-230 $\mu V\ K^{-1}$, and it can have either a positive or negative value depending on if it is p- or n-type (Rowe & Min 1997).

2.7 RECENT DEVELOPMENTS IN THE SOLAR THERMOELECTRIC SYSTEMS

There are good effort on the research area of Solar TEG from quite long ago, even lately become more attractive especially after the recent progress in the field (Kraemer et al., 2011). For instance Chen (1996) reported a calculation technique based on thermodynamic analysis to determine the best performance of a solar-driven thermoelectric generator. While Rockendorf et al. (1999) have carried out a comparative study of the performance of a solar TEG and a solar PV, where both systems were used for combined heat and power application. It was found that the thermal and electric efficiency of the solar thermoelectric generators are approximately 45% and 3.2%, respectively, whereas that of a PV/T system reaches 10% for electricity production. Accordingly, they concluded that solar thermoelectric system will only be of interest for special applications and purposes. However, their conclusion was drawn from a special case where the geometry of thermoelectric module was fixed and the geometrical influence had been neglected. Juanicó and Rinalde (2009) present another economic comparison between PV and TEG solar panels, based on a field study

examining the provision of lighting for isolated homes in rural of Argentina. They find that the panel with TEG produces electricity at a lower cost, even though both panels are similar in terms of construction cost. This difference is due to a greater flexibility of TEGs to operate with any thermal source, such as the chimney of a stove, while PV is restricted only to operation during periods with sufficient sun light. (Juanicó & Rinalde, 2009). Omer and Infield (2000) designed and produced a two-stage solar TEG system using a concentrated collector. The design has been demonstrated to provide efficient solar concentration without the need for frequent tracking adjustment. The system has been successfully employed in a small combined heat and thermoelectric power generation unit. It was found that the major heat loss from the system was due to radiation more than convection, and the overall heat loss coefficient were related to the pressure level and the tilt angle (Omer & Infield 2000). Significant efforts have been made to achieve the improved performance of rooftop solar thermoelectric systems with focuses on implementing different designs of collectors and identifying the best position / orientation for the TEG collectors. The failure to observe such an action is likely to result in unsatisfactory performance. He et al. (2012) reported an experimental solar TEG system based on a glass evacuated-tubular solar collector as shown in Figure 2.18, A TEG placed in between a hot copper plate and a water flow channel. The study concludes that the optimum power output obtained when the load resistance is larger (not equal) than TEG internal resistance, this was at the condition of constant temperature difference across a thermoelectric module, this finding is different from what previously stated, which is the maximum power output can be achieved when the TEG resistance and the load resistance are equal in value. They also reported that both the thermal and electrical efficiencies of the proposed module decrease with an increase in the cold water temperature (input water), as the electrical efficiency is decreased by 23%, and the thermal efficiency also decreased by 10% when the input water temperature was increased from 25°c to 55°C.

However, the geometrical influence of thermoelectric module was neglected in their investigation.

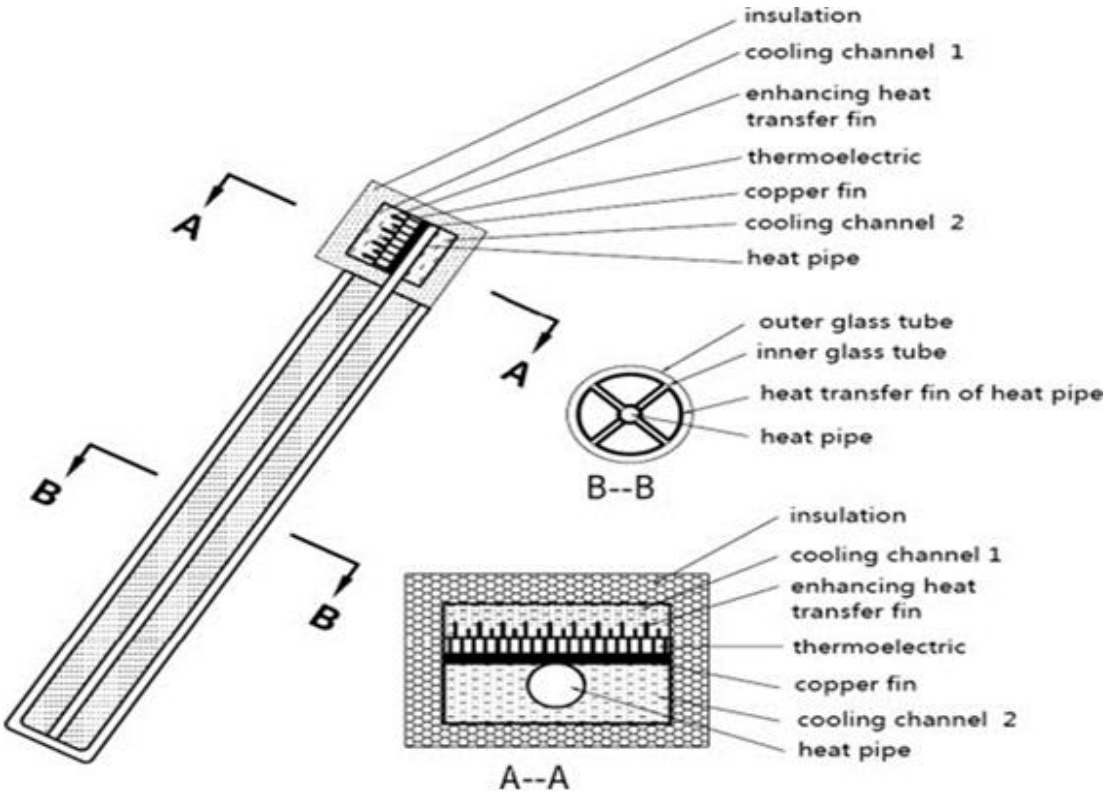

Figure 2.18 Schematic diagram of the STEG system based on evacuated-tube collector presented by Wei He et al, (2012).

Miljkovic and Wang (2011) reported a system, in which the TEG is attached to a parabolic concentrator with an evacuated tubular absorber. As shown in Figure 2.19, the TEG is placed between the inner tube (the cold side) and the outer absorber (hot side). An overall efficiency of 52.6% for combined heat and electrical power generation has been achieved by such a system, under conditions of a working temperature range between 300–1200 ^{o}K and solar concentration in the range of 1–100 suns (Miljkovic & Wang, 2011). The advantage of the concentrated system is to provide higher temperature at the hot side of TEG and consequently result in high electrical conversion efficiency. However, it requires optical tracking device, making the system complicated.

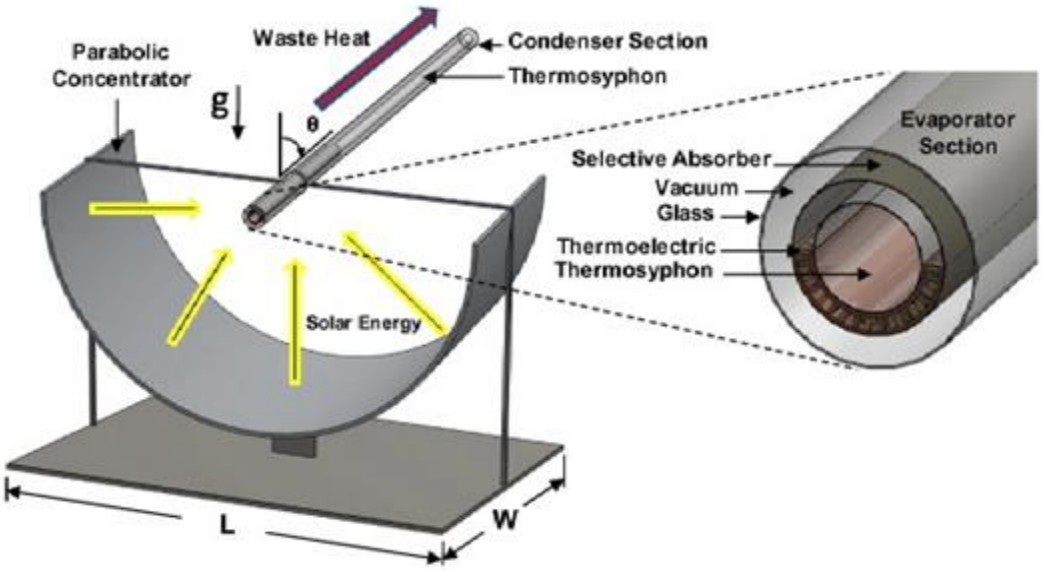

Figure 2.19 Schematic diagram of the concentrated solar thermoelectric system using a parabolic collector with an evacuated tubular absorber (Miljkovic and Wang, 2011).

In order to avoid using the optical tracing device but achieving higher temperature operation, a thermal concentrator using a flat copper plate was employed as shown in Figure 2.20 (Kraemer et al. 2011). The work carried out by Kraemer et al. at M.I.T. demonstrated that an efficiency of 5.2% for electrical power conversion is achieved using a flat panel solar TEG system operated in an enclosure system with a vacuum level of $5x10^{-6}$ mbar, with corresponding TEG temperature difference of 100 ^{o}C. This is the highest conversion efficiency achieved to date in a solar thermoelectric system. It is to be noted that the work was only focused on achieving high efficiency of electrical power generation and the effect on the efficiency of heat production was not investigated.

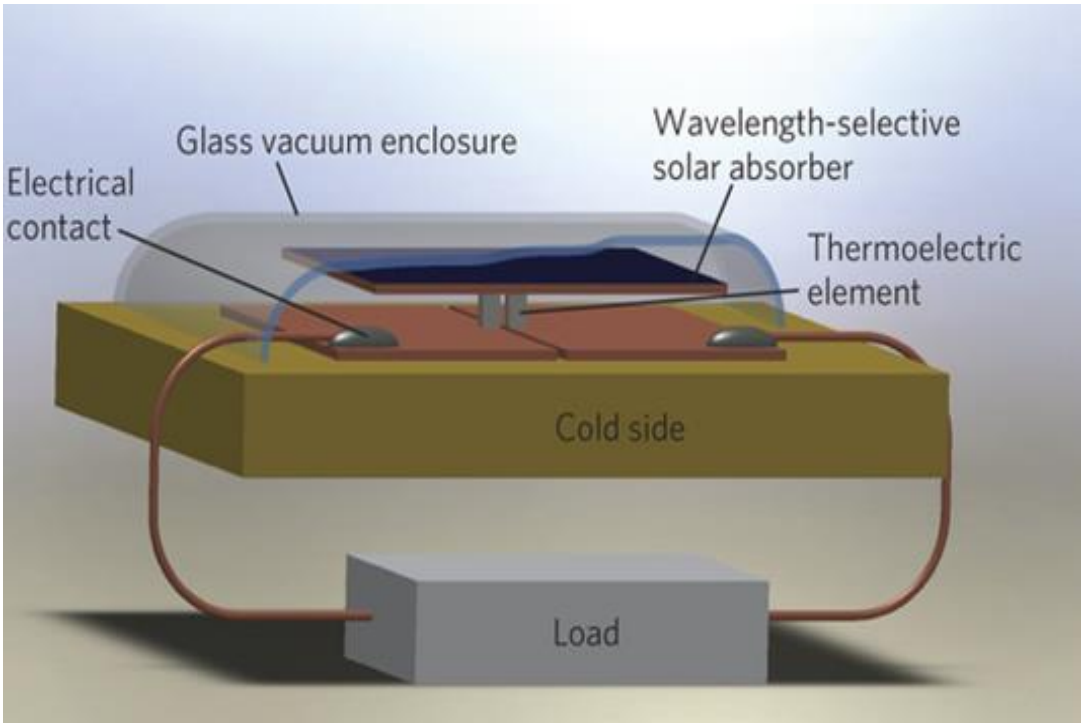

Figure 2.20 Evacuated STEG with Flat-Panel solar absorber (Kraemer et al, 2011).

It is apparent from literature survey above that solar thermoelectric system is a promising energy technology that has potential to harvest sunlight for combined heat and electricity production. In particular, the solar thermoelectric system based on a stationary flat-panel collector appears to provide a simple, low cost and rooftop system for domestic applications. However, there is lack on the research area, where the effect of TEG geometries to the optimum heat and electric power has not been investigated, especially when vacuum level is applied. There is a need to identify the parameters that are crucial to the efficiency of the system for both thermal energy and electrical energy production in order to improve its economic viability. To date, no work has been carried out in this aspect. The work reported in the following chapters is our attempts to fill in this gap through a systematic experimental investigation.

CHAPTER 3: RESEARCH METHODOLOGY

3.1 INTRODUCTION

This chapter describes the experimental techniques employed to investigate the performances of the proposed solar thermoelectric (STEG) system, in particular, the effects of TEG geometries on the heat and electrical power outputs of the STEG system. A laboratory-scale STEG system was designed and constructed. The experimental techniques developed based on this system will be used to determine the crucial parameters of the STEG, these include the thermal energy generated by the absorber, heat conducted through and electrical power generated by TEG, thermal and electrical efficiencies of the STEG. Finally a simplified theoretical model of this experimental system was presented.

3.2 EXPERIMENTAL SYSTEM DESCRIPTION

A solar TEG system was designed and constructed as shown in Figure 3.1. The system consists of a halogen lamp (as light source) and a copper plate (as solar absorber). The TEG was positioned between the heat absorber and the heat exchanger, which were immersed in a water container. The solar absorber measured 130mm x 130mm x 1mm. In order to ensure high absorption rate of light, the top surface of a solar absorber was painted with black high temperature paint (pnm type, see Appendix A1 on page 160). A channel was made on the reverse of the absorber to accommodate a k-type thermocouple, used to measure the temperature of the absorber, which is also the hot side temperature (T_h) of the TEG. Another thermocouple was placed in a groove at the top of an aluminium heat exchanger to measure

the TEG's cold side temperature (T_c). The heat exchanger was submerged in a water container with a magnetic stirrer to improve the heat transfer between heat exchanger and water and to ensure the temperature of the water is uniform in the container. The temperature of the water (T_w) was measured by a thermocouple, which was placed in the middle section of water container. To ensure the long-term stability of the radiation incident on the absorber, a halogen lamp was employed as suggested by Riffat and Mayere (2012). The halogen provides a better approximation of the solar spectrum than many other light sources. Although a solar simulator is available in our laboratory which provides the best match to solar spectrum, it has very limited irradiation area and limited operation period. Therefore, a halogen lamp was employed, which was placed 75mm above the surface of the solar absorber during experiments.

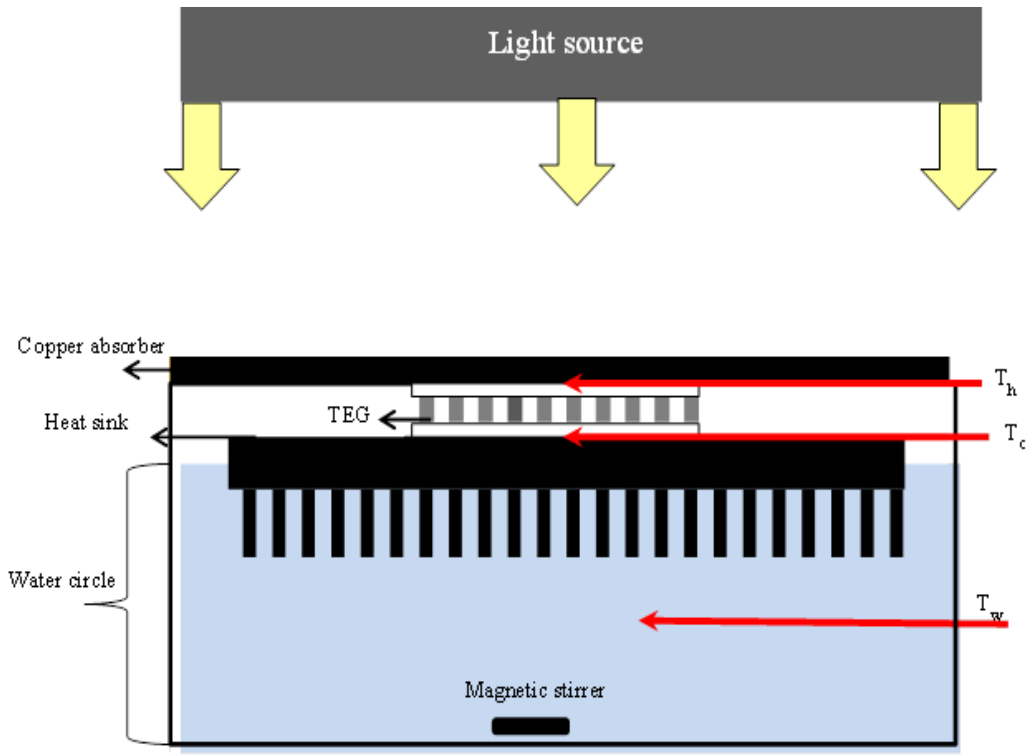

Figure 3.1 Schematic of the experimental setup, which represents a laboratory-scale solar thermoelectric system using a flat-panel collector for combined heat and power generation.

Figure 3.1 represents a simplified solar thermoelectric generator (TEG) system, which harvests solar radiation to produce electrical power and hot water. The solar radiation is converted into thermal energy by the copper absorber, which passes through the TEG module. Consequently, the TEG converts some of this thermal energy into electricity, and the rest passes through the heat exchanger into the water (producing hot water). Clearly, this system represents a simple yet effective co-generation configuration, which is particularly suitable for rooftop applications in remote areas.

3.3 DEFINITION OF THE SYSTEM CONVERSION EFFICIENCIES

The energy conversion processes of the proposed experimental system are illustrated schematically in Figure 3.2 below. Since this study involves determination of the efficiencies of several conversion processes, a clear definition of these efficiencies is necessary and is given as follows:

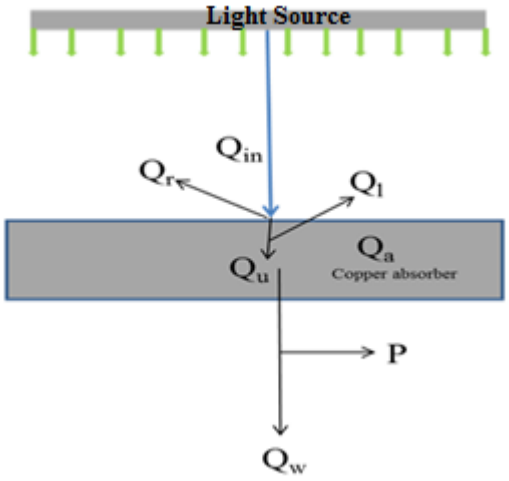

Figure 3.2 Schematic diagram of energy flow in the experimental system of Figure 3.1.

The absorber efficiency concerns with the ability of absorber to convert solar irradiation into thermal power, which is defined as

$$\eta_a = \frac{Q_a}{Q_{in}} \qquad (3.1)$$

where, Q_u is the thermal power produced by the absorber and Q_{in} is the incidence of light irradiation upon the absorber.

The efficiency of the thermoelectric generator concerns with the ability of a thermoelectric that convert heat into electricity, which is defined as

$$\eta_E = \frac{P}{Q_a} \qquad (3.2)$$

Where, P is the electrical power generated by the TEG.

The efficiency of heating concerns with the system ability to produce hot water, which is defined as

$$\eta_H = \frac{Q_w}{Q_a} \qquad (3.3)$$

Where, Q_w is the heat flux used to heat the water through heat exchanger.

The overall efficiency concerns with the combined heat and electricity production of the system, which is defined as

$$\eta = \frac{Q_w + P}{Q_a} \qquad (3.4)$$

In order to study the characteristics of this system and to investigate the system optimisation, a number of key parameter needed to be determined. This included heat absorption, heat lost and power generated. Experimental techniques for this purpose were proposed, and their feasibility investigated below.

3.4 DETERMINE THE HEAT ABSORBED BY THE ABSORBER

Figure 3.2 provides the principle of the experimental technique employed to determine the amount of thermal energy converted from solar radiation by the absorber. For this purpose, the experiment was carried out when the solar absorber was exposed to a light source but the rest of the system (TEG, heat exchanger and water container) was disconnected from the absorber, meaning both $P = 0$ and $Q_w = 0$.

By exposing only the solar absorber to the radiation from the light source (Q_{in}), some of the irradiation energy (Q_r) was reflected. The remaining irradiation energy was received and converted into heat by the absorber (Q_u)

$$Q_{in} = Q_r + Q_u \qquad (3.5)$$

In this investigation, it is crucial to determine the heat flux produced in the absorber (Q_u). When the remaining system is not attached to the absorber, the thermal energy converted from the solar radiation (Q_u) is equal to the sum of the heat flux retained in the absorber (Q_a), and the heat lost from the absorber to the ambient surroundings (Q_l)

$$Q_u = Q_a + Q_l \qquad (3.6)$$

This heat loss (Q_l) is mainly due to convection and radiation, and it is proportionate to the temperature difference between the absorber and surrounding ambient (ΔT). At a small ΔT, Q_l is usually very small and can be neglected. Consequently, equation 3.6 can be approximated as:

$$Q_u \approx Q_a \qquad (3.7)$$

The heat flux retained in the absorber (Q_a) is equal to the product of the absorber mass (m), the specific heat capacity (C_p) and the rate of temperature change ($\frac{\Delta T}{\Delta t}$)

$$Q_a = m \cdot c_p \cdot \frac{\Delta T}{\Delta t} \qquad (3.8)$$

Therefore, at very small ΔT, we have

$$Q_u \approx m \cdot c_p \cdot \frac{\Delta T}{\Delta t} \qquad (3.9)$$

Equation (3.9) indicates that Q_u can estimated by measuring $\frac{\Delta T}{\Delta t}$ for a material with known m and c_p. It is clear that ΔT has to be particularly small for the technique to be valid. Such validity can be checked by the linearity of ΔT vs. Δt. Figure 3.3 shows the classic heating curve of the absorber temperature, where the temperature is plotted as a function of time. Although the overall heating curve is not linear, an approximate linear relationship between ΔT and Δt can be seen during the initial irradiation period, as shown clearly by the inset in Figure 3.3. This result indicates that equation 3.9 can be employed to determine the thermal energy flux converted from solar radiation by measuring the slope of the heating curve during the initial linear period (Note: the results shown in this chapter are intended to demonstrate

the validity of the experimental techniques only. For clarity, experimental details are not included here but will be reported in Chapter 4).

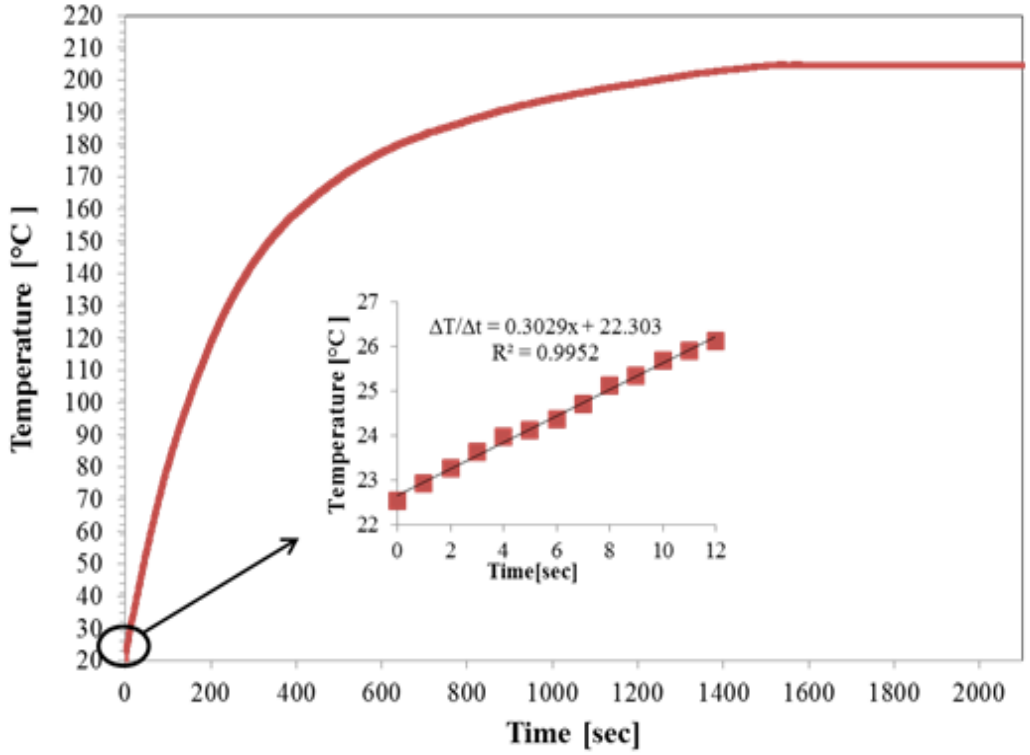

Figure 3.3 Classic heating curve of a solar absorber. The inset represents the temperature change of the absorber during the initial period of irradiation, which shows a linear relation between ΔT & Δt.

3.5 DETERMINE THE HEAT LOST FROM THE ABSORBER

With increasing temperature, the heat loss from the solar absorber will increase until reaching a constant value where the heat generated by the absorber is equal to the heat lost from it. In order to determine and improve the system efficiency, it is necessary to have the knowledge of the heat loss from the absorber. Two different methods were employed and described below.

3.5.1 *SLOPE TECHNIQUE BASED ON TEMPERATURE PROFILE*

The heat retained in the absorber (Q_a) decreases with increasing temperature of the absorber due to heat loss (Q_l). Q_a at any given time can be estimated by determining the corresponding slope on the temperature profile of the heating curve shown in Figure 3.3. Using an approximate approach, the slopes ($\Delta T/\Delta t$) was calculated at every three minute intervals. The corresponding Q_a can he determine as a function of temperatures as shown in Figure 3.4.

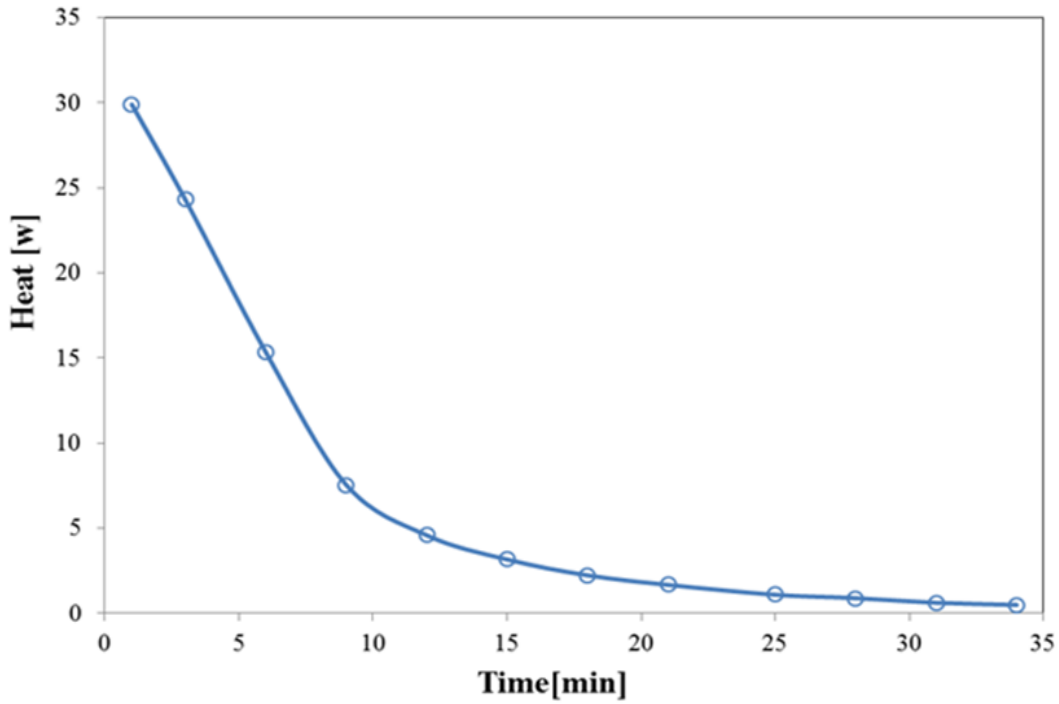

Figure 3.4 The net heat produced and retained in the absorber as a function of time (estimated using the slope method).

With the knowledge of Q_u and Q_a, which were determined from Figure 3.3, the heat loss (Q_l) from the absorber can be estimated using equation 3.6 ($Q_l=Q_u-Q_a$). The results are shown in Figure 3.5 (solid blue line and circles).

3.5.2 CALCULATION FROM CONVECTION AND RADIATION

It is anticipated that the heat loss from the absorber is mainly caused by convection and radiation. Based on fundamental heat transfer theory, the heat loss due to convection (on the first term and radiation on the second term) can be estimated using the flowing equation:

$$Q_1 = [hA_c(T_h - T_a)] + [\varepsilon\sigma A_c({T_h}^4 - {T_a}^4)\ ] \quad (3.10)$$

Where, h is the convection coefficient, A_c is the absorber area, T_h is the absorber temperature, T_a is the surrounding temperature, ε is the emissivity of the absorb surface, and σ is a Stefan Boltzmann constant. The first term on the right of equation 3.10 is due to convection and the second term is due to radiation. The values for ε and h were obtained from the literature, which gives ε =1 (Nellis & Klein 2008) and h= 5.7 Wm^{-2} K^{-1} (Fan et al, 2011). Using the temperatures T_h and T_a from the experiment, the heat loss from the absorber can be calculated which is shown by the dashed line in Figure 3.5. It can be seen that the results estimated from both methods are in a reasonably good agreement. These results demonstrate the validity of experimental techniques employed for this research.

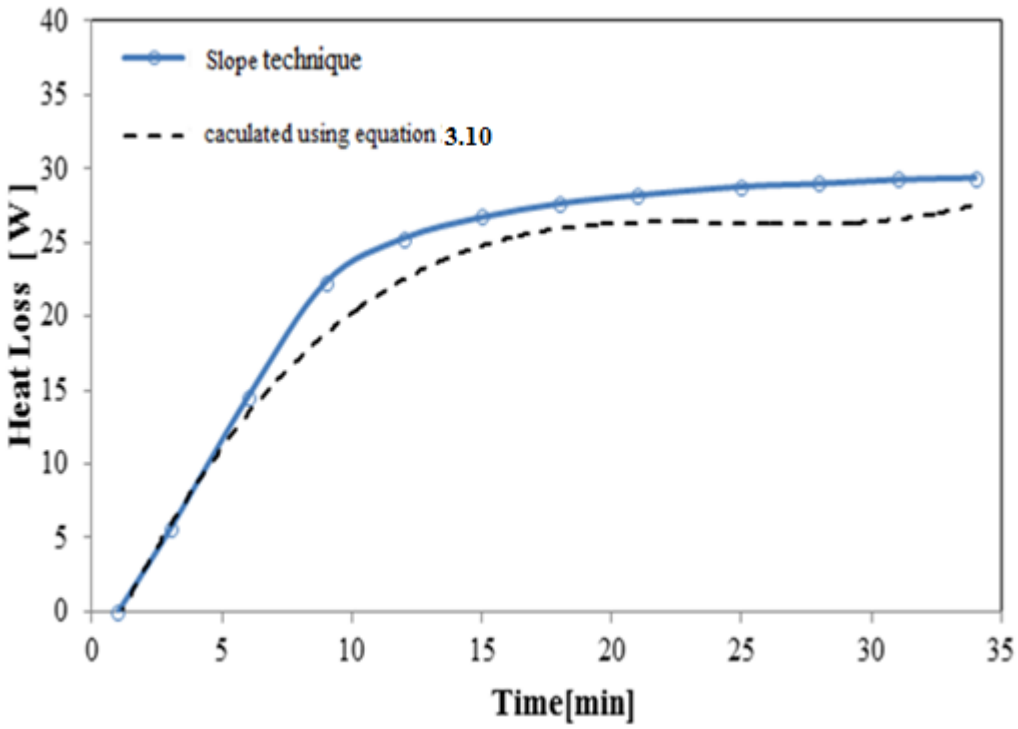

Figure 3.5 Heat loss determined using the slope technique, compared with that calculated based on heat transfer theory.

3.6 DETERMINING HEAT ABSORBED BY THE WATER

Based on the experimental set-up described by Figure 3.1, the heat power generated by the system (i.e., thermal energy transferred into the water) can be estimated using two different approaches:

1) The first approach uses the same principle of the slope technique described in section 3.5.1. Based on the equation (3.8), m and C_p in this case are the mass and the specific heat of the water, respectively. $\frac{\Delta T}{\Delta t}$ Was obtained by monitoring the water temperature profile (T_w) at the initial period of the operation where the temperature change with time shows a linear relationship. However, it is to be noted that a thermal lag will occur due to the presence of the TEG, where the thermal energy is initially absorbed by the TEG and heat sink before entering into the water. As a result, this will introduce additional errors to this technique. This

technique measures the net heat gained by the water (i.e, the heat transferred into the water minus the heat lost from the water to surrounding ambient).

2) A second approach is to determine the heat transfer through the TEG (Q_{TEG}) using equation below

$$Q_{TEG} = \frac{kA_{TEG}(T_h - T_c)}{L} \qquad (3.11)$$

Where, T_h is the temperature at the hot side of the TEG and T_c is the temperature of the heat sink that emerged in the water. A_{TEG} is the total area of the thermoelements in the TEG and L is the length of thermoelements. k is the thermal conductivity of thermoelectric materials. In this investigation, TEG modules using Bi_2Te_3 materials were employed, which has a thermal conductivity of 1.5 W $m^{-1}K^{-1}$ (Min, 2010). This approach is only valid under assumption that all the heat passing through the TEG and heat sink is transferred into the water (i.e., no heat loss to the surrounding ambient). Since the TEG and heat sink has relative large heat conductance and majority of the heat sink is emerged into the water, this assumption is approximately valid. Unlike the slope technique, this method determines the thermal energy transferred into the water, not the net gain of the heat by the water. In addition, equation (3.11) can be applied to both transient and steady state. However, the method was dependent on the measuring of the temperature difference across the TEG (T_h - T_c). This method is only valid when the temperature difference is measured when the TEG is under an open circuit condition. In a closed circuit, the temperature difference across the TEG would have been altered because the Peltier effect occurs. In this research, the heat and electrical power generated by the system was mainly investigated during the steady state under open circuit conductions, with the thermal power determined using the second technique.

3.7 DETERMINE THE ELECTRICAL POWER OUTPUT

The work presented in this section highlights how the electrical power of the system shown on Figure3.1 was determined and measured. It begins by describing how the open circuit voltage (Vo), and electrical resistance value of the TEG were measured. The internal resistance was determined on the electrical power being maximized, as shown with the electrical circuit below.

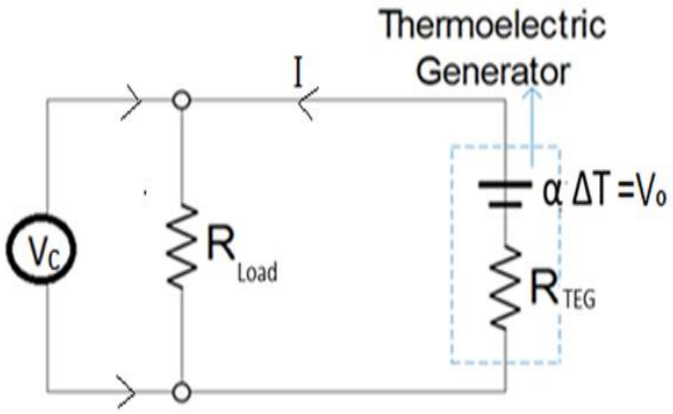

Figure 3.6 Measuring the TEG's internal resistance, which achieves the maximum power.

The TEG (R_{TEG}) was connected in a series with variable external resistance (R_{Load}) to complete the loop, and the voltage drop (V_c) was measured with different load resistances (R_{Load}). The maximum power was recorded when the TEG resistance matched the load resistance. Such power in a closed circuit can be calculated using equation (2.2) on chapter 2. The plotted curve represents the electrical power output as a function of the resistance value. The best available was the one representing the maximum power, as shown in (Figure 3.7).

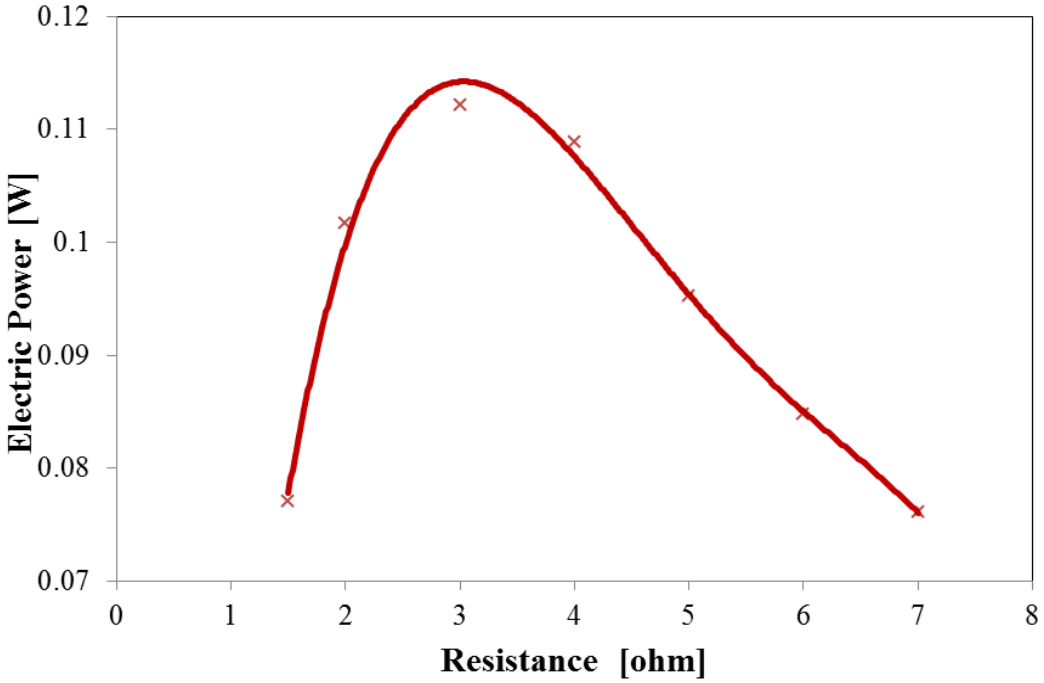

Figure 3.7 Maximum power as a function of load resistance of TEG.

As the internal resistance of the TEG was defined, the electrical power in an open circuit was determined by measuring the open circuit voltage, then the maximum power at open circuit can be identified using equation (2.3), which driven from equation (2.2) as previously presented (chapter 2) (Min, 2010). Figure 3.6 is electric circuit equivalent of figure 2.14. Based on figure 3.6, the voltage created by the Seebeck effect at the TEG can be calculated if the temperature difference across the junctions (ΔT) and the Seebeck coefficient (α) of the semiconductor materials are known:

$$Vo = \alpha \, \Delta T \qquad (3.12)$$

$\Delta T = T_h - T_c$, were T_h and T_c are the temperatures at the hot and cold side of the thermoelectric device, respectively).

$$V = \alpha \, \Delta T \approx I \, (R_{TEG} + R_{Load}) \qquad (3.13)$$

Equation 3.13 gives:

$$I = \frac{\alpha \Delta T}{R_{TEG} + R_{Load}} \quad (3.14)$$

As $V_c = IR_{Load}$ then:

$$Vc = \frac{\alpha \Delta T}{R_{TEG} + R_{Load}} . \ R_{Load} \quad (3.15)$$

$$\text{And as } P = V_c I \approx \left(\frac{\alpha \Delta T}{R_{TEG} + R_{Load}} . R_{Load} \right) \left(\frac{\alpha \Delta T}{R_{TEG} + R_{Load}} \right) \quad (3.16)$$

$$P = \frac{(\alpha \Delta T)^2 . R_{Load}}{(R_{TEG} + R_{Load})^2} \quad (3.17)$$

In condition of $R_{Load} = R_{TEG}$, maxim power at open circuit can be driven as :

$$P = \frac{(V_0)^2}{4R_{TEG}} \quad (2.18)$$

Even though equation 2.2 is more accurate in determining electrical power than equation 2.3, the latter is used to avoid any uncertainty of the temperature difference value introduced by the Peltier effect in closed circuit conditions. Additionally, the power generated by the TEG will be directly measured by measuring the TEG voltage.

3.8 THEORETICAL MODEL

A theoretical model, that enable the prediction of the optimal TEG geometries needed to achieve the optimum heat and electrical power output from the solar thermoelectric system, is needed to assist the experimental investigation. In this section, a simplified and approximate model was developed based on the experimental system shown in Figure 3.1 and the energy flow described in Figure 3.2. In a steady state, the heat (Q_u) produced in the solar absorber for a given irradiation is balanced by the heat lost from the system and the heat transferred through the TEG into the water,

$$Q_u = Q_l + Q_{TEG} \qquad (3.19)$$

The heat loss (Q_l) from the system is mostly from the absorber through convection and radiation (equation 3.10) which represent the first term (eq 3.20). The heat transferred through the TEG is due to Fourier heat conduction described by equation 3.11. Consequently, the heat transfer equation of the solar thermoelectric system (Figure 3.1) in a steady state can be expressed as:

$$Q_u = \left[hA_c(T_h - T_a) + \varepsilon\sigma A_c\left(T_h{}^4 - T_a{}^4\right) \right] + \left[\frac{kA_{TEG}(T_h - T_c)}{L}\right] \qquad (3.20)$$

Equation 3.19 enables investigation of the absorber temperature (T_h) in relation to the TEG geometries (A_{TEG} and L). In a STEG system shown in Figure 3.1, the heat transfer parameters including h, ε, σ and κ are known once the materials of the system are chosen. The system usually operates under a given sunlight irradiation (Q_u) for a given surrounding

temperature T_a. In addition, it can be shown (see Table 4.4) that T_c of the system investigated in a steady state remains approximately constant at ~70 ^{o}C. Under such circumstances, the relationship of the absorber temperature (T_h) to the TEG geometries (A_{TEG}/L) can be determined. Once the absorber temperature is determined, the heat power produced in hot water can be calculated using equation 3.11 and the electrical power generated by the TEG can be calculated using equation 3.20 (Min G, 2010),

$$P = \frac{(N\alpha)^2 A \Delta T^2}{2\rho(n+L)(1+\frac{2rLc}{L})^2} \qquad (3.21)$$

where, α is the Seebeck coefficient of TEG materials (with a typical value of ~200 μV/K), ρ is the electrical resistivity (with a typical value of 1×10^{-5} Ω.m), *Lc* is the thickness of the ceramic contacts layers in TEG (with a typical value of 0.5 ~ 1mm), r is the ratio of thermal contact resistance to that of the bulk (with a typical value of 0.2), n is the ratio of electrical contact resistance to that of the bulk (with a typical value of 0.1mm), and N is the number of thermocouples in the TEG. The calculation technique presented in this section facilitates calculation of both the heat and electrical powers produced by a STEG system shown in Figure 3.1 as a function of the TEG geometries. Consequently, it enables the investigation of the optimal TEG geometries needed to achieve the maximum heat and electrical power outputs from a STEG system.

3.9 CONCLUSIONS

A laboratory scale STEG system was designed and constructed. The experimental techniques for investigating the performances of the STEG system were proposed. Based on

fundamental heat transfer theories, it was shown that the heat power generated in the solar absorber can be determined using the “slope technique”. In addition, it can also be used to estimate the heat losses from the system. The heat power produced in hot water can be determined using the “slope technique,” while the heat transferred into the hot water can be determined using the Fourier’s law. The electrical power generated by TEG can be determined from direct power output measurement or calculated using an established thermoelectric device theory.

A calculation technique of the constructed experimental system (Figure 3.1) was also established, which facilitates estimation of the heat and electrical power output of a solar thermoelectric system as a function of TEG geometry. The model has been employed in the following chapters to investigate the optimal TEG geometries for obtaining the maximum heat and power outputs.

CHAPTER 4: EFFECT OF TEG GEOMETRY ON SOLAR THERMOELECTRIC SYSTEM

4.1 INTRODUCTION

This chapter describes an experimental investigation of the influence of TEG geometry on the performances of a solar thermoelectric system using the constructed laboratory scale system (Figure 3.1) and experimental techniques described in Chapter 3. The objective is to determine the optimal geometries of TEG for obtaining the maximum heat power or electrical power. The experimental results obtained from this investigation were also used to validate the theoretical model established in Section 3.8.

4.2 DESCRIPTION OF EXPERIMENTS

The investigation was carried out using the constructed experimental setup as described in Figure 3.1. The experiment aims to study the effect of the TEG geometry on the thermal and electrical power production of a solar thermoelectric system. For this purpose, 5 appropriate TEGs were chosen, which have significantly different geometries. The selection of the appropriate TEGs are based on a useful geometrical parameter referred to as the aspect ratio, which is defined as $(A_{TEG}.2N)/L$, where A_{TEG} is the cross-sectional area of thermoelements in TEG, N is the number of thermocouples in TEG (i.e., 2N is the number of the thermoelements in TEG) and L is length of the thermo elements. Guided by this parameter, 5 suitable TEGs were identified from a large number of commercially available thermoelectric modules (see Section 4.4 for details). The experiments were performed under a fixed sunlight irradiation of 1700 $W \cdot m^{-2}$ (a halogen light with this intensity was employed in this investigation because it is the only available light source that can last for long time and has approximate spectrum to the sunlight). The experimental investigation involves

determination of the temperature difference across the TEGs, the thermal power transferred into hot water and electrical power output generated using the techniques described in Chapter 3. Experimental work investigated both the transient and steady state, while the calculation technique (to estimate the optimum TEG geometry) will focus only on the steady state because of the limitation of the technique. Although the transient state contributes to heat and power production, the steady state is likely to be dominant operating state in a solar thermoelectric application and will be the focus of this work.

4.3 VALIDATING THE SLOPE TECHNIQUE

The absorber temperature profiles, induced under the three light intensities, were obtained using the "slope technique." The results are shown in Figure 4.1, which show classic heating curves. It can be seen that in the initial period the rate of temperature change under higher light intensity of irradiation are larger than those under lower light intensity of irradiation. Also, the final steady state temperature is higher for these with higher light intensity. In the opening seconds the temperature increased sharply, which indicates that the heat loss to the surroundings is minimal. An initial period that corresponding to a temperature difference of less than 6 ^{o}C between the absorber and the surroundings was selected to investigate the linearity of the rate of temperature change, $\Delta T/\Delta t$. The data in the initial period of Figure 4.1 was collected and plotted in Figure 4.2. Straight lines are evident for all three light intensities, with linearity coefficients of > 0.995. This indicates that the heat losses during this initial period are negligible and the heat absorbed by the heat absorber can be calculated using equation 3.8. Using the slope determined from Figure 4.2, the mass (0.250 kg) and specific heat capacity (400 Jkg^{-1} K^{-1}) of the copper (the material for the solar absorber in this study), to estimate the heat power absorbed by the solar absorber. The results are displayed in Table 4.1.

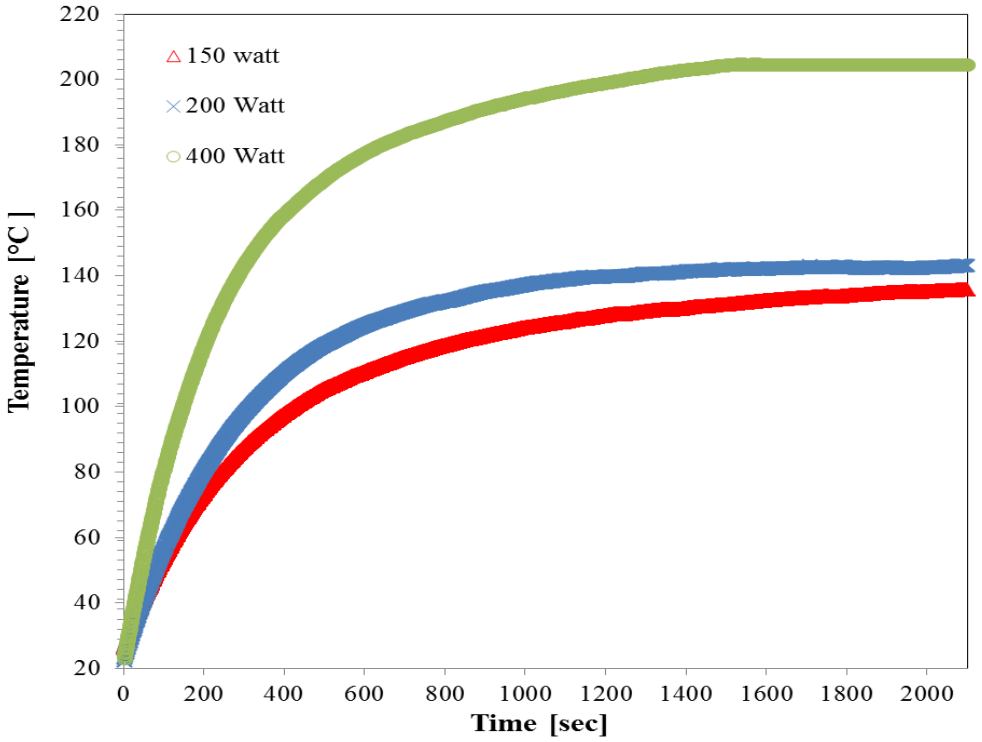

Figure 4.1 The absorber temperatures as a function of time for three different lighting power (Intensities).

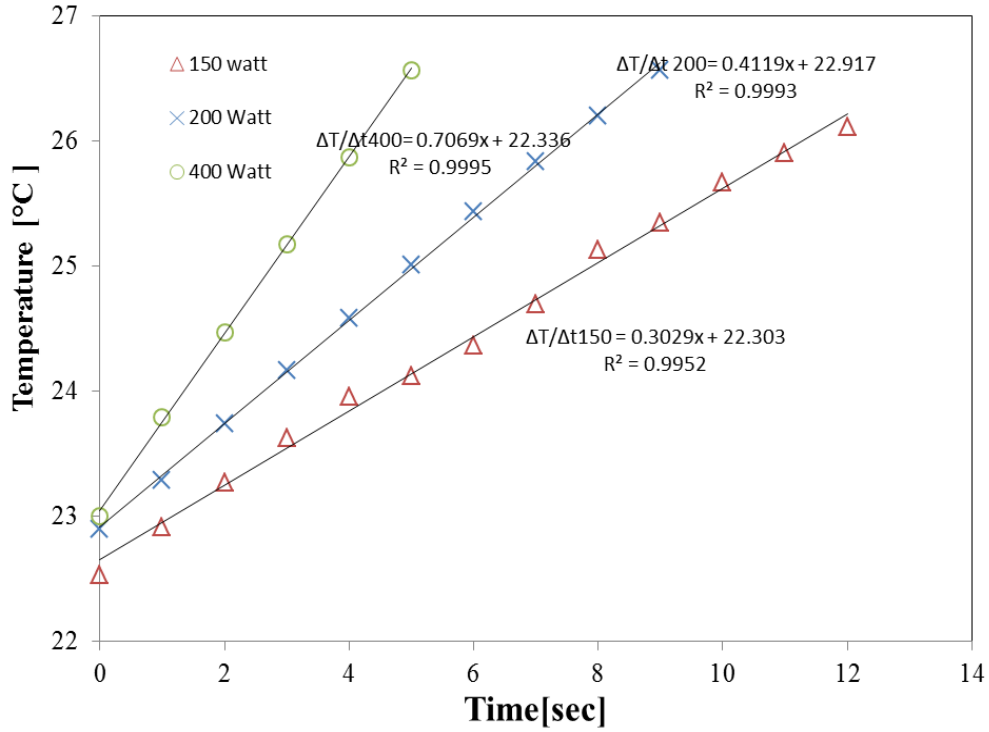

Figure 4.2 The absorber temperatures during the first 12 seconds under three different lighting power.

In order to validate the slope technique, the results obtained from the slope technique were compared with the results obtained from direct measurements of light irradiation power. An intensity meter (Pyranometer) of a Kipp & Zonen CMP11 type was used to measure the light intensities generated by three halogen bulbs employed in this study. To ensure accurate comparison, the intensity meter was placed under the light sources in the same distance to that of the solar absorber. An average of five measurements were taken at different locations in the same plane of the solar absorber, which has an area of 130 mm x 130 mm (see Figure 4.3 below). The readings obtained by the Pyranmeter under the light irradiation by the 400 watt light bulb are also displayed in the figure below. The results of light intensity measurement for other two light bulbs (150 and 200 Watt) are shown in Appendix A2 on page 161.

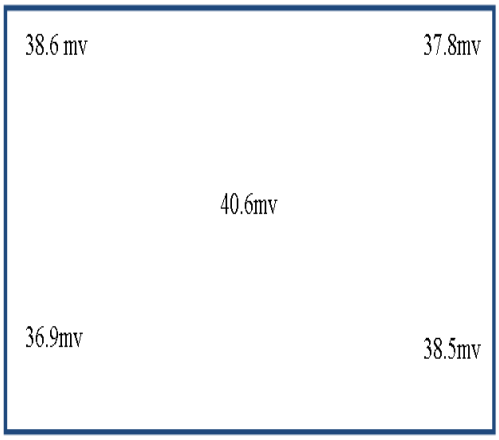

Figure 4.3 Readings obtained from measurements using the Pyranmeter at 5 different locations on solar absorber plane.

Using the sensitivity of the Pyranmeter (8.66×10^{-6} V/Wm^{-2}), the power of light irradiation from the three halogen bulbs can be calculated. The sensitivity is defined as the voltage (V) generated by unit light irradiation (Wm^{-2}). The results calculated from Pyranmeter measurement are also collected in Table 4.1. Since the conversion efficiency of light energy into thermal energy using black paint on copper is over 90% (Kennedy, 2002, p. 11), it is

expected that the results obtained from the slope technique will be close to the light power directly measured from Pyranmeter if the slope technique is valid. It can be seen from Table 4.1 that the results obtained using the slope technique are in reasonably good agreement with these obtained from direct measurements using Pyranmeter. With a deviation between 2 % and 5%, the Pyranmeter results were consistently higher than those obtained using the slope technique. The light bulb with an intensity of (1816W.m^{-2}) was employed for the study hereafter.

Table 4.1 Comparison of the heat power determined from the slope technique and the power in the light irradiation measured using Pyranmeter.

Light ID	$\frac{\Delta T}{\Delta t}$	**Intensity [Pyranometer] [W.m^{-2}]**	**Heat [slope technique] [W.m^{-2}]**
150	0.30	1816	1775
200	0.41	2560	2420
400	0.70	4400	4150

In order to ensure the repeatability of the measurements, the experiment was repeated three times and the results are shown in Figure 4.4, which is obtained using the halogen bulb of the intensity of 1816 W.m^{-2}. The results from the two other bulbs are documented in the Appendices A3 on page 162. All results demonstrate a very good repeatability.

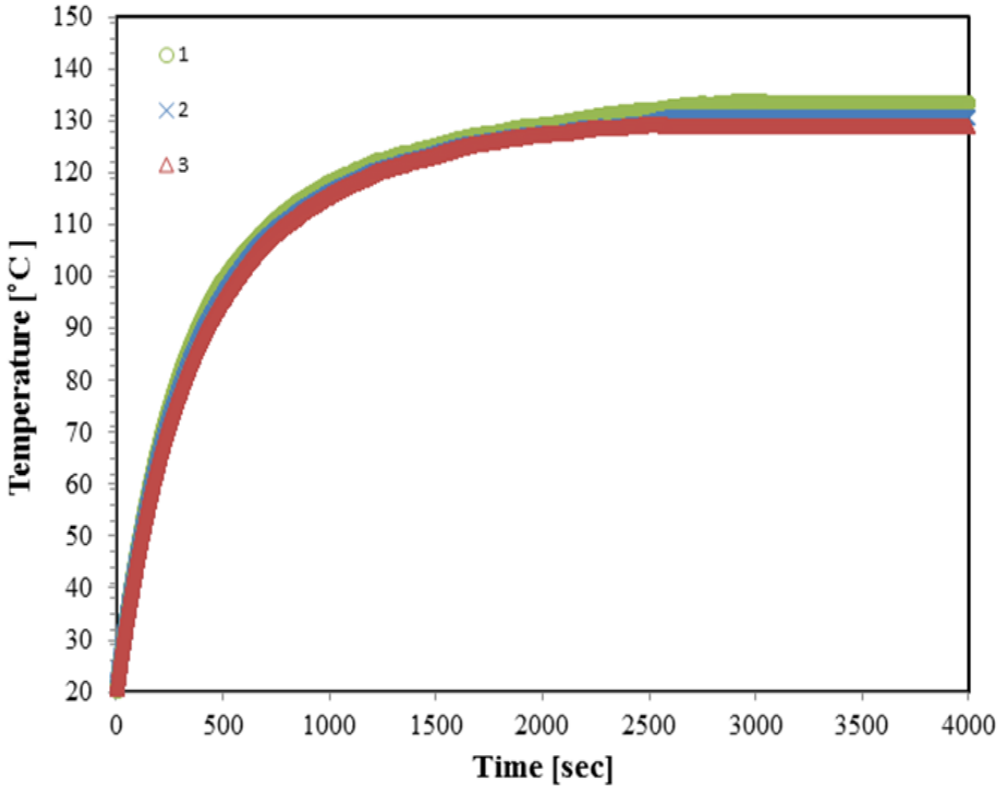

Figure 4.4 Three tests of the absorber temperature profile to show good repeatability of the experiments.

4.4 SELECTION OF TEGS FOR EXPERIMENTS

Suitable TEG for this study is selected from commercially available thermoelectric modules. Although there appear to be a large number of different modules available on the market, finding a wide selection of TEGs proved difficult. They were chosen based on the aspect ratio. In addition, the operating temperature is also considered. Five TEGs that have significant different aspect ratios were identified as shown in Table 4.2. The manufacturers' specifications of these TEGs are shown in Appendix A4 on page 163.

Table 4.2 The geometrical parameters of TEGs selected for this study.

Sample ID	N	A (m^2)	L (m)	Aspect ratio (Ax2N)/L-(m)	Measured-R (Ω)
S1	72	$1.6x10^{-6}$	$1.7x10^{-3}$	0.136	1.8
S2	127	$1x10^{-6}$	1.5×10^{-3}	0.169	6.5
S3	127	$2x10^{-6}$	1.7×10^{-3}	0.299	3.5
S4	127	$7.6x10^{-6}$	3.6×10^{-3}	0.536	1.6
S5	48	$1.7x10^{-5}$	2.4×10^{-3}	0.680	0.2

To calculate the electrical power, the value of each TEG's internal resistance (R) was determined through experimentation. The results of this are shown in Table 4.2. The TEG's internal resistances were determined by performing the matched load experiments described in Section 3.7. The result of the matched load experiment based on a TEG module with small aspect ratio of 0.136 is shown in Figure 4.5. The results of the matched load experiments for the other 4 TEG modules are displayed in Appendix A5 on page 164.

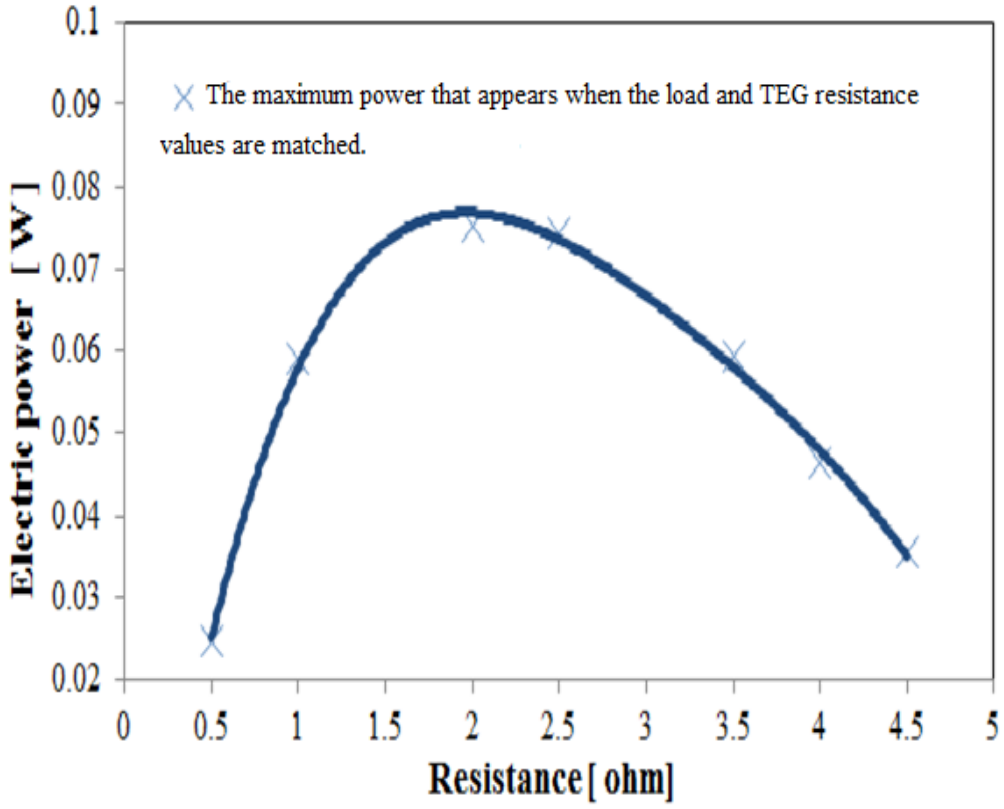

Figure 4.5 Determination of the internal resistance (1.8 Ω) of the TEG with sample ID of S1 and an aspect ratio of 0.136.

4.5 EFFECT OF TEG ON SOLAR HOT WATER SYSTEM

Evaluating the effect of adding a TEG to the solar hot water system on its thermal power output is particularly important. Experiments were conducted based on the system illustrated in Figure 3.1 on chapter 3 to evaluate the thermal performance of the system with and without TEG devices. The evaluation started with examining the performance of SHW system based on the structure of the proposed system; this was conducted by placing the solar absorber directly on the top of the heat sink which was partly submerged in water. Evaluating the thermal performance of the system required to measure the system temperature, two thermocouples were attached to the system, one thermocouple was inserted

between the absorber and the heat sink to measure T_h, while the other thermocouple placed in the water tank to measure the T_w. The temperatures of both systems were monitored from the first second of turning the light on. The results are illustrated in Figure 4.6. By investigating the water temperature at the first 8 minutes of the operation starting time, and determining the rate of temperature change $\Delta T/\Delta t$ (Figure 4.6), together with the water mass (0.450 ml) and specific heat (4184J.kg-1.K-1), the thermal power of proposed SHW system can be calculated using Equation 3.9 mentioned on chapter 3.

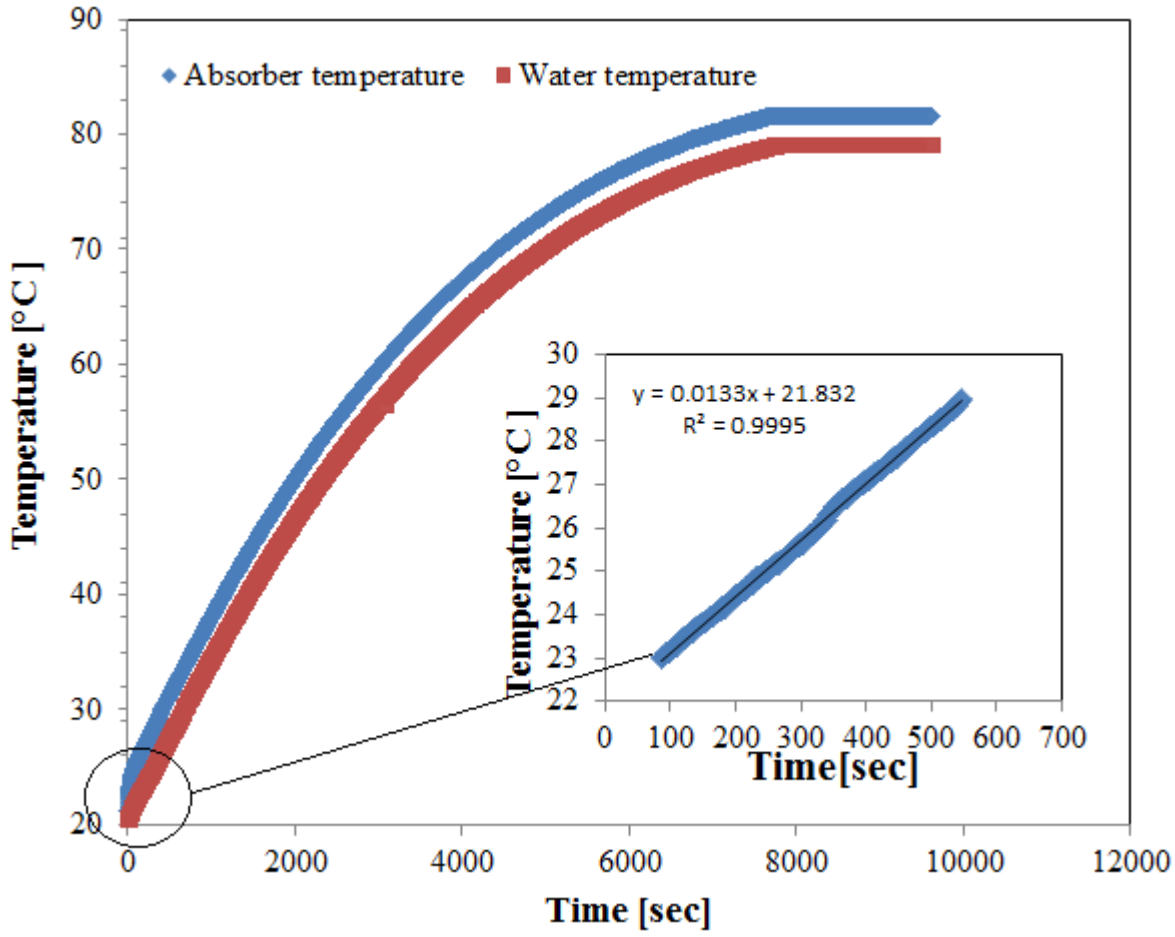

Figure 4.6 The absorber and water temperature of the SHW system

Figure 4.6 shows the absorber and the water temperature of the SHW system based on the proposed structure in Figure 3.1 on chapter 3. The difference in temperatures recorded between the absorber and water at the steady state was 2°C. The inset Figure shows the rate

of the water temperature and time change during the initial period ($\Delta T/\Delta t$), which show good linear relationship, with slope coefficient of 0.0133. The thermal power of the system was calculated as following:

$$Q_{w1} = (0.450\text{kg})\ (4184\ \frac{\text{J}}{\text{kg.K}})\ (0.0133\text{K/se}) = 25\ \text{Watt} \qquad (4.1)$$

The thermal performance of the proposed SHW system was also investigated in a different way. A copper plate with similar dimensions to the largest TEG device was machined to replace the TEG and was placed between the absorber and the heat sink, as illustrated in Figure 3.1 on chapter 3; this was to obtain fair results to the system which included the TEG in terms of heat transfer conditions. The thermal powers of the systems with and without TEG were obtained using the slope technique during the transient state. By monitoring the water temperature, the slope coefficient of the rate of temperature change over time, $\frac{\Delta T}{\Delta t}$, was obtained, together with the water mass (0.450 ml) and specific heat ($4184 J.kg^{-1}.K^{-1}$); the thermal power of the system with and without TEG were calculated.

Figure 4.7, shows the absorber and the water temperature of the system when TEG is not attached (copper plate attached instead). The T_h, T_w ($Tw \approx T_c$) of the system without TEG are plotted as a function of time. The recorded T_h & T_w, in the steady state, show small differences (3^oC), which indicates that heat flows easily from the solar absorber into the water.

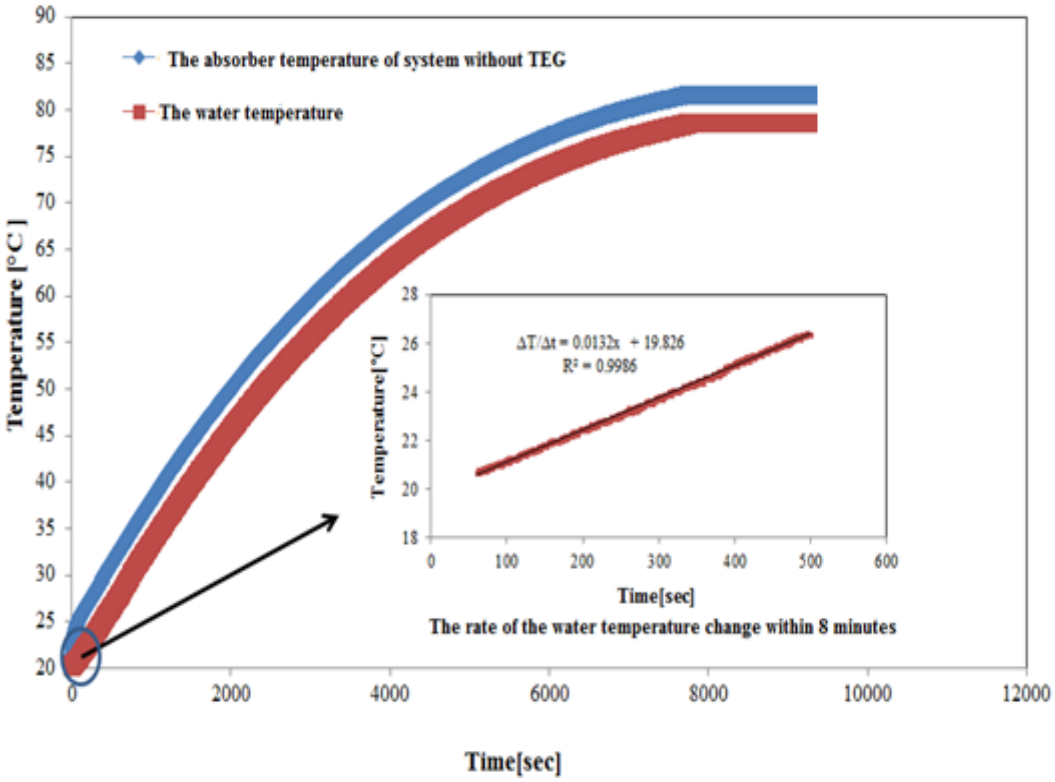

Figure 4.7 The absorber and water temperature of the system, without a TEG, as a function of time.

The rate of temperature change during the first few minutes $\frac{\Delta T}{\Delta t}$ of the system with copper plate was determined using the slope technique as shown in the inset of Figure 4.7. The inset Figure shows the water temperature change during the initial period. A good linear relationship was evident, with a value of 0.013K/sec. Therefore, the thermal power of the system without TEG can be calculated by using equation 3.9 as :

$$Q_w = (0.450\text{kg})\ (4184\ \frac{J}{kg.K})\ (0.0132K/se) = 24.8\ \text{Watt} \qquad (4.2)$$

While, when a TEG was attached to the system and replaced the copper plate, an increase in the temperature difference between T_h and T_w was observed (40 ^oC). This was due to a significant thermal resistance caused by the TEG devices. Using the slope technique, the thermal powers of all five TEGs samples were determined. Figure 4.8 shows the results

obtained from a TEG with sample ID of S5 and an aspect ratio of 0.68. Similar patterns of the temperature change were obtained for other 4 TEGs of different aspect ratios. These results are shown Figure 4.8, while the relationship between the changes of the water temperature ΔT in respect of the time change during the initial period for other 4 TEGs of different aspect ratios are shown in in Appendix A6 on page 166.

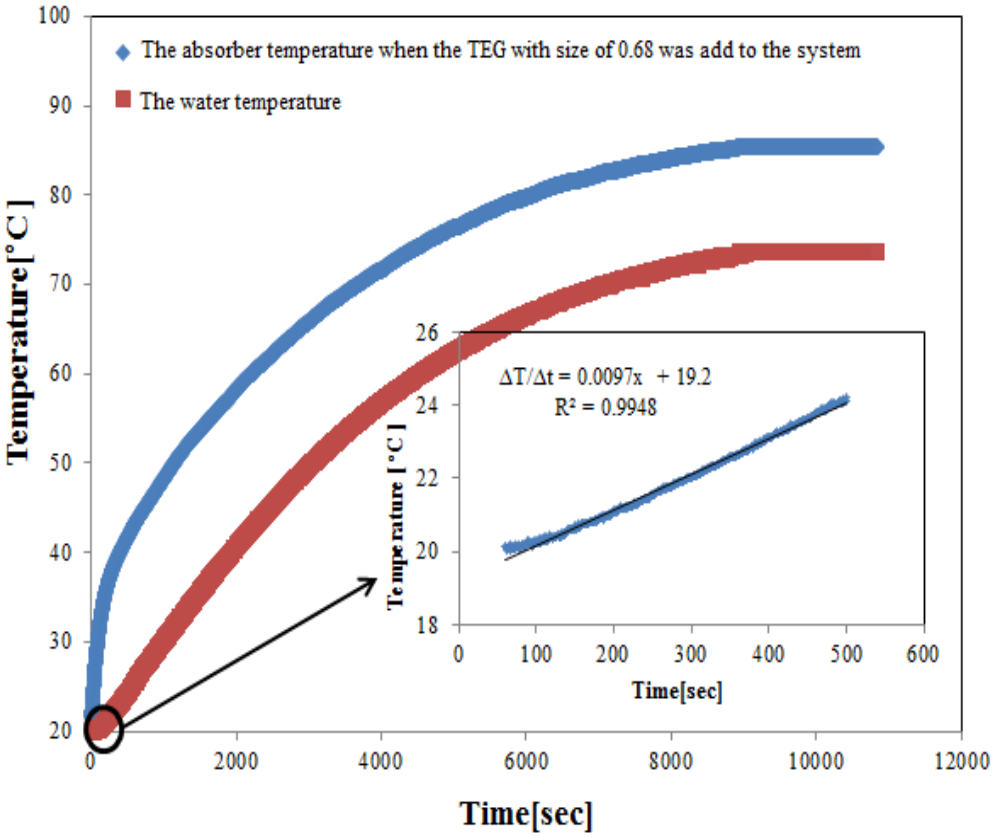

Figure 4.8 The temperature profiles of the absorber and the water of the system with the TEG that has sample ID of (S5) and an aspect ratio of 0.68.

Figure 4.8 shows system temperature when the TEG attached. The inset is the temperature profile of the water during the initial period. A linear relationship between ΔT and Δt is evident. The thermal power absorbed by the hot water of the system can be calculated using the slope technique at the initial period of the first eight minutes. The slope($\frac{\Delta T}{\Delta t}$) of the TEG with sample ID of S5 and aspect ratio of 0.68 can be determined from the inset of Figure 4.8.

Together with the mass of the water in the system (0.45 kg) and the specific heat capacity of the water (4184 $Jkg^{-1}K^{-1}$), the thermal power was calculated by:

$$Q_w 0.68 = (0.450\text{kg}) \left(4184 \frac{\text{J}}{\text{kg.K}}\right) (0.0097\text{K/sec}) = 18.2 \text{ Watt} \qquad (4.3)$$

It can be seen that the thermal power transferred into the water is reduced in the case when a TEG is employed compared with the case of using copper plate. This is due to the thermal conductance of the TEG which is smaller than that of the copper plate. It is anticipated that the thermal power transferred into the hot water of the system will be depended on the aspect ratio of the TEGs employed. Using the same slope technique and the experimental data shown in Appendix A6 on page 166, the thermal power transferred into the hot water using the other 4 TEGs of different aspect ratios were calculated and listed in Table 4.3. The results appear to show that the value of thermal power transferred into water through all samples at the transient state are almost similar, while the results obtained at the steady state shows different results between the samples and compare to the transient state results. This is due to existence of heat convection between the solar absorber and hot water. This will be discussed in details in Chapter 6. The thermal efficiency of the solar hot water system which obtained at the transient state of system without TEG (with copper plate) was estimated to be 82% (based on an input heat value of 30W). While the thermal efficiency at the transient state of the system with the five TEG samples and aspect ratio were in the range of 48- 60%. In general, the thermal efficiency at the transient state has small increase with increasing the aspect ratio of the TEGs. In addition to the thermal power, the system also produces electrical power as discussed in Section 4.4

4.6 DETERMINE THE OPTIMAL TEG GEOMETRY FOR OBTAINING MAXIMUM HEAT AND ELECTRICAL POWER OUTPUTS

The results obtained in section 4.5 demonstrated that thermal efficiency of producing hot water is affected by incorporation of a TEG in the solar hot water system. This section aims to investigate the optimum size ratio between the TEG and solar absorber. In this investigation, the size of the solar absorber remained unchanged (0.13m x 0.13m x 0.001 m), while the size of the TEG varied by using 5 different TEGs samples listed in Table 4.2. The suitable TEG geometry for obtaining the best thermal performance, the best electrical performance, and the best combined performance were investigated, respectively.

4.6.1 DETERMINATION OF THERMAL POWER TRANSFERRED INTO HOT WATER

As described in Section 3.6, the thermal energy transferred into the hot water during the steady state can be estimated from the temperature difference across the TEG. The temperature of the system with the TEG that has an aspect ratio of 0.680 is shown in Figure 4.8 above. The temperature profiles (T_h and T_w) of the system, which were integrated with the other 4 TEGs samples, were also determined and are displayed in Figure 4.9 below for the TEGs with the aspect ratios of 0.136, 0.169, 0.299 and 0.536, respectively.

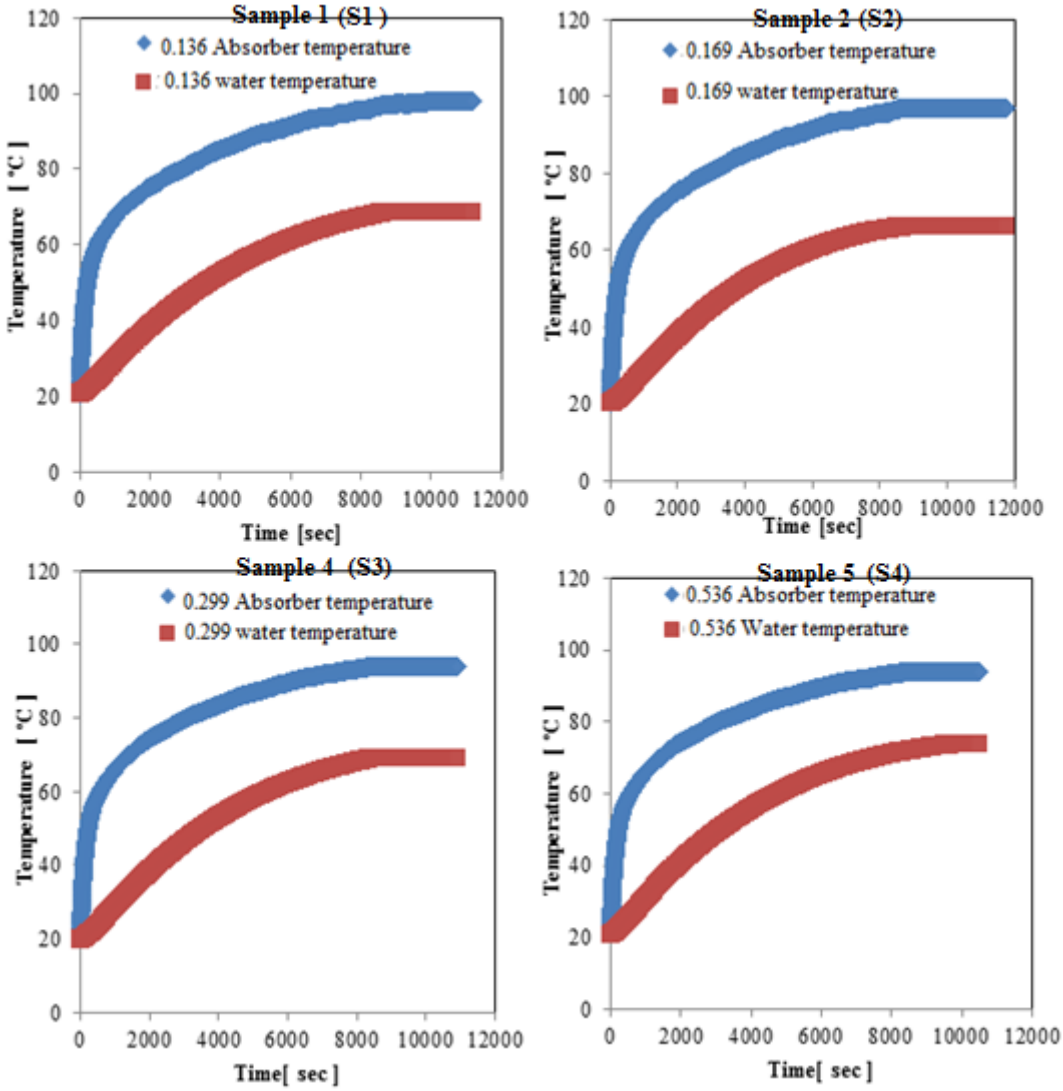

Figure 4.9 The absorber and water temperature of the other 4 system with the other ID samples, plotted as a function of time.

It's evident from Figure 4.9 that the temperature difference ($T_h - T_w$) increase by decrease the aspect ratio, and using the ΔT to calculate the thermal powers transferred into the hot water during the steady state period using equation 3.19, where the thermal conductivity of the TEG materials (which use Bi2Te3 based alloys) is assumed to be 1.5 $W.m^{-1}.K^{-1}$. Mean time the thermal power was also determined at the transient state (using the slop technique), and both results are illustrated in Table 4.3.

Table 4.3 The heat power delivered by the solar TEG modules, using two alternative methods in the same time period.

Sample I.D	**Module size [2N.A.L^{-1}] in meter**	**Thermal power at the steady state condition [Q_{TEG}] in Watt**	**Thermal power at the transient state [Q_W] in Watt**
S 1	0.136	4.00	13.90
S 2	0.169	6.00	14.60
S 3	0.299	9.50	15.68
S 4	0.536	15.00	17.50
S 5	0.680	14.00	18.38

It can be seen clearly that the thermal power of a solar thermoelectric system increases with increasing the aspect ratio of the TEGs during the steady state period. This indicates that a TEG with a larger aspect ratio is better for transferring the heat into the water. It appears that the results obtained from the initial transient state using the slope technique are different from those obtained from the final steady-state period (using Fourier's law). The deviation is mainly due to the results obtained using Fourier's law neglected the heat transfer due to the heat convection between the solar absorber and the hot water (see detailed discussion in Chapter 6).

4.6.2 DETERMINATION OF ELECTRICAL POWER OUTPUT

The effect of the TEG's geometry on the electrical power output was investigated. The electrical power outputs from the TEGs in the steady state were calculated using equation 2.3, which requires knowledge of the open-circuit voltage and internal resistance of the TEGs. The internal resistances of the TEGs were determined from the matched load experiment and the results are listed in Table 4.2. The open circuit voltage (V_o) and the temperature difference across the TEGs were monitored once the light source was switched. The calculated electrical power outputs and temperature differences across the TEG, as a function of time for the system with 5 different TEGs, are shown in Figure 4.10. The electrical power and temperature difference reached a peak at about 30 minutes (after the light source was switched on) for all cases of different TEGs. Following this, both variables began decreasing until they reached the steady state, which was between 2.5-3 hours from the start. The system with larger size TEG reached the steady state faster than smaller ones. The electrical power output can also be determined by measuring the closed circuit voltage with the matched load resistance connected to the circuit. In general, the measurements under a closed circuit condition are more accurate than are those of an open circuit. Nevertheless, in this study, the measurements under an open circuit condition were employed due to the rapidness and simplicity of measurements.

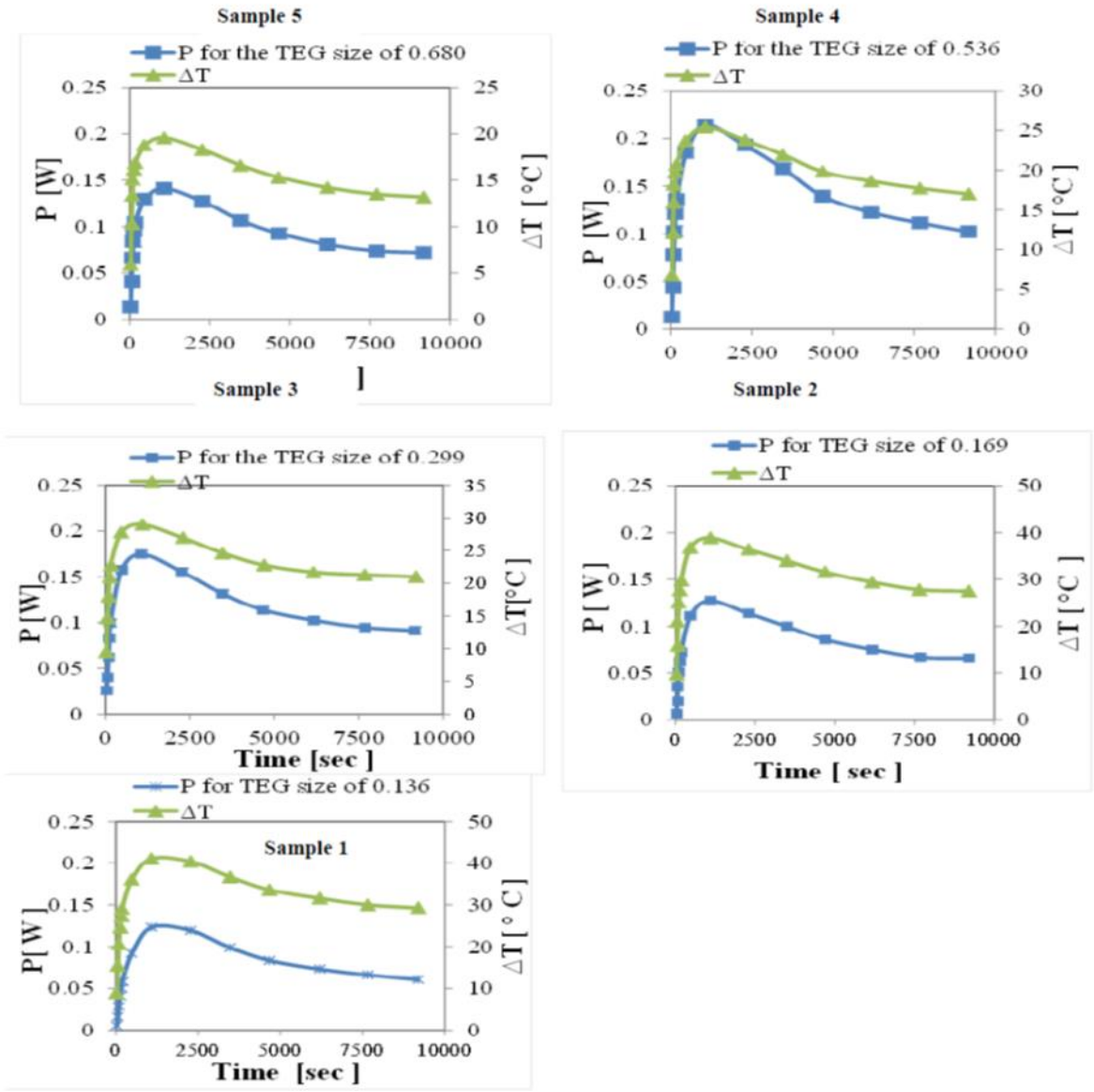

Figure 4.10 The electrical power and temperature difference of all system sizes, as functions of time.

Given the geometry of the TEG and the properties of materials employed, the electrical power output can also be calculated using equation 3.20. Figure 4.11 displays the electrical power outputs as a function of temperature difference for all TEG samples. The points represent the experimental results while the solid lines represent the theoretical calculation results. All results show a reasonably good agreement between experiment and theory. In order to obtain realistic calculation, the geometry of thermoelements in a TEG needs to be

determined. The cross-sectional area (A) and length (L) of the thermoelements in a TEG were measured using a microscope (see Appendix A7 on page 168 for details). The measured A and L were also compared with the data provided by the manufacturer's datasheets whenever it is possible (Appendix A4 on page 163). Since it is difficult to determine experimentally the material properties from a TEG device, the typical literature values of thermoelectric properties and contact properties were used, which were given in Section 3.8.

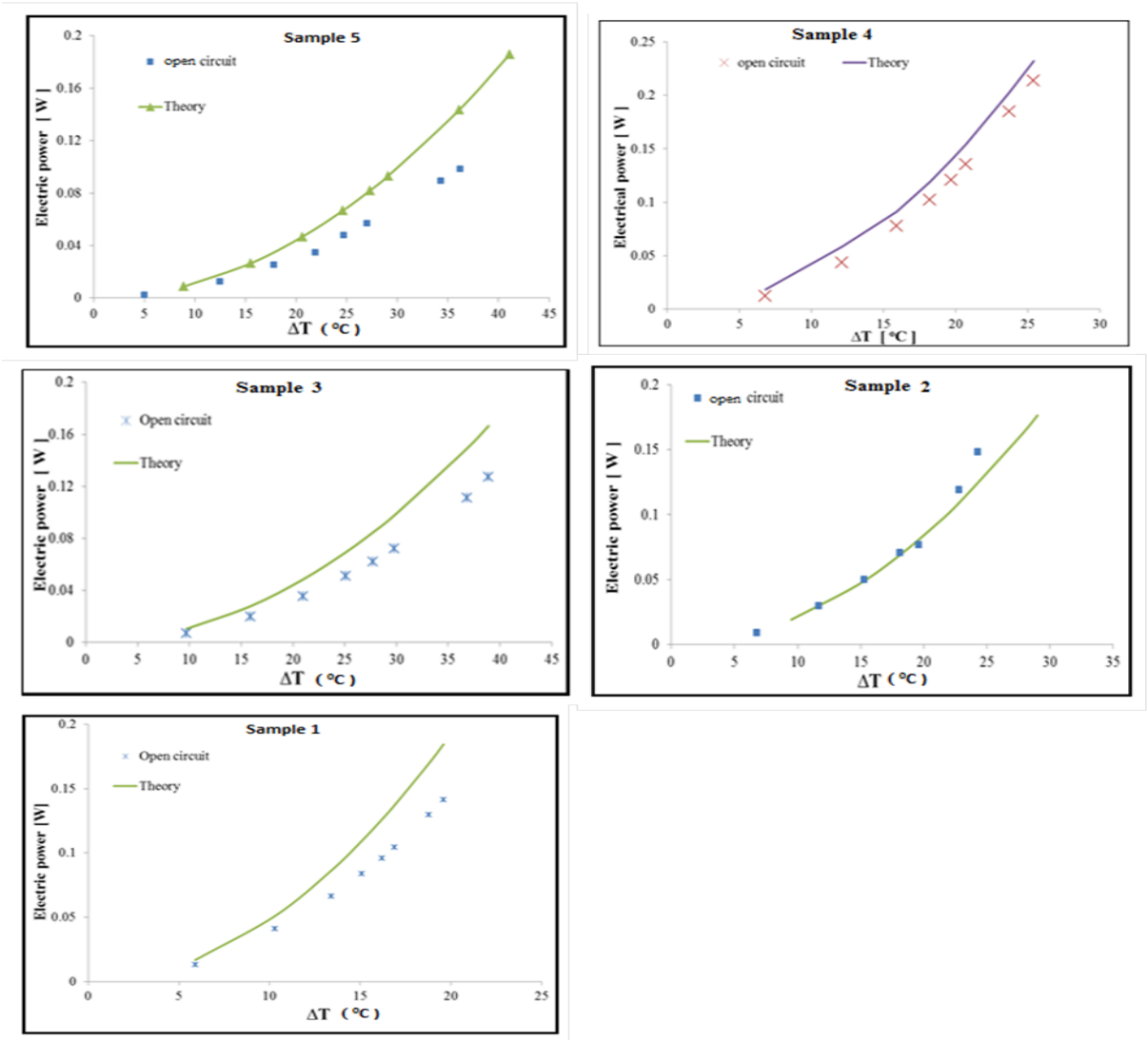

Figure 4.11 The electrical power output of the All TEG samples and aspect ratio as a function of temperature difference ΔT.

Even with using the literature values, the results show that the experimental data is broadly in line with the theoretical calculation, with a difference of less than 20%. At small ΔT values, the difference is small, and increasing the ΔT increases the difference. It can also be seen that both the measured and calculated results show parabolic curves, which is expected from the TEG theory. The experiments were repeated to demonstrate the reproducibility of the electrical power measurements. Figure 4.12 shows the results of two tests using all TEG samples and aspect ratio The maximum deviation is less than 12%.

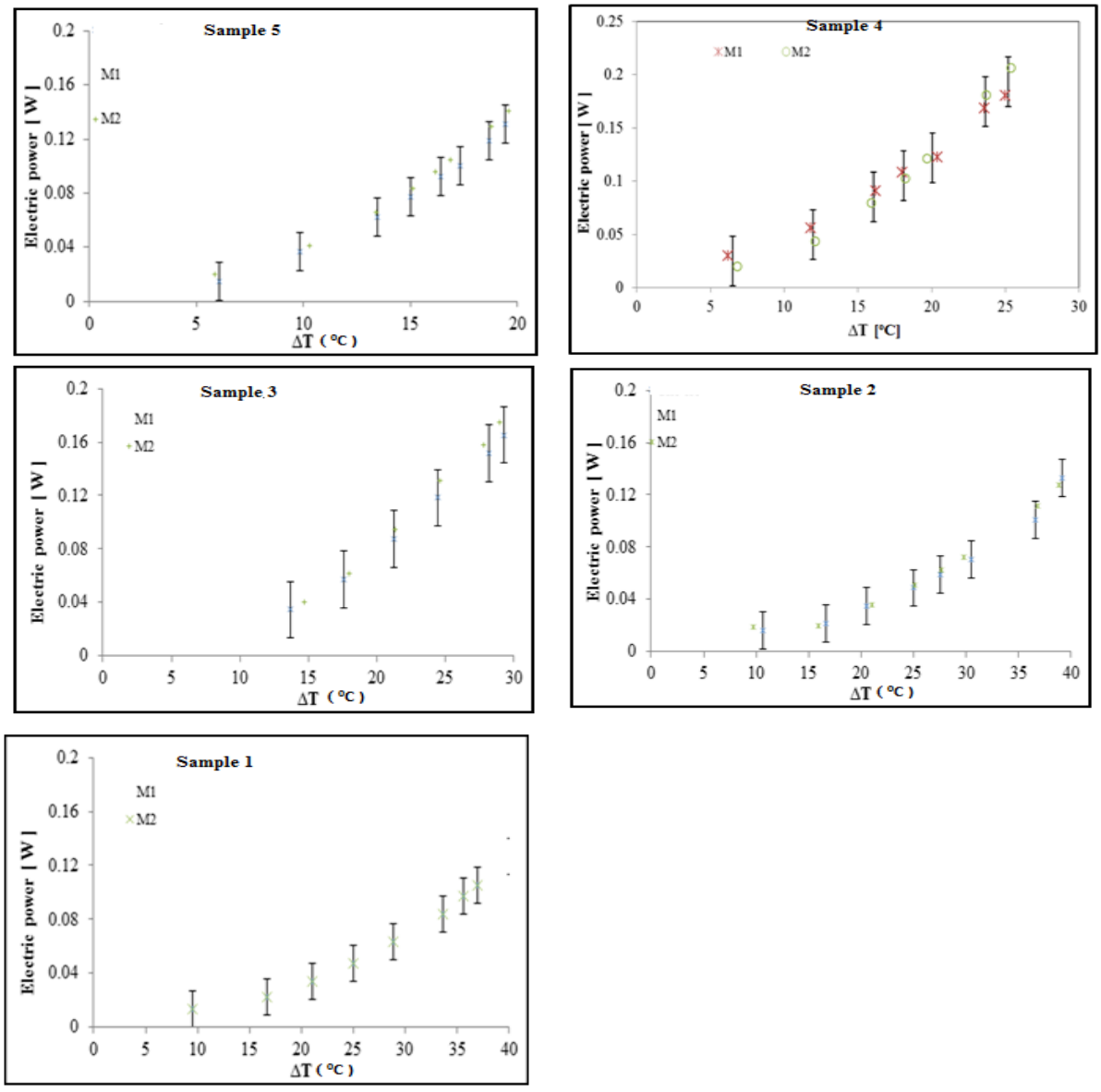

Figure 4.12 Two measurements (M1 and M2) of the electrical power output as function of ΔT to demonstrate the reproducibility of electrical power measurements.

4.6.3 *DETERMINING THE OPTIMUM TEG GEOMETRY FOR HEAT AND POWER PRODUCTION*

As the thermal and electrical powers of all sizes were obtained, the effect of TEG geometries on thermal and electrical power production can be evaluated experimentally. Furthermore, these experimental results can be used to obtain realistic parameters required by the theoretical model and to validate it. As previously stated, the theoretical model developed in Section 3.8 requires two initial parameters: the power of light irradiation and the cold side temperature (T_c) of the TEG. The value of the light irradiation power was determined using the slope technique, which gives 30 W (equivalent to 1700 $W.m^{-2}$). The value of the cold side temperature T_c at steady state was chosen from the average of experimental data shown in Table 4.4. It can be seen from the table that the cold side temperature for the given system remains approximately around 71 ^{o}C, which the temperature difference across the TEG changed more significantly. The average value of T_c was used in calculation technique developed in equation 3.19.

Table 4.4 The measured TEG T_c and ΔT.

Sample ID	system size	T_c [˚C]	?T [˚C]	The averge T_c
S1	0.136	69	29	
S2	0.169	68	27	
S3	0.299	70	21	71˚C
S4	0.536	74	17	
S5	0.680	75	13	

The main aim of the developed theory model is to predict the corresponding ΔT across the TEGs for different TEG sizes using equation 3.19. ΔT is an important parameter on which the heat and electrical power can be calculated. The ability to calculate ΔT will lead to the capability of calculating the heat and electrical power of the system. Figure 4.13 shows comparison of the measured and calculated ΔT as a function of TEG size (aspect ratio). The cold side temperatures (Tc) of the experimental results are shown in Table 4.4, while it is assumed to be 71 ^{o}C in theoretical calculation which based on equation 3.20, the values of remaining constant employed, such as convection coefficient, the Boltzmann constant, emissivity, were obtained from the literature as shown on chapter 3. It can be seen that the theoretical calculation is in a reasonably good agreement with experimental results. The largest deviation between theory and experiments is approximately 16%, which occurs in the smallest TEG size (sample S1 with aspect ratio of 0.136). ΔT increases with decreasing in the aspect ratio, which is expected from the Fourier's law.

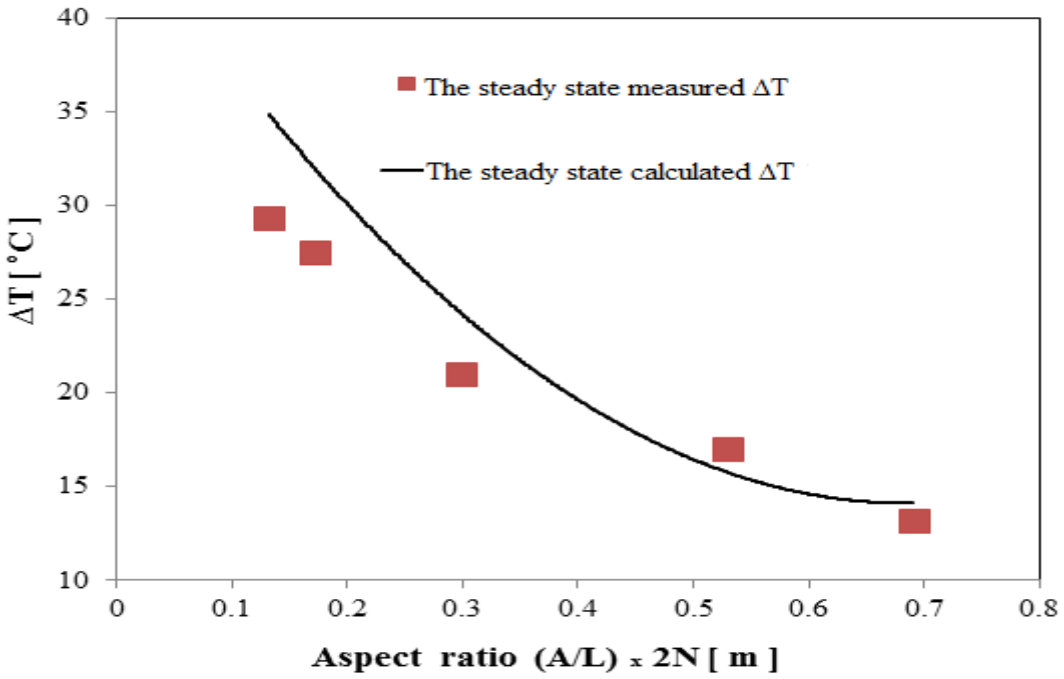

Figure 4.13 The temperature difference across a TEG (ΔT) as a function of TEG size (aspect ratio). The squares represent experimental results and the line represents the calculation technique .

Figure 4.14 shows the data of the data of electric power obtained at the steady state by theoretical calculation (dashed line) and experimentally measured (square points), the theory results is broadly in line with the experimental results, which predicted a similar optimum value. Although the theoretical values for smaller aspect ratios are higher than the experimental values (20 % as the largest deviation), it shows a clearly decrease from the optimum value. It can be seen from that Figure 4.13 that the errors may be further reduced by selecting more appropriate heat convection and radiation parameters. Based on ΔT shown in Figure 4.13, the heat and electrical power outputs of the system at steady state can be calculated using equations 3.19 and 3.20, respectively. The results are shown in Figures 4.14 and 4.15 for electrical and heat power output, respectively. The results show clearly an optimum TEG geometry for electrical power output from the system. For the system investigated, the maximum electrical power was obtained in a TEG with sample S1 and aspect ratio of 0.536. Increasing or decreasing the aspect ratio against this optimum value will lead to a reduction in the electrical power output. This can be explained by the fact that the change of TEG aspect ratio results in opposite change in ΔT. As indicated by equation 3.20, obtaining a large electrical power output requires both large ΔT and large aspect ratio. Consequently a trade-off is achieved at an optimum value.

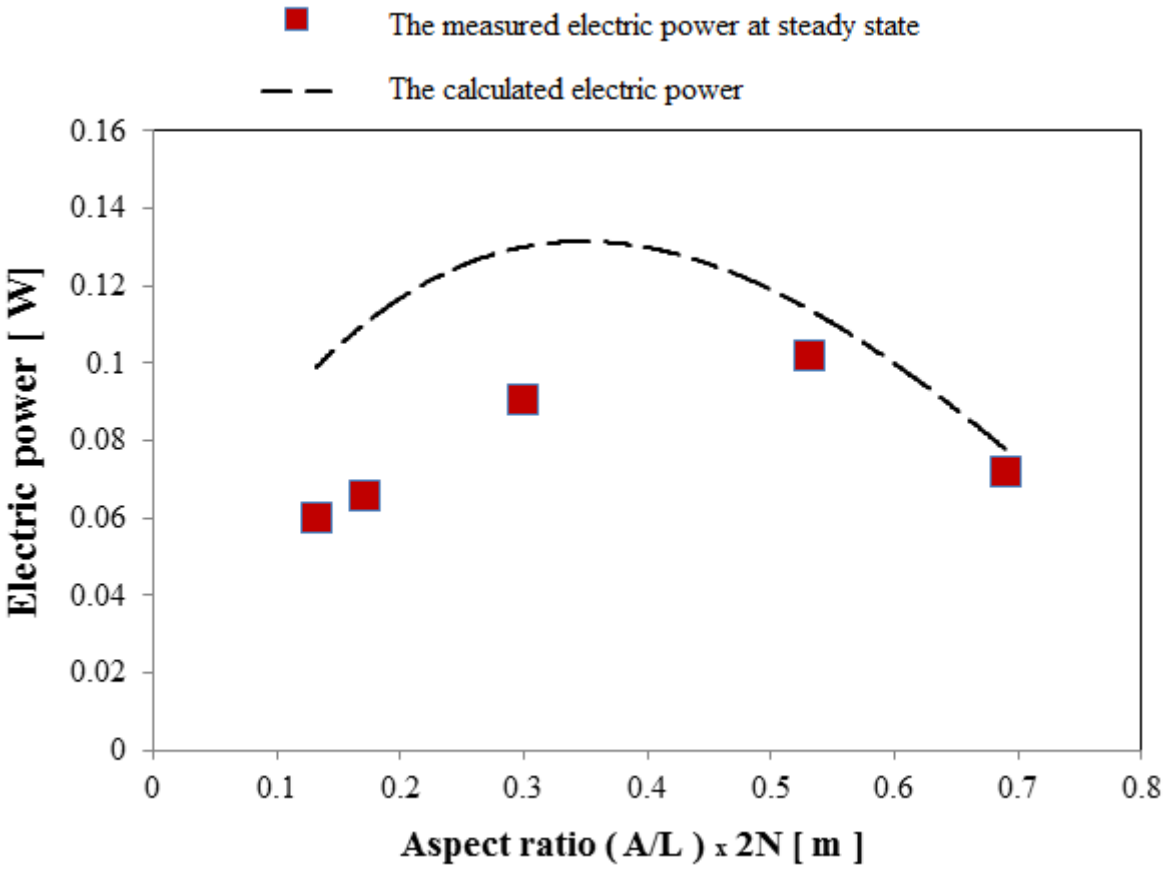

Figure 4.14 The experimental and the calculated electrical power output as a function of the TEG size.

Figure 4.15 compares the experimental thermal power output to the theoretical calculation, plotted as a function of the TEG aspect ratio. The results show the deviation between the theory and experiments is less than 10%. The thermal power output (hot water) of the system increases with increasing the aspect ratio as expected from equation 3.20. However, it can be seen that the difference between the largest TEG, with sample ID S5 and aspect ratio of 0.68 and the optimum one which has sample ID of S4 and aspect ratio of 0.536 is very small. Consequently, the TEG with the TEG with sample ID of S4 and aspect ratio of 0.536 also produces the largest total power (electrical + thermal) output as shown in Table 4.5.

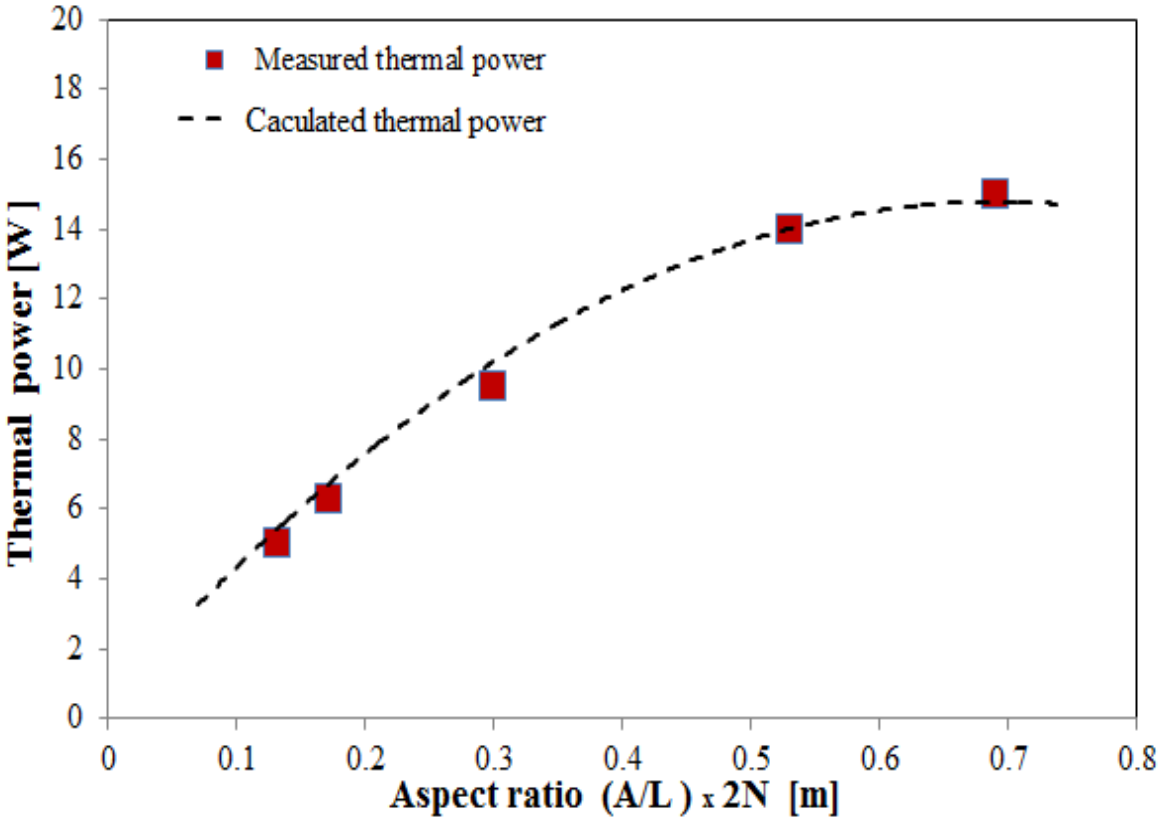

Figure 4.15 The measured and calculated heat power, as a function of TEG geometrical size.

Figures 4.14 and 4.15 confirm there was an optimal TEG size, where the maximum heat and electrical power are achieved. Based on experimental and theoretical results of the investigated system, the TEG with Sample ID of S4 and aspect ratio of 0.536 is the best TEG geometry for obtaining maximum combined thermal and electrical power output. A good agreement between the experimental results and theoretical calculation also provide validation for the developed thermoelectric model, which will be employed for investigation of thermal and electrical power output under different atmospheres in Chapter 6.

Table 4.5 Comparison between measured and estimated electrical power in addition to the thermal power and total heat and power from the system at the steady state condition for each TEG size.

Sample ID	Module ratio [A*2N/L]	Estimated electric power [W]	Measured electric power [W]	Thermal power [W]	The system total H & P efficiency %
S1	0.136	0.085	0.064	4.00	13.5
S2	0.169	0.09	0.07	6.00	20.2
S3	0.299	0.104	0.091	10.00	33.6
S4	0.536	0.108	0.102	15.00	50.36
S5	0.680	0.08	0.072	15.00	50.24

Table 4.5 shows the results obtained by all samples at the steady state condition. The thermal power of Samples S1, S2, S3 could be less estimated, further discussion about the accuracy of the steady and transient state results will be detailed in Chapter 6.

4.7 CONCLUSION

This chapter presented an experimental investigation and analysis of the performances of a solar thermoelectric system in relation to the TEG geometry. The results obtained in this

chapter show that the system performance, in terms of electrical and heat power, is clearly dependent on the TEG aspect ratio (length, cross-sectional area and number of thermocouples). For the system investigated in this chapter, the results show that an optimal TEG aspect ratio is 0.536 (sample S4), in which the best system performance is achieved at a lesser cost than that of using the largest TEG. The experimental results obtained from this investigation also establish the validity of the theoretical model described in Chapter 3. Given the input light irradiation and the required hot water temperature (i.e., Tc for TEG), the theoretical model is capable of determine the temperature difference (ΔT) across TEG for different aspect ratios and consequently is able to predict the thermal and electrical power outputs of a solar thermoelectric system for a given geometry. This is a very useful outcome because the experimental investigation is limited to available TEGs, while this theoretical model can be employed to investigate any TEG size and operating conditions, such as in vacuum (see chapter 6).

CHAPTER 5: DESIGN AND CONSTRUCTION OF AN IMPROVED SOLAR THERMOELECTRIC SYSTEM WITH VACUUM ENCLOSURE

5.1 INTRODUCTION

This chapter is focusing on designing and constructing experimental setup. This enables the experiments to be carried out in a controllable atmospheric condition. The structure of this new experiment setup is similar to the previous one described in Chapter 3 (Figure 3.1), but with two main differences explained as follows:

1. A vacuum chamber was built to allow the system to work in an enclosed space. This was made to investigate the effect of the heat lost from the system to the surroundings (mainly convection), and the subsequent the performance of the system.
2. Xenon light is employed instead of the previous halogen as a light source, as Xenon can be used as an excellent model for sunlight (Quill et al, 2007). The light intensity was higher than that of a typical bulb (1000wm^{-2}), and this was changed to investigate the effect of concentrated light on the system's performance.

As demonstrated in Chapter 4, the optimum TEG size for obtaining the maximum electrical power output is substantially smaller than the size of the solar absorber in order to obtain larger temperature difference across the TEG. This will inevitably increase the heat loss from the solar absorber to the surroundings through heat convection. The rationale to develop this improved experimental setup is to provide the ability to investigate the influence

of heat convection on the TEG geometry optimisation and resultant thermal and electrical power outputs from a solar thermoelectric system. Figure 5.1 shows a comparison of the electrical power outputs of a solar thermoelectric system in ordinary ambient atmosphere with that in vacuum. The results were calculated using the theoretical model described in section 3.8 and the TEGs investigated in Chapter 4, with taking into consideration of heat convective losses with or without vacuum. It can be seen that the electrical power output can be increased by up to 50% if the convective heat losses is completely eliminated by using vacuum.

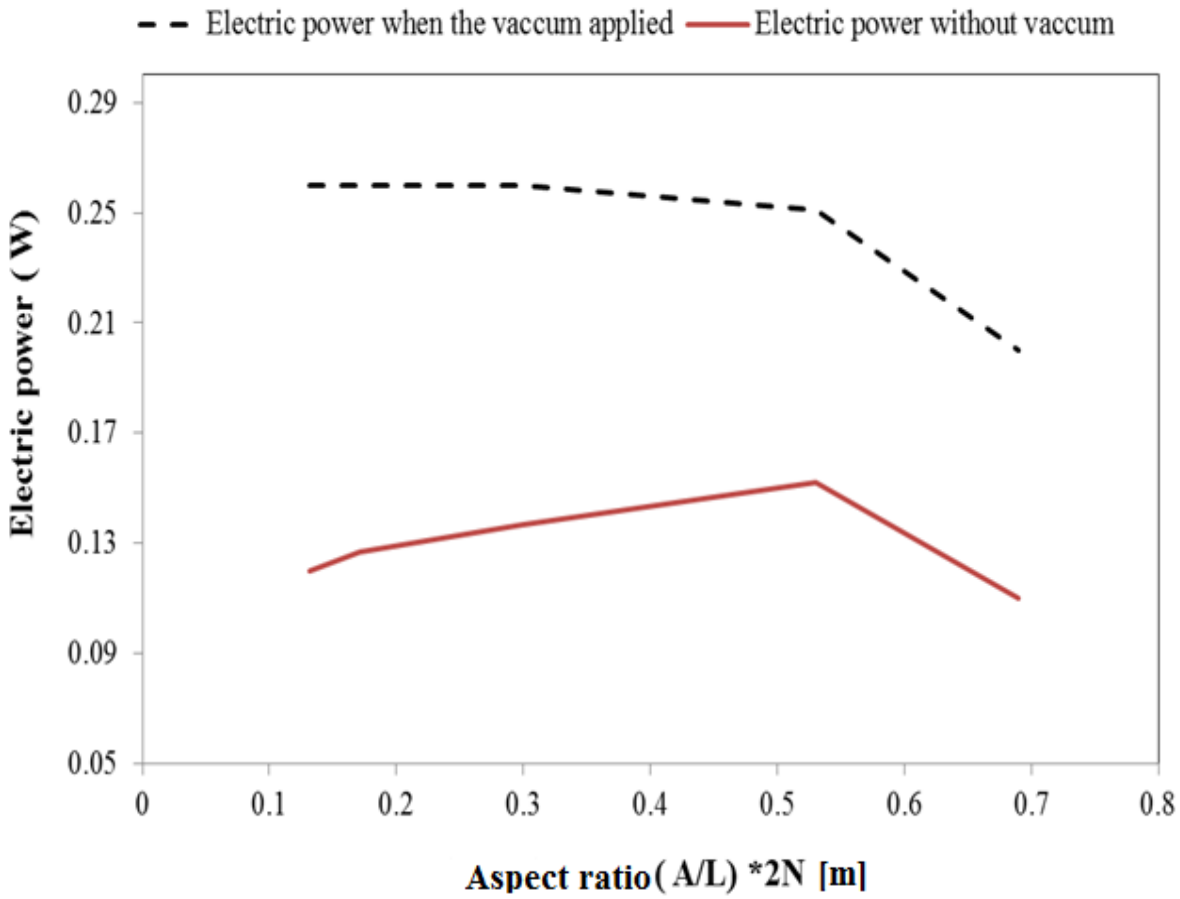

Figure 5.1 The calculated electrical power outputs of the solar thermoelectric system operated in ordinary ambient atmosphere and in vacuum.

5.2 EXPERIMENTAL SETUP

Figure 5.1 predicated a promising increase of the power output with the use of vacuum. As a consequence, the new solar thermoelectric system was designed following a similar setup of the previous solar thermoelectric system, but included a vacuum chamber. This setup consists of three major parts - a vacuum cavity, a heat sink and a water container. Figure 5.2 shows the photograph of the constructed system. The details of this experimental setup are explained below. A schematic diagram of the experimental setup is shown in Figure 5.3. The solar absorber and the TEG are placed in an aluminium vacuum chamber, which is sealed from the top by a special glass and from the bottom by a heat sink. The TEG is sandwiched between the solar absorber and the heat sink. In order to facilitate the measurement of temperatures, the backside of the solar absorber and the topside of the heat sink were grooved with channels, in which two thermocouples were inserted for temperature measurements of the cold and hot side of the TEG, respectively. To ensure good thermal contact, the solar absorber were pressed against the TEG and in turn against the heat sink by four plastic screws with the gaps filled with the heat sink compound (thermal paste). As shown in Figure 5.4, the assembly, consisting of the solar absorber, the TEG and the heat sink, was inserted into the opening at the bottom of the aluminium vacuum chamber and was sealed with an O-ring that was placed on the edge of the heat sink and that was secured with four screws. As a result, the top parts of the assembly (including the solar absorber, the TEG and the heat sink) were kept in the vacuum enclosure, while the lower parts of the assembly (i.e., the heat sink fins) were outside the vacuum chamber, and were submerged in a thermally insulated water container.

As mentioned above, the top seal of the vacuum chamber is a piece of special glass measuring 170 mm x 170 mm x 5 mm. The glass seal allows light irradiation to enter the vacuum chamber and to shine onto the solar absorber. The light energy absorbed by the solar absorber is converted into thermal energy. It passes through the TEG and the heat sink into the water. The control of the vacuum level in the chamber leads to control of the heat losses. This is the main advantage of this new experimental setup compared with the one employed in Chapter 4. To ensure safety during experiments, the whole setup was placed inside a metal box with a transparent door (Figure 5.2). The safety box is needed because the top seal of the vacuum chamber is a square piece of glass that facilitates the light entering into the vacuum chamber. The safety box had an opening on the top - 17 cm x 14 cm - where the light source was mounted. In addition, another two small holes, with diameters of 5cm, were made in the each side of the box for pumping tube and electrical wires to connected to the vacuum chamber. During testing of the setup, implosion of the glass occurred a few time, which proved the necessity of the safety box.

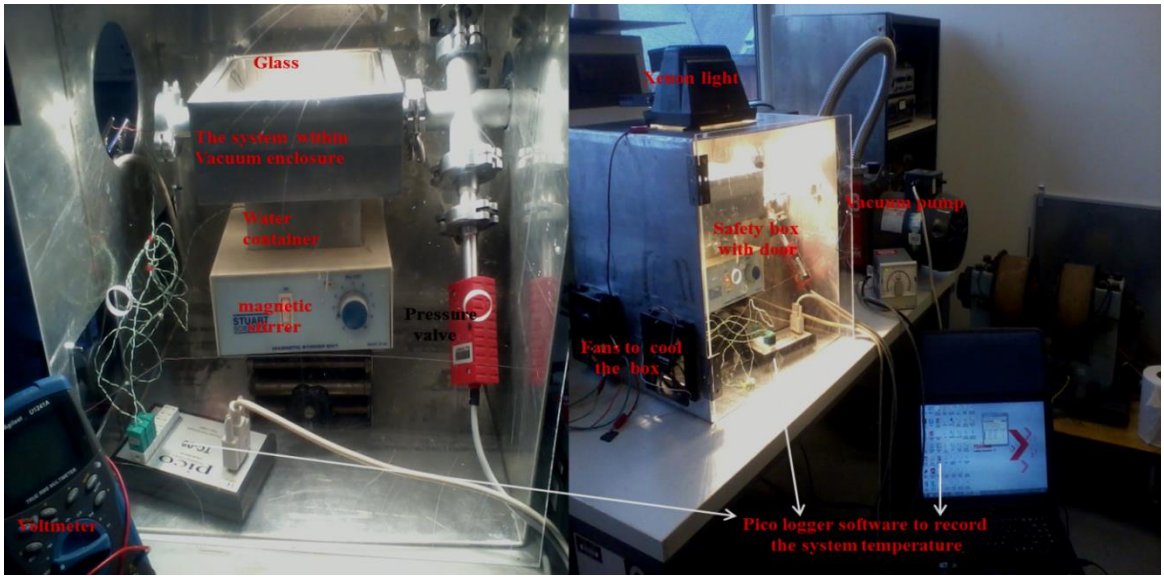

Figure 5.2 Photograph of the complete experimental setup in a safety metal box. The solar absorber and the TEG are sealed in an aluminium vacuum chamber from top by a special glass and from button by metal heat sink block.

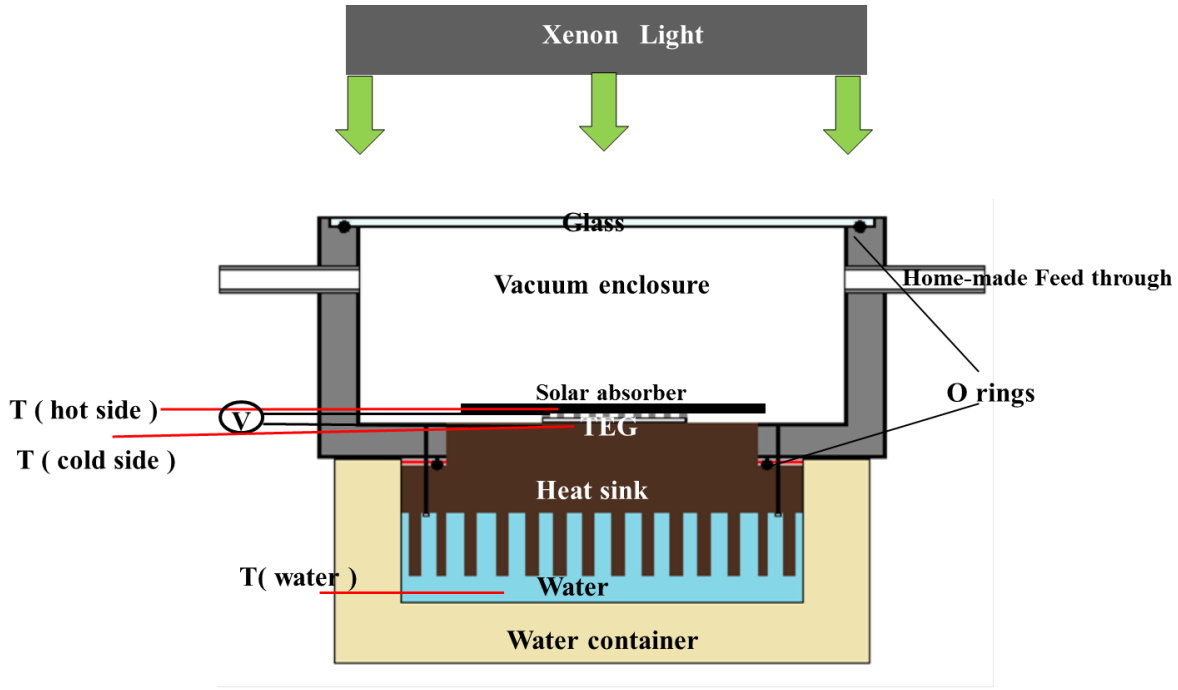

Figure 5.3 The experimental set-up in further detail.

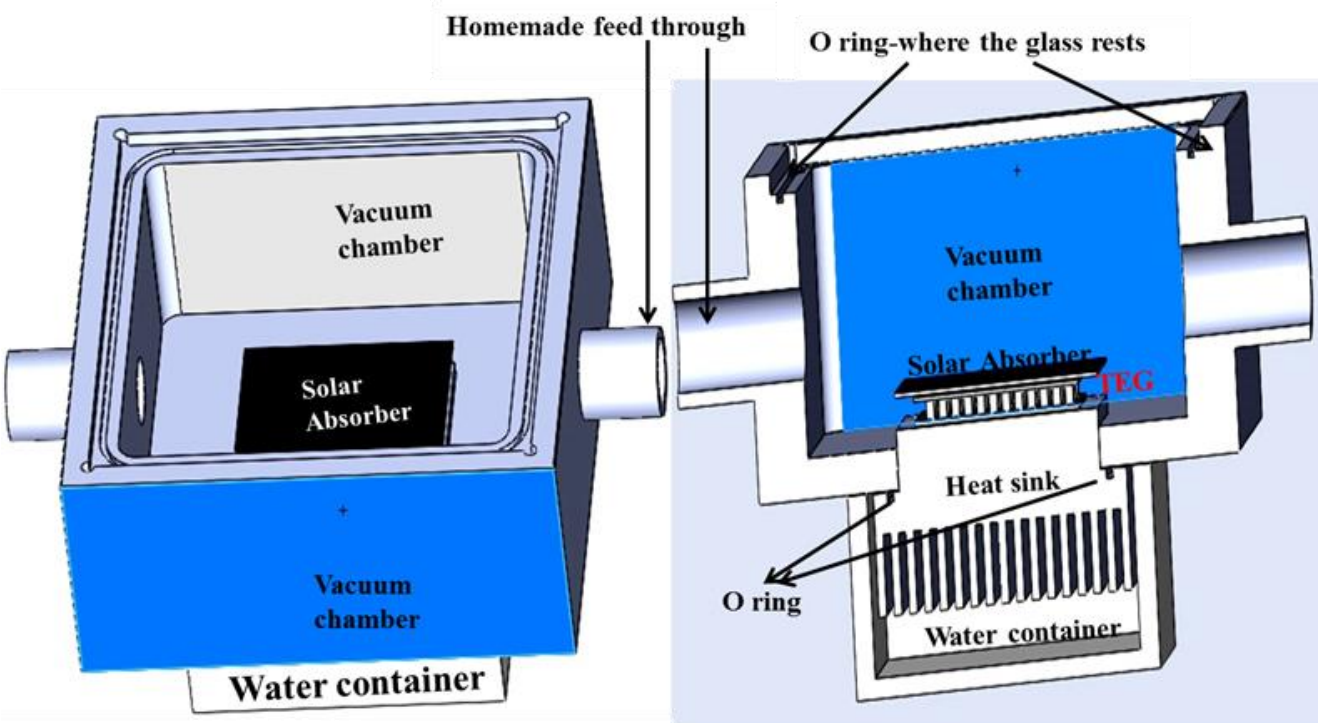

Figure 5.4 The cross section of the experimental kit.

5.2.1 *THE LIGHT SOURCE*

As the experiment was conducted indoors, a suitable light source needs to be selected. An important criterion in identifying a suitable light source is to examine its spectrum and ensure it has a similar spectrum to the sun. In previous experiments a halogen bulb was used as the heat source due to the cost and availability. However, the halogen bulb produces lots of energy in the infrared region. This can lead to the findings obtained from those experiments deviating from those when operating under real sunlight. Xenon light is the most common source used as a solar simulator (Figure 5.5). From the figure where the left Y axis representing Xenon, halogen and mercury radiation, while the right Y axis representing the sun irradiation, the Xenon spectrum is relatively close to the sun's spectrum (Pandolfini et al. 2013). Therefore, a 118mm tube Xenon light bulb, with the ability to consume 400 Watts of power, was therefore purchased.

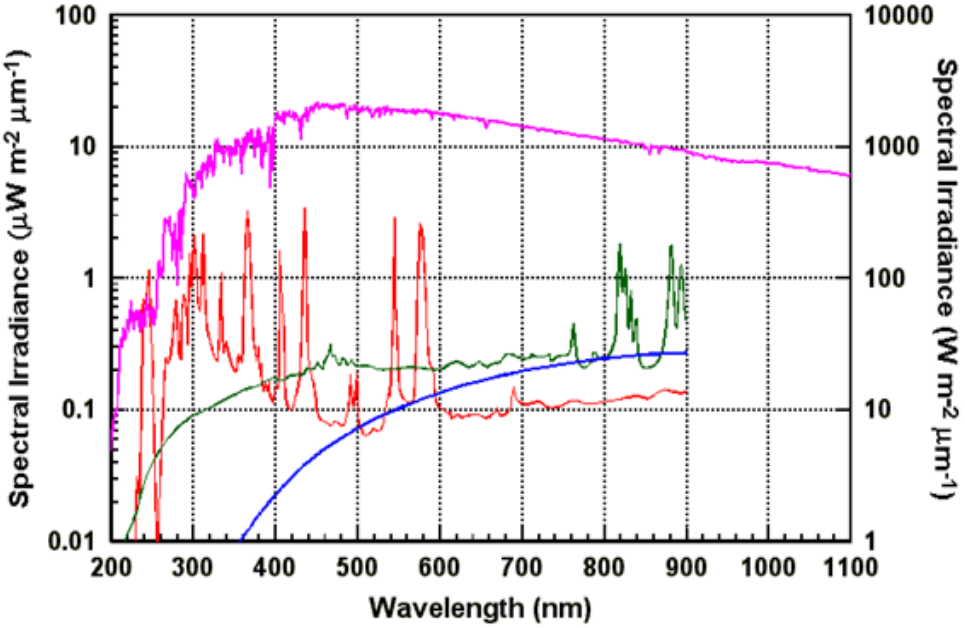

Figure 5.5 The Spectral irradiance of xenon (green), halogen (blue) and mercury (red) light bulbs (left axis) compared to spectral irradiance from the sun (purple, corresponding to the right axis). (D Alan, 2007).

5.2.2 THE GLASS

It was important to find the appropriate type of glass to fulfil the experimental design and requirements. Initially, the priority was high spectrum transmittance, as Quartz glass-fused silica was found to be the best glass type after research – it had a high light transmission. The other crucial requirement was that if its able to resist the mechanical load resulting from pressure difference, and work at a high temperature. In terms of temperature, level Quartz glass-fused silica can resist temperatures of up to 1000^{o} C (K Buchwald – 2007). To avoid the danger of broken glass under a vacuum, safety precautions were considered - a safety metal box with a transparent door to accommodate the system within its enclosure was made. A slot at the top of the safety box was created as the same size to the light box (170mm x 150mm). In addition, initial calculations to find out the mechanical load applied to the glass and its load resistance were carried out. The calculations were as follows:

Glass bending moment

A unit width of the glass was taken and analysed to check the glass' capability to resist the applied vacuum. The maximum applied bending moment was calculated from a supported glass strip as, $\frac{WL^2}{8}$ where, W is the uniform distributed load applied to the glass, and L is the effective glass span, as shown below:

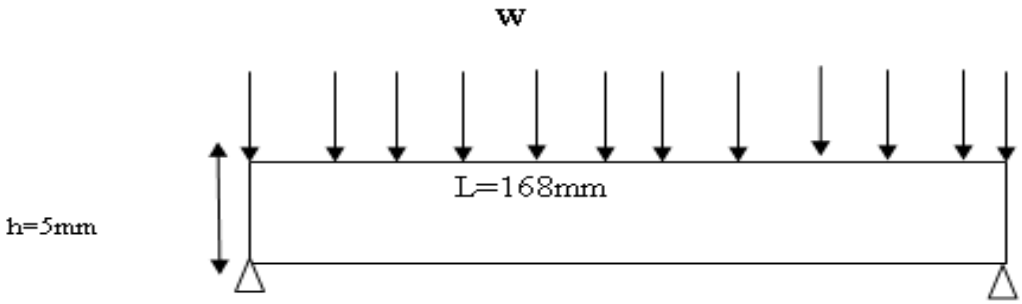

When operating under a vacuum condition, the pressure difference between the inside and outside vacuum chamber is,

P = outside pressure – inside pressure

P = 1- $8x10^{-2}$ = 0.92 bar = 0.092 N/ mm^2

Then,

W=P*1 (as a unit width has been taken) .

As a result, the maximum bending moment can be obtained as,

$$M_{max}=\frac{WL^2}{8}=\frac{0.092*(168)^2}{8}=\ (324\ N.mm)$$

Based on the diagram shown below, the glass internal resistive moment was calculated as follows:

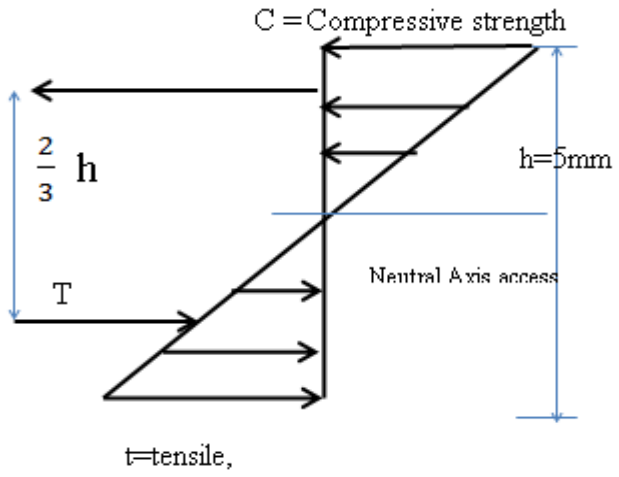

$$M_r = \frac{th^3}{6},$$

Where, t is the maximum tensile stress (t= 40 N/mm^2) (www.saint-gobain.com), and h is the flexural working stress theory, the h value was obtained from literature as (5) (R.J.D.Tiley, 2004), then the internal resistive moment was calculated as:

$$M_r = 833 \text{ N.mm}$$

The Factor of Safety (FOS) of the glass against flexural bending can be calculated using

$$FOS = M_r / M_a$$

Consequently, we obtain,

$$FOS = 833/324 = 2.57$$

The initial calculation showed that the chosen glass can resist the maximum bending force that is produced due to pressure difference under vacuum. Therefore, the risk of breaking the glass was low. However, the glass did not survive the combination effect of the vacuum and the heat stresses produced by the light source. When the system was examined under each

condition alone, the glass survived, but the glass cracked when operating under the vacuum and light stress together. This was due to the thermal expansion of the glass, which made the pressure stress enhanced. The quartz fused silica had a thermal expansion of $0.55\times10-^{6}/^{o}K$ (Mats Blomqvist et. al. 2011). Clearly, the glass with lower thermal expansion coefficient was the only choice as a replacement. The most suitable choice was Schott glass, which is a type of Robax ceramic glass (mainly used in electric stoves). Since its thermal expansion is almost zero $(0 \pm 0.05)\ x10^{-6}/^{o}K$ (www.schott.com), it can work in an extreme temperature condition. In addition, Schott Robax glass is a highly transparent glass (Figure 5.6 and 5.7). Consequently, Schott Robax glass with dimensions of 168mm x 168mm and a thickness of 5mm was chosen for the experiment.

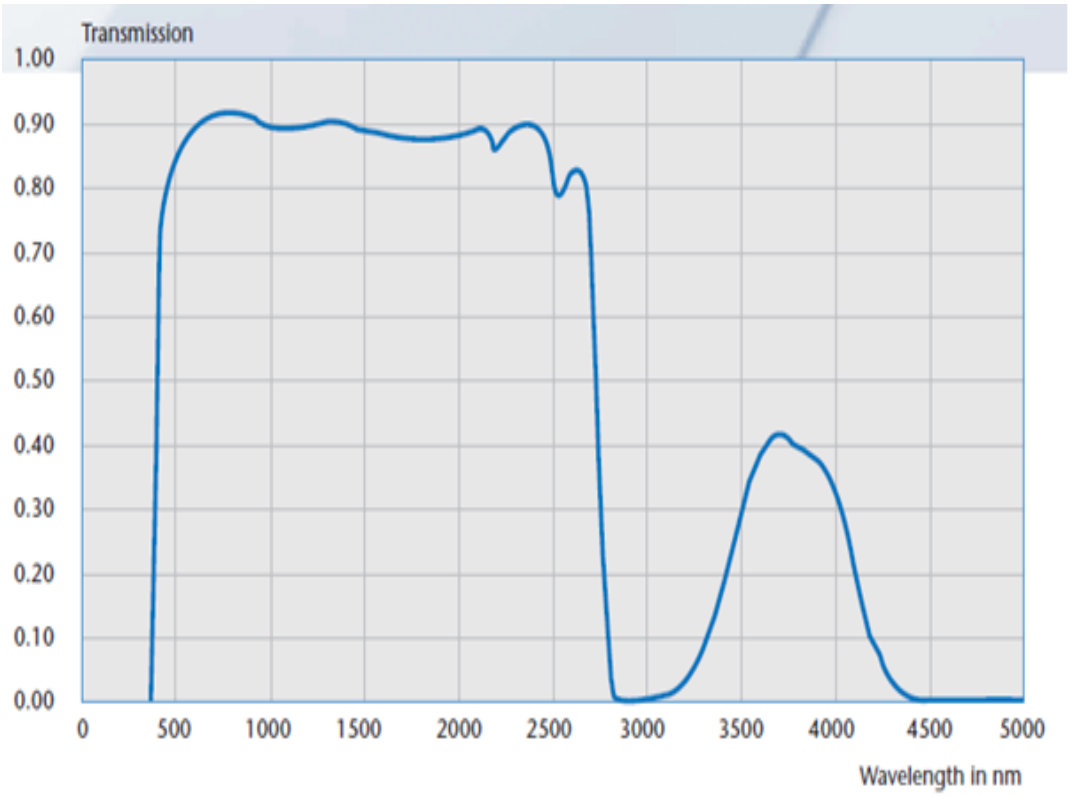

Figure 5.6 Light transmission of Robax glass with a thickness of 5mm(www.schott.com).

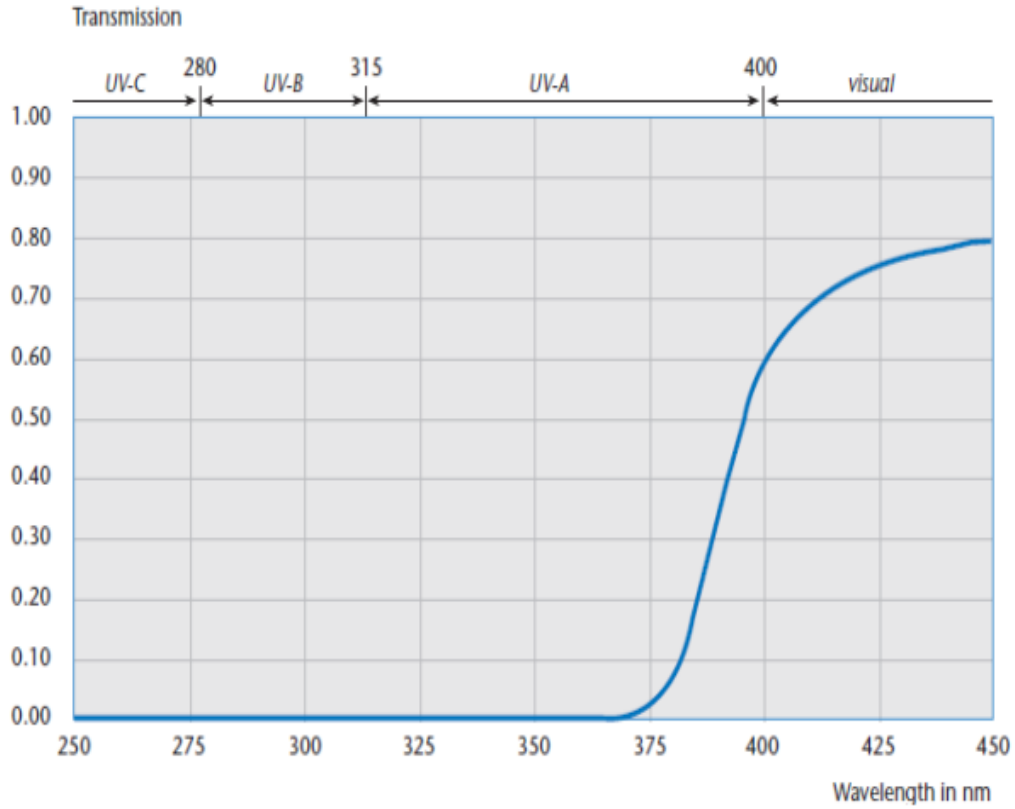

Figure 5.7 UV transmission of Robax glass (www.schott.com).

5.2.3 THE VACUUM CHAMBER

A vacuum chamber was designed and constructed from an aluminium block because the chamber has to be ridged enough to resist the stress applied by vacuum and heat, and yet easy to be machined. The aluminium block has an overall dimension of 205 mm x 205mm x101 mm. As shown in Figure 5.8, a cavity was made in the middle of the block to form the vacuum chamber, the engineering drawing of the vacuum chamber and Klein Flanges (KF) are shown on the appendix B1 on page 171. The vacuum chamber is sealed from the top by placing a Robax glass on the recessed edges of the chamber with an O-ring in between. The

Robax glass enables the light irradiation of all sun spectrums to enter into the chamber where the solar absorber/TEG is located. An opening of 80mm x 80mm is made at the bottom of the chamber, where the solar absorber, the TEG and the top part of the heat sink is inserted into the chamber and is sealed by the lower part of the heat sink with O-rings in between. Two holes were made on the side walls of the chamber and two KF were welded. One of the KF flanges is used for connecting the chamber to the vacuum pump, while the other is attached to a feedthrough for electrical and temperature connections. The feedthrough was made by drilling 1mm diameter holes on blank flange cover and sealed using heat resistant epoxy. Figure 5.9 shows the home-made feedthrough and related attachments.

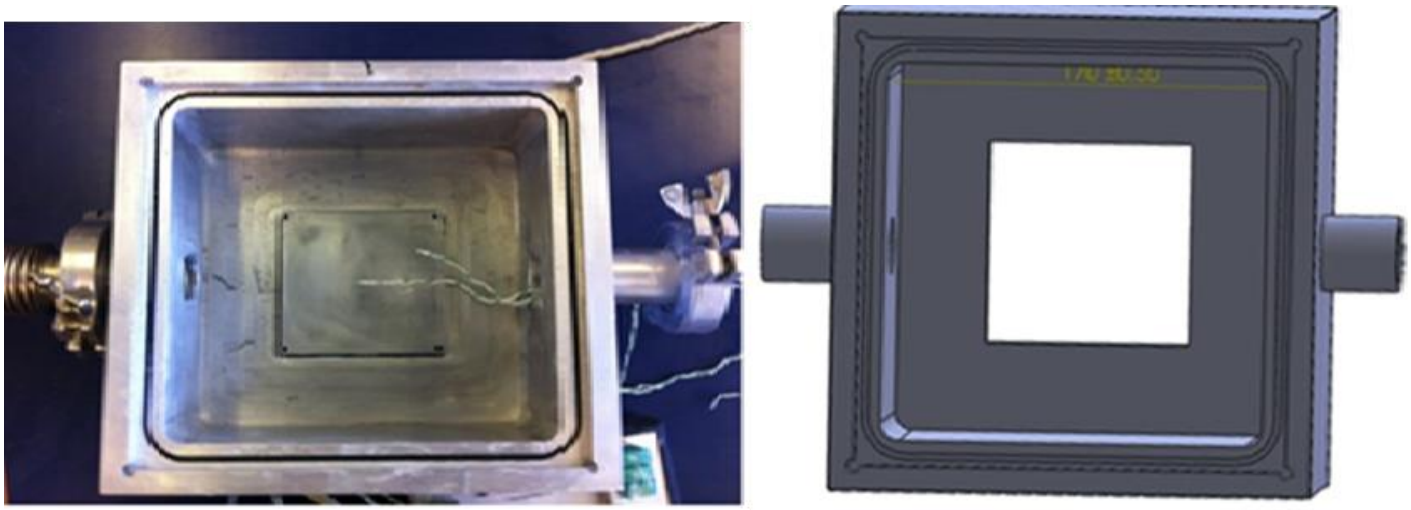

Figure 5.8 The vacuum chamber.

Figure 5.9 Home-made feed through using a blank cover, which can be attached to the standard KF flange.

5.2.4 THE SOLAR ABSORBER

The solar absorber was designed to fit within the vacuum enclosure and, therefore, the size was restricted to the space available. A copper plate, with an area of 80 mm^2 and thickness of 1mm, was chosen. The plate was painted with high temperature black matt paint (pnm type) from the top, this to maximize its heat absorption ability and the use of copper provides high thermal conductivity. Additionally, a groove was machined on the backside of the copper plate to accommodate a thermocouple, which is used to measure the temperature of the absorber and the TEG's hot side (T_h). The solar absorber was fixed on to the heat sink

(with the TEG in-between) using four plastic screws. The plastic screw has very low thermal conductivity that minimise the direct heat loss from the solar absorber to the heat sink. To ensure good thermal contact, thermal conductive compound was applied to the interfaces between the hot and cold side of the TEG .

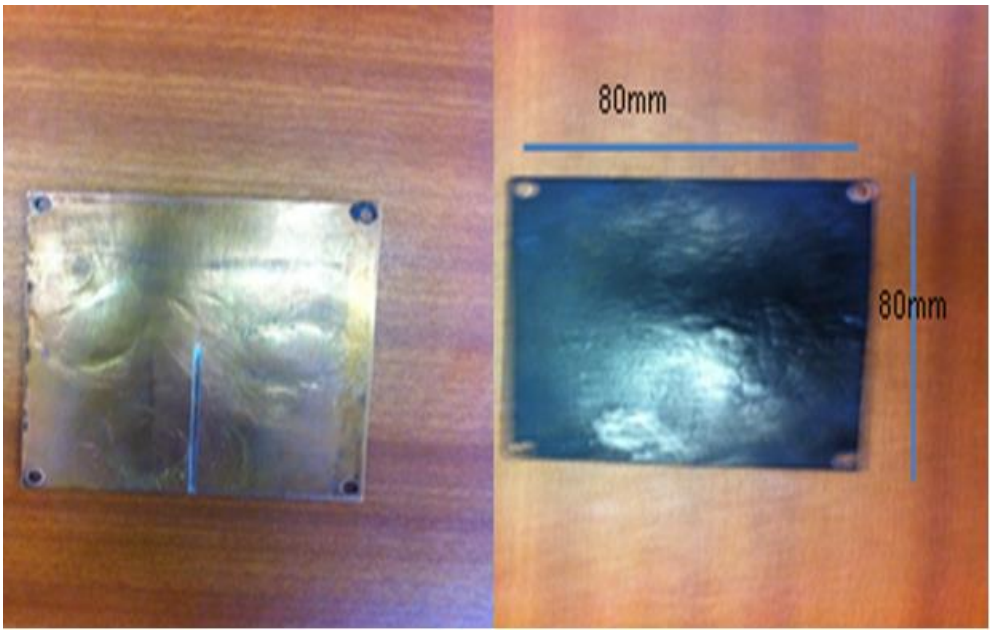

Figure 5.10 The backside (left) and front side of the solar absorber.

5.2.5 THE HEAT SINK

An aluminium heat sink, with an area of 100 mm x 80 mm x 50 mm, was designed and fabricated as shown in Figure 5.11 and the engineering drawing on the appendix B2 on page 172. The heat sink fins were built-in fins, each at 30 mm long and 3mm thick. In addition to its main function as heat exchanger, the heat sink servers as the support for solar absorber/TEG assembly and the bottom seal for the vacuum chamber. It is attached to the vacuum chamber from the bottom using four screws with an O-ring in between to ensure no leakages. The top part of the heat exchanger is an extended square base of 20 mm (with

dimensions of 80mm^2), on which the solar absorber and TEG are mounted and inserted inside the vacuum chamber. A groove was also made at the top of the extended base to accommodate a thermocouple for measurements of TEG's cold side temperature and heat sink temperature.

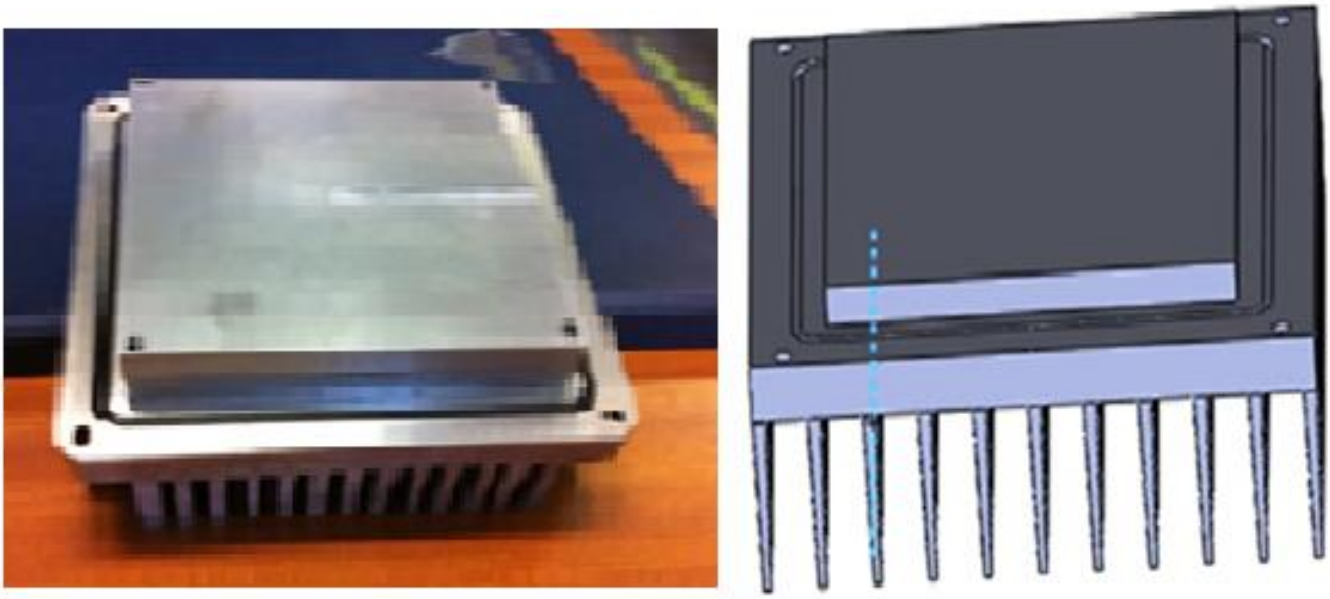

Figure 5.11 The photograph of the fabricated heat sink (left) and its design drawing (right).

5.2.6 THE WATER CONTAINER

The system is completed by attaching a water container to the bottom part of the heat sink. With the fins of the heat sink submerged into the water in the container, the thermal energy flowing through the TEG and heat sink will enter into the water to produce hot water. In order to minimise conductive heat loss from the container, a polypropylene plastic, with a

thermal conductivity of 2 - 3W/m-K, was employed. The dimension of the water container is 120 mm x 115 mm x 500 mm (Figure 5.12), which has a volume of 300 ml.

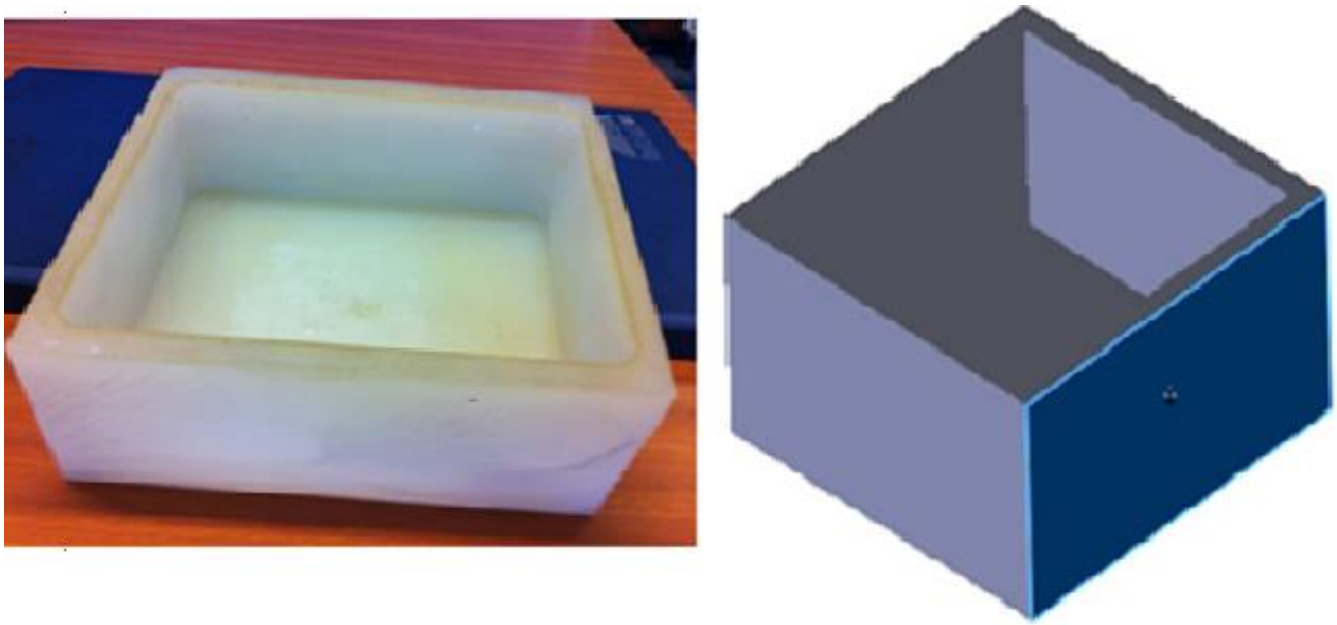

Figure 5.12 Photograph of the fabricated water container (left) and its design drawing (right).

CHAPTER 6: RESULTS AND DISCUSSION

6.1 INTRODUCTION

This chapter explores the performance of the different size systems, through investigations and tests under different environmental conditions. The results were discussed and analysed, with regards to the effects of applying different vacuum levels and concentrating the light intensity on the performance of the system. This was previously described in Chapter 5. Consequently, the results were analysed, based on the methods presented in the methodology chapter. The amount of heat absorbed was determined, using the slope technique, as well as the system's thermal power. The results were investigated by changing the environmental conditions in response to the convection heat lost from the system, and therefore to the system thermal performance. Following this, the system's electrical power output was resolved in all sizes. Moreover, different conditions were applied, and the effect of minimizing the convection heat lost by changing the environmental conditions on system size optimization was evaluated. Finally, the optimal system size and conditions were the most advantageous efficiencies obtained. This, as well as an analysis of the results, provided the optimum ratio for thermo element area and length (A/L).

6.2 DETERMINATION OF THE LIGHT INTENSITY ON THE ABSORBER

In order to evaluate the system performance, the heat power absorbed by the absorber has to be determined. The experiment was conducted based on the slope technique following the

same approach as described in section 4.3, but using the new absorber constructed in Chapter 5 and a Xenon light source (rather than a halogen light bulb). The absorber temperature (T_h) was recorded as a function of time. The results display an identical trend as those of Figure 4.1. To avoid "repetition," the results obtained from this experiment are included in Appendix B3 on page 172. From data analysis, we can see that the solar absorber reached a steady state in approximately 30 minutes after the light was switched on. The maximum T_h recorded was 204 ^{o}C. The rate of temperature change over the initial time period was determined using the slope technique and the heat absorbed was calculated, which gives a value of 21.4 Watt, the value of the heat power absorbed obtained by the slope technique is corresponds to a light intensity of 3340 W m^{-2} (Given the absorber area, mass and specific heat were 0.0064 m^2, 0.08kg and 400 $j.kg^{-1}$. K^{-1}, respectively) if the absorber efficiency is 100%. To ensure the results obtained were reliable, the light intensity was also measured directly using a light intensity meter (Pyrometer, Kipp & Zonen CMP11) with a factor of $5.2x10^{-6}$ $VW^{-1}.m^{-2}$. The intensity meter was placed at the same location as the absorber and exposed to the light under the same conditions. The measurements were taken at five different points within an area of 8 cm^2 (i.e., the same area of the absorber). An average was taken. Light intensity of 3700 wm^{-2} was obtained (See Appendix B4 on page 173 for more details), the average of the heat power obtained by measurement was 23.5 Watt.

6.3 DETERMINATION OF THERMAL POWER

Experimental study was carried out using the equipment developed in Chapter 5 (Figure 5.2), aiming to investigate the influence of the environment on the power performance and geometry optimisation of the system. The influence of the environment on the system performances is anticipated due to the level of convective heat loss of the system is strongly

depended on its surrounding atmosphere. In this study, the experiments were performed in five different environmental conditions and levels. They are categorised as follows:

Condition 1: The system without glass (an unglazed system), at atmospheric pressure.

Condition 2: The system with glass cover (a glazed system), but at atmospheric pressure.

Condition 3: A glazed system at a vacuum level of $2x10^{-1}$ mbar.

Condition 4: A glazed system at a vacuum level of $8x10^{-2}$ mbar.

Condition 5: A glazed system at a vacuum level of $5x10^{-2}$ mbar.

Five TEG devices with different sizes were employed. The dimension, aspect ratio and internal resistance of these devices are shown Table 6.1. Four of the devices shown in Table 6.1 have actually used in the experiments described in Chapter 4 (Table 4.2). Unfortunately, one of the devices, which has sample ID of S2 and aspect ratio of 0.169, was damaged and no identical device is available. Consequently, another device, which given an ID as Z1 and aspect ratio of 0.031, was replaced and employed.

Table 6.1 The dimensions, aspect ratios, internal resistances and cost of the TEG devices that are employed in this experiment.

Sample ID	N	A (m^2)	L (m)	Aspect ratio [Ax2N]/L (m)	R (Ω)	Cost [£]
Z1	62	$1x10^{-6}$	$2x10^{-3}$	0.031	1.7	15
S1	72	$1.6x10^{-6}$	$1.7x10^{-3}$	0.136	1.8	30
S3	127	$2x10^{-6}$	1.7×10^{-3}	0.299	3.5	32
S4	127	$7.6x10^{-6}$	3.6×10^{-3}	0.536	1.6	65
S5	48	$1.7x10^{-5}$	2.4×10^{-3}	0.680	0.2	50

In order to determine the thermal power, the temperature differences (Th -Tc) of the TEGs were recorded from the moment when the light source was switched on until the period when the system reached the steady state. The measurement was repeated for each TEG under each of the 5 different environmental conditions. The results of the measurements are shown in Figure 6.1, which displays the hot side temperature (T_h) of the TEG as a function time. It can be seen that the hot side temperature of the TEG increased when the vacuum level were increased. In particular, the increase is more significant for the system with the smallest TEG. By comparing the results of Condition 2 and Condition 3, it is clear that the hot side temperature (T_h) increased by approximately 16% for the system with sample of Z1 and aspect ratio of (the smallest TEG). This improvement was a direct consequence of minimizing the convective heat loss because the vacuum is applied to the system.

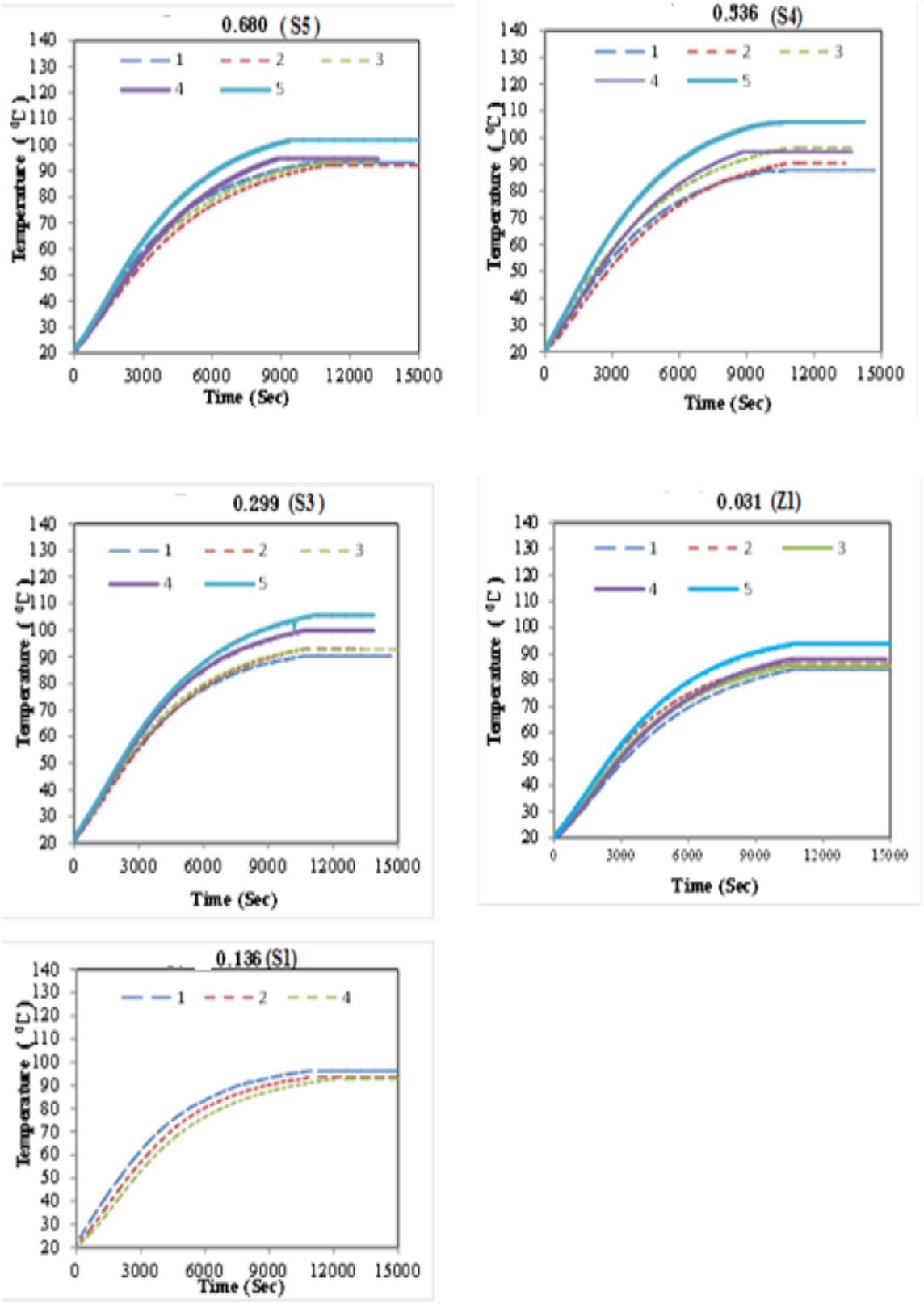

Figure 6.1 The hot side temperatures of the TEG as a function of time for all samples under 5 different environmental conditions.

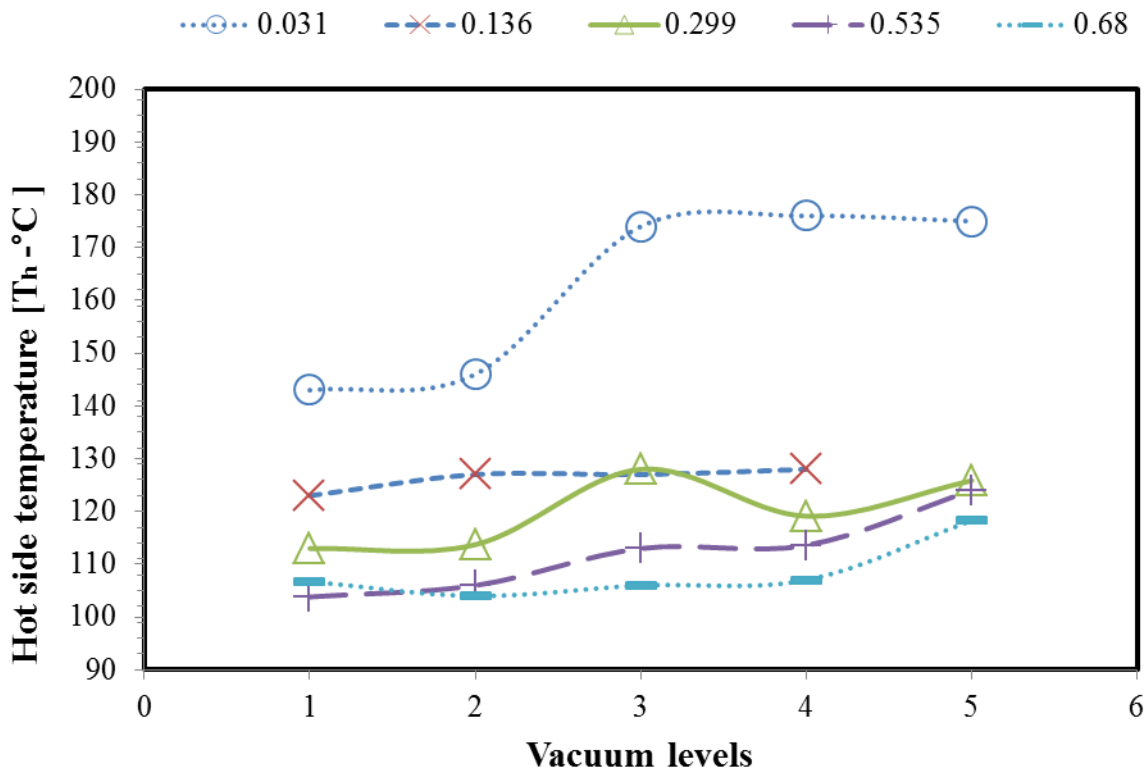

Figure 6.2 The steady state hot side temperatures (Th) of all samples as functions of the environmental conditions.

Using the steady state data from Figure 6.1, the dependence of the hot side temperature (T_h) on the environmental conditions is shown in Figure 6.2 for all 5 TEGs samples. It can be seen that the hot side temperature (T_h) of the TEG depends on both the aspect ratio and operating environment. The hot side temperature is higher for the TEGs with smaller aspect ratio. Furthermore, the operating environment has more significant effect on the TEGs with smaller aspect ratios than those with larger aspect ratio. This can be explained by the fact the convective heat loss is more significant in the TEGs which have smaller aspect ratios. The convective heat loss is more significant in the TEGs with smaller aspect ratios than those with larger aspect ratios because the hot side temperature of the TEGs with smaller aspect ratios is higher than those with larger aspect ratios under the same operating condition. The operation in vacuum will help to minimise the convective heat loss, resulting in more

significant improvement in the TEGs with smaller aspect ratio. This is clearly demonstrated by the change in the hot side temperature of the smallest TEG (with sample ID of Z1 and aspect ratio of 0.031) in Figure 6.2.

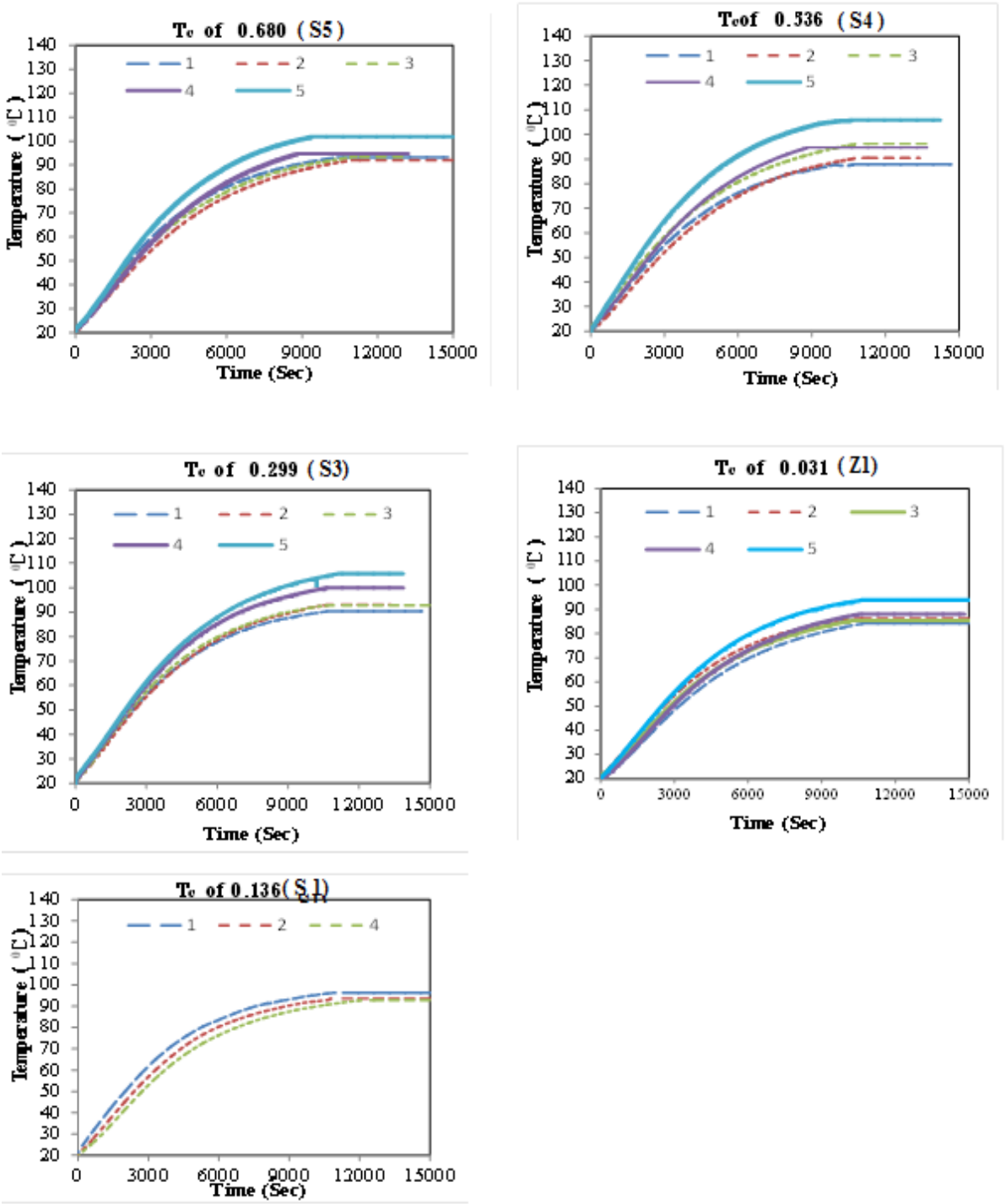

Figure 6.3 The TEG cold side temperatures of all samples, as functions of time, at the different vacuum levels.

The cold side temperature (T_c) of the TEG is also affected by both the aspect ratio and operating environment. Figure 6.3 shows the cold side temperature profiles of 5 TEGs investigated as a function of time, which were recorded from the moment when the light source was switched on to the period when the system reached the steady state. As illustrated in Figure 6.3, the operating environment appears to have less influence on the cold side temperature (T_c). Nevertheless, it shows a trend of very small increase with increasing the vacuum level. Since the thermal power and electrical power produced by the system depend directly on the temperature difference (ΔT) across the TEG, it is more intuitive to plot the ΔT. Figure 6.4 shows the temperature differences across the TEGs at the steady state as a function of the operating vacuum level for 5 different TEG.

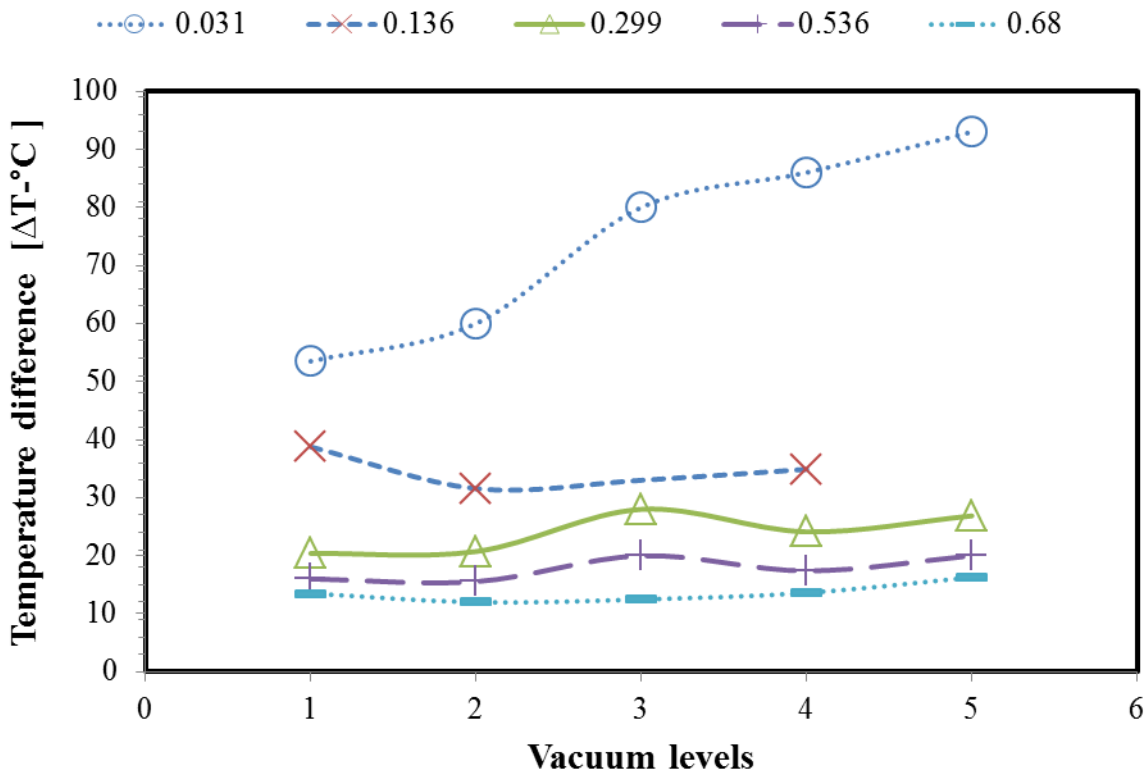

Figure 6.4 The temperature differences (ΔT) across the 4 different TEGs' aspect ratios at the steady state as a function of the operating vacuum levels.

Figure 6.4 proves that increasing the vacuum levels enhances ΔT - this is due to minimizing the heat loss. The smaller a TEG is used in the system and the significant the enhancement is. An increase of 25% was obtained in the system with the smallest TEG when the operating environment changed from the Condition 2 (non-vacuum) to Condition 3 (low vacuum). A maximum increase in ΔT is 37 %, which corresponds to the change of the operating environment from Condition 1 to Condition 5.

The trend of temperature change in the system that has sample ID of S1 and aspect ratio of 0.136 is a bit unusual - the ΔT value showed a decrease when the operating environment changes from Conditions 1 to Condition 2. It is unclearly what has caused this change. Unfortunately, the TEG employed was damaged during the investigation. As a result, only the experimental data corresponding to the test environments of Conditions 1, 2 and 4 was available. It was not possible to confirm the result of Condition 1 by repeating the experiment.

Table 6.2 Comparison of ΔT between Condition 5 and Condition 1 in the steady state.

Sample ID	Aspect ratio [Ax2N]/L (m)	Condition 1 ΔT (^{o}C)	Condition 5 ΔT (^{o}C)	The increase %
Z1	0.031	58.76	93.00	37
S3	0.299	20.40	26.87	24
S4	0.536	16.00	20.00	20
S5	0.680	13.50	16.27	17

The temperature differences across different TEGs under Condition 1 and Condition 5 at a steady state are compared and the results are shown in Table 6.2. Condition 1 represents

a completely open system where the convective heat loss will be very significant while Condition 5 corresponds to a vacuum level of $5x10^{-2}$ mbar, in which condition the convective heat loss should be minimised. The results show a clear dependence of the temperature difference on the operating environment. Increasing the vacuum level improves the ΔT. This effect is more significant in a system with smaller aspect ratio. This can be understand by the influence of vacuum on convective heat loss. With the knowledge of the ΔT obtained from the experiment for each system, the thermal power (Q_{TEG}) at the steady state can be calculated using equation 3.19 (in Chapter 3). Using a typical value of 1.5 $W.m^{-1}.K^{-1}$ for the thermal conductivity of Bi_2Te_3 materials (the thermoelectric materials employed in those commercial available modules), the thermal powers transferred into hot water under 5 operating conditions were calculated and are displayed as a function of the aspect ratio of the TEGs in Figure 6.5 below. The dependence of thermal power on the aspect ratio is evident. It can be seen that the thermal power is ~2.5 W for the smallest TEG with sample ID of Z1 and aspect ratio of 0.031, while it is ~12 W for the largest TEG with sample ID of S5 and aspect ratio of 0.68 when operating under Condition 1. The thermal power also increases with increasing vacuum level. However, the increase by improving vacuum level is limited if compared with the amount of increase that can be achieved by changing the aspect ratio. This is clearly shown in Figure 6.6, in which the thermal power is plotted as the function of operating environmental conditions using the same sets of data employed in Figure 6.5. The thermal power increases slowly along the line as changing the operating conditions, which jumping across the lines when changing the TEGs.

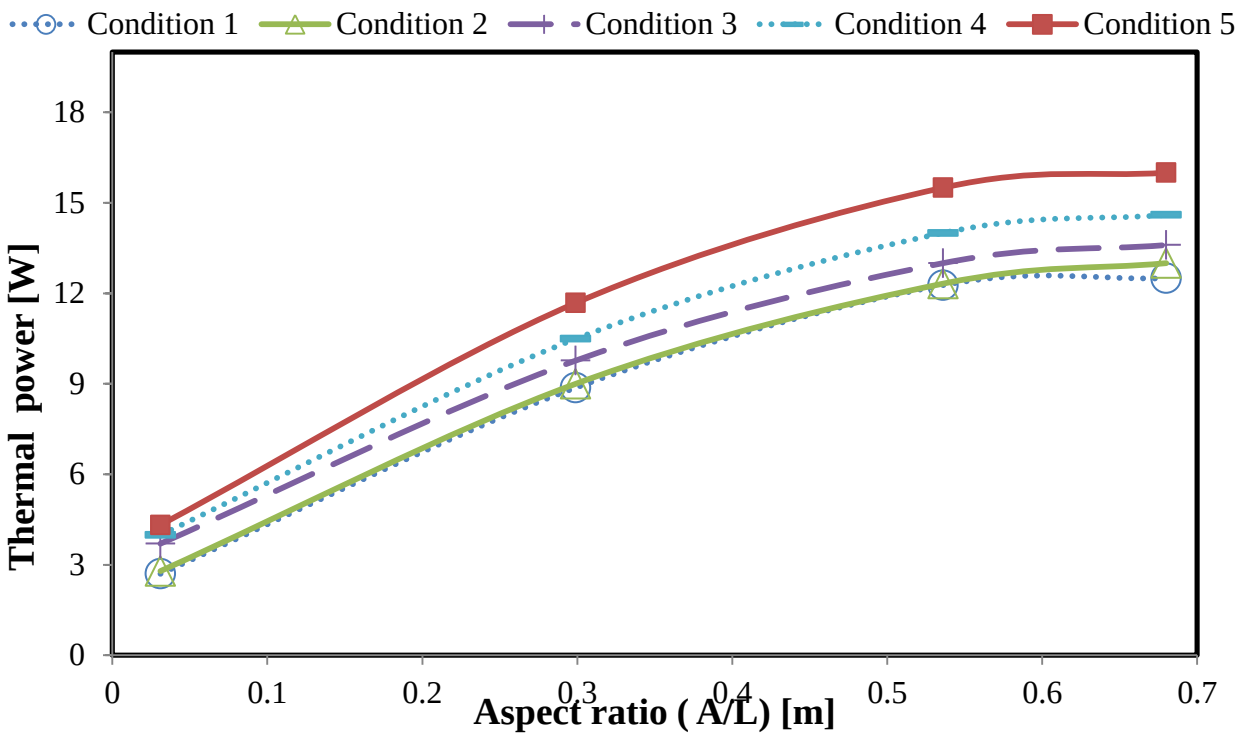

Figure 6.5 Thermal powers transferred into hot water of the solar thermoelectric system at the steady state, calculated using the conduction method (Q_{TEG}), displayed as a function of the aspect ratio of the TEG.

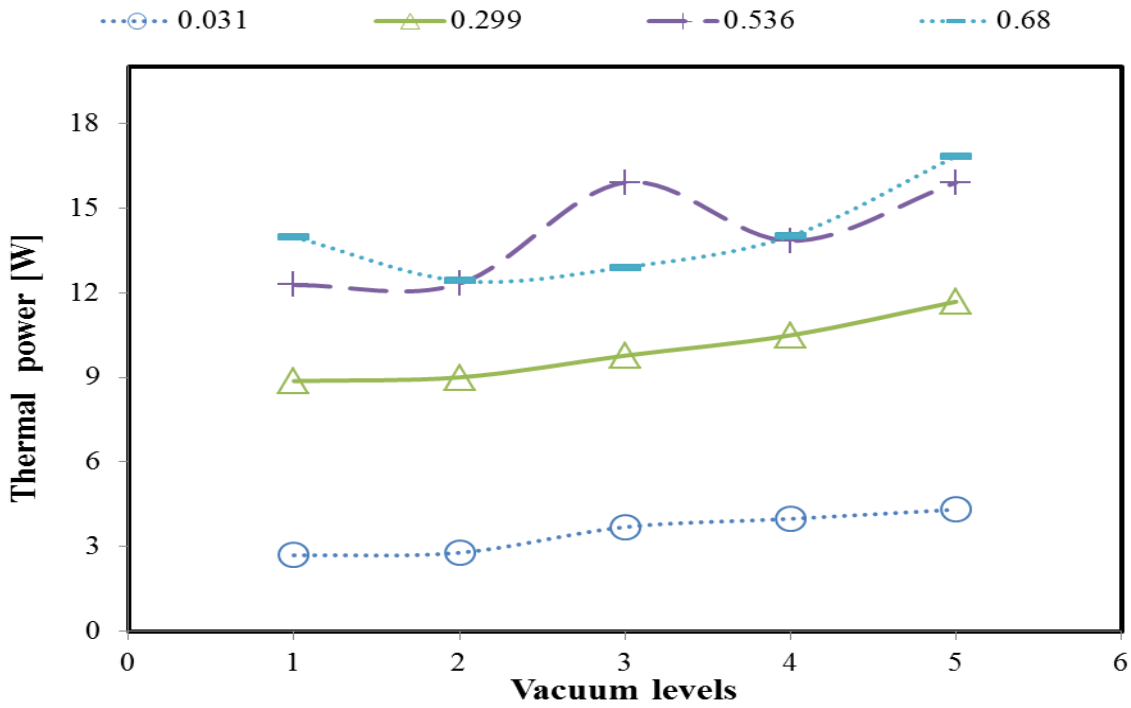

Figure 6.6 Thermal power transferred into the hot water in a steady state as a function of the operating vacuum levels for the systems of different aspect ratios. The results were calculated using the conduction method (Q_{TEG}).

The thermal power transferred into hot water can also be determined in the transient state using the slope technique (Q_w). The results obtained using the slope technique were compared with these obtained using the conduction method (Q_{TEG}) during the same initial period (i.e., the first eight minutes). Following the experimental procedures described in Chapter 4.4, the temperature profiles of the hot water as a function of time were recorded and the rate of the temperature change ($\frac{\Delta Tw}{\Delta t}$) of the water was determined from the slope of the temperature profile recorded. (See Appendix B5 on page 173). To calculate the thermal power using the slope technique (equ. 3.9), the mass of the water in the container is measured, which is 0.275 kg. The specific heat of the water was obtained from literature which gives 4184 $J.kg^{-1}.K^{-1}$. The results were plotted as a function of the aspect ratio of the TEGs, and are shown in Figure 6.7.

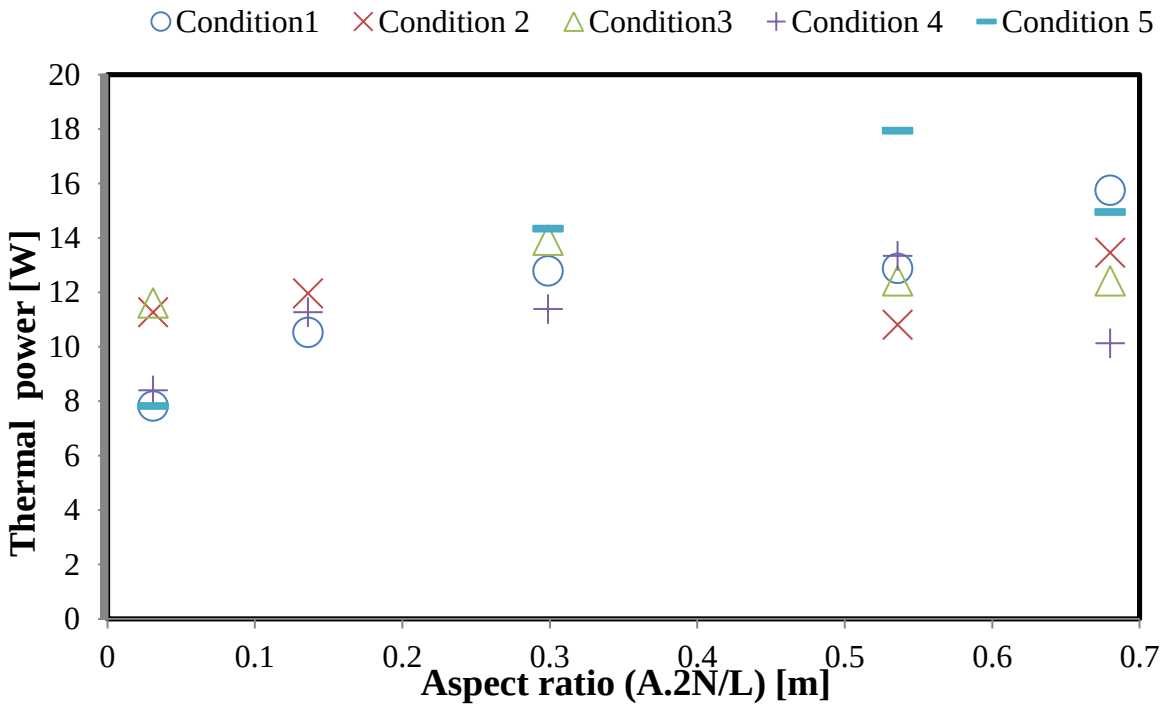

Figure 6.7 Thermal power determined using the slope technique, plotted as a function of the aspect ratio of the TEGs for different vacuum levels.

The thermal power transferred into the hot water during the same initial transient period (i.e., the first eight minutes) can also be determined using the conduction method (equation 3.11) from the measurements of the average temperature difference across the hot and cold side of the TEGs during this period. The results were plotted as a function of the aspect ratio of the TEGs for different operating environmental conditions and are shown in Figure 6.8.

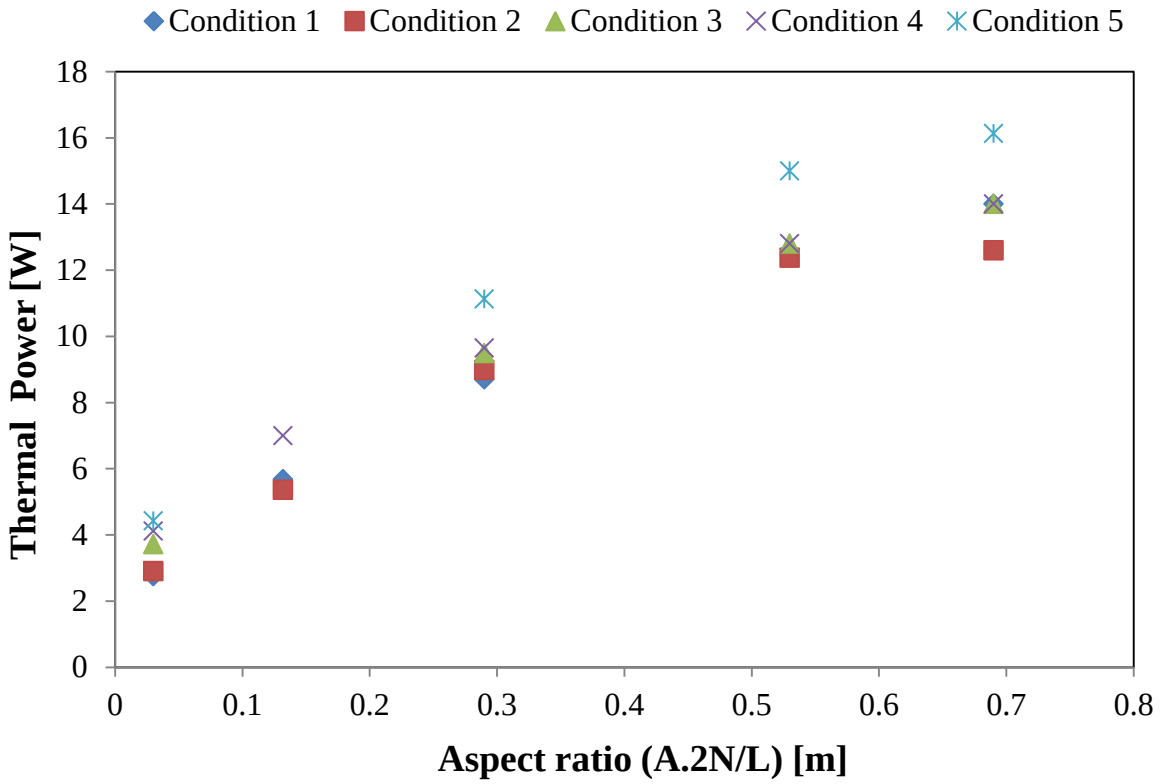

Figure 6.8 Thermal power determined using the conduction method during the period of the first 8 minutes as a function of the aspect ratio of the TEGs at different operating vacuum levels.

Similarly, Figure 6.8 also shows that thermal power increases with increasing the aspect ratio of the TEG and the vacuum level of operating environment. However, by comparing both results in detail, it can be seen that there are differences in the values of thermal power outputs. In particular, for the TEGs with small aspect ratios, the thermal powers obtained using the slope technique is significantly larger than those obtained using the conduction

technique. Difference appeared in the TEGs with smaller aspect ratios, while the differences become smaller in the TEGs with larger aspect ratios. On the other hand, for the TEGs with larger aspect ratios, the thermal powers determined using both techniques agree with each other. This observation can be explained by taking into account the heat radiation. It is to be noted that the slope technique determines the thermal power from the water temperature change that take into account all thermal energy transferred into the hot water, that include contribution from conduction, convection and radiation. However, the conduction technique only determines the thermal energy transfer due to heat conduction. The contribution due to convection and radiation are neglected. For large TEGs, the conduction area is very close to the area of the solar absorber. It is anticipated that the heat conduction will be the dominant heat transfer process in this case and consequently the thermal power estimated using the conduction technique will very close to the values that are actually transferred into the hot water. As being shown in Figures 6.7 and 6.8, the results by both techniques are very similar for a TEG that has a larger area. However, if a TEG has a small area, this indicates that a large area is available between the back surface of the solar absorber and the hot water (or top or the heat exchanger). This could result in a noticeable contribution to the heat transfer from the solar absorber to the hot water directly by heat radiation. When heat radiation between the solar absorber and the hot water was taken into consideration, it was estimated that the heat transfer due to heat radiation in the case of the smallest TEG is approximately 4.2W, while it is only approximately 0.2W in the case of the largest TEG. Clearly, the difference between Figures 6.7 and 6.8 can be understood. For detailed explanation, please see Appendix B6 on page 183. The results indicate that the thermal power determined using the slope technique is more reliable than the conduction technique because the slope technique includes the contributions from all heat transfer processes. The conduction technique, as a method to estimate the thermal power transferred into the hot water, is only valid when the area of the

TEG is similar to that of the solar absorber. In addition, the results also indicate that a decrease in heat conduction due to the use of a small TEG could be partially compensated by an increased heat radiation, Consequently, thermal power transferred into the hot water is much higher than the predicted value from the conduction technique.

6.4 DETERMINATION OF THE ELECTRICAL POWER OUTPUT

The open circuit voltages from the output terminals of the TEGs were recorded as function of time from the moment when the light source was switched on to the period when the system reached the steady state. With the knowledge of the internal resistances of the TEGs, the electrical powers generated by the TEGs were calculated using equation 2.3 and the results were displayed as a function of time shown in Figure 6.9.

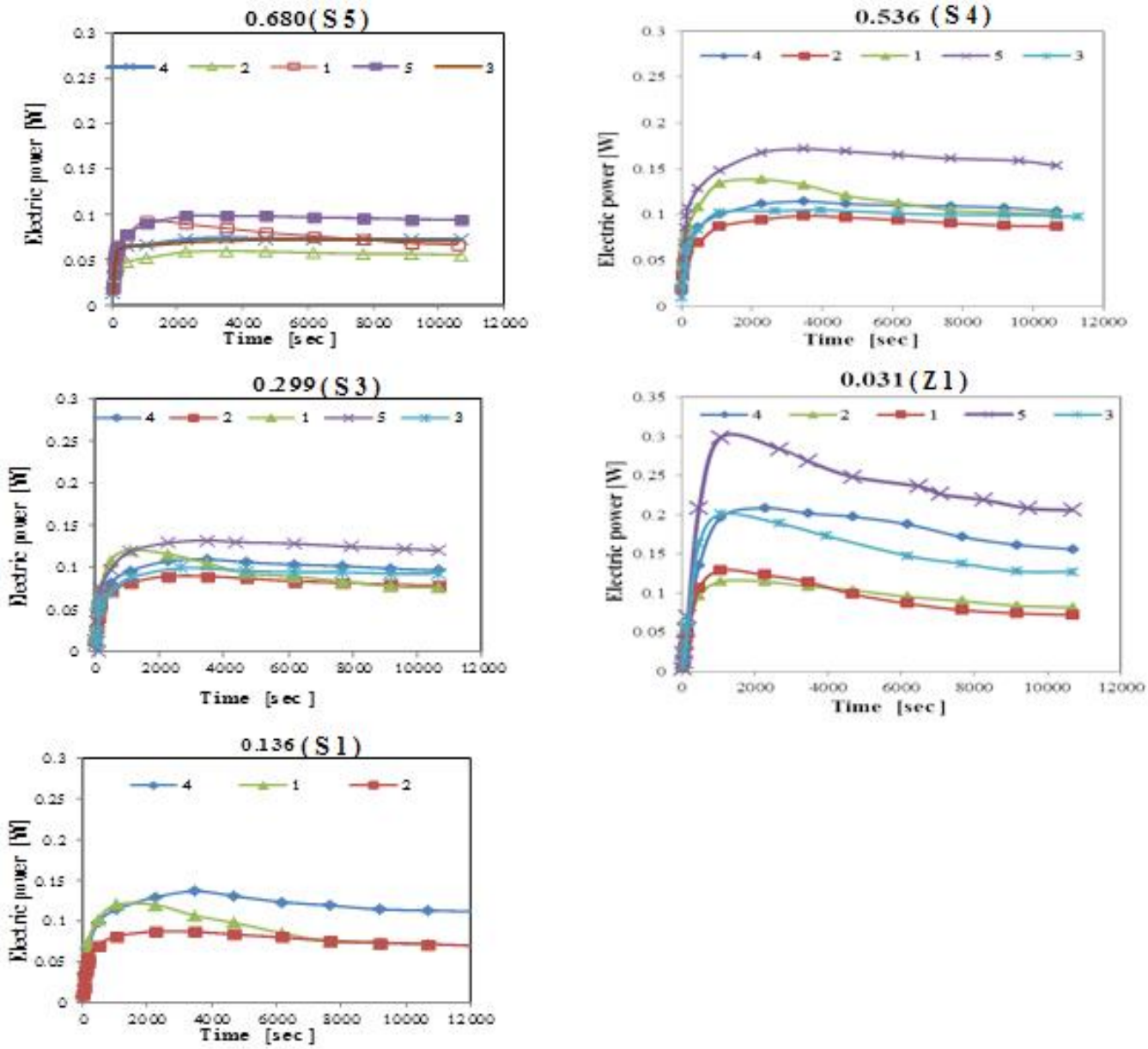

Figure 6.9 The electrical powers generated by the TEGS as a function of time at different operating vacuum levels.

It can be seen that at the initial period the electrical power increases with increasing time until it reaches a maximum value after approximately 20 minutes from the start. It appears that the time required to reach the maximum power level is almost the same for all TEGs under all operating conditions. Afterwards, the power level decreases with further increase in time until it reaches a steady state. This is due to the fact that the temperature difference

across the TEGs reaches the maximum value during a transient state. Once again, it appears that the time required to reach the steady state is almost the same for all systems with different TEGs and operating under different environments. The power levels at steady state are lower than the maximum value and the degree of decrease depends on the aspect ratio of the TEGs and environmental conditions of operation. The electrical power drop between the maximum value and the steady state value is the most significant for the TEG with smallest aspect ratio and operating in high vacuum, whereas it shows little difference for the TEG with the largest aspect ratio. Clearly, this reflects the dependence of electrical power output on both the TEG aspect ratio and operating environments. While the power (thermal and electrical) production during the transient period can contribute to the total energy generation of the system, the main contribution is anticipated from the operation in the steady state. Figure 6.10 shows the electrical power outputs as a function of 5 operating environmental conditions for different aspect ratios. It can be seen that the operating environment has a significant impact on the electrical power output of the system. When operating in a normal atmosphere (Condition 1), all 5 TEGs of different sizes appear to generate more or less similar power levels (0.07 W – 0.1 W). However, when the TEGs were operated in high vacuum (Condition 5), the difference in electrical power output among different TEGs became much more significant (0.1 W - 0.2 W), this is because the improvement of minimising the convection heat lost, which was very high at the TEG with the smallest aspect ratio, due to substantial gap left between the absorber and the water system – an increase by 64% from operating in Condition 1 to Condition 5, while the improvement is much less in the TEGs that have large aspect ratios. The optimal aspect ratio to obtain the maximum electrical power output is also affected by the operating environment conditions. Figure 6.11 shows the electrical power outputs as a function of the aspect ratio of the TEGs for different operating environmental conditions. It can be seen that, when operating in Condition 1, the maximum

power output of 0.1 W was obtained using the TEG with the aspect ratio of 0.536, which corresponding to the second largest TEG investigated. However, when operating in Condition 5, the maximum power output of 0.2 W was obtained from the TEG with the smallest aspect ratio. This result clearly demonstrates that selecting a TEG with appropriate aspect ratio is crucial to obtain the best available power output for a given operating environmental condition. It brings significant benefits in both improving the maximum electrical power output (0.1 W to 0.2 W) and reducing the cost of TEG by using small size modules ($0.536/0.031 \approx 17$ times of reduction in volume, consequently the thermoelectric materials cost). Significant increase in the electrical power output of the TEG with smallest aspect ratio is due to the fact that the temperature difference across the TEG increased significantly when the convective heat loss is reduced through the use of vacuum. Both the measured and simulated results of the temperature differences across the TEGs, together with the measured open circuit voltages, are included in Appendix B7 on page 185 for reference. The validity of the measurements of electrical power outputs for all 5 TEGs under all operating environmental conditions are also demonstrated as shown in Appendix B8 on page 187.

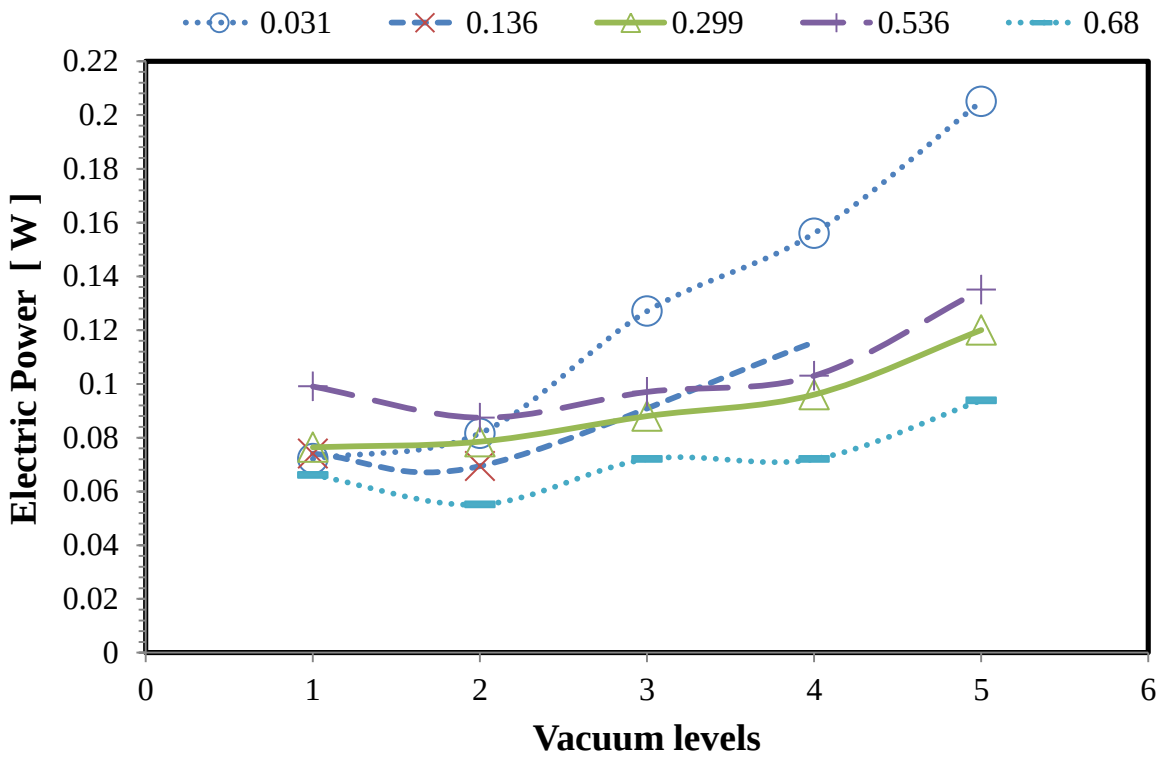

Figure 6.10 The electrical power of as a function of the operating vacuum levels for 5 different TEGs Samples.

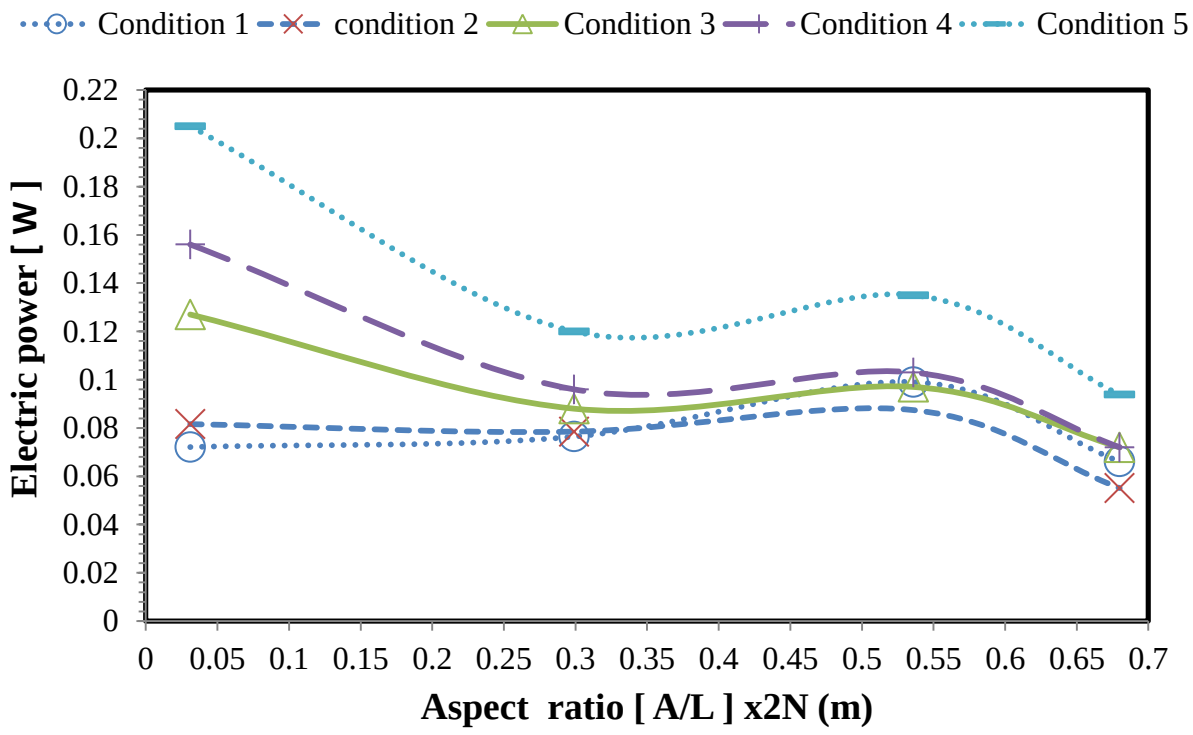

.

Figure 6.11 The electrical power outputs as a function of the aspect ratio of the TEGs at different vacuum levels.

6.5 OPTIMAL TEG SIZE FOR MAXIMUM THERMAL AND ELECTRICAL POWER

The results obtained in sections 6.3 and 6.4 indicate that the aspect ratio required to obtain the maximum thermal power output is different from that required for the electrical power output. The optimisation is also affected by the operating environmental conditions, which are clearly shown in Figures 6.5 and 6.11. In general, a large aspect ratio is required if the system is required to produce maximum thermal power output. On the other hand, a small aspect ratio with a high vacuum operating condition is needed if the system is designed to produce as much electrical power as possible. For the system investigated, if the relative contribution of thermal and electrical power is specified, the optimal aspect ratio for the TEG can be determined using the plots obtained from this experiment, which are displayed in Appendix B9 on page 190. Furthermore, the experimental results obtained from this studies shows a reasonably good agreement with the calculated results using the theoretical model described in Chapter 3. The validation of the theoretical model provides a powerful tool to investigate the optimisation of the system. Based on the results obtained, which are mainly shown in Figures 6.5 and 6.11, the best system size which offers the optimal heat and electric power performance can be determined. This enabled the researcher to define the best size optimization based on a solar absorber size of 0.08m x 0.08m.

6.6 DETERMINATION OF SYSTEM EFFICIENCIES

As explained in Section 3.2, the system's overall efficiency (η), the TEG's electricity converting efficiency (η_E) and the system's thermal efficiency (η_H) needed to be determined. To find out η_E and η_H, the absorber's efficiency in converting the input energy into heat (η_a) has to be determined. This was based on the energy input (Q_{in}) which was measured using the intensity meter. While the heat absorbed by the absorber ($Q_{a)}$ was obtained by the slope technique. The values of those two essential parameters are shown in the equation below,

$$Q_a = 21 \text{ W}, \quad Qin = 23 \text{ W}.$$

Consequently, the absorber's efficiency can be determined by,

$$\eta_a = \frac{Qa}{Qin} = 91\%$$

η_E and η_H can be calculated by using the following equations,

$$\eta_E = \frac{P}{Qa} \quad \text{and} \quad \eta_H = \frac{Qw}{Qa}$$

Once the essential parameters, Qa and Q_{in} , as well as P and Qw were calculated using the data obtained by measurements, the efficiencies of the system of different sizes under different environmental conditions, are presented in the section below.

6.6.1 THE EFFICIENCIES OF THE SYSTEMS UNDER CONDITION 1

The TEG's conversion efficiencies (η_E) under Condition 1 ranged from 0.31 -0. 47 %. The largest system was the least efficient, while the second largest was the most efficient in terms of electricity generation. The thermal efficiency (η_H) of these systems ranged from 11% - 60% with the larger system showing the higher thermal efficiency. Decreasing the aspect ratio of the system decreases the thermal efficiency. The detailed results are presented in a table below.

Table 6.3 The efficiency results of all system sizes under Condition 1.

Aspect ratio	η_E %	η_H %	η %
0.031	0.34	11	11.34
0.136	0.35	24	24.35
0.299	0.36	38	38.36
0.536	0.47	55	55.47
0.680	0.31	60	60.31

6.6.2 THE EFFICIENCIES OF ALL SYSTEMS UNDER CONDITION 2

When glass was added to the experiment, the results altered slightly when compared to Condition 1, even though the addition of the glass was an attempt to cut 5% of the input energy. The overall efficiencies of the smallest system sizes with samples ID Z1, S1 and S3 and aspect ratio of 0.031, 0.136 and 0.299 were increased, while the remaining samples (S4

and S5) with larger sizes' (aspect ratio of 0.536 and 0.680) efficiencies were decreased. The detailed results are presented in the table below.

Table 6.4 The efficiency results for all system sizes under Condition 2.

Aspect ratio	η_E %	η_H %	η %
0.031	0.38	12	12.38
0.136	0.36	27	27.36
0.299	0.37	39	39.37
0.536	0.41	54	54.41
0.680	0.26	54	54.26

6.6.3THE EFFICIENCIES OF ALL SYSTEMS UNDER CONDITION 3

When a vacuum level of 2 x 10^{-1} mbar was applied under Condition 3, the total efficiency showed a noticeable improvement, particularly in the case of the smallest module. The TEG's conversion efficiency increased by 36%, 16%, 10% and 21%, respectively for the four samples (Z1, S3,S4 and S5), with aspect ratio of 0.031,0.299,0.536 and 0.680 compared to the electrical power shown in Condition 2. The thermal efficiency only increased in the two smallest sizes, and remained similar in the largest two.

Table 6.5 The efficiency results for all system sizes under Condition 3.

Aspect ratio	η_E %	η_H %	η %
0.031	0.60	16	16.60
0.299	0.44	43	43.44
0.536	0.46	54	54.46
0.680	0.33	54	54.33

6.6.4 THE EFFICIENCIES OF ALL SYSTEMS UNDER CONDITION 4:

When the vacuum level was increased further to 8 x 10^{-2} mbar, the TEG's conversion efficiency in the TEG with smallest size (Z1 and aspect ratio of 0.031) was doubled compared with those of Conditions 1 and 2, and increased by 19% compared with that under Condition 3. Similarly, the thermal efficiency was increased more significantly in the smaller sizes than that in the larger sizes. The table below shows the detailed results.

Table 6.6 The efficiency results of all system sizes under Condition 4.

Aspect ratio	η_E %	η_H %	η %
0.031	0.74	17	17.74
0.136	0.52	30	30.52
0.299	0.45	46	46.45
0.536	0.49	60	60.49
0.680	0.34	61	61.34

6.6.6 THE EFFICIENCIES OF ALL SYSTEMS UNDER CONDITION 5

When a vacuum level of 5 x 10^{-2} mbar was applied, the TEG conversion efficiency of all sizes increased. However, the greatest increase recorded was particularly noticeable in the smallest system (Z1 and aspect ratio of 0.031), as this showed an increase of 65% compared to the results under Condition 1. Improvements of 60%, 36% and 22 % were recorded, if compared to Conditions 2, 3 and 4. There was a reasonable improvement of thermal efficiency for all sizes under this condition if compared to that of the previous one. This is shown in the table below.

Table 6.7 The efficiency results of all system sizes under Condition 5

Module size	η_E %	η_H %	η %
0.031	0.95	19	19.95
0.290	0.57	51	51.57
0.530	0.64	69	69.64
0.690	0.44	72	72.44

As the electric and heat power efficiency of this proposed system has been presented on table 6.7. The efficiency for similar system reported on the literature has been summarised on the following table.

Table 6.8 The efficiency results similar systems developed by other research groups.

Aurther-Year	System Type	TEG ΔT	System efficiency %	
			Electric efficiency	Thermal efficiency
Lertsatitthanakorn et al 2008	Glazed Flat plate – Experiment results based on 24 TEG modules	22°C	0.14	80.3
Rockendorf et al. 1999	Vacuum tube – experiment results	70°C	3	45
Kreamer at al 2011	Vacuum glazed flat plate- estimation	100°C	5	
He et al 2012	Glass evacuated-tube solar collectors- Experiment	45°C	1.25	55
Edgar Arturo et al 2013	2-axis sun-tracking concentrator (Dish) collector –The results based on experiment work with 6 TEG devices	150°C	5	50

As seen in the table above, the STEG system shows a good potential to maximise the electric efficiency of the rooftop system. The literature suggests that STEG maximum power efficiency of 5% can be achieved. Even the purpose of this research was to design a prototype STEG to contribute further to solar energy market; however, the steady state power efficiency recorded in this research was only 1 %. Even though the electricity provided by this system is low compared to some results reported, it is still to be accounted as a stand-alone system to provide electricity in addition to the hot water powered from clean energy source. This small electricity provided could make a big difference in circumstances where providing electricity and maintenance would be particularly difficult, such as in a desert or distant places.

The research contributed to the STEG energy field by providing calculation techniques; one of the techniques was developed to estimate the heat absorbed and lost by the solar absorber, and by analysing the balance of heat transfer and losses through the STEG system. Another technique to estimate the optimum design ratio of thermoelectric legs (cross sectional area and length), which can be added to the SHW system in order to achieve the optimum heat and electric power was developed. The established technique contributes to the research area by suggestion the optimum STEG system optimisation; the optimisation provides a trade-off between the TEG aspect ratio and SHW size, which improves the overall STEG system efficiency. The optimisation also provided a guide to the designer (manufacturer) and users with good prediction of what size they should use. This will save the user's time of examining different TEGs with different aspect ratios and save manufacturing cost by using less material.

6.7 THERMAL AND ELECTRICAL POWER OUTPUT FROM A REALISTIC SYSTEM

The smallest system under Condition 5 provides the highest electrical power under vacuum operation, based on the results obtained from this investigation. To determine the optimal TEG geometry (i.e., the ratio of area to length (A/L) for maximum electrical power output, the developed calculation technique was employed using the parameters based on the TEG module of the smallest size. The TEG area (A x 2N) was given a constant value as ($1x10^{-3}m^2$ x 62), the input heat power was assumed to be 23 W and Tc was assumed to be maintained at 95 ^{o}C. By examining various length values, the corresponding temperature difference was established and, consequently, the thermal and electrical power was estimated. The results are shown in Figure 6.12 below.

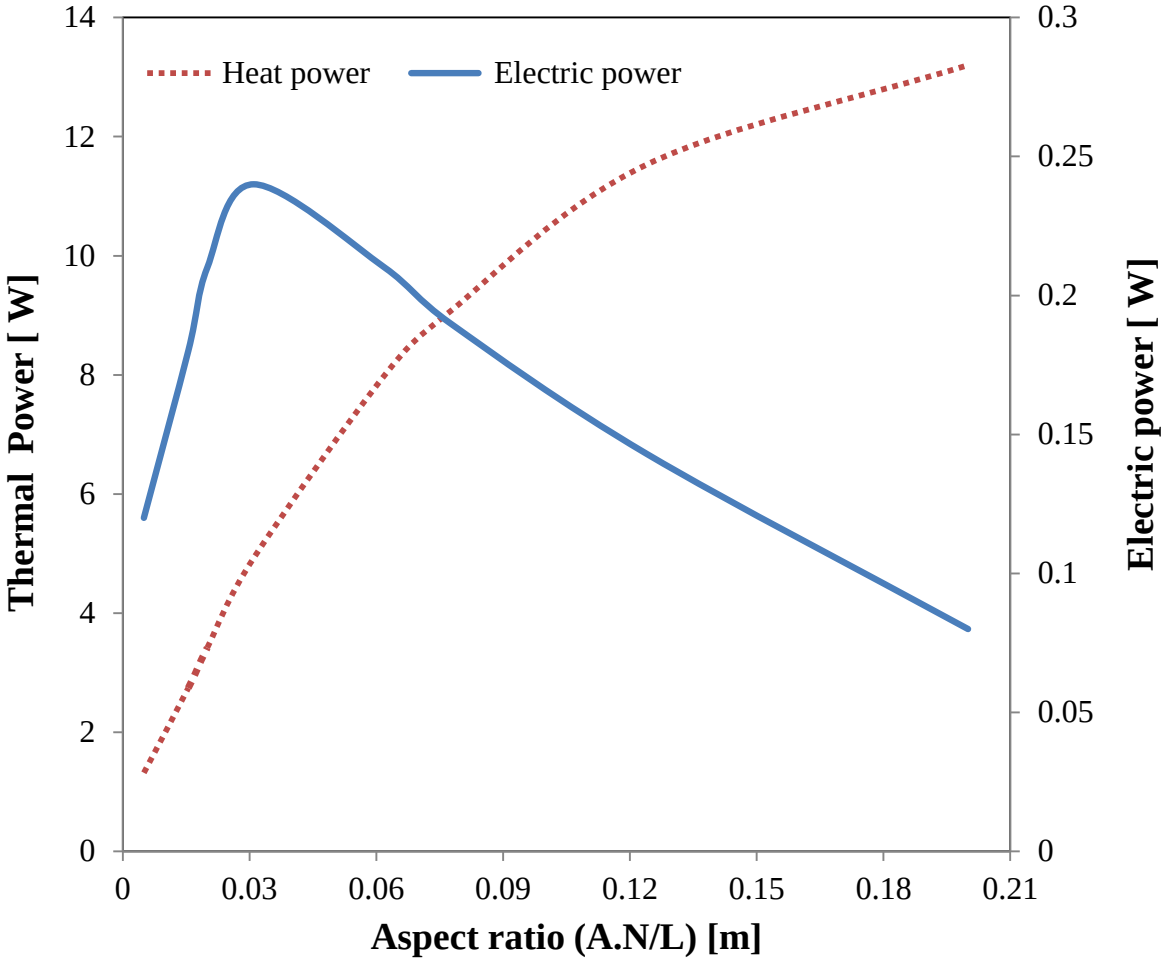

Figure 6.12 Calculated thermal and electrical power as a function of deferent aspect ratio of the area to length of the thermo element in a TEG.

As shown, the calculated values for the thermal and electrical power are displayed as a function of the ratio (A/L) of the thermo element in a TEG. This shows similar parameters to those of the system with the smallest TEG operating at a higher vacuum level (where the convective heat loss was neglected in the calculation (equation 3.19). Comparing the calculated results to the experimental results (for the system with Sample Id of Z1 and aspect ratio of 0.031), it can be seen that the estimated result was higher than the measured results by 14%. The optimal ratio for thermo elements of the TEG to obtain the maximum electrical

power can be determined from Figure 6.12, which gives a dimension of 1 mm x 1 mm x 2mm as shown in Figure 6.13.

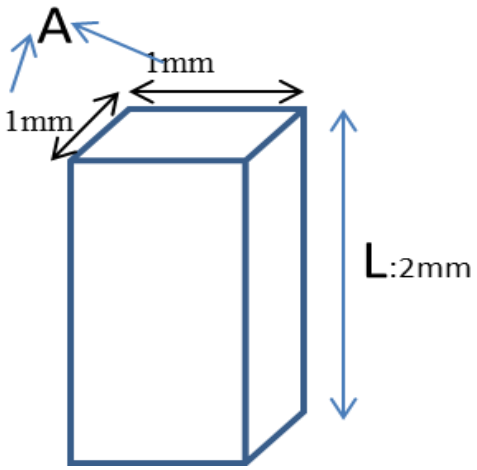

Figure 6.13 The optimal aspect ratio of area to length for the thermo elements in a TEG to obtain maximum electrical power output indicated by both the experimental and calculated results.

The experimental results were obtained from the constructed laboratory scale systems with an absorber area of 0.08 x 0.08 m^2. The maximum electrical output is achieved in a system that uses the smallest TEG under Condition 5. To estimate the electrical output of a realistic system that has an absorber area of 1 m^2, a total of 155 TEGs is required, which would provide approximately 31 W of electricity and 1 kW of thermal power, if there was a vacuum level of $5x10^{-2}$ mbar and light intensity was concentrated to 3500 $W.m^{-2}$. An additional cost to the solar hot water system would be expected at approximately £2,500 (this estimates is based on the price of the TE module purchased from retailers on a small quantity, the real cost is expected significantly lower if large quantity is required). Based on the results obtained from the system that uses the largest TEG and operates under Condition 5, it is estimated that approximately 21 W of electricity and 2.5 kW of thermal power would be expected from a realistic solar absorber with an area of 1 m^2. This would be using a total of 155 largest TEGs, with an additional cost in the region of £4600 (similarly, it is likely to be

overestimated). The system with the smallest TEG size under Condition 5 is more suitable if more electricity is required, while the system with the largest TEG size is more preferable if large thermal power output is overwhelming consideration.

6.8 CONCLUSION

The behaviour of heat and electrical power production, from a flat panel solar thermoelectric system under different environmental conditions, was investigated. The results showed that minimising the convective heat loss has a positive effect on system performance. The conversion efficiencies of heat and electricity generation are improved by reducing the heat loss from the system, achieved by operating the system under vacuum environment. Comparing the results obtained from the operation without vacuum to those under a vacuum level of 5×10^{-2} mbar, the electrical power efficiency of the system with the smallest TEG is improved by approximately 65% and the thermal power by approximately 37%. Furthermore, the results obtained from this investigation provide essential knowledge and experimental confirmation of the role of the TEG geometry on the thermal and electrical power outputs under different operating conditions. The understanding in this aspect is crucial to the optimal design of solar thermoelectric systems for achieving maximum efficiencies and power outputs.

CHAPTER 7: CONCLUSIONS AND FUTURE WORK

7.1 CONCLUSIONS

This project investigated the feasibility and performances of combined heat and power generation using a solar thermoelectric system based on a flat panel solar collector. A unique aspect of this system is the dual role of thermoelectric generator that serves as both heat exchanger and generator. Prototype systems on a laboratory-scale were designed and constructed to facilitate the experimental investigation, which is supported by theoretical simulation. The main focus of this research concentrated on the study of geometrical influence of the thermoelectric generator on the performances of heat and power production of the proposed solar thermoelectric system. The main achievements are as follows:

A technique to determine the light absorption by a solar absorber was established and its suitability for this investigation was validated. The technique, referred to as the "slope technique," provides a simple and effective method to estimate the thermal energy generated in the solar absorber by light irradiation. In addition, this technique also proved to be useful in determining the thermal energy transferred from the solar absorber into the hot water. Compared with the usual technique based on the Fourier's law, the slope technique provides more accurate estimation of the thermal energy transferred into the hot water because it takes into account the contribution from the radiation. The ability to determining the input energy facilitates the evaluation of the efficiencies of the proposed system.

A laboratory-scale solar thermoelectric system was designed and constructed based on an initial prototype built and tested in the first stage of this investigation. The system facilitates the study of performances of the solar thermoelectric system in different environmental conditions, in particular, under different vacuum levels. The capability of the system being able to operate in different environmental conditions is crucial in determining the optimal thermoelectric generator for achieving the maximum thermal and electrical power output. Apart from meeting the requirement of controlling of the operating environmental conditions, the system allows the light irradiation over the full-spectrum to enter into the vacuum chamber with minimal losses.

A systematic experimental investigation was carried out in an attempt to understand the effect of the size of a thermoelectric generator on the performances of heat and power generation in relation to various heat losses in the system. This involved a series of experiments with 5 thermoelectric generators of different sizes and tested in 5 different operating environmental conditions during the transient and steady-state. A substantial amount of experimental data has been collected from this detailed investigation. The experimental results reveal that the power outputs of both heat and electricity generated by the solar thermoelectric system are strongly depended on the aspect ratio of thermoelectric generators. In general, thermal power output increases with increasing the aspect ratio of the thermoelectric generator, while the maximum electrical power output is obtained at an optimal aspect ratio that depends on the intensity of light irradiation and operating environmental conditions. In addition, the optimal aspect ratio decreases with an increase in vacuum level. This indicates that a small size thermoelectric generator is needed in order to achieve the maximum electrical power output if operated in high vacuum level. This finding can have a significant impact on the cost of the system.

A simplified model was developed to provide theoretical support for studying the geometrical influence of thermoelectric generators on the performances of the proposed flat-panel solar thermoelectric system. The model was validated using the experimental data obtained from this investigation. The results show a good agreement between the calculated and observed values. The benefit of the developed model is that it facilitates the investigation of a wide range of the sizes of thermoelectric generators, which are not available from commercially available products, and different operating environmental conditions, which is not achievable using the existing facilities.

The experimental results, together with the calculated results from the developed technique, indicate that a flat-panel solar thermoelectric system can convert some of the thermal energy (converted from light irradiation) into electricity. However, the amount of electricity generated is significantly lower than the thermal energy generated. This is due to the thermal energy density and temperature in a solar thermal system is much lower than the ideal application case required by thermoelectric generators. Consequently, based on the state-of-the-art thermoelectric technology, a flat-panel solar thermoelectric system will primarily be used for hot water production with the capability of generating a small portion of electricity. Furthermore, the amount of electricity generated by the system can be varied to some extent by changing the aspect ratio of thermoelectric generator. The maximum power output that can be achieved from such a system is close to 1% using small thermoelectric generator operating in vacuum at expense of reduced thermal power output. This represents an electrical power output of ~ 30 W and thermal power output of ~2 kW from a typical rooftop solar thermal collector of 6 m^2.

7.2 FURTHER WORK

There are a number of interesting areas, which have not been investigated due to the time constraint or outside the scope of this investigation, but worth of exploring in the future work. These include:

1. It has been observed that the thermal energy transferred from the solar absorber to the hot water is significant higher for small size TEGs when measured using the slope technique than that determined using the Fourier's law. This difference may be explained by the fact that the technique based on the Fourier's law neglected the convection and radiation heat transfer between the solar absorber and the hot water, leading to the actual thermal energy transfer into the hot water underestimated. If this is confirmed by the further work, the thermal efficiency of the system using smaller TEG will be much higher than these currently estimated.

2. An effect way to increase the electrical power output and conversion efficiency of TEGs is to increase the temperature difference across the TEG. High temperature at the hot side of TEG can be achieved by employing high concentration technologies such as parabolic mirrors or heliostats. The investigation in this direction may provide high electrical power output solar thermoelectric system than these flat-panel systems.

3. Further development of theoretical model to improve the accuracy and its predictive power. Carrying out detailed simulation study to identify the optimal size of TEG for given applications.

4. Increasing the vacuum level decreased the heat loss due to the convection, and henceforth this increases the temperature difference across TEGs, leading to an improvement

in the system efficiency. The proposed system could be implemented on a larger scale in the practical world, and the vacuum level could be increased to the typical vacuum level of evacuated solar hot-water tubes. It has been suggested by Yin (2005) and Ayompea et al (2011) that a vacuum level of 10^{-6} mbar can be achieved using evacuated tube, which would lead to reduced heat loss and consequently, improvement in the system efficiency.

5. To investigate the feasibility of improving the system efficiency by incorporating TEG with a PV system. There is heat generated in PV cells. In addition, the irradiation in the infrared wavelength is not utilised by PV cells, which can be further used by TEG to convert it into electricity.

REFERENCES

1. Alamiri, Abdallah. 2013. The Energy efficiency guidebook: The Gulf Organization for Industrial Consulting. Available online at http://www.goic.org.qa/Arabic/documents/Energy%20Guide%20Book-2013.pdf . Accessed on 17/January/2013.

2. Al-Karaghouli, Ali. 2007. Renewable energy research in critical investment for Arab Region. WIPO/IDB Regional Seminar for Arab Countries on Intellectual Property and Transfer of Technology, Riyadh Saudi Arabia, 4-6 June 2007. Available online on http://www.wipo.int/edocs/mdocs/arab/en/wipo_idb_ip_ryd_07/wipo_idb_ip_ryd_07_2.pdf. Accessed on 22/January/2013.

3. Amatya, R. and Ram, R. 2010. Solar thermoelectric generator for micropower applications. *Journal of Electronic Materials* 39(9): 1735–1740.

4. Amrutkar, S.K., Ghodke, S. and Patil, K.N. 2012. Solar Flat Plate Collector Analysis. IOSR Journal of Engineering 2(2): 207-213.

5. Andreas Bitschi, 2009. Modelling of thermoelectric devices for electric power generation - Phd Thiess. Swiss Federal Institute of Technology –Zurich. Diss. ETH No. 18441 .Available online at: http://e-collection.library.ethz.ch/eserv/eth:470/eth-470-02.pdf. Accessed on 24/September/2014.

6. Andy Walker. 2013. Solar Energy. Technologies and project delivery for buildings. John Wiley & Sons, Inc. Walker ISBN: 978-1-118-13924-0

7. Arturo, E. Urbiola, C. and Vorobiev, Y. 2013. Investigation of Solar Hybrid Electric/Thermal System with Radiation Concentrator and Thermoelectric Generator. International Journal of Photoenergy 2013: 1-7.

8. Arvizu, D., P. Balaya, L. Cabeza, T. Hollands, A. Jäger-Waldau, M. Kondo, C. Konseibo, V. Meleshko,W. Stein, Y. Tamaura, H. Xu, R. Zilles, 2011: Direct Solar Energy. In IPCC Special Report on Renewable Energy Sources and Climate Change Mitigation [O. Edenhofer, R. Pichs-Madruga, Y. Sokona,K. Seyboth, P. Matschoss, S. Kadner, T. Zwickel, P. Eickemeier, G. Hansen, S. Schlömer, C. von Stechow (eds)], Cambridge University Press, Cambridge, United Kingdom and New York, NY, USA.

9. Azarbayjani, M. and Anderson, J. 2008. Assessment of Solar Energy Conversion Technologies-Application of Thermoelectric Devices in Retrofit an Office Building. Proceedings of the Sixteenth Symposium on Improving Building Systems in Hot and Humid Climates, Plano, TX, December 15-17, 2008. ESL-HH-08-12-29.

10. Baker, S,E. and Parker, J,D. 2009. Use of alternative energy. In Doty, S. and Turner, W.C. (Eds.) Energy Management Handbook. Seventh Edition. Publisher Fairmont Press. ISBN-10: 142008870X.

11. Bob Ramlow and Benjamin Nusz. 2010. A Comprehensive Guide to Solar Water and Space Heating Systems: Revised and expanded edition. New Society Publishers. First addition, ISBN139781550924497.

12. Boinpally Bhargav. 2010. Solar Energy, the best solution to crisis. California Takshila University,Electrical Engineering. Available online at http://www.ctuniv.org/magzine_solar_en_bhargav.pdf. Accessed on 24/September/2014.

13. Boubault, B. Claudet, O. Faugeroux, G. Olalde,2013. Accelerated aging of a solar absorber material subjected to highly concentrated solar flux, Energy Procedia 49 (2014) 1673 – 1681.

14. Bradford, Jaryn. Bean, Frances. Chapman, Tom. and Byrne, Tom. 2011. Here comes the sun, a field trial of solar water heating systems . The Energy saving trust 2011. Available online at http://www.energysavingtrust.org.uk/content/download/29047/348320/version/3/file/Here+comes+the+sun+-+solar+hot+water+report.pdf. Accessed on 22/September/2013.

15. Brown, S. R., Kauzlarich, S. M., Gascoin, F. and Snyder, G. J. 2006, Yb14MnSb11: New High Efficiency Thermoelectric Material for Power Generation. Chem Inform, 37: no. doi: 10.1002/chin.200625011.

16. Buchwald, Kristian. 2007. White paper- fused silica transmission gratings. Ibsen Photonics Publication, Version: 1.0 March 2007 Available online at: http://www.dops.dk/pictures/pdf/ibsen_whitepaper.pdf. Accessed on 18/September/2014.

17. Cai, Yonghua. Xiao, Jinsheng. Zhao, Wenyu. Tang, Xinfeng. and Zhang, Qingjie. 2011. A General Model for the Electric Power and Energy Efficiency of a Solar Thermoelectric Generator. Journal of Electronic Materials 40(5): 1238-1243.

18. Camacho, E.F. Berenguel, M. Rubio, F,R. and Martínez, D. 2012. Control of Solar Energy Systems. ISBN 978-0-85729-915-4. DOI 10.1007/978-0-85729-916-1.Springer London Dordrecht Heidelberg New York.

19. Chetan Singh Solanki. 2013. Solar Photovoltaic Technology and Systems. A Manual for Technicians, Trainers and Engineers. Publisher: Prentice-Hall of India Pvt.Ltd (1 Mar 2013). ISBN-10: 8120347110.

20. Chittum, Anna. 2013. How electric utilities can find value in CHP. The piplication of council of an energy –efferent economy (ACEEE) . White paper. July 2013.Available online at : http://aceee.org/white-paper/electric-utilities-and-chp . Accessed on 17/July/2014.

21. Chu, Yinghao, 2011. Review and comparison of different solar energy technologies, Tech. rep. Global Energy Network Institute (2011).

22. D. Champier, J. P. Bedecarrats, M. Rivaletto and F. Strub. 2010. Thermoelectric Power Generation from Biomass Cook Stoves. Energy, Vol. 35, No. 2, 2010, pp. 935-942. http://dx.doi.org/10.1016/j.energy.2009.07.015.

23. D. Mills. 2001. Advances in solar thermal electricity technology. Solar Energy. Volume 76, Issues 1–3, January–March 2004, Pages 19–31.Solar World Congress 2001.

24. Das, Kishor, Nand . Mihir Kr. Das. Anirudha Narain and Vibhaw Prakash Ranjan.2010. Fuzzy model representation of thermosyphon solar water heating system. Solar Energy. Volume 84, Issue 6, June 2010, Pages 948–955.

25. De Winter, Francis. 1991. Solar Collectors Energy storage and Materials. Publisher: The MIT Press. ISBN-10: 0262041049.

26. Deutsche Gesellschaft Für Sonnenenergie (DOG),2009. Planning & Installing Solar Thermal Systems, Second edition. ISBN-13: 978-1-84407-760-1.Publisher Earthscan Ltd.

27. Dey, Christopher. 2004.Heat transfer aspect of an elevated linear absorber. Solar Energy, 76(1-3), 243-249. doi:10.1016/j.solener.2003.08.030.

28. Doolittle, Alan. 2007. Lecture 2: The nature of light, reading assignment – Chapter 2 of PVCDROM. Available online at http://users.ece.gatech.edu/~alan/ECE4833/Lectures/Lecture2_PropertiesOfSunlight.pdf. Accessed on 04/ July/ 2014.

29. Du, Qungui. Xinqiang Jiang . Xiaodan Zhang And Junling Gao 2011. Influence of structure parameters on performance of the thermoelectric module. Journal of Wuhan University of Technology-Mater. Sci. Ed., vol. 26, no. 3, pp. 464-468, Jul. 2011. DOI 10.1007/s11595-011-0250-0.

30. Duffie, John A and A. Beckman, William. 2013. Solar Engineering of Thermal Processes. Fourth Edition. Publisher: John Wiley and Sons, Inc. ISBN: 978-0-470-87366-3.

31. Edgar Arturo, Chávez Urbiola and Yuri Vorobiev. 2013. Investigation of Solar Hybrid Electric/Thermal System with Radiation Concentrator and Thermoelectric Generator. International Journal of Photoenergy.Volume 2013, article ID 704087, 7 pageshttp://dx.doi.org/10.1155/2013/704087.

32. Energy Saving Trust. 2006. Solar water heating systems– guidance for professionals, conventional indirect models. London www.greenspec.co.uk/files/energy/EST-solarWaterHeating.pdf.(2006).

33. Enrico Zambolin. 2011. Theoretical and Experimental Study of Solar Thermal Collector Systems and Components. Ph.D Thesis,Università degli Studi di Padova. Available online at: http://paduaresearch.cab.unipd.it/3461/1/tesivers4.pdf. Accessed on 17/June/2014.

34. EUREC Agency. 2011. The Future for Renewable Energy 2: Prospects and Directions. Publisher: Routledge; 2nd edition. ISBN-10: 190291631X.

35. European Photovoltaic Industry Association (EPIA), 2014. Global Market Outlook for Photovoltaics until 2016, EPIA, Brussels.http://files.epia.org/files/Global-Market-Outlook-2016.pdf.

36. Fan, Hongnan., Randeep Singh, Aliakbar Akbarzadeh.2011. Electric Power Generation from Thermoelectric Cells Using a Solar Dish Concentrator.Journal of Electronic Materials May 2011, Volume 40, Issue 5, pp 1311-1320.

37. Franz Mauthner and Werner Weiss, 2014.Solar Heat Worldwide Markets and Contribution to the Energy Supply 2012. publications of the Solar Heating and Cooling Programme (SHC)- International Energy Agency(2012).

38. Fulya Verdier 2011. Desalination using renewable energy. Final report. Middle East and North Africa, World Bank, 2012, ISBN (paper): 978-0-8213-8838-9.

39. Global Energy Writing Team. 2012. Global Energy Assessment: Toward a Sustainable Future. Publisher: Cambridge University Press. First addition.ISBN 9781 10700 5198.

40. Goetzbergera, Adolf, Christopher Hebling and Hans-Werner Schockb.2002. Photovoltaic materials, history, status and outlook. Materials Science and Engineering: R: Reports.Volume 40, Issue 1, 1 January 2003, Pages 1–46.

41. Green Systems UK. A questions and answers on solar hot water. Available online at: http://greensystemsuk.com/questions-and-answers/questions-answers-on-solar-hot-water/. Accessed on 20/July/2014.

42. Greening ,Benjamin and Azapagic, Adisa. 2014. Domestic solar thermal water heating: A sustainable option for the UK? Renewable Energy, Volume 63, March 2014, Pages 23–36.

43. Gregory Nellis and Sanford Klein. 2009. Heat Transfer book. Chapter 10, example 10.4-1: Absorptive and Emissivity of a Solar Selective Surface. Publisher : Cambridge University Press– ISBN 10: 0521881072 / 0-521-88107-2.

44. He, W. Sub, U. Wanga, Y. Riffat, S. and Jia, J. 2012. A study on incorporation of thermoelectric modules with evacuated-tube heat-pipe solar collectors. Renewable Energy **37**(1): 142–149.

45. Homola, C.A. 2009. Solar domestic hot water heating systems design, installation &maintenance. Available online at ; http://www.asseplumbing.org/chapters/NOH%20SolarWtrHtg%20Pres.pdf. Accessed on 17/June2014.

46. Hueck, U. 2013. An innovative concept for large-scale concentrating thermal power plants. In Stolten, D. and Scherer, V. (Eds.) Transition to Renewable Energy Systems. Weinheim, Germany: Wiley-VCH Verlag GmbH & Co. KGaA, Weinheim, Germany. doi: 10.1002/9783527673872.ch10. Publisher : Wiley-VCH Verlag GmbH & Co. KGaA. First addition.

47. International Committee of the Red Cross. 2012. Solar water heating system. A how to manual. Available online at: http://www.icrc.org/eng/assets/files/2012/icrc-solar-water-heating-systems.pdf. Accessed on 23/June/2014.

48. J. Pandolfini, B. Greska and A. Krothapalli. 2011. ESC cost effective solar simulator. Poster submitted to Florida Energy & Sustainability Centre. Available online at:

http://www.floridaenergy.ufl.edu/wp-content/uploads/Poster-5_32-ESC-Cost-Effective-Solar-Simulator-09-20101.pdf. Accessed on 22/June/2014.

49. J.-P. Fleurial, G.J. Snyder, J.A. Herman, M. Smart and P. Shakkottai. 1999. Miniaturized Thermoelectric Power Sources. SAE Technical Paper 1999-01-2569, 1999, doi:10.4271/1999-01-2569.

50. Jeffery Quill. Greg Fedor. Patrick Brennan and Eric Everett. 2007. Quantifying the indoor light environment. Testing for light stability in retail & residential environments. International Conference on Digital Printing Technologies. Pages 514-1043., pp. 689-698(10).

51. Jercan, Andrei Ştefan. 2006. The simplified calculation of the Flat plate solar collector. Proceedings of International Conference on Sustainable Energy Technologies, Nottingham, UK. 2006, p. 1-5.

52. Jincan, Chen. 1996. Thermoelectric analysis of a solar-driven thermoelectric generator. Journal of Applied Physics 79(5): 2717-2721.

53. Juanicó, L.E. Rinalde, G.F. 2009. Comparative analysis of photovoltaic and thermoelectric panels for powering isolated homes. Journal of Renewable and Sustainable Energy **1** 043107. http://dx.doi.org/10.1063/1.3180391.

54. K Gelin, DPhil Thesis,2004. Preparation and characterization of sputter deposited dpectrally selective solar absorbers, Uppsala University, Sweden (2004).Available online at : http://www.diva-portal.org/smash/get/diva2:164328/FULLTEXT01.pdf. Accessed on 24/September/2014.

55. Kaddour, A. Benyoucef, B. 2013. Influence of Cooling Constant on the Stirling Dish System Efficiency. Journal of Earth Science & Climate Change 4(4): 150-152.

56. Kalogirou, Soteris .2004. Solar thermal collectors and applications. Progress in Energy and Combustion Science . Volume 30, Issue 3, 2004, Pages 231–295.

57. Kennedy, C.E. 2002. Review of mid- to high-temperature solar selective absorber materials.Tech. Rep. TP-520-31267, National Renewable Energy Laboratory (2002).

58. Kraemer, Daniel. Poudel, Bed. Ping Feng, Hsien. Caylor, Christopher. Xiao. Yu, Bo. Xiao,Yan. Wang, Xiaowei. Wang, Dezhi. Muto, Andrew. Kenneth, McEnaney. Matteo, Chiesa. Ren, Zhifeng and Chen, Gang. 2011. High performance flat panel solar thermoelectric generators with high thermal concentration, Nature Materials 10,532–538(2011)doi:10.1038/nmat3013.

59. Kumara, Ashwani. Kumarb, Kapil. Kaushikc, Naresh. Sharmaa,Satyawati and Mishrad ,Saroj. 2010. Renewable energy in India: Current status and future potentials. Renewable and Sustainable Energy Reviews. Volume 14, Issue 8, October 2010, Pages 2434–2442.

60. L,M, Ayompea. A, Duffya. S,J, McCormackb and M,Conlon. 2011. Validated TRNSYS model for forced circulation solar water heating systems with flat plate and heat pipe evacuated tube collectors. Applied Thermal Engineering, Volume 31, Issues 8–9, June 2011, Pages 1536–1542.

61. L.M. Ayompea, A. Duffya, d, S.J. McCormackb, and M. Conlonc. 2011. Validated TRNSYS model for forced circulation solar water heating systems with flat plate and heat pipe evacuated tube collectors. Applied Thermal Engineering. Volume 31, Issues 8–9, June 2011, Pages 1536–1542.

62. Lewis, Nathan and Crabtree, George. 2005. Basic Research Needs for Solar Energy Utilization: report of the Basic Energy Sciences Workshop on Solar Energy Utilization, April 18-21, 2005. US Department of Energy, Office of Basic Energy Science, Washington, DC. Available online at: http://authors.library.caltech.edu/8599/. Accessed on 22/July2014.

63. Li Xu Zhifeng Wang. Xin Li, Guofeng Yuan. Feihu Sun. Dongqiang Lei. 2013. Dynamic test model for the transient thermal performance of parabolic trough solar collectors. Solar Energy.Volume 95, September 2013, Pages 65–78.

64. Liu Lei. Zhang Suo-Liang. Ma Ya-Kun. Wu Guo-Hao. Zheng Shu-Kai and Wang Yong-Qing. 2013. Modelling and structure optimization of flat-panel thermal concentrated solar thermoelectric device. Acta Phys. Sin 2013, Vol. 62 Issue (3): 038802.doi:10.7498/aps.62.038802.

65. Luque, A and Hegedus, S. 2003. Handbook of Phovoltaic Science and Engineering. Publisher: John Wiley & Sons, Inc. First addition. 1132 pages. ISBN 0-471-49196-9.

66. M, Kubo. M, Shinoda. T, Furuhata and K, Kitagawa. 2005. Optimization of the incision size and cold-end temperature of a thermoelectric device. Energy, Vol. 30, No. 11-12, 2005, pp. 2156-2170.

67. M, Lina. K, Sumathyb. Y, J, Dai. R,Z,Wanga. Y, Chena. 2013. Experimental and theoretical analysis on a linear Fresnel reflector solar collector prototype with V-shaped cavity receiver. Applied Thermal Engineering. Volume 51, Issues 1–2, March 2013, Pages 963–972.

68. Mahtani, Pratish. Yeghikyan, Davit. Kherani, Nazir P and Stefan Zukotynski. 2007. The use of amorphous silicon in fabrication a photovoltaic thermal system, 2nd Canadian solar buildings conference Calgary, June 10 -14.2007.

69. Mancini, Mancini, Thomas R.; James Chavez,; Gregory Kolb,. 1994. Solar thermal power today and tomorrow Mechanical Engineering-CIME. Journal Name: Mechanical Engineering; (United States); Journal Volume: 116:8. DOE:AC04-76DP00789.

70. Masters, G,M. 2013. Renewable and Efficient Electric Power Systems. Publisher:: John Wiley & Sons, Inc. 2nd Edition..ISBN: 978-1-118-14062-8.

71. Mats, Blomqvist. Ola, Blomster. Stuart, Campbell. Magnus, Pålsson. Frank, Becker and Wolfram, Rath. 2011. All-in-Quartz Optics for Low Focal Shifts, SPIE Photonics West Conference in San Francisco, Proc. SPIE 7912, Solid State Lasers XX: Technology and Devices, 791216 (February 15, 2011); doi:10.1117/12.874597.

72. Michael Kohl, Michaela Georgine Meir , Philippe Papillon , Gernot M. Wallner and Sandrin Saile 2012. Polymeric Materials for Solar Thermal Applications. First addition, Wiley-VCH, Weinheim (2012).

73. Miljkovic , Nenad and Evelyn N. Wang. 2011. Modeling and optimization of hybrid solar thermoelectric systems with thermosyphons. Solar Energy.Volume 85, Issue 11, November 2011, Pages 2843–2855.

74. Mills, D. 2004.Advances in solar thermal electricity technology, Solar Energy, Volume 76, Issues 1–3, January–March 2004, Pages 19–31.

75. Min,Gao. 2010. Thermoelectric energy harvesting, Energy Harvesting for Autonomous Systems. Publisher: Artech House. 308 pages (2010) 135-157. ISBN 978156937185.

76. Mohamed, Ahmed. Al-Habaibeh, Amin. Abdo, Hafez and Juma,Mohamed. 2013. An investigation into the current utilisation and prespecctive of renewable energy resources and techniques. Energy Research Journal 4 (1): 15-23, 2013. ISSN: 1949-0151.

77. Morrison, G, L. 2013. Solar collectors: Solar energy the state of the art. Gordon J. (Ed). ISES position papers, Publisher Routledge, 2013. ISBN 1134275897, 9781134275892. 2001, 724 pages. pp. 145-221.

78. Naito, H. Kohsaka, Y. Cooke, and Arashi, H. 1996. Development of a solar receiver for a high-efficiency thermionic/ thermoelectric conversion system. Energy. Volume 58, Issues 4–6, October–December 1996, Pages 191–195. Selected Proceedings of the ISES 1995: Solar World Congress. Part II.

79. Natalia Kulichenko and Jens Wirth. 2012. Concentrating solar power in developing countries. Regulatory and financial incentives for scaling up. A World Bank study. ISBN (electronic): 978-0-8213-9608-7.

80. Ngô, Chirstian and Natowitz, Joseph. 2009. Our Energy Future: Resources, Alternatives and the Environment. Publisher: John Wiley & Sons. First addition, ISBN-10: 0470116609.512 pages.

81. Ogbonnaya, Emmanuel and Wises, Leland. 2013. Micro Solar thermal power harvesting using thermoelectric generator. National Society of Black Engineers. Proceedings of 38th Annual Convention, Pittsburgh, PA.

82. Ojike O, 2011. Characterization of a flat plate double glazed solar collector. Continental J. Renewable Energy 2 (2): 10 – 18. ISSN: 2251 – 0494.

83. Omer, S.A. and Infield, D.G. 2000. Design and thermal analysis of a two stage solar concentrator for combined heat and thermoelectric power generation. Energy Conversion and Management 41(7): 737-756.

84. Omer,S. A. and Infield, D. G. 1998. Design optimization of thermoelectric devices for solar power generation. Solar energy materials and solar cells. VOL 53(ISSUE 1-2), 67-82.

85. P,M,E, Koffi. H,Y, Andoh. P,Gbaha. S, Touréb. G, Ado. 2008. Theoretical and experimental study of solar water heater with internal exchanger using thermosiphon system. Energy Conversion and Management. Volume 49, Issue 8, August 2008, Pages 2279–2290.

86. Patyk, Andreas. 2013. Thermoelectric generators for efficiency improvement of power generation by motor generators – Environmental and economic perspectives, Applied Energy. Volume 102, February 2013, Pages 1448–1457.

87. Pearce, J.M. 2009. Expanding photovoltaic penetration with residential distributed generation from hybrid solar photovoltaic and combined heat and power systems. Energy. Volume 34, Issue 11, November 2009, Pages 1947–1954.

88. Performance. Petros J. Axaopoulos, and Emmanouil D. Fylladitakis,2013. Performance and economic evaluation of a hybrid Photovoltaic/Thermal solar system for residential applications. Energy and Buildings. Volume 65, October 2013, Pages 488–496.

89. Pitz-Paal, R., Buck, R., Heller, P., Hirsch, T. and Steinmann, W.-D. (2013). Solar thermal power production in transition to renewable energy systems (eds D. Stolten and V. Scherer), Wiley-VCH Verlag GmbH & Co. KGaA, Weinheim, Germany. doi: 10.1002/9783527673872.ch17.

90. Qi Zhang, Amen Agbossou, Zhihua Feng and Mathieu Cosnier. 2010. Solar micro-energy harvesting based on thermoelectric and latent heat effects. Part II: Experimental analysis. Sensors and Actuators A: Physical. Volume 168, Issue 2, 10 August 2011, Pages 335–342.

91. R. Amatya and R. J. Ram. 2010. Solar Thermoelectric generator for micro power applications. Journal of Electronic Materials, Vol. 39, No. 9, 2010, pp. 1735-1740. http://dx.doi.org/10.1007/s11664-010-1190-8.

92. Renewables. 2012. Global Status Report (Paris: REN21 Secretariat).

93. Richard. J. D. Tilley. 2004. Understanding solids: the science of materials. John Wiley & Sons, New York (2004). ISBNs: 0 470 85275 5 (Hbk) 0 470 85276 3 (Pbk).

94. Rockendorf, G., Sillmann, R., Podlowski, L. and Litzenburger, B. 1999. PV-hybrid and thermoelectric collectors. Solar Energy . Volume 67, Issues 4–6, 1999, Pages 227–237 .

95. Rowe, D.M. 1999. Thermoelectrics, an environmentally-friendly source of electrical power. Renewable Energy. Volume 16, Issues 1–4, January–April 1999, Pages 1251–125616.

96. Rowe, D.M. 2006. Thermoelectric waste heat recovery as a renewable energy source. International Journal of Innovations in Energy Systems and Power, Vol. 1, no. 1 (November 2006)

97. Rowe, D.M. and Min, G. 1997. Evaluation of thermoelectric modules for power generation. Journal of Power Sources. Volume 73, Issue 2, 15 June 1998, Pages 193–198.

98. Rowe, M and Min,G. 1996. Design theory of thermoelectric modules for electrical power generation. IEE Proceedings - Science, Measurement and Technology, vol. 143, no. 6, p. 351, 1996. ISSN :1350-2344.

99. Rupeni Mario, 2000. Efficiency monitoring of solar how water systems in the Fiji Islands and the United kingdom of Tonga. SOPAC Technical Report 318.available online at: http://ict.sopac.org/VirLib/TR0318.pdf . Accessed on 14/September/2014.

100. S, Rittidech. A, Donmaung. K, Kumsombut. 2009. Experimental study of the performance of a circular tube solar collector with closed-loop oscillating heat-pipe with check valve (CLOHP/CV). Renewable Energy. Volume 34, Issue 10, October 2009, Pages 2234–2238.

101. S. Blundell, K. 2006. Concepts in Modern Physics. Oxford University Press. ISBN 78-019-856769-1(2006) 247.

102. S. Meir, C. Stephanos, T. H. Geballe and J. Mannhart. 2013. Highly-efficient thermoelectronic conversion of solar energy and heat into electric power, Journal of renewable and sustainable energy 5,043127.2013.

103. Saffa Riffat and Abdulkarim Mayere. 2012. Performance evaluation of V-Trough solar concentrator for water desalination applications. Applied Thermal Engineering. Volume 50, Issue 1, 10 January 2013, Pages 234–244.

104. Saffa Riffat and Xiaoli Ma. 2003. Thermoelectrics: a review of present and potential applications. Applied Thermal Engineering 23(8): 913-935.

105. Saint Gobain Glass. Glass Physical properties, Mechanical properties. Available online at: http://ro.saint-gobain-glass.com/upload/files/physical_properties.pdf. Accessed on 19/June/2014.

106. Salvatore Abate, Riccardo Barberi, Giovanni Desiderio, Giuseppe Lombardo, 2012. Solar radiation heat absorber for a stirling motor- Patents- Applicant Innova Solar Energy S.R.L. Publication number WO2012016873 A1 .Application number PCT/EP2011/062744. PCT number PCT/EP2011/062744.

107. Santora, R. and Maronde, S. 2011. The advantage of the thermoelectric devices. Available online at: http://me1065.wikidot.com/thermoelectrics.Accessed on 15/August/2014.

108. Sargent and Lundy. 2003. Assessment of parabolic trough and power tower solar technology cost and Performance forecasts. NREL Subcontracted Report. Sargent & Lundy LLC Consulting Group. Chicago, Ill. October 2003.

109. Schott Robax-Transparent glass ceramics for extreme temperature. Available online at. http://www.vitrea.fi/images/images_muut_tuotteet/schott_brosch_robax_e.pdf . Accessed on 14/June/2014.

110. Sharma, A.M., Tyagi, W., Chen, C.R. and Buddhi, D. 2009. Review on thermal energy with phase change materials and applications. Renewable and Sustainable Energy Review. Volume 13, Issue 2, February 2009, Pages 318–345.

111. Sharma,Atul.Tyagi ,V,V. Chen, C,R. Buddhi, D. 2009. Review on thermal energy storage with phase change materials and applications, Renewable and Sustainable Energy Reviews. Volume 13, Issue 2, Pages 318–345.

112. Solar Energy Industries Association. 2012. Concentrating Solar Power. Available online at: http://www.seia.org/sites/default/files/cspfactsheet-120223144940-phpapp01.pdf . Accessed on 15/September/2014.

113. Sudhansu S. Sahoo, Suneet Singh and Rangan Banerjee, 2012. Steady state hydrothermal analysis of the absorber tubes used in Linear Fresnel Reflector solar thermal system. Solar Energy. Volume 87, January 2013, Pages 84–95.

114. Suter, C, Tomes, P, Weidenkaff, A. and Steinfeld, A. 2011. A solar cavity-receiver packed with an array of thermoelectric converter modules. Solar Energy. Volume 85, Issue 7, July 2011, Pages 1511–1518.

115. T. M. Tritt, H. Böttner and L. Chen. 2008. Thermoelectrics: Direct Solar Thermal Energy Conversion, MRS Bulletin, Vol. 33, No. 4, 2008, pp. 366-368.

116. Terry Hendricks. 2006. Engineering scoping study of thermoelectric generator systems for industrial waste heat recovery. Industrial Technologies Program, U.S. Department of Energy (2006).

117. Thirugnanasambandam, M., Iniyan, S. and Goic, R. 2010. A review of solar thermal technologies. Volume 14, Issue 1, January 2010, Pages 312–322.

118. Tian, Y. And Zhao, C.Y. 2013. A review of solar collectors and thermal energy storage in solar thermal applications. Applied Energy. Volume 104, April 2013, Pages 538–553 Applied Energy 104: 538-553.

119. Tripathi, M.N. and Bhandari, C.M. 2005. Material parameters for thermoelectric performance. Pramana Journal of Physics.Vol 65. Vol.3. Pages: 469-479.

120. US Department of Energy. 2013. The History of Solar. Washington, D.C.: Energy Efficiency and Renewable Energy. US Department of Energy. Available online at: http://www1.eere.energy.gov/solar/pdfs/solar_timeline.pdf.Accessed on 24/September/2014.

121. Viebahn, P., Kronshage, S., Trieb, F. and Lechon, Y. 2008. Final Report of Technical Data, Costs, and Life Cycle Inventories of Solar Thermal Power Plants. New Energy Exteralities Developments (NEEDS). Available online at: http://www.needsproject.org/RS1a/RS1a%20D12.2%20Final%20report%20concentrating%20solar%20thermal%20power%20plants.pdf . Accessed on 24/September/2014.

122. Volker Quaschning. 2010. Renewable Energy and Climate Change, John Wiley & Sons, Ltd. Second addition.ISBN 978-0-470-74707-0.

123. W. He, Y. Su, Y. Q. Wang, S. B. Riffat, and J. Ji. 2012. A study on incorporation of thermoelectric modules with evacuated-tube heat-pipe solar collectors. Renewable Energy, vol. 37, no. 1, pp. 142-149, Jan. 2012.

124. Watts, G.W. 2000. Legionnaires Disease: An Overview. Available online at: http://www.saudiaramco.com/content/dam/Publications/Environews/Environews%20Winter%202011/Legionnaires_Disease.pdf . Accessed on 15/July/2013.

125. Weinstein, L.A., McEnaney, K. and Chen, G. 2013. Modelling of thin-film solar thermoelectric generators. Journal of Applied Physics.Vol 113.Issue16. http://dx.doi.org/10.1063/1.4803123.

126. Weiss, W., Bergmann, I. and Faninger, G. 2003. Solar heating worldwide markets and contribution to energy supply 2003. International energy Egency (IEA) Solar Heating & Cooling Programme. Available online at: http://www.iea-shc.org/Data/Sites/1/publications/shc_annual_report_2005.pdf. Accessed on 22/January/2013.

127. Werner Weiss and Franz Mauthner. 2012. Solar heat worldwide markets and contribution to the energy supply 2010. Available online at: http://solarthermalworld.org/sites/gstec/files/Solar%20Heat%20Worldwide_Edition_2012%20(3).pdf . Accessed on 17/January/2013.

128. William B. Stine and Richard B. Diver. 1994. A compendium of solar Dish/Stirling Technology. Sandia National Laboratories, Report SAND-7026 UC-236, USA. available online at: www.osti.gov/scitech/servlets/purl/10130410 . Accessed on 17/January/2013.

129. World Scientific Publishing Co. Pte. Ltd. ISBN-13 978-981-4324-74-8. pp. 171-197. doi: 10.1142/9789814324755_0008. Available online at: http://www.worldscientific.com/worldscibooks/10.1142/7942. Accessed on 17/ January/2014.

130. X. Gou, H. Xiao and S. Yang. 2010. Modelling experimental study and optimization on Low-temperature waste heat thermoelectric generator system. Applied Energy, Vol. 87, No. 10, 2010, pp. 3131-3136. http://dx.doi.org/10.1016/j.apenergy.2010.02.013.

131. Xi, H., Luo, L. and Fraisse, G. 2007. Development and applications of solar-based thermoelectric technologies. Renewable and Sustainable Energy Reviews. Volume 11, Issue 5, June 2007, Pages 923–936.

132. Xu Xinjian, Yang Lei, Zhang Xiaosong and Peng Donggen. 2009. Review on the Development of Flat-Plate Solar Collector and its Building-Integrated Designing. Proceedings of ISES World Congress 2007 (Vol. I – Vol. V) 2009, pp 623-626.

133. Y. Y. Hsiao, W. C. Chang and S. L. Chen. 2010. A Math- ematic Model of Thermoelectric module with applications on waste heat recovery from automobile engine. Energy, Vol. 35, No. 3, 2010, pp. 1447-1454. http://dx.doi.org/10.1016/j.energy.2009.11.030.

134. Yang Mu and Pan Rongfang. 2011. Harvesting sunlight: Solar photovoltaic industry in China. China's Industrial Development in the 21st Century. Published by World Scientific Publishing Co. Pte. Ltd. ISBN-13 978-981-4324-74-8. ISBN-10 981-4324-74-4. Available online on : http://www.worldscientific.com/worldscibooks/10.1142/7942#t=toc. Accessed on 25/Septemper/2014.

135. Yazawa, K., Wong, V.K. and Shakouri, A. 2012. Thermal challenges for solar concentrator thermoelectric CHP system. A paper published in 13th IEEE ITHERM Conference. San Diego, CA. May 30 2012-June 1 2012. Digital Object Identifier :10.1109/ITHERM.2012. Page(s):1144 – 1150. 6231552. ISBN: 1087-9870. Available online at: http://ieeexplore.ieee.org/xpl/login.jsp?tp=&arnumber=6231552&url=http%3A%2F%

2Fieeexplore.ieee.org%2Fstamp%2Fstamp.jsp%3Ftp%3D%26arnumber%3D6231552 . Accessed on 17/July/2014.

136. Yin Zhiqiang and Zhou Xiaowen 2011, Developments of solar thermal utilization in china. Available online at: http://active.cput.ac.za/energy/past_papers/DUE/2011/PDF/43.Zhiqiang%20Y.pdf. Accessed on 25/September/2014.

137. Yin Zhiqiang. 2005. Development of solar thermal systems in China. Solar Energy Materials and Solar Cells. Volume 86, Issue 3, 31 March 2005, Pages 427–442.

138. Yu, C. and Chau, K.T. 2010. Thermoelectric automotive waste heat energy recovery using maximum power point tracking. Energy Conversion and Management Volume 50, Issue 6, June 2009, Pages 1506–1512.

139. Zalba, B., Martin, J.M., Cabeza, L.F. and Mehling, H. 2003. Review on thermal energy storage with phase change: materials, heat transfer analysis and applications.Applied Thermal Engineering. Volume 23, Issue 3, February 2003, Pages 251–283.

140. Zhang, L. and Li, C. 2008. The research of solar-heated generation system using CPC collector. The international multi conference of engineers and computer scientists. Vol II. IMECS 2008, 19-21 March, 2008, Hong Kong. ISBN: 978-988-17012-1-3.

BIBLIOGRAPHY

1. Abraham Kribus , Daniel Kaftori, Gur Mittelman , Amir Hirshfeld, Yuri Flitsanov and Abraham Dayan,2006/ Aminiature concentrating photovoltaic and thermal system/ Energy Conversion and Management, Volume 47,Issue20, December 2006, Pages 3582-3590.

2. Ashok Gadgil, Sara Al-Beaini, Merwan Benhabib, Samantha Engelage, Adam Langton. 2007. Domestic solar water heater for developing countries, available online at : http://energy.lbl.gov/staff/gadgil/docs/2007/solar-water-heater-rpt.pdf . Accessed on 06/04/2013.Accssed on 25/September/2014.

3. Baljit Singh and M. Y. Othman 2009.A review on photovoltaic thermal collectors. Journal of renewable and sustainable energy. Volume 1, Issue 6. http://dx.doi.org/10.1063/1.3266963.

4. Chris Vernon 2007, Concentrating Solar Power, available online at: http://www.theoildrum.com/node/2583. Accessed on 25/September/2014.

5. Chuang Yu and K.T. Chau2010, Thermoelectric automotive waste heat energy recovery using maximum power point tracking, Energy conversion and management, Volume 50, Issue 6, Pages 1506-1512.

6. Energy Efficiency Office, Department of the Environment, Small-scale combined heat and power for buildings. Guide 176, Good Practice Programme, UK, 1996. Available online at : http://www.cibse.org/pdfs/GPG176.pdf#search='guide%20176%20smallscale . Accessed on 3/10/ 2012.

7. Energy saving trust 2006, solar water heating systems– guidance for professionals, conventional indirect models .Available online at: http://www.solartwin.com/PDF/Solartwin_response_to_ESTs%20solar_document_CE_131.pdf . Accessed: 25/September/2014.

8. Greenpeace international 2009.Concentration solar power outlook, available onlie at http://www.greenpeace.org/international/en/publications/reports/concentrating-solar-power-2009 . Accessed on 25/September/2014.

9. H. Zhai, Y.J. Dai, J.Y. Wu, R.Z. Wang and L.Y. Zhang 2010, Experimental investigation and analysis on concentrating solar collector using linear Fresnel lens, Energy Conversion and Management, Volume 51, issue 1, January 2010, Pages 48-55.

10. Heng Xiao and Suwen Yang 2010, Modeling, experimental study and optimization on low-temperature waste heat thermoelectric generator system. Applied energy. Volume 87, Issue 10, Pages 3131-3136.

11. K. Qiu, and A.C.S. Hayden2008, Development of a thermoelectric self-powered, Journal of Power Sources, Volume 180, Issue 2, Pages 884-889.

12. Lixi Zhang, Chunlei Li 2008. The Research of Solar-heated Generation System Using CPC Collector. Proceedings of the International MultiConference of Engineers and Computer Scientists 2008 .Vol II. IMECS 2008, 19-21 March, 2008, Hong Kong. Available on line at: http://www.iaeng.org/publication/IMECS2008/IMECS2008_pp1751-1754.pdf. Accssed on 25/September/2014.

13. Maria Brogren, Per Nostell and Björn Karlsson 2001, optical efficiency of a PV–thermal hybrid CPC module for high latitudes ,solar energy, Volume 69, Supplement 6, July-December 2001, Pages 173-185.

14. Mitch fincer.org, The advantage and disadvantages of solar PV technology. Available online at http://www.fincher.org/Misc/AlternateEnergy.shtml accessed on 15/September/2014.

15. Nand Kishor, Mihir Kr. Das, Anirudha Narain and Vibhaw Prakash Ranjan,2010, Fuzzy model representation of thermosyphon solar water heating system , Solar Energy, volume 84, issue 6, June 2010, Pages 948-955.

16. National renewable energy laboratory 2009, Concentrating Solar Power. Available online at http://www.nrel.gov/learning/re_csp.html .Accessed on 15/September/2014.

17. Neil McNiven 2008. Evacuated tube solar water heating.Available online at http://www.reuk.co.uk/Evacuated-Tube-Solar-Water-Heating.htm. Accessedon 20/September/2014.

18. Nicola Armaroli and Vincenzo Balzani 2006, The Future of Energy Supply: Challenges and Opportunities Renawable energy, DOI: 10.1002/anie.200602373. Available online at: http://ethic-forum.unife.it/E602373e_ev-Balzani.pdf . Accessed on 25/September/2014.

19. Onovwiona H. I and Ugursal V.I, 2004, Residential cogeneration systems: review of the current technology, International journal of hydrogen energy. Vol 33, issue 13, pp 3506-3510.

20. P.G. Charalambous G.G. Maidment, S.A. Kalogiro and K. Yiakoumetti, Photovoltaic thermal (PV/T) collectors:A review, Applied thermal engineering, Volume 27, issues 2-3, February 2007, Pages 275-286 .

21. Pascal Affolter, Wolfgang Eisenmann, Hubert Fechner, Matthias Rommel, Anton Schaap, Henrik Sørensen, Yiannis Tripanagnostopoulos, Herbert Zondag,2005.PV/T road map, European guide for the development and market introduction of PV-Thermal technology, European Union under contract no 502775 (SES6). Available online at : http://www.pvtforum.org/pvtroadmap.pdf . Accessed on 11/02/2013.

22. Paul Eccleston 2007, Solar panels-what's on the market. Available online at: http://www.telegraph.co.uk/earth/3295556/Solar-panels-whats-on-the-market.html . Accessed: 06/April/2013.

23. Renawable.com 2010, PV market report, available online at http://www.renewbl.com/2010/03/19/solarbuzz-world-solar-pv-market-reached-6-43-gw-in-2009.html . Accessed: 20/June/2010.

24. Ryan Santora and Scott Maronde, The advantage of the thermoelectric devices. Available online at http://me1065.wikidot.com/thermoelectrics . Accessed on 18/April/2013.

25. S. Maneewan, J. Khedari, B. Zeghmati, J. Hirunlabh, and J. Eakburanawat, 2004, Investigation on generated power of thermoelectric roof solar collector, Renewable Energy Volume 29, Issue 5, April 2004, Pages 743-752.

26. Solar buzz2010, solar module price highlight. Available online at. http://www.solarbuzz.com/facts-and-figures/retail-price-environment/module-prices . . Accessed on 30/April/2013.

27. Sun Max, information guide :solar storage tanks .Available online at: http://www.sunmaxxsolar.com/pdfs/SHW-GIB-005-solar-storage-tanks.pdf . Accessed: 1/June/2013.

28. T. Bergene and O.M. Lovvik 1995, Model calculation on a flat-plate solar heat collector with integrated solar cells. ,Solar Energy Vol. 55, No. 6, pp. 453-462.

29. T.N. Anderson, M. Duke, G.L. Morrison and J.K. Carson,2009,Performance of a building integrated photovoltaic/thermal (BIPVT) solar collector, Solar Energy, volum83, isuue4, April 2009, Pages 445-455.

30. T.T. Chow2010, A review on photovoltaic/thermal hybrid solar technology, Applied Energy, Volume 87, Issue 2, February 2010, Pages 365-379.

31. Thermo technologies, collector efficiency, available online at http://www.thermomax.com/Efficiency.php , accessed on 15/August/2011.

32. USA department of energy. Solar Energy Technologies Program – 2008-2012 Available online at: http://www1.eere.energy.gov/solar/pdfs/solar_program_mypp_2008-2012.pdf. Accessed: 27/Feb/2010.

33. Zhang, Q, Agbossou, A., Feng, Z. and Cosnier, M. 2010. Solar micro-energy harvesting based on thermoelectric and latent heat effects. Part II: Experimental analysis. Sensors and Actuators A: Physical. Volume 163, Issue 1, September 2010, Pages 284–290. DOI: 10.1016/j.sna.2010.06.027.

APPENDIX

Appendix A:

A1: The specification for the black paint used on this research (PAM type) High Temperature Paints

400ml - 400ml

Product code: PNM400 - PAM400

Industrial grade paints, with very good thermal resistance (up to 650°C). Aluminium Grey or Matt Black in colour, with a polyphenylmethylsiloxane resin base along with high-quality pigments and extenders. The heat-resistant paints are perfectly suited to the painting of objects exposed to high temperatures, for example furnaces, car exhaust systems, engines and motorcycles, barbecues etc

---

Key Properties:

- Heat resistant paints suitable for objects exposed to temperatures up to 650°C
- Excellent coverage and flow characteristics
- Good adhesion and anti-corrosion properties
- Available in matt black (PNM) and aluminium grey (PAM)

Electrolube (A division of HK Wentworth Ltd) Ashby Park, Coalfield Way, Ashby de la Zouch,
Leicestershire LE65 1JR United Kingdom

Tel: +44 (0)1530 419600 Email: info@electrolube.com

A2: The results of light intensity measurement for the light bulbs of 150 and 200 Watt

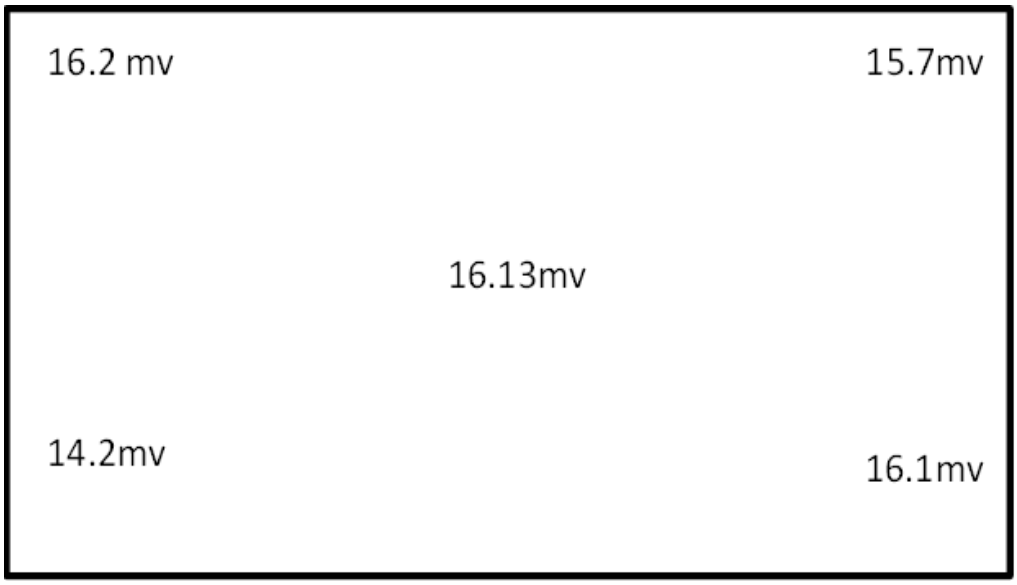

The results in voltage which obtained by payronmeter for the light bulb with intinsity of 150 watt .

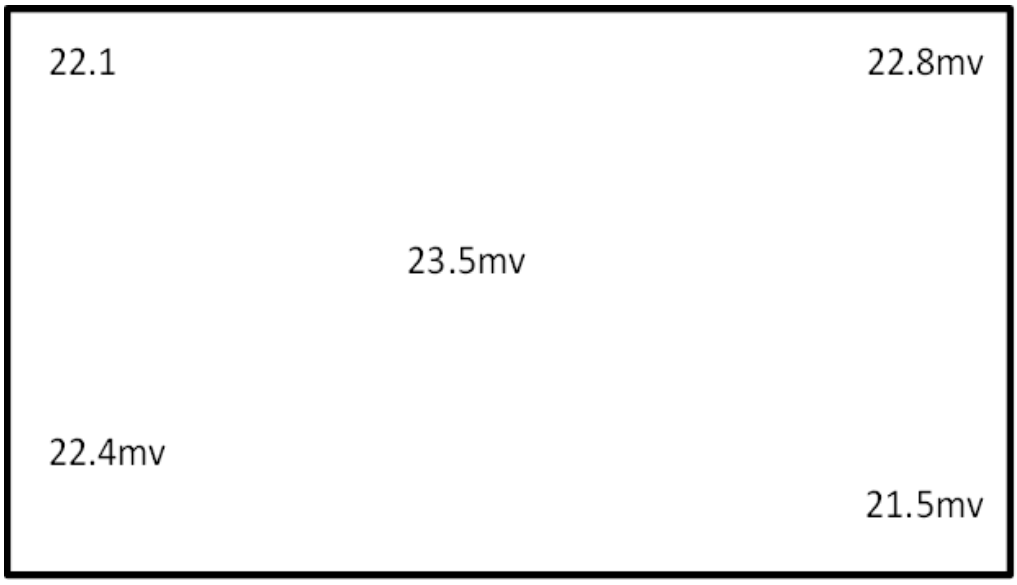

The results in voltage which obtained by payronmeter for the light bulb with intinsity of 200 watt

A3: the repeatability measurements of the light bulbs intensities of 200 & 400 Watt

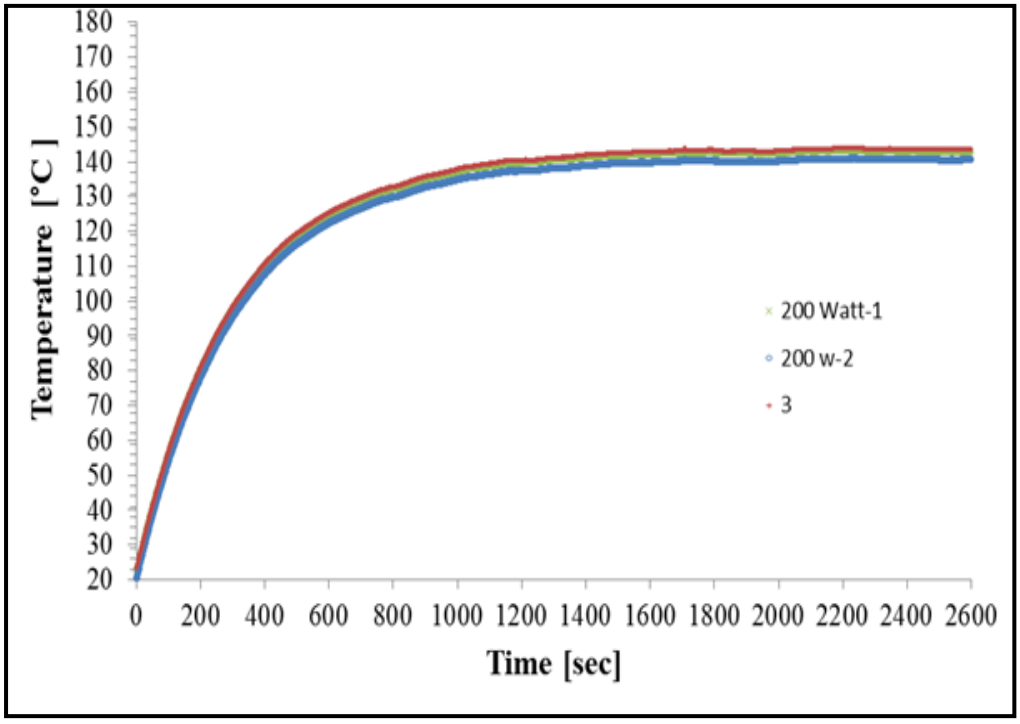

The absorber temperatures (Th) as a function of time in with 3 different measurement of halogen light ID of 200watt.

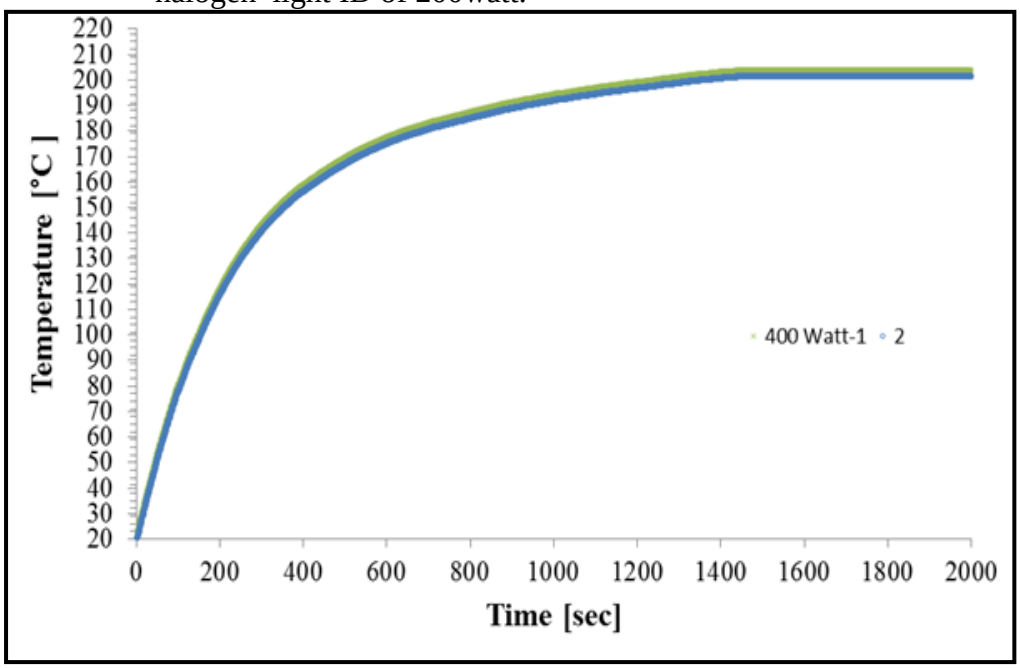

The absorber temperatures (Th) as a function of time in with 3 different measurement of halogen light ID of 400watt.

A4: The manufacturers' data sheets of the used TEG parameters specification.

200°C TEG (Tested at Hot Side Temperature: 200°C, Cold Side Temperature: 50							
RS Part No.	MPN	Couples	V_{oc} (V)	R_{in} (Ω)	I_{max} (A)	P_{max} (W)	T_{max} (°C)
6937028	GM200-127-10-15	127	7.00	7.70	1.60	1.60	200
6937030	GM200-71-14-16	71	3.90	2.10	1.80	1.80	200
6937043	GM200-127-14-16	127	7.00	4.00	3.10	3.10	200
6937040	GM200-31-28-35	31	1.70	0.56	1.30	1.30	200
6937059	GM200-127-28-35	127	7.00	2.30	5.30	5.30	200
6937056	GM200-49-45-30	49	2.50	0.28	5.60	5.60	200
6937068	GM200-49-45-25	49	2.50	0.23	6.80	6.80	200

250°C TEG (Tested at Hot Side Temperature: 250°C, Cold Side Temperature: 50							
RS Part No.	MPN	Couples	V_{oc} (V)	R_{in} (Ω)	I_{max} (A)	P_{max} (W)	T_{max} (°C)
6937071	GM250-127-10-15	127	9.40	7.90	0.59	2.80	250
6937078	GM250-71-14-16	71	5.30	2.40	1.10	2.90	250
6937080	GM250-127-14-16	127	9.40	4.30	1.09	5.10	250
6937093	GM250-31-28-35	31	2.30	0.59	1.95	2.20	250
6937090	GM250-127-28-35	127	9.40	2.40	1.96	9.20	250
6937103	GM250-49-45-30	49	3.60	0.31	5.80	10.60	250

A5: The experiments results to determine the TEG's internal resistances value.

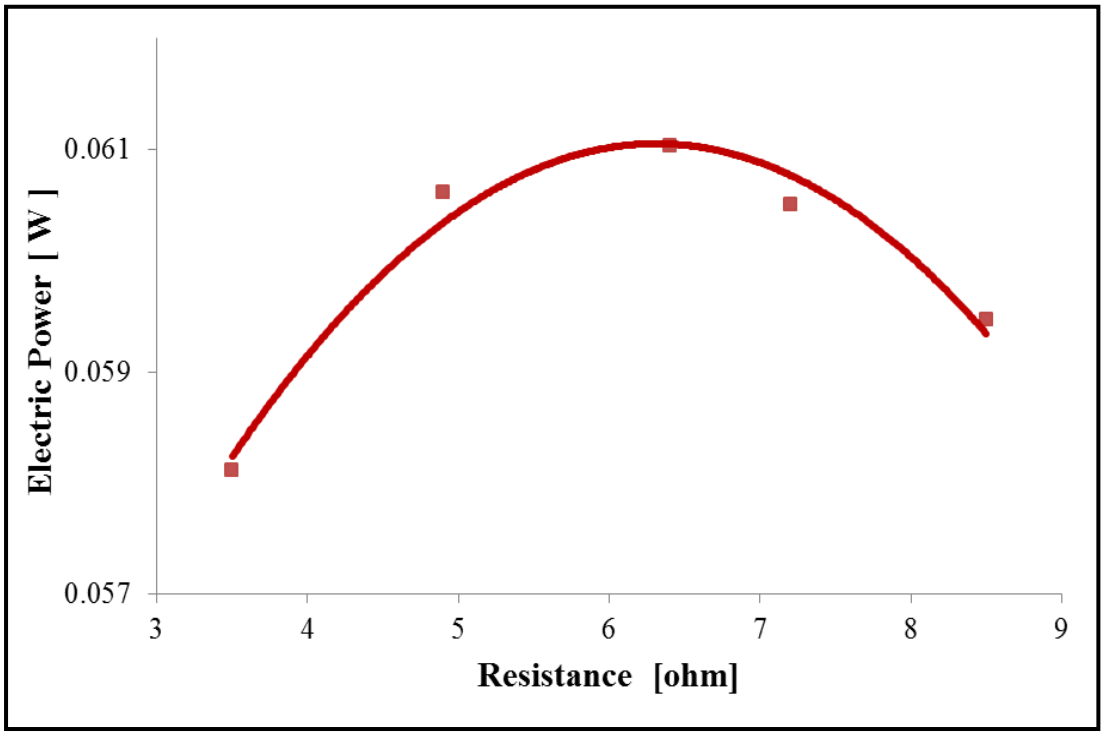

Determined the resistance value (6.5 Ω) of the TEG size with 0.169.

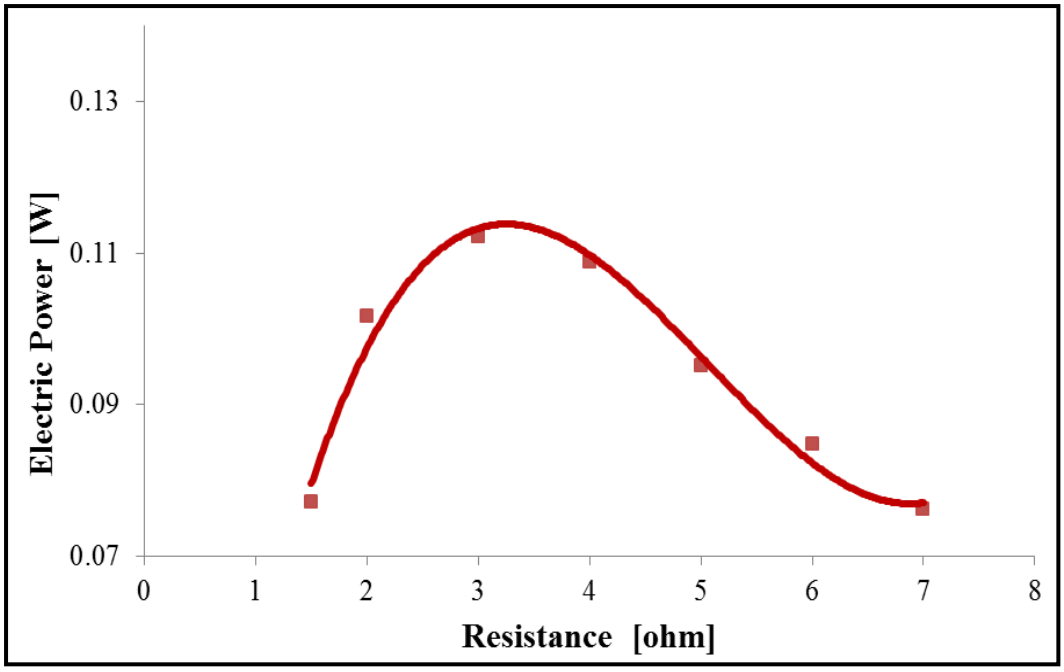

Determining the resistance value (3.5 Ω) of the TEG with size of 0.299.

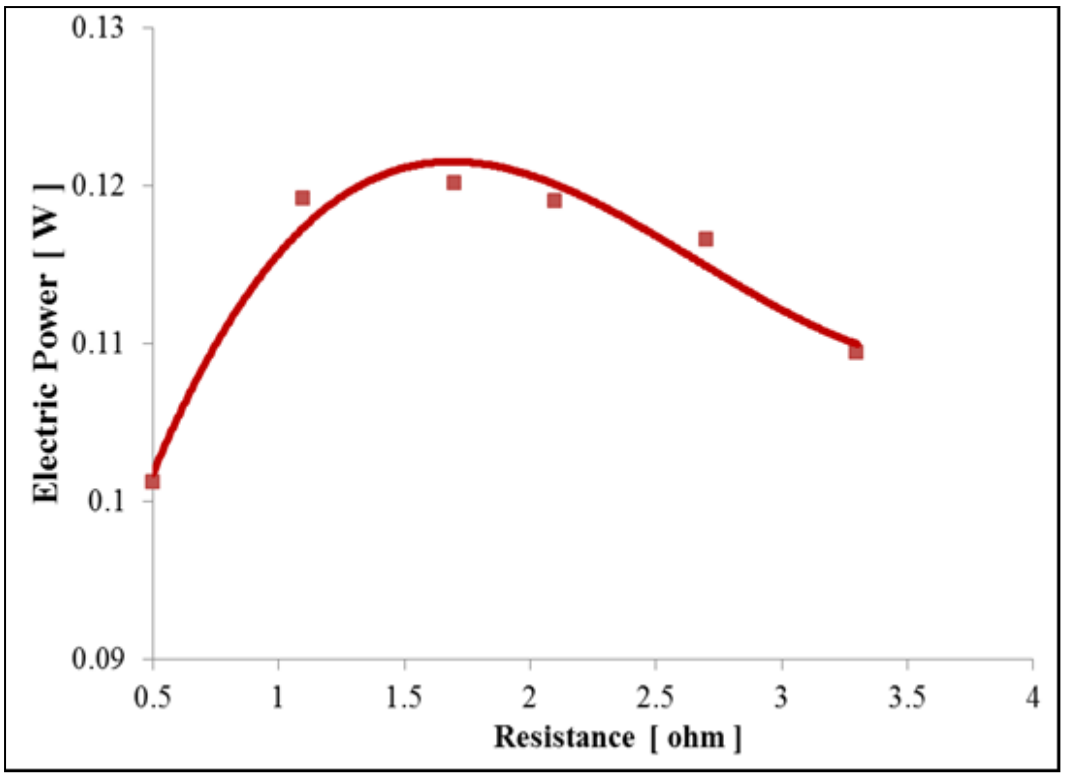

Determining the resistance value (1.6 Ω) of the TEG with size of 0.536.

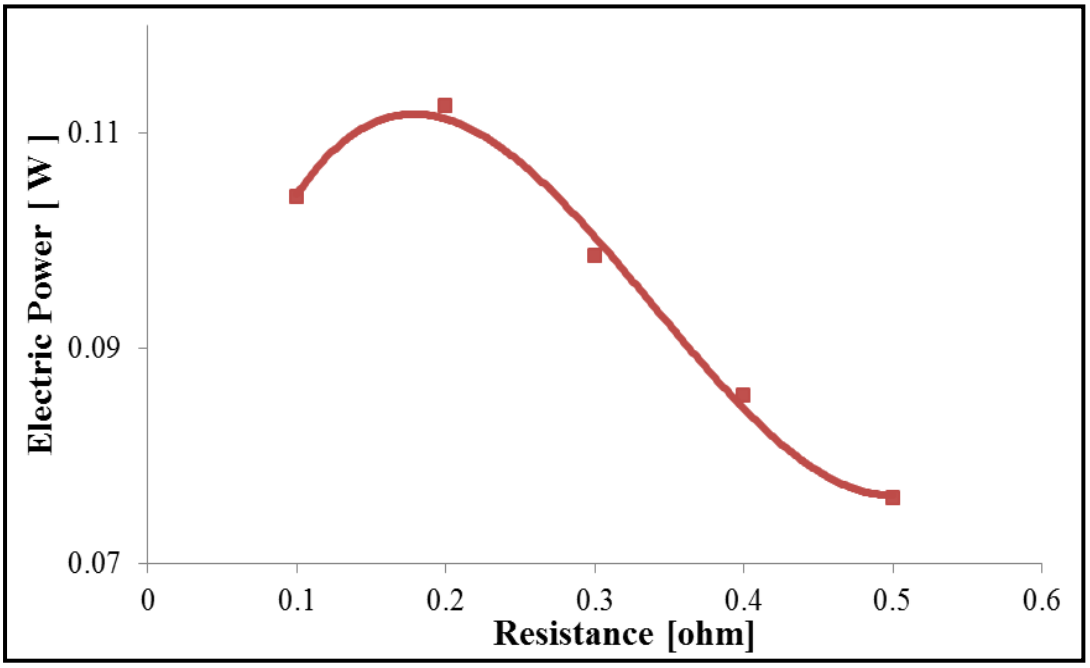

Determining the module internal resistance value (0.2Ω) for the TEG with size of 0.680.

A6: Determine the thermal power (slope technique) from ΔT and Δt relationship.

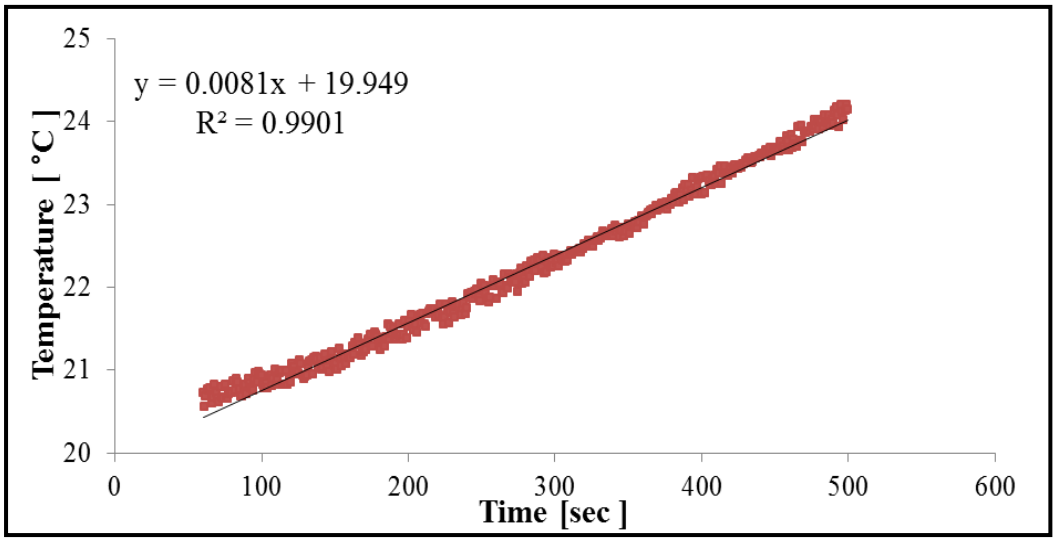

The rate of the Water temperature of system with TEG module ratio of 0.136 as function of time under atmospheric condition.

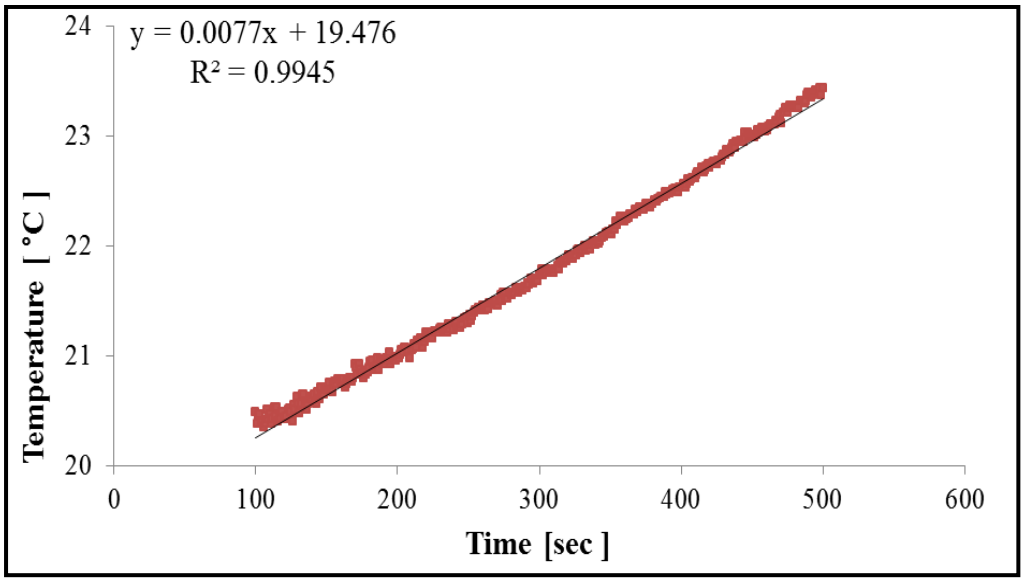

The rate of the water temperature of system with TEG module ratio of 0.169 as function of time under atmospheric condition.

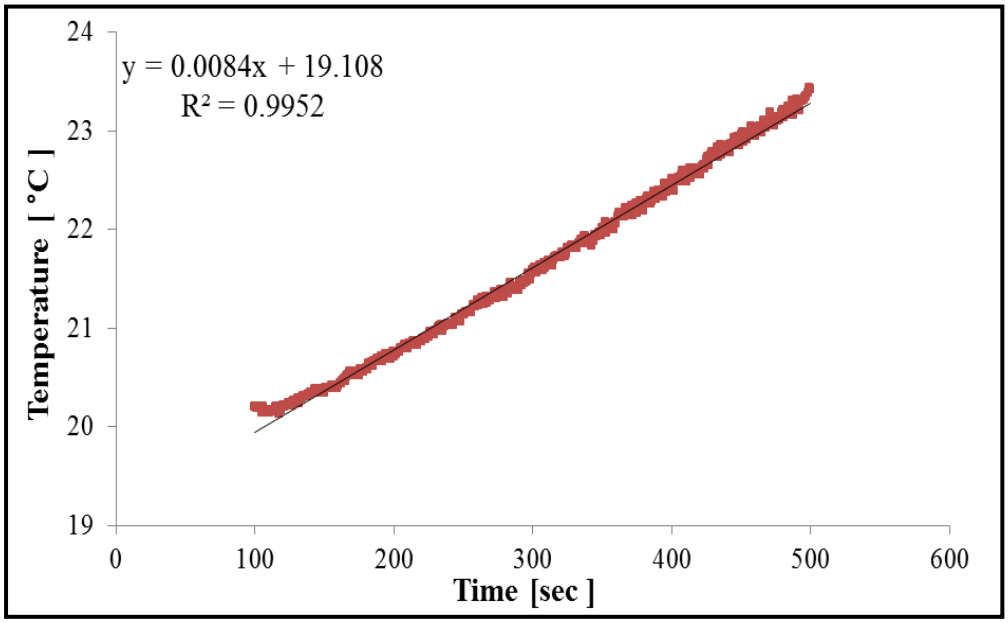

The rate of the water temperature of system with TEG module ratio of 0.299 as function of time under atmospheric condition.

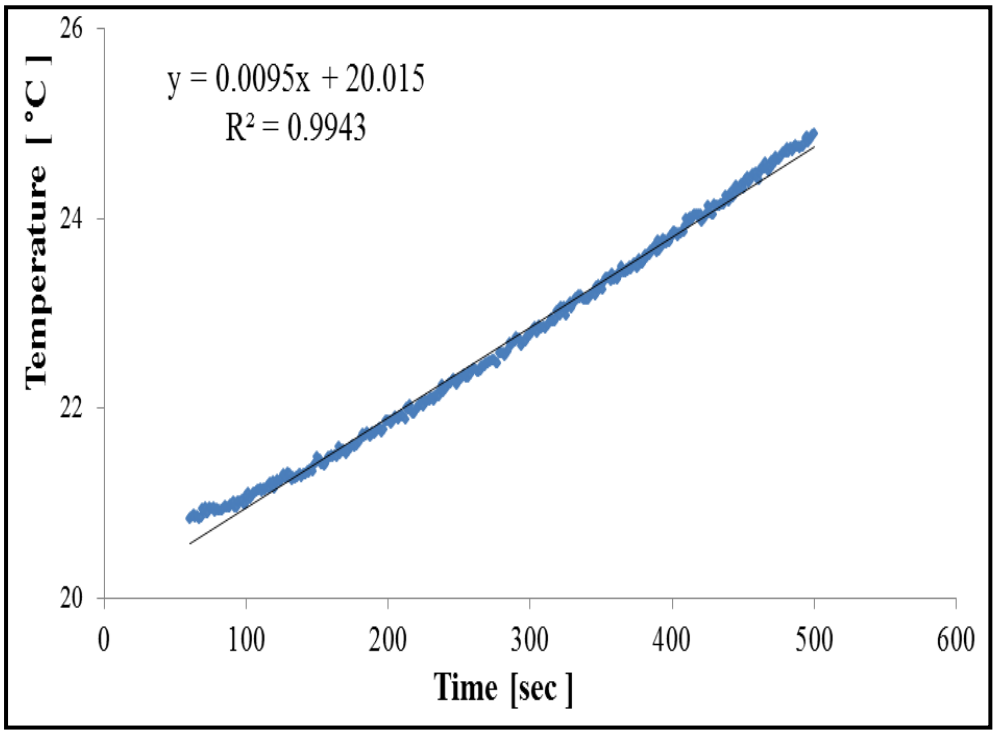

The rate of the water temperature of system with TEG module ratio of 0.536 as function of time under atmospheric condition.

A7: The measurements of the cross-sectional area (A) and length (L) of the thermoelements in all a TEG's.

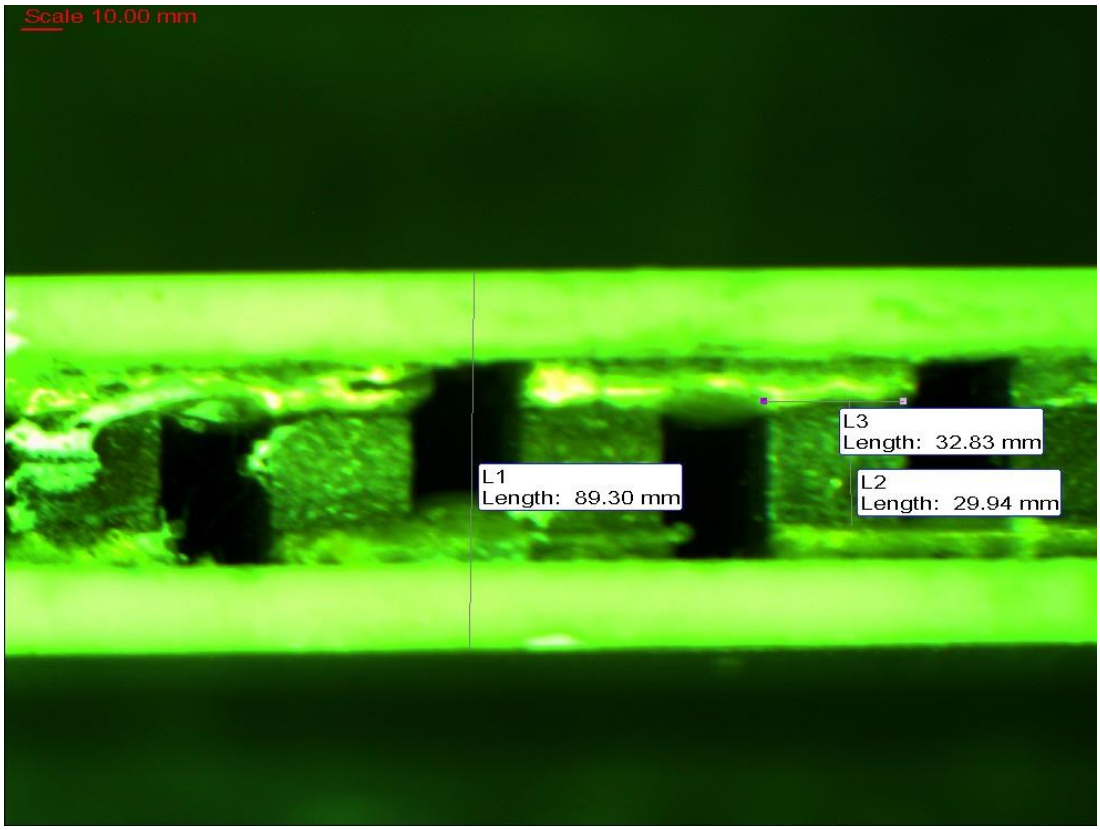

Determination of the geometries of the module size of 0.136.

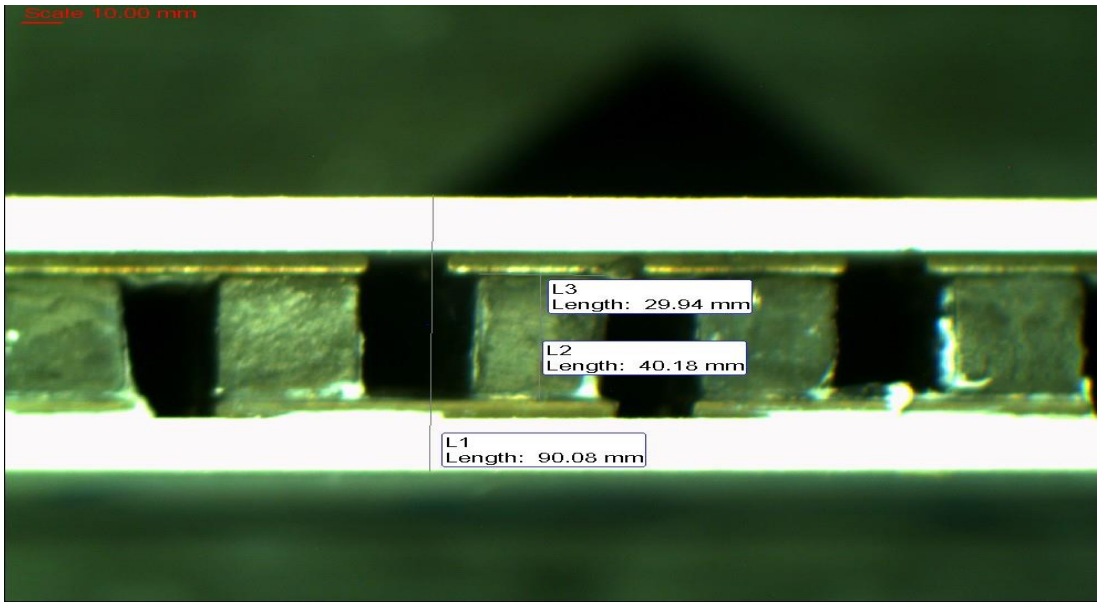

Determination of the geometries of the module size of 0.169

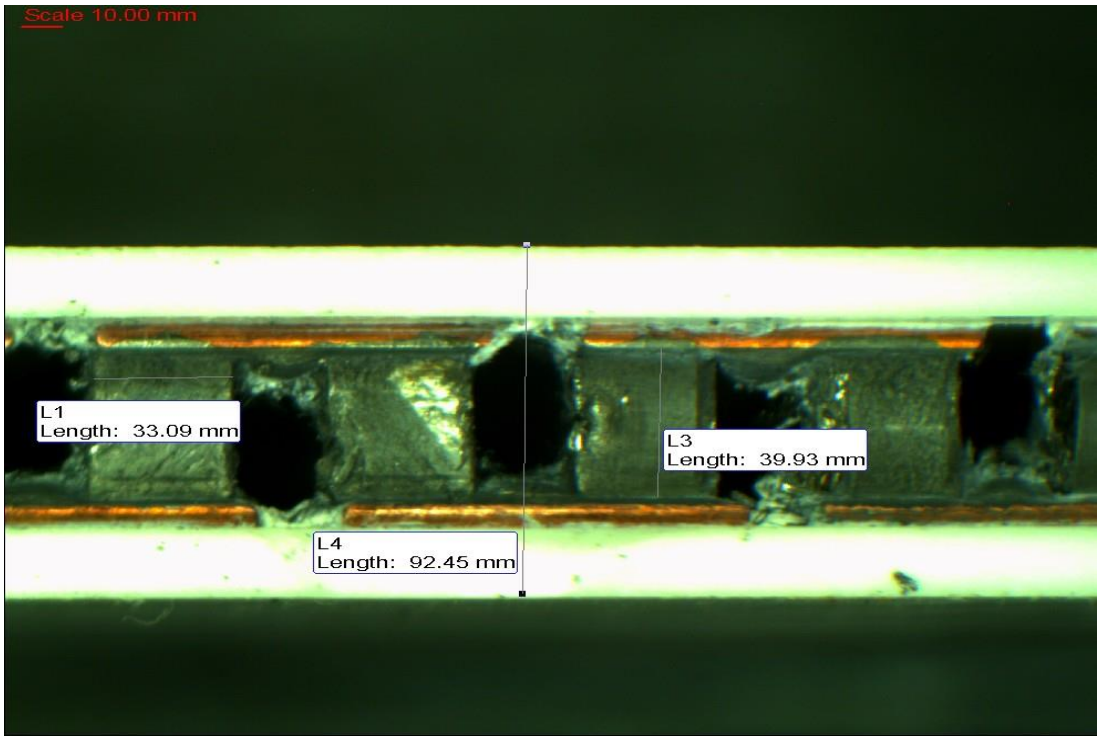

Determination of the geometries of the module size of 0.299.

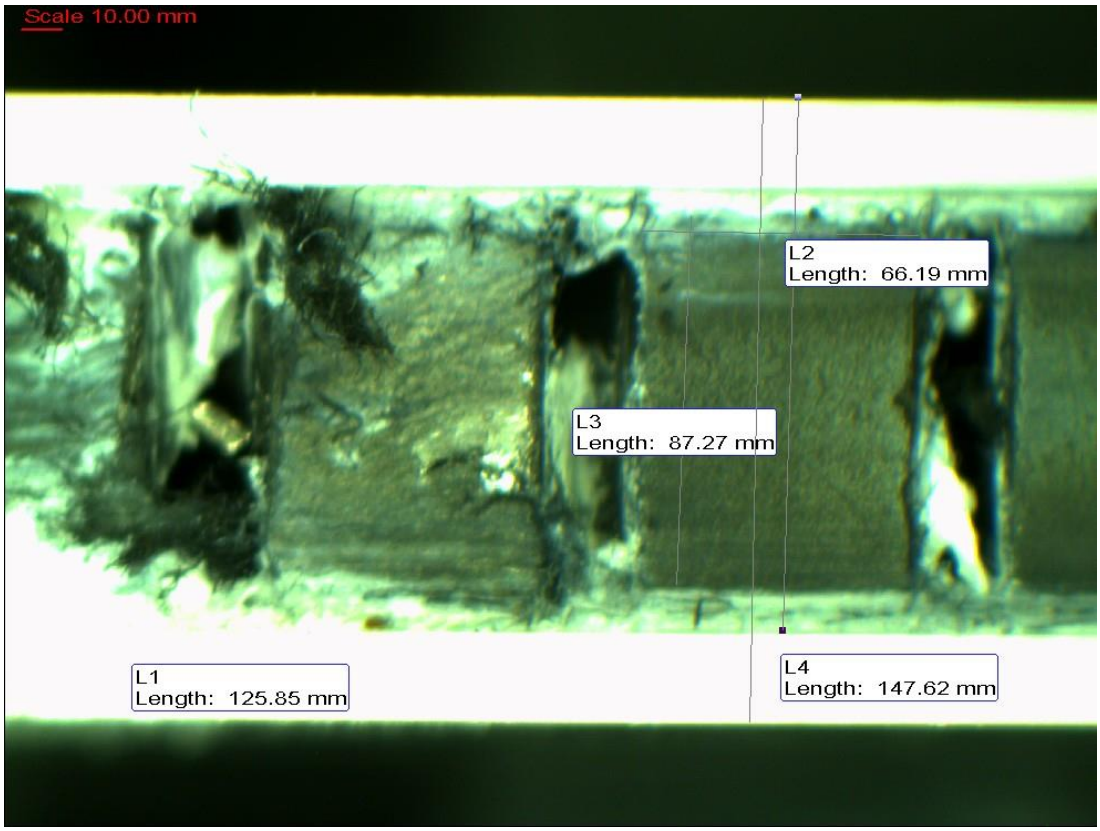

Determination of the geometries of the module size of 0.536.

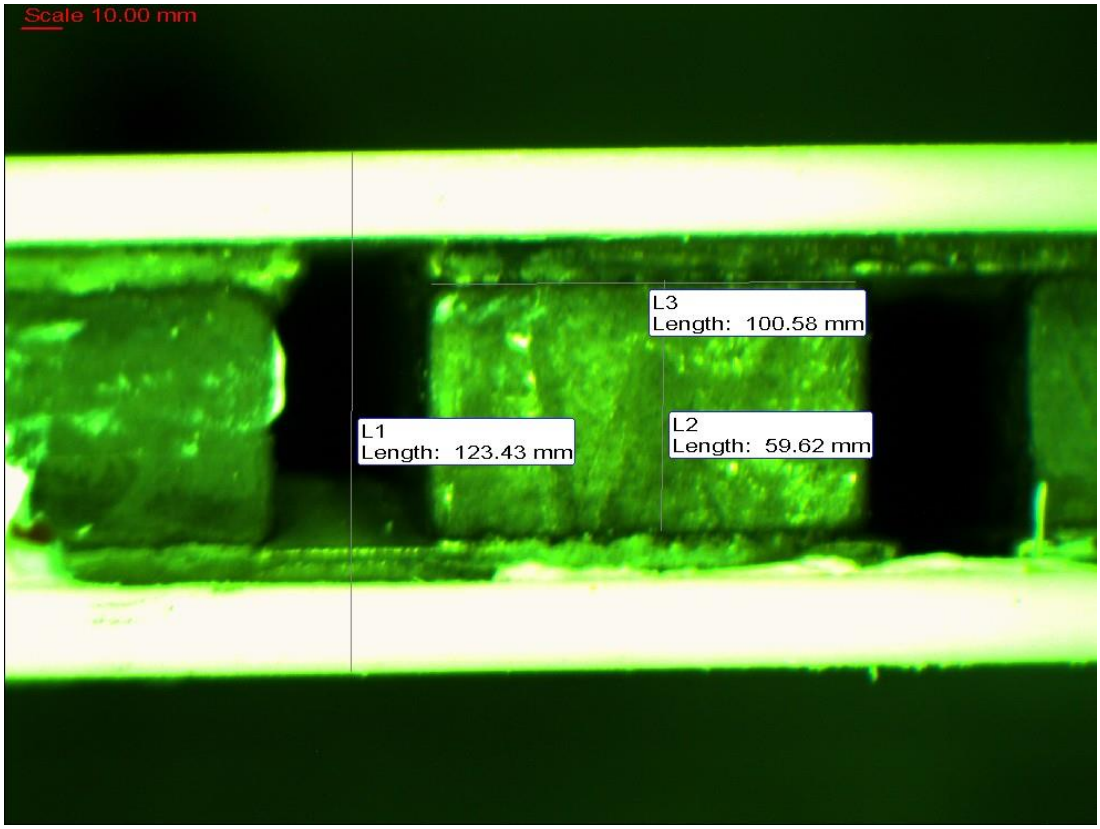

Determination of the geometries of the module size of 0.680.

Appendix B

B1: The engineering drawing of the vacuum chamber and the KF

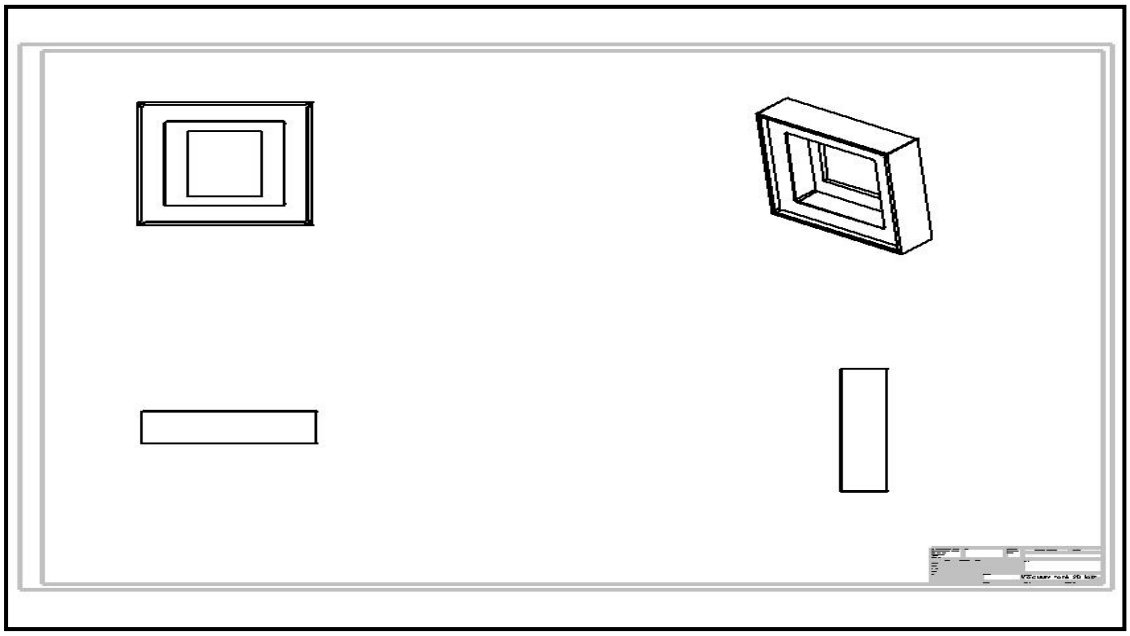

The engineering drawing of the vacuum chamber

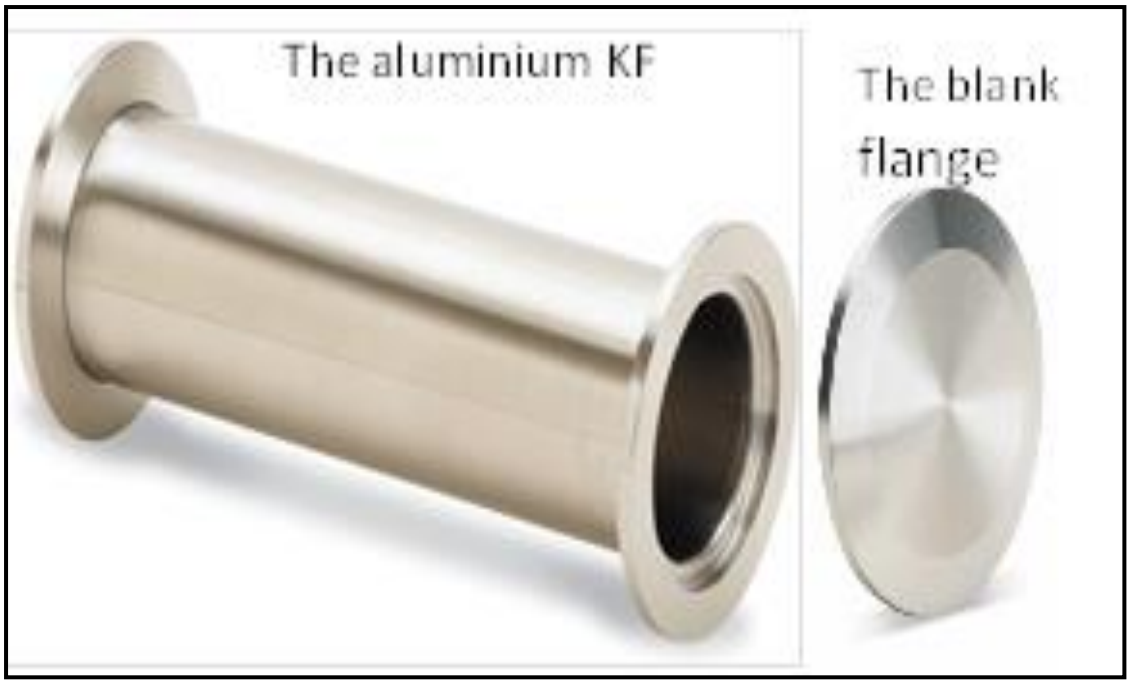

The KF used to connect the vacuum system to the vacuum pump

B2: The engineering drawing of the heat sink used on the vacuum experiments.

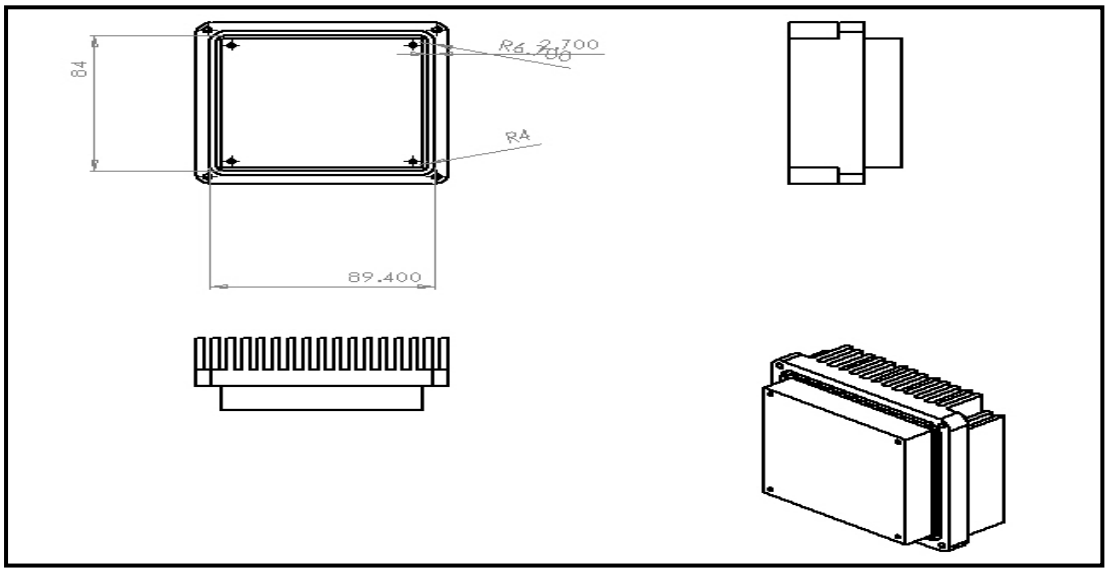

B3: Calculating the heat absorbed by the absorber under the xenon light bulb.

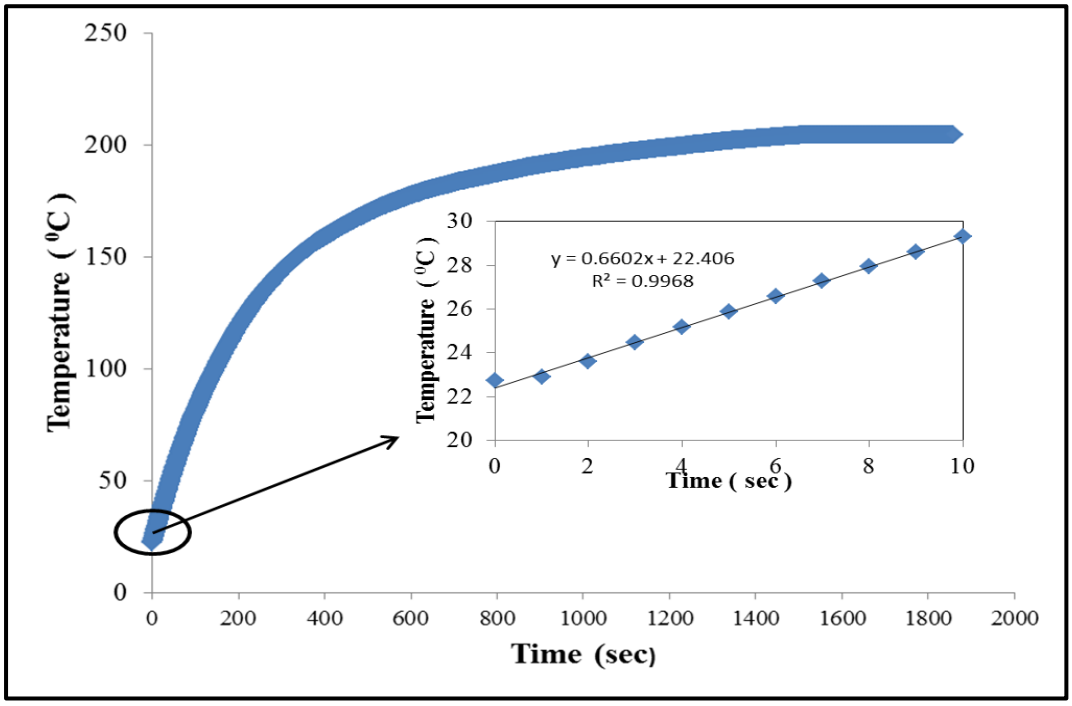

B4: Measuring the Xenon light intensity using the intensity meter.

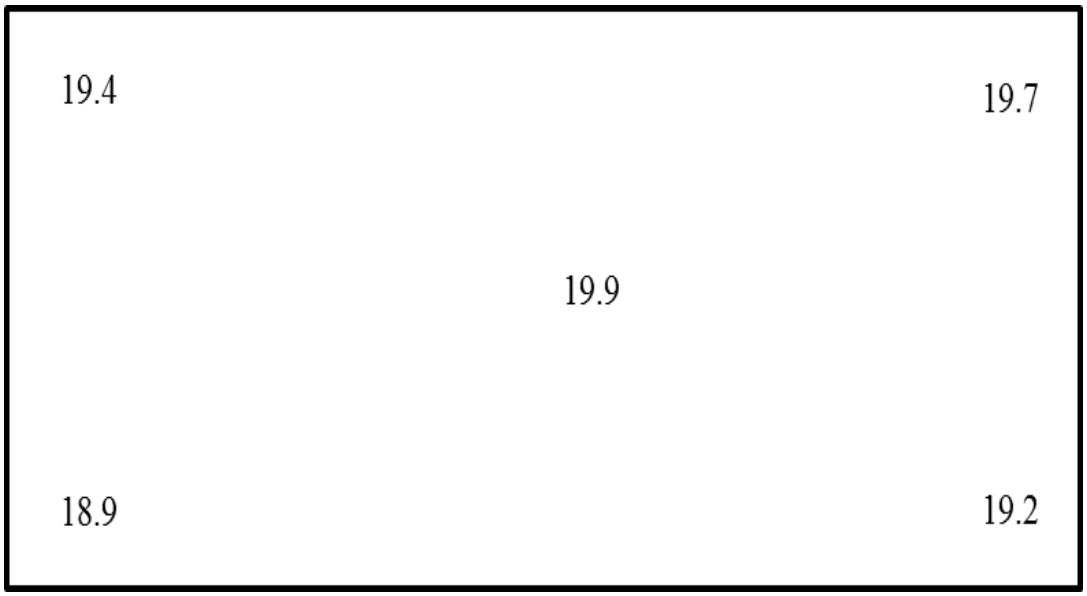

B5:ΔT as function of Δt to calculate the thermal power using the slope technique.

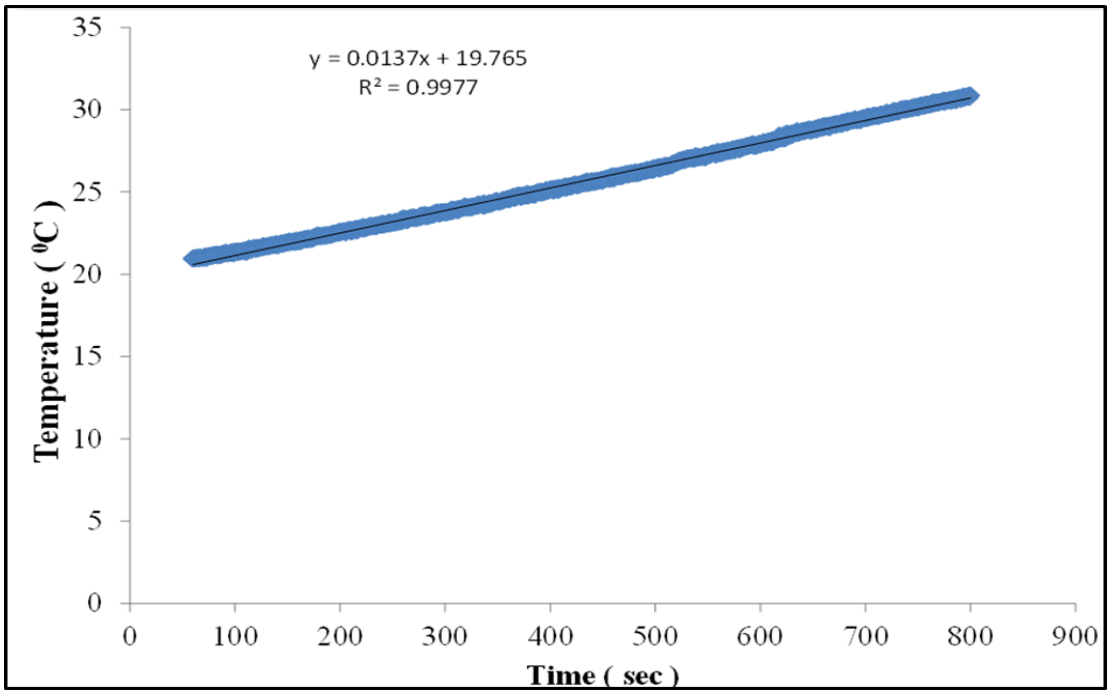

The rate of the water temperature at the first 8 minutes of the system with TEG size of 0.68 at condition 1 .

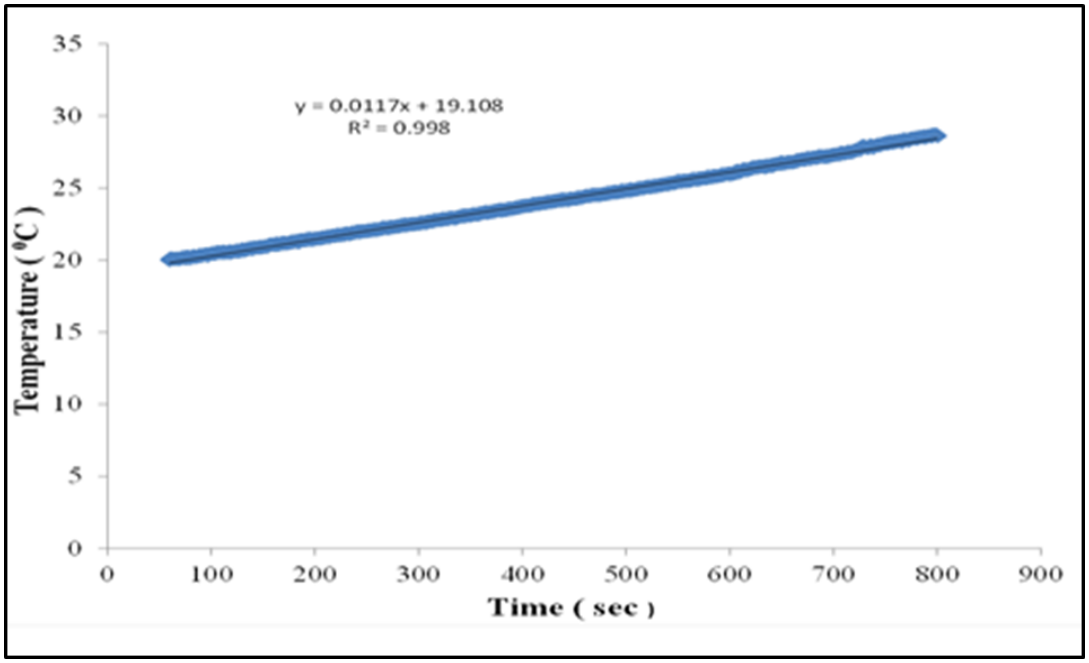

The rate of the water temperature at the first 8 minutes of the system with TEG size of 0.68 at condition 2 .

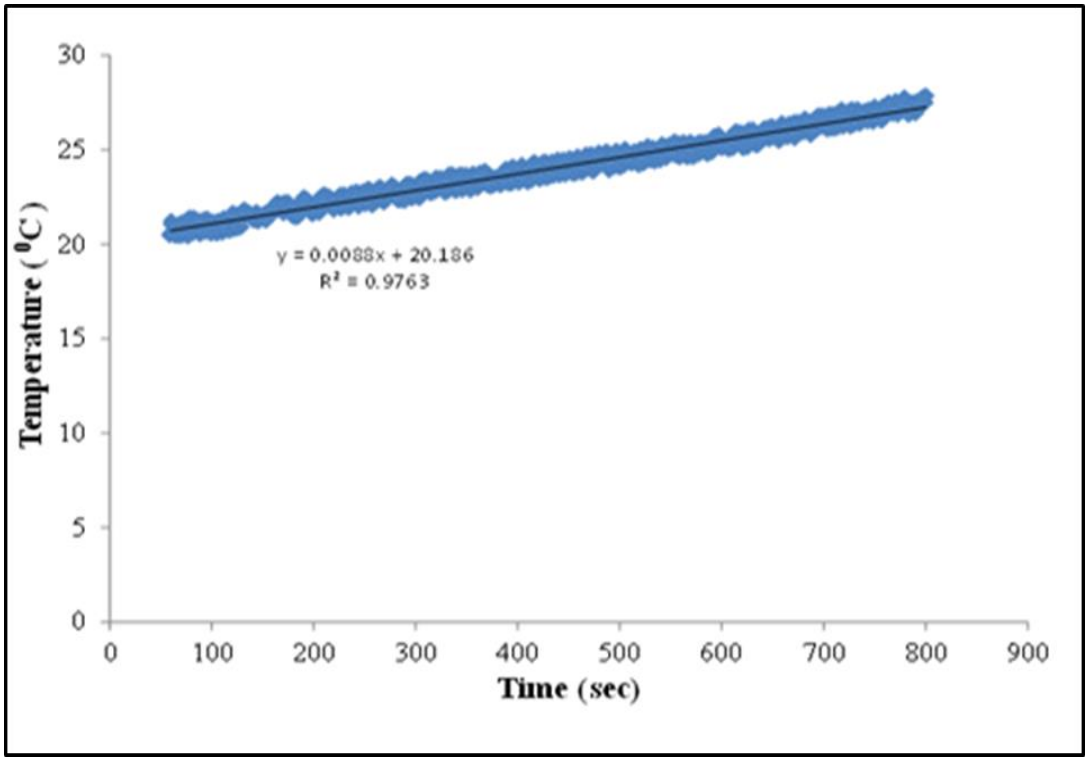

The rate of the water temperature at the first 8 minutes of the system with TEG size of 0.68 at condition 3 .

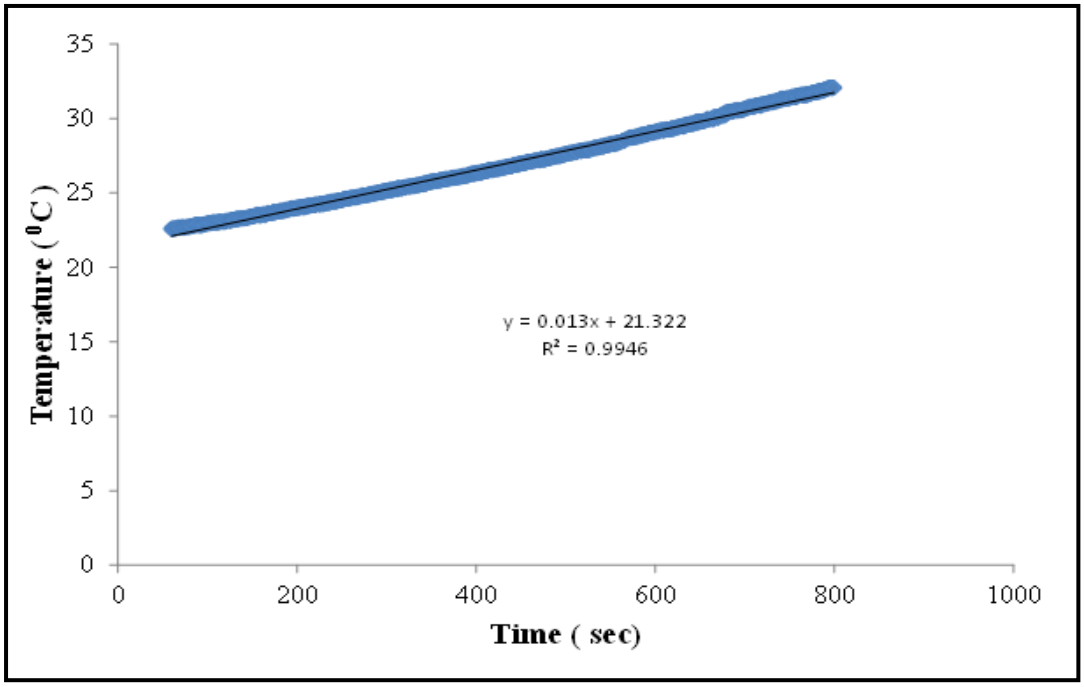

The rate of the water temperature at the first 8 minutes of the system with TEG size of 0.68 at condition 4 .

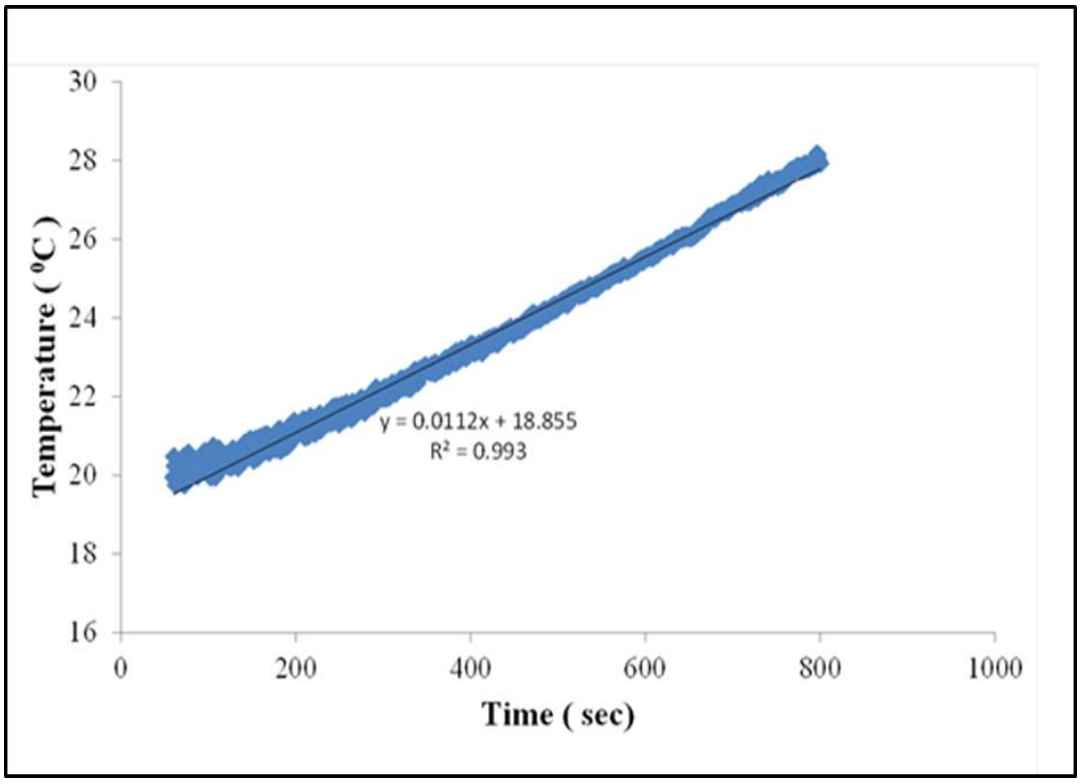

The rate of the water temperature at the first 8 minutes of the system with TEG size of 0.536 at condition 1 .

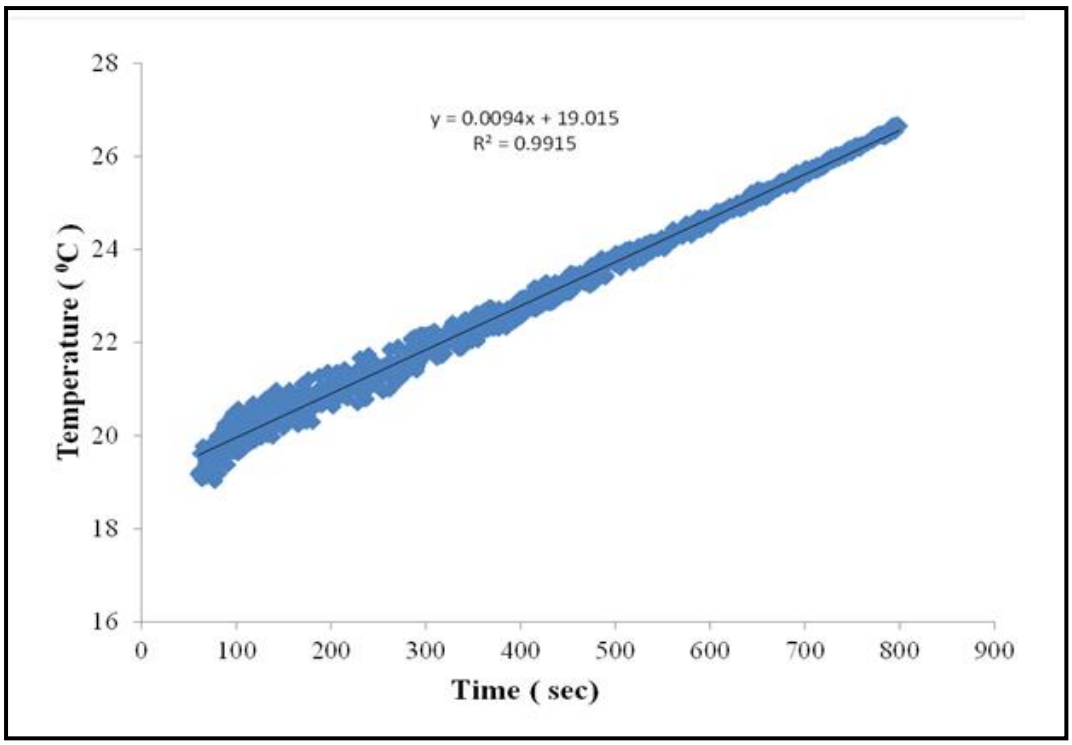

The rate of the water temperature at the first 8 minutes of the system with TEG size of 0.536 at condition 2 .

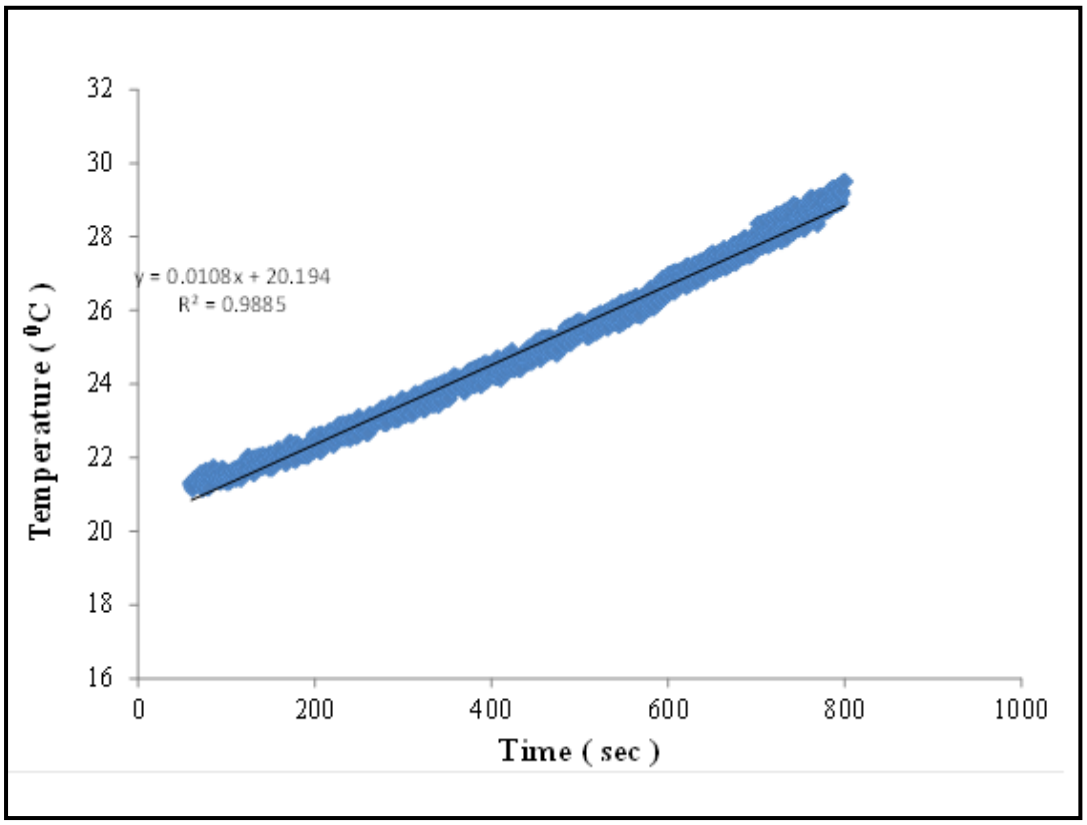

The rate of the water temperature at the first 8 minutes of the system with TEG size of 0.536 at condition 3 .

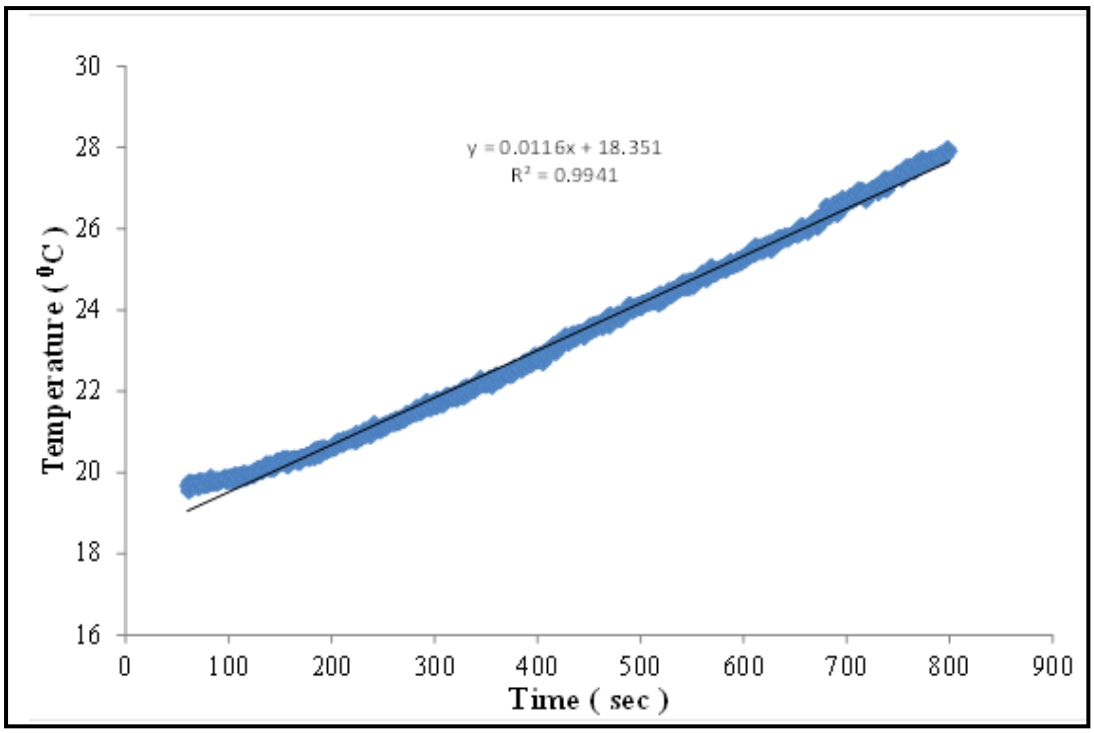

The rate of the water temperature at the first 8 minutes of the system with TEG size of 0.536 at condition 4 .

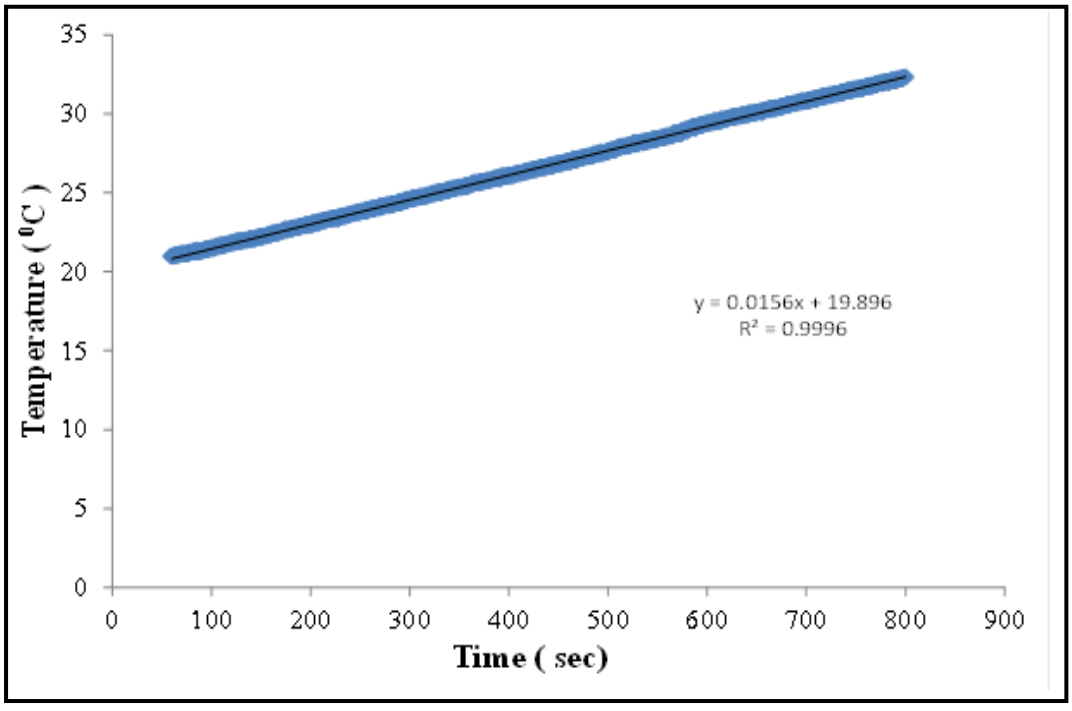

The rate of the water temperature at the first 8 minutes of the system with TEG size of 0.536 at condition 5 .

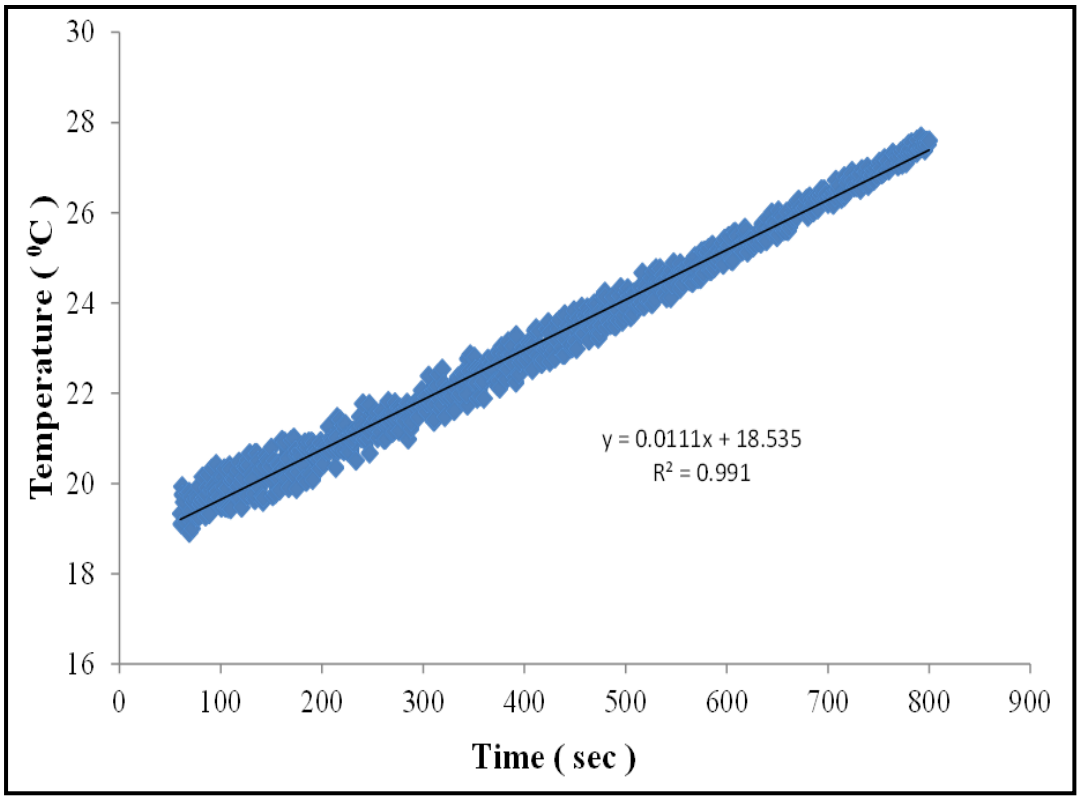

The rate of the water temperature at the first 8 minutes of the system with TEG size of 0.299 at condition 1 .

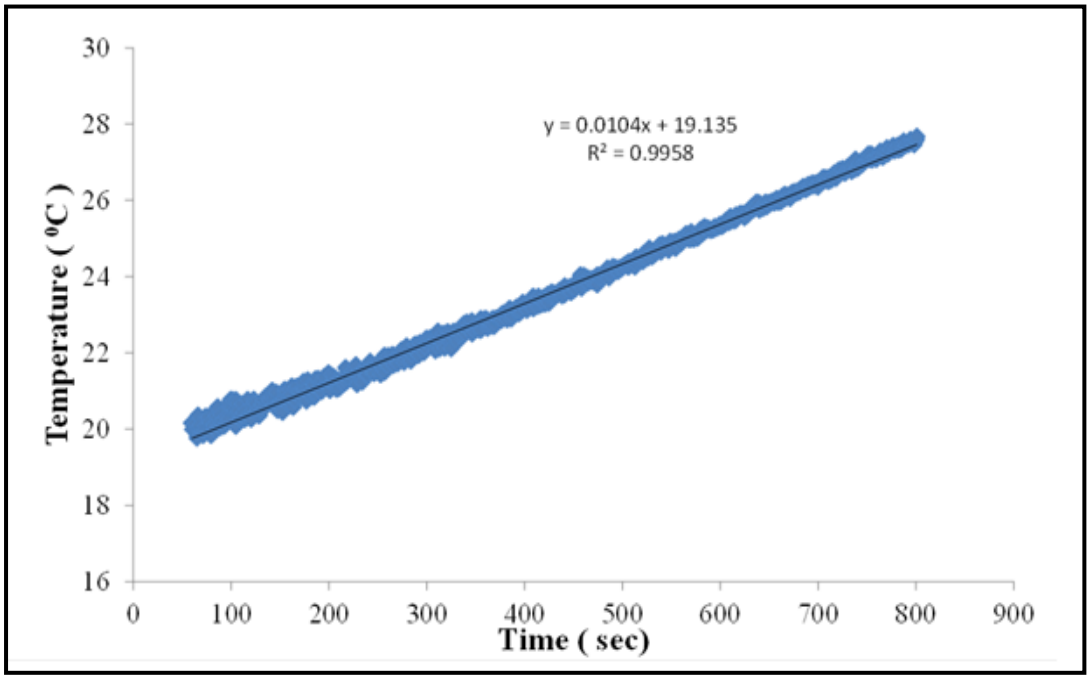

The rate of the water temperature at the first 8 minutes of the system with TEG size of 0.299 at condition 2 .

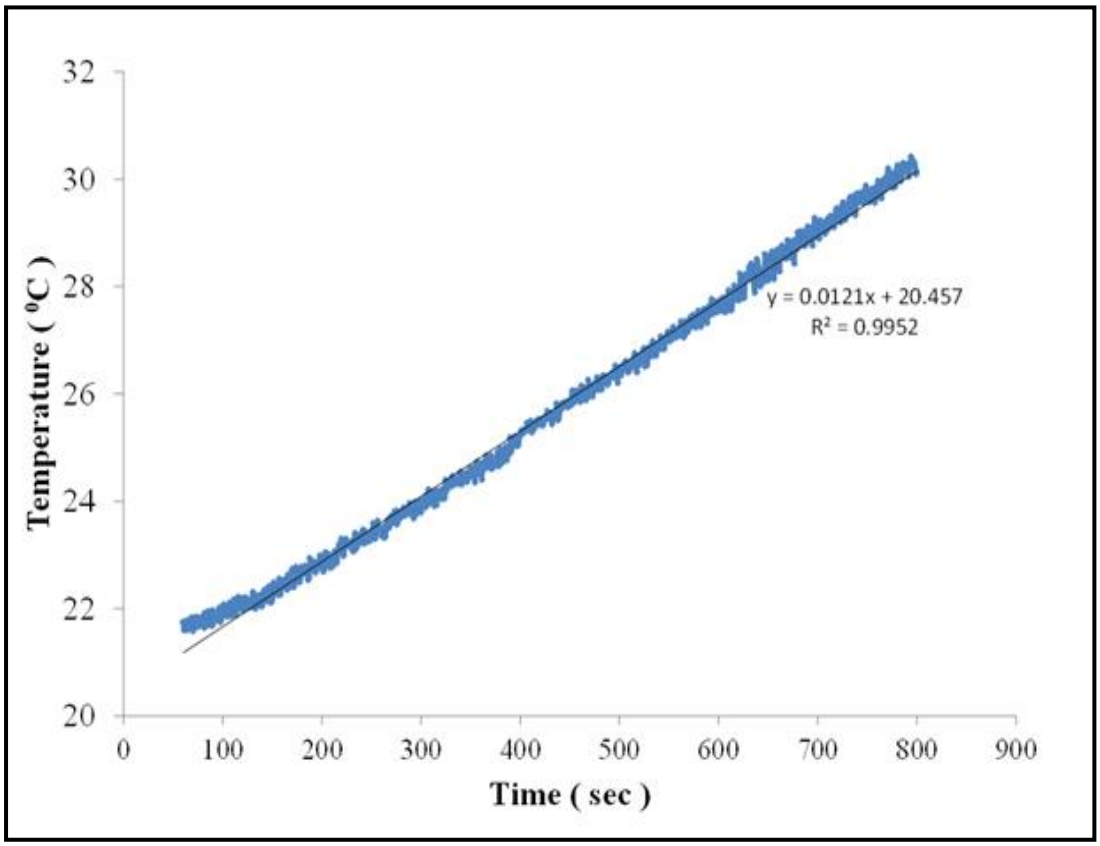

The rate of the water temperature at the first 8 minutes of the system with TEG size of 0.299 at condition 3 .

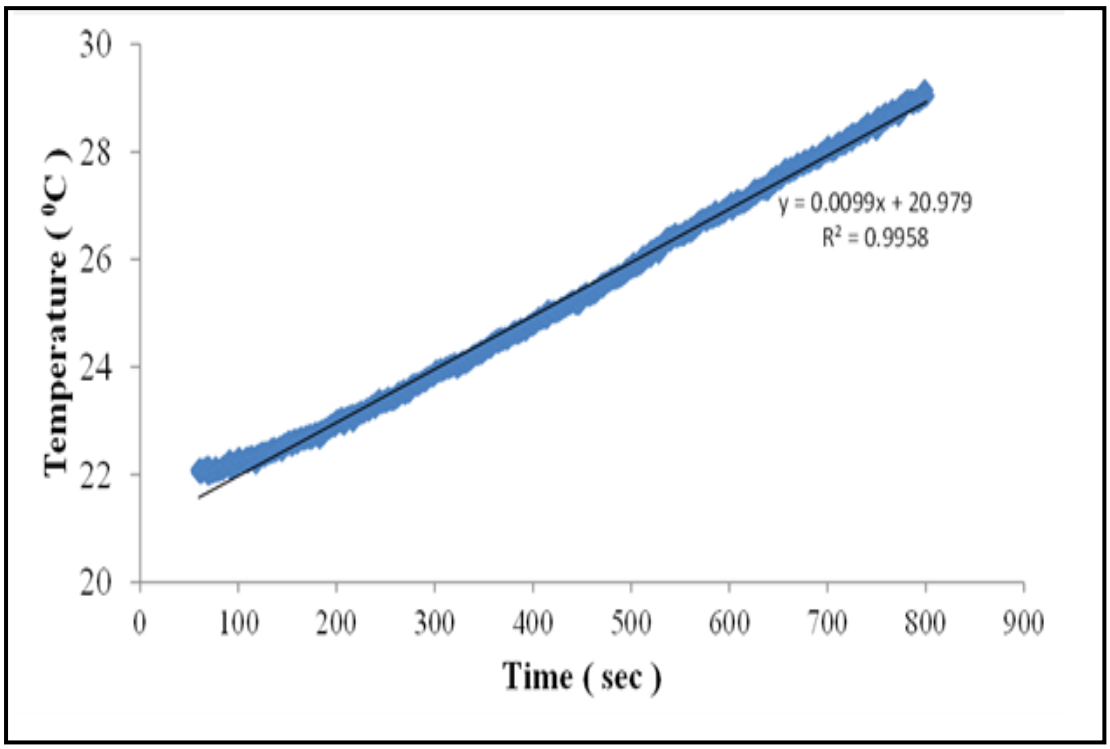

The rate of the water temperature at the first 8 minutes of the system with TEG size of 0.299 at condition 4 .

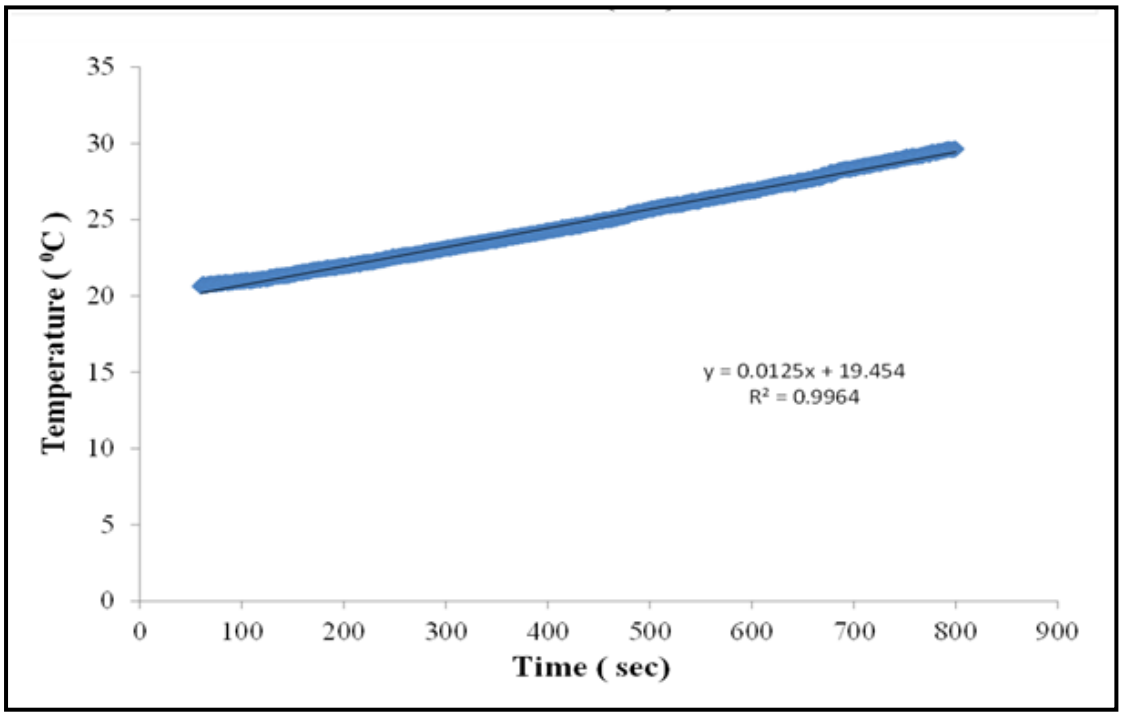

The rate of the water temperature at the first 8 minutes of the system with TEG size of 0.299 at condition 5 .

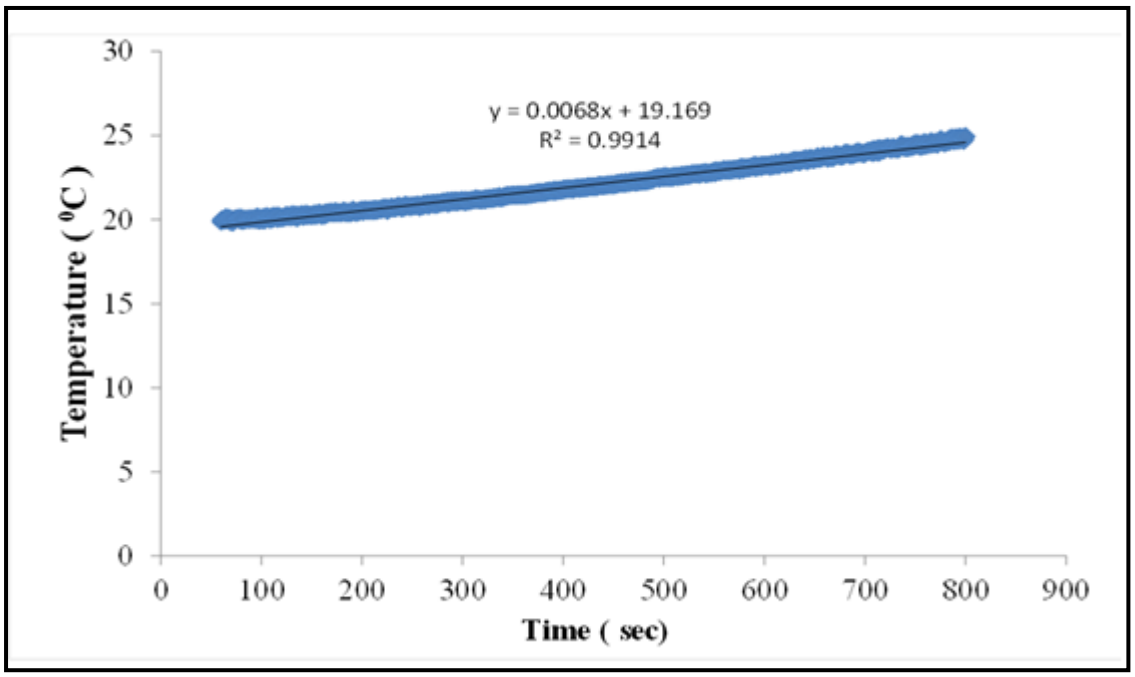

The rate of the water temperature at the first 8 minutes of the system with TEG size of 0.031 at condition 1 .

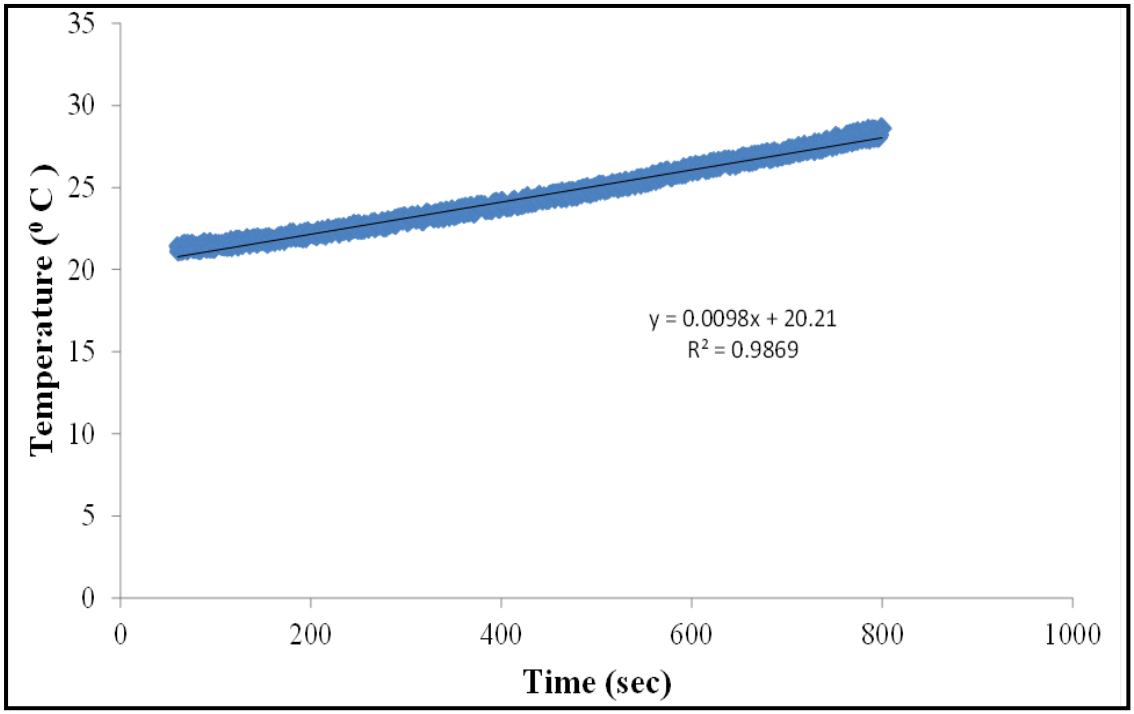

The rate of the water temperature at the first 8 minutes of the system with TEG size of 0.031 at condition 2 .

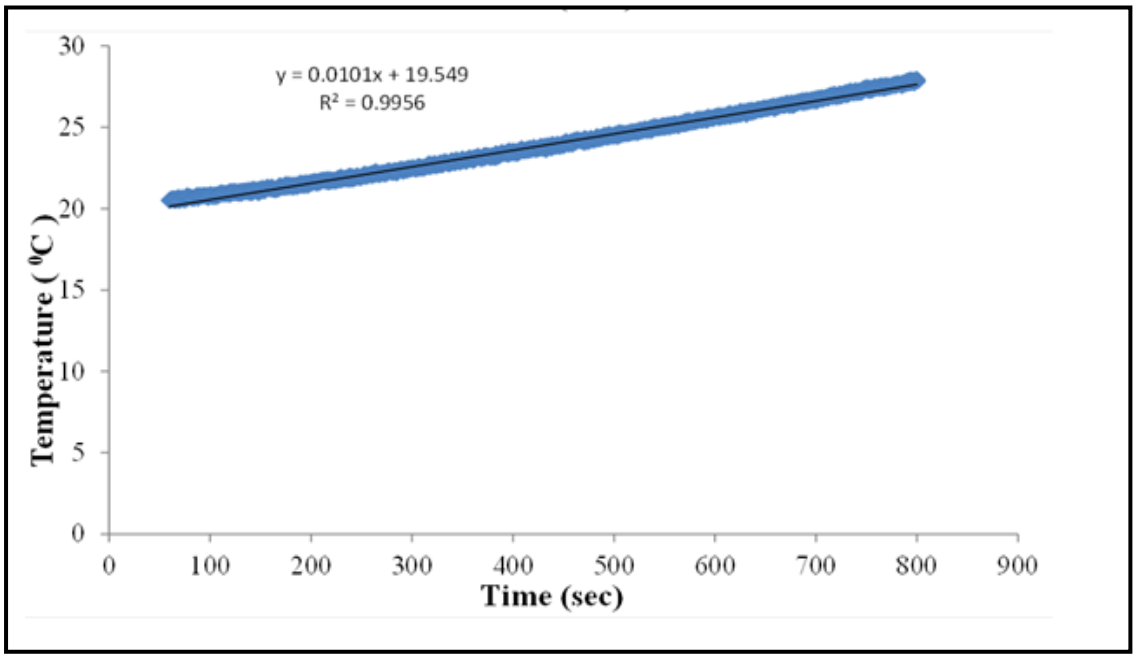

The rate of the water temperature at the first 8 minutes of the system with TEG size of 0.031 at condition 3 .

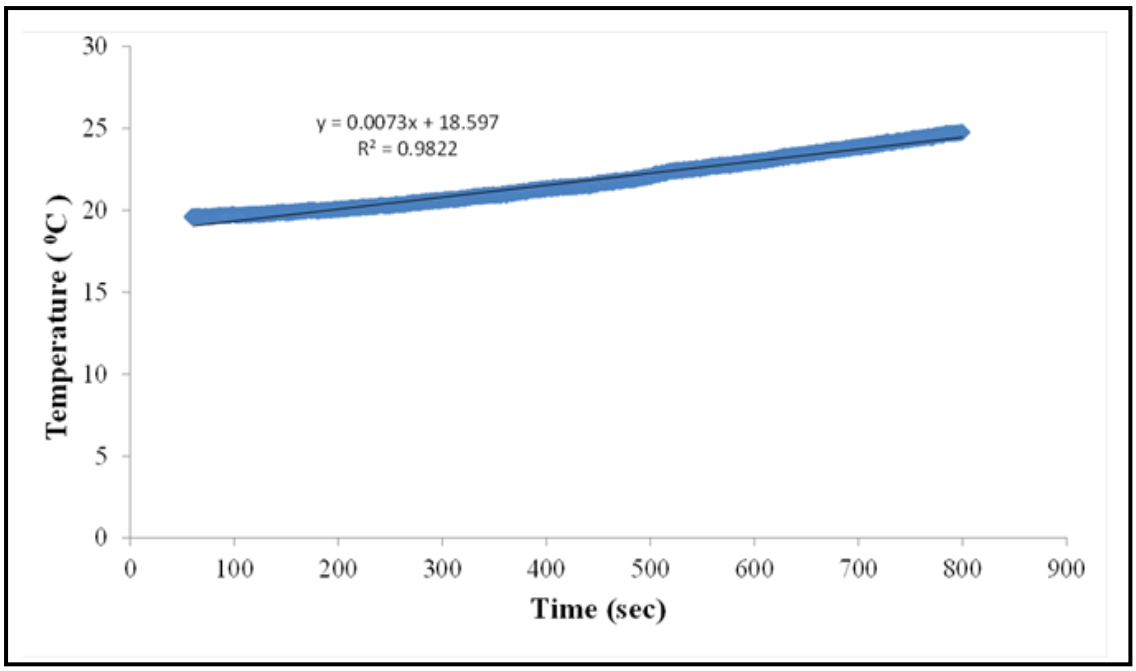

The rate of the water temperature at the first 8 minutes of the system with TEG size of 0.031 at condition 4 .

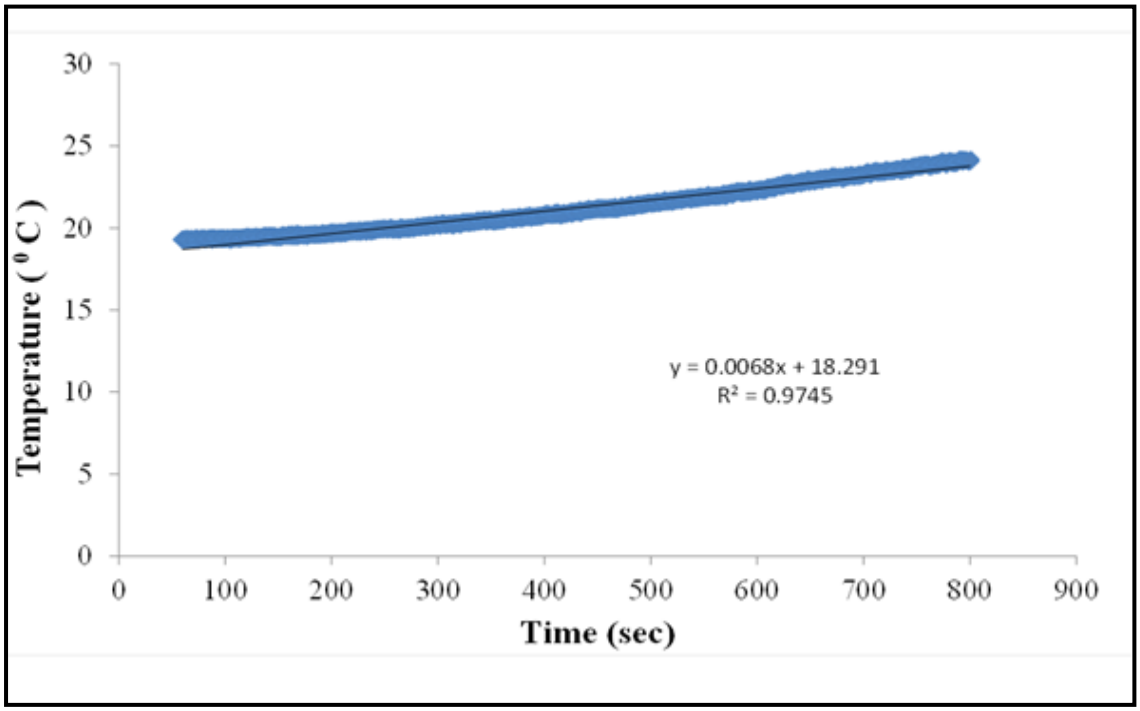

The rate of the water temperature at the first 8 minutes of the system with TEG size of 0.031 at condition 5 .

B6: Calculation example to investigate the difference in the value of the heat power obtained by the two different methods.

From the graphs shown on 6.7 and 6.8, the heat power generated by the smallest and the largest module sizes under condition 5 (where the heat lost by convection is considerably smaller), at the steady state condition was 4.3 and 16.8 Watt, while the results at the transient state conditions of the same module sizes were 7.8 and 14.95 watt. In order to investigate this further, a brief calculation to estimate the heat lost by the radiation effect (considering that convection heat lost is small and negligible) through the smallest and largest modules, as examples, is carried out as following:

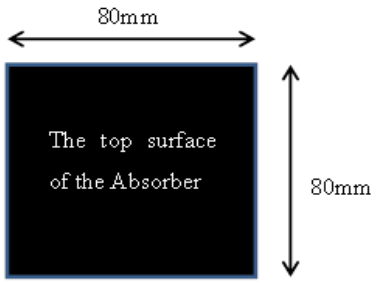

The size of the solar absorber

Calculating the heat lost by radiation , where equation 3.6 is applied, taking into account that the convection effect is not considered, the heat lost from the absorber can be determined as :

$$Q\,rad = \varepsilon\sigma\, A_c\, (T_h + 273)^4 - (T_c + 273)^4)$$

Where the value of the absorber emissivity (ε) was estimated as 0.5, the absorber hot side temperature (T_h) was recorded from the experiments as 176^o C, for the smaller, and 106^o C, for the larger module size, while the cold side (T_c) was 88^o C for the small module and 93^o C for the larger module size. The absorber radiates heat from both sides of its surface (A_c =2x

0.0064 $m^{2)}$, however, at the absorber's lowest surface, the TEG is attached and the radiation lost is no longer applied, therefore, the calculation of the radiation of the surface area becomes:

$$A_c = [2x (0.0064)] – (\text{TEG surface area area}) .$$

The TEG surface area is 0.000225 m^2 for the small, and 0.003844 for the larger module size. The radiation loss results for the smaller size is 8.3 watts, and 0.67 watts for the larger size. As was noticed, the heat transfer by radiation effect was too small for the larger size compare to the conduction effect, and *vice versa*.

As heat power calculated through the TEG (both modules) by the conduction effect at the steady state is :

4.24 Watts for the small module

12.84 Watts for the large module.

Considering the calculated radiation and conduction heat lost from the absorber and the rubber seal added for both modules:

For the small module = 4.24+8.28= 12.5 watt.

While, for the large module = 12.84+0.67= 13.5 watt.

Considering the heat lost's value, especially in the smallest modules, explains why there is a large difference between the two methods (Q_w and $Q_{TEG)}$ of determining the heat power .

B7: Temperature difference, open voltage, the measured and calculated electrical power of Chapter 6 Section 4.

Table M. 1.The electrical power results of all module sizes under unglazed condition at steady state.

Module ID	Module ratio [A*2N/L]	ΔT	V	Measured Power Watt	Calculated power Watt
15B	0.031	58.76	0.7	0.072	0.0717
30B	0.132	28.69	0.73	0.074	0.074
40A	0.290	20.4	1.034	0.0763	0.076
62A	0.530	16	0.802	0.1	0.1035
62B	0.690	13.5	0.23	0.066	0.087

Table M. 2.The electrical power results of all module sizes in glazed systems at steady state.

Module ID	Module ratio [A*2N/L]	ΔT	V	Measured Power Watt	Calculated power Watt
15B	0.031	60	0.745	0.0816	0.0807
30B	0.132	31.56	0.707	0.069	0.0807
40A	0.290	20.73	1.048	0.078	0.078
62A	0.530	15.54	0.748	0.087	0.101
62B	0.690	12.	0.21	0.055	0.071

Table M. 3.The electrical power results when a vacuum level of 2x10 -1 mbar is applied to the systems.

Module ID	Module ratio [A*2N/L]	ΔT	V	Measured Power Watt	Calculated power Watt
15B	0.031	80.05	0.93	0.127	0.131
30B	0.132	-	-	-	-
40A	0.290	22.47	1.14	0.093	0.1
62A	0.530	20	0.79	0.097	0.1
62B	0.690	12.47	0.24	0.07	0.083

Table M. 4.The electrical power results of all modules under vacuum level of 8x10 -2 mbar at steady state condition.

Module ID	Module ratio [A*2N/L]	ΔT	V	Measured Power Watt	Calculated power Watt
15B	0.031	86	1.03	0.156	0.160
30B	0.132	34.89	0.91	0.11	0.115
40A	0.290	24.13	1.16	0.096	0.103
62A	0.530	17.4	0.81	0.103	0.109
62B	0.690	13.6	0.24	0.072	0.0886

Table M. 5.The electrical power results of all module sizes under vacuum level of 5x10 -2 mbar at steady state condition.

Module ID	Module ratio [A*2N/L]	ΔT	V	Measured Power Watt	Calculated power Watt
15B	0.031	93	1.152	0.200	0.190
30B	0.132	-	-	-	-
40A	0.290	26.87	1.296	0.120	0.136
62A	0.530	20	0.99	0.135	0.150
62B	0.690	16.	0.274	0.093	0.117

B8: Measurements validation of electrical power outputs

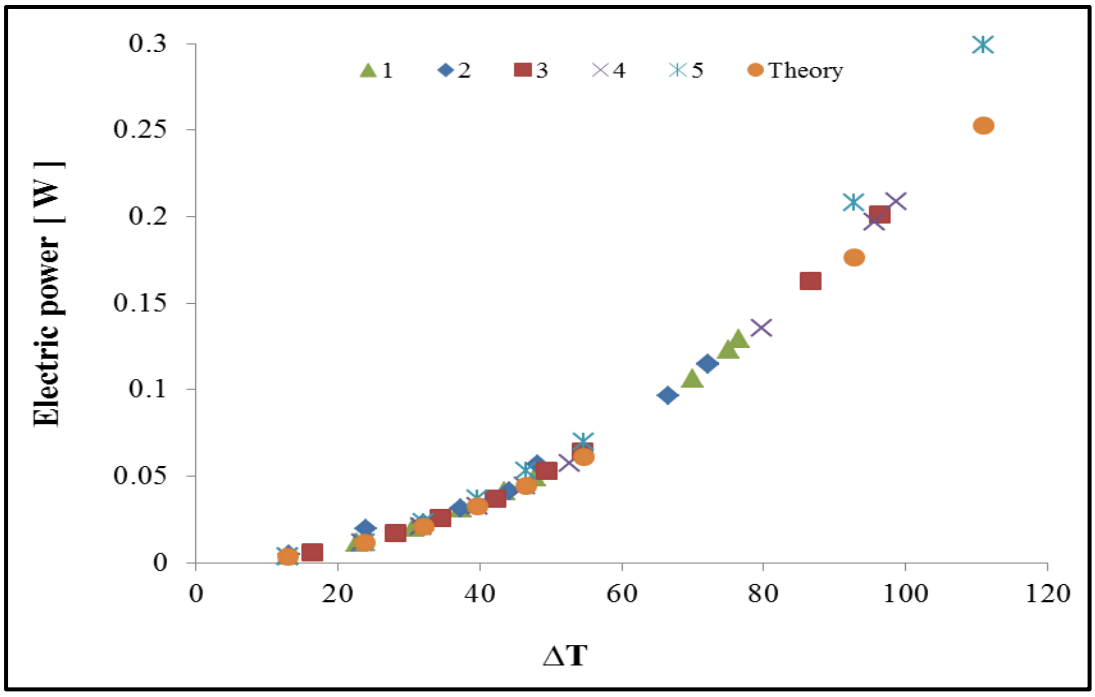

The electrical power of the module size of 0.031 as a function of ΔT under different environmental conditions.

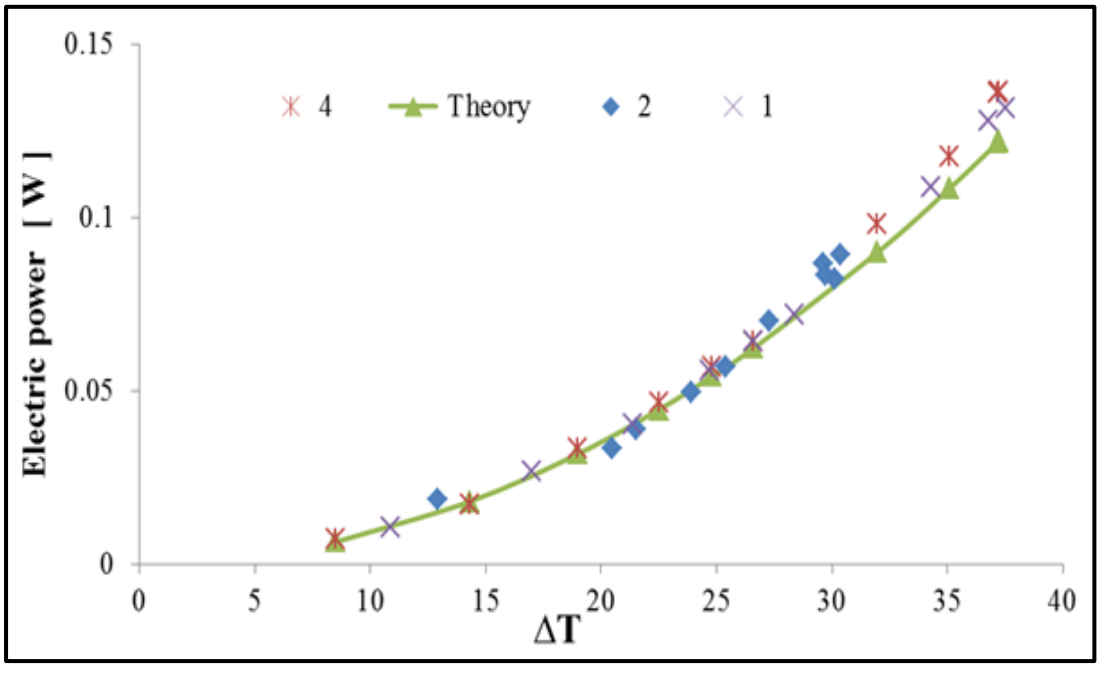

The electrical power of the module size of 0.136 as a function of ΔT under 3 different environmental conditions.

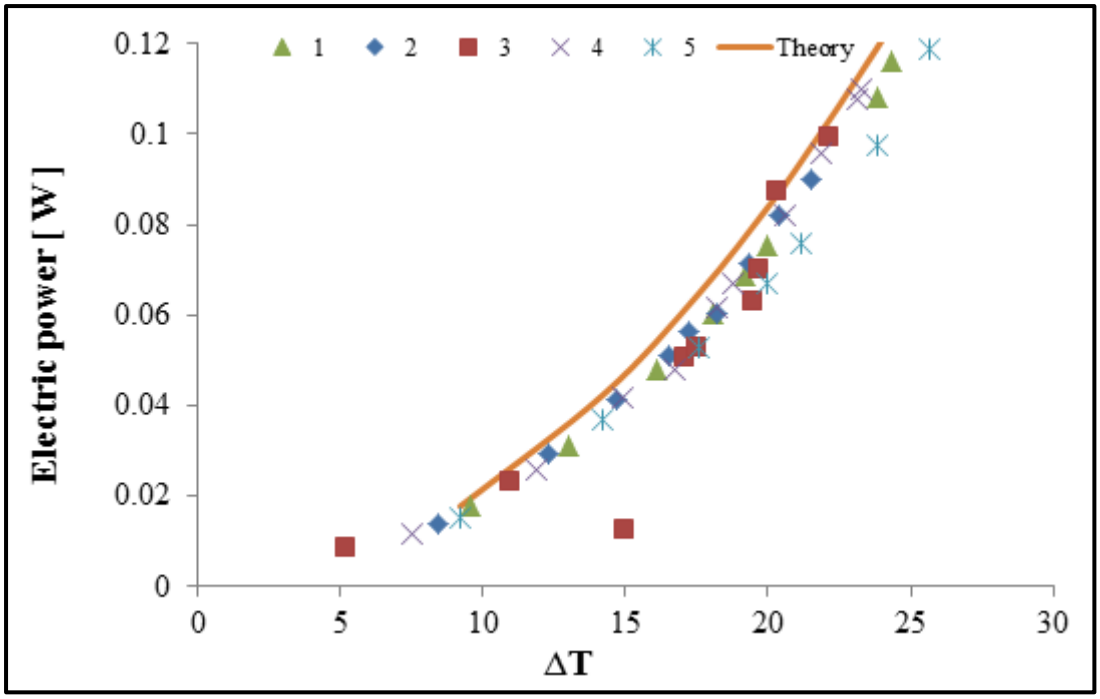

The electrical power of the module size of 0.299 as a function of ΔT under different environmental conditions.

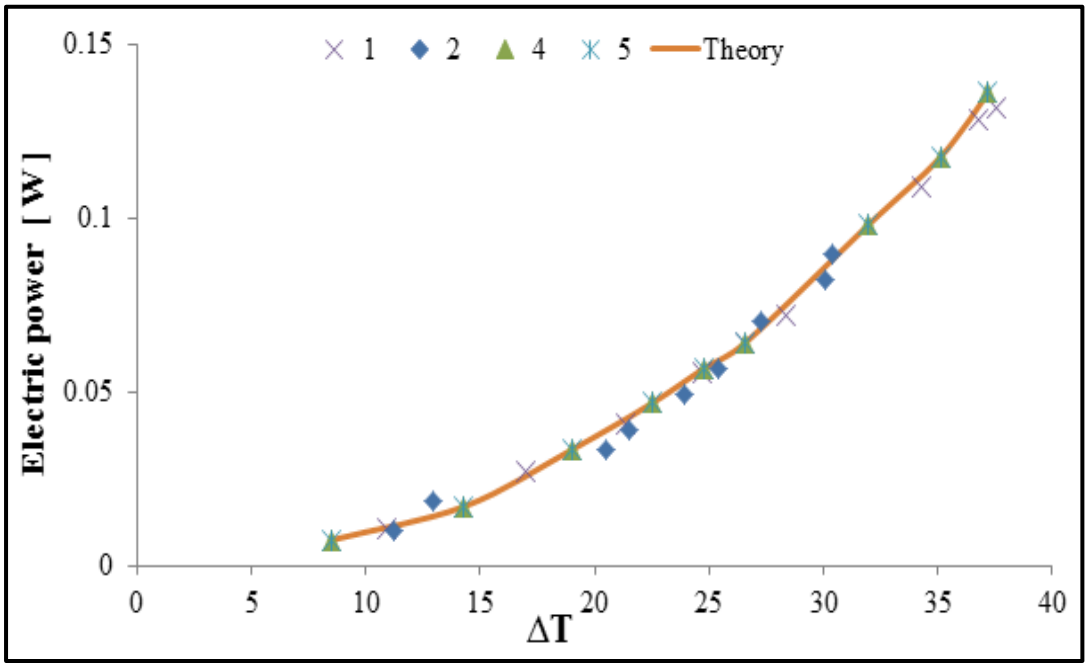

The electrical power of the module size of 0.536 as a function of ΔT under different environmental conditions.

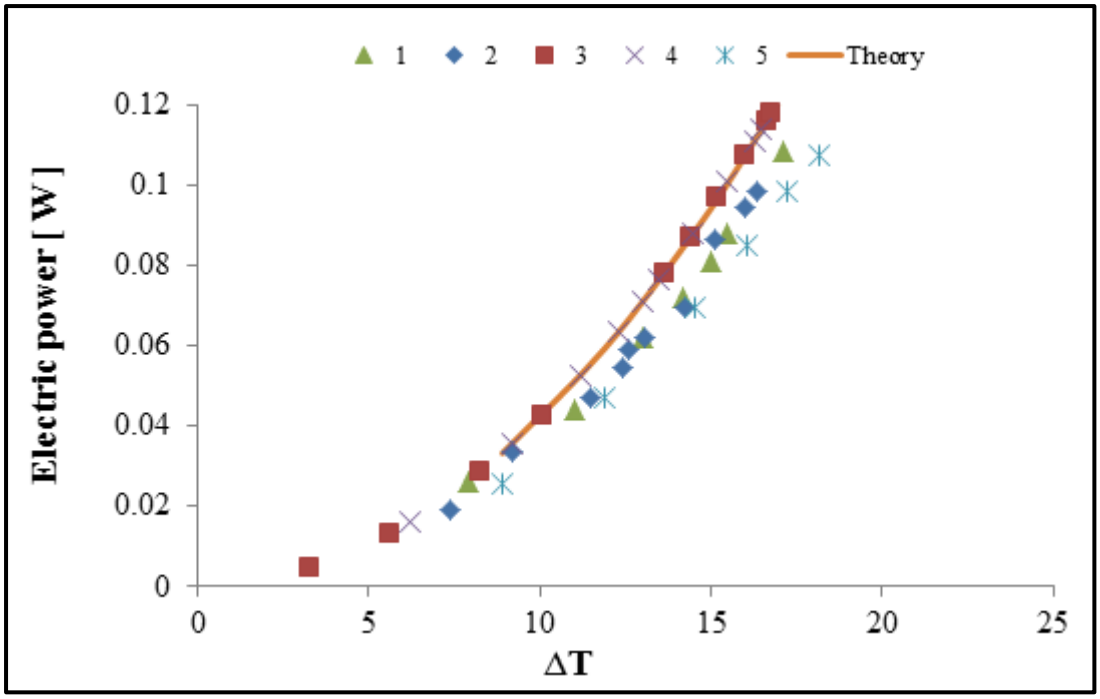

The electrical power of the module size of 0.680 as a function of ΔT under different environmental conditions.

B9: The heat and electrical power of each system size under each environmental condition.

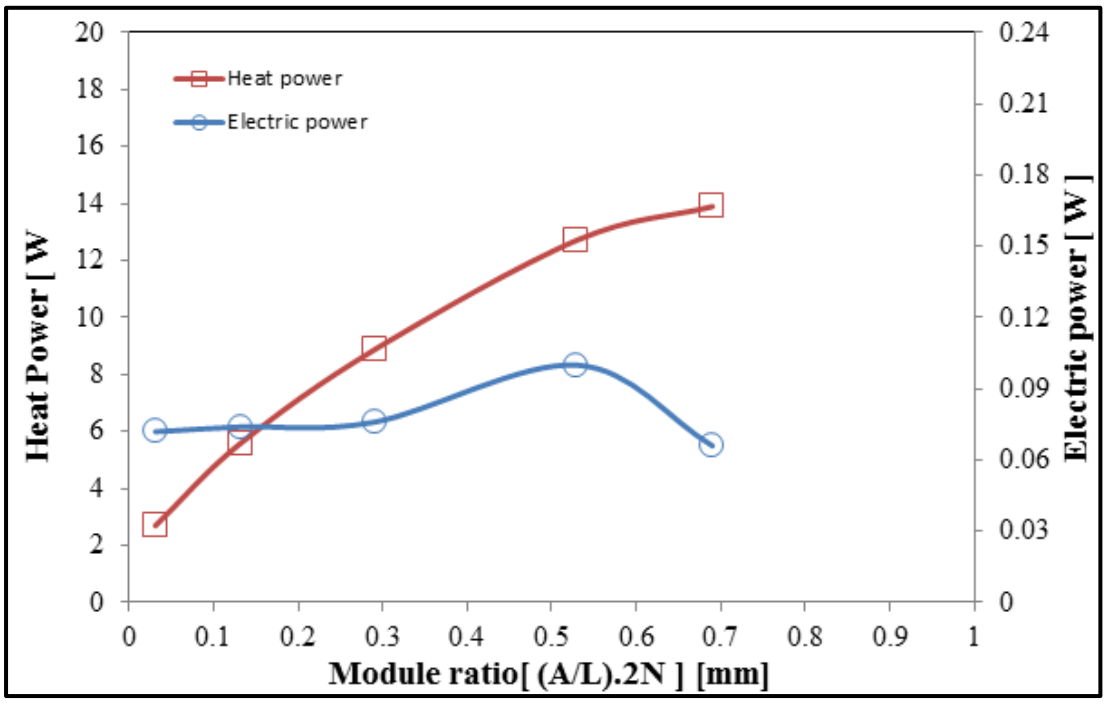

The optimum heat power and electrical power at steady state condition as a function of the module ratio on condition 1. (The line is here as an eye guide).

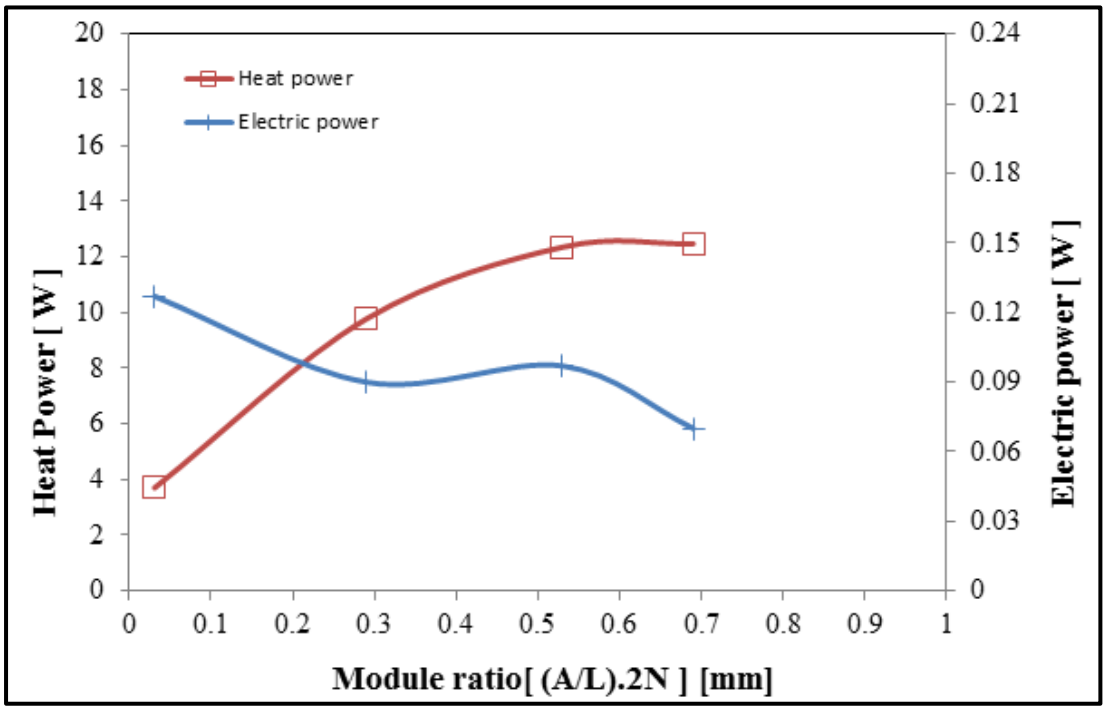

The optimum heat power and electrical power at steady state condition as a function of the module ratio on condition 2.

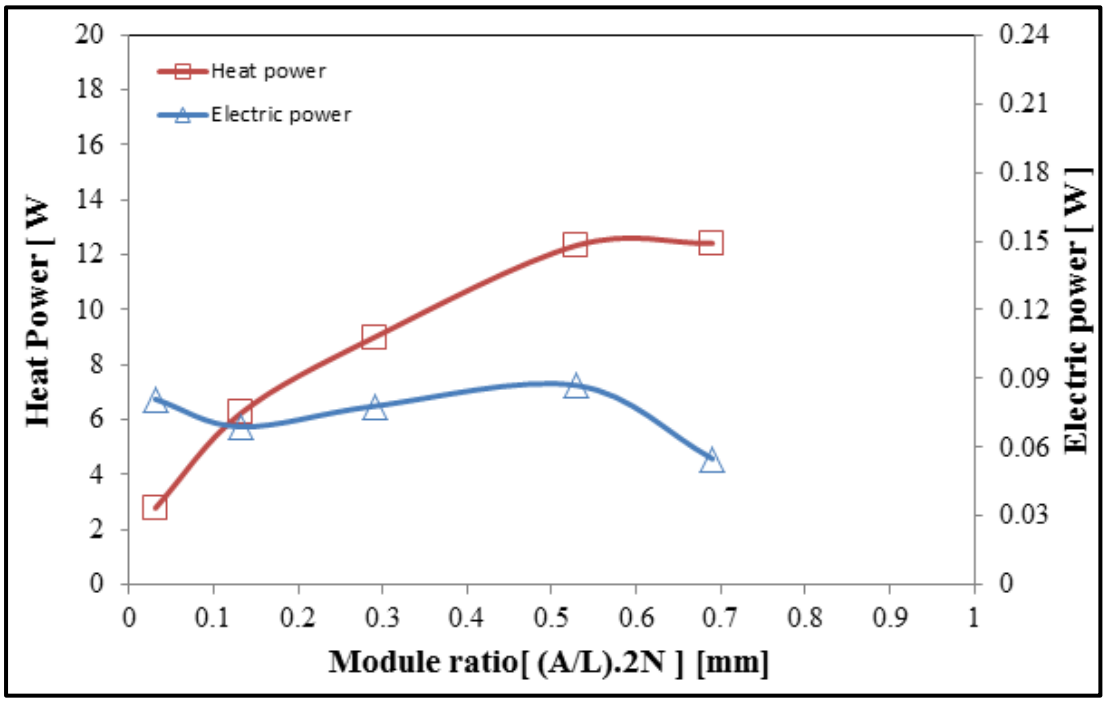

The optimum heat power and electrical power at steady state condition as a function of the module ratio under condition 3.

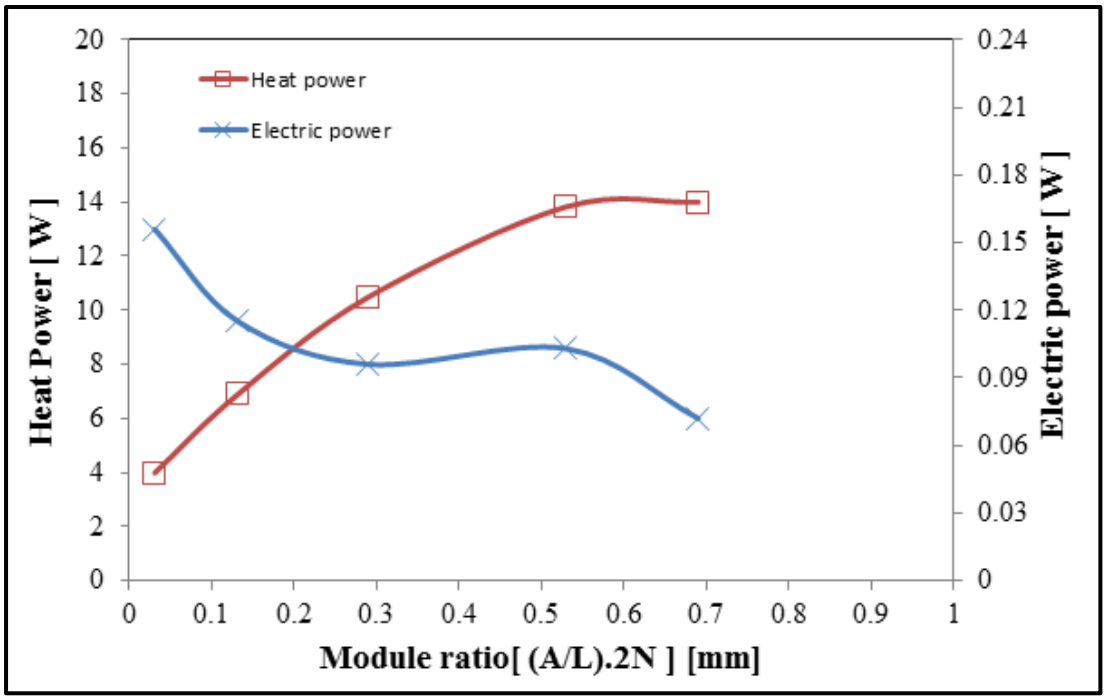

The optimum heat power and electrical power at steady state condition as a function of the module ratio under condition 4.

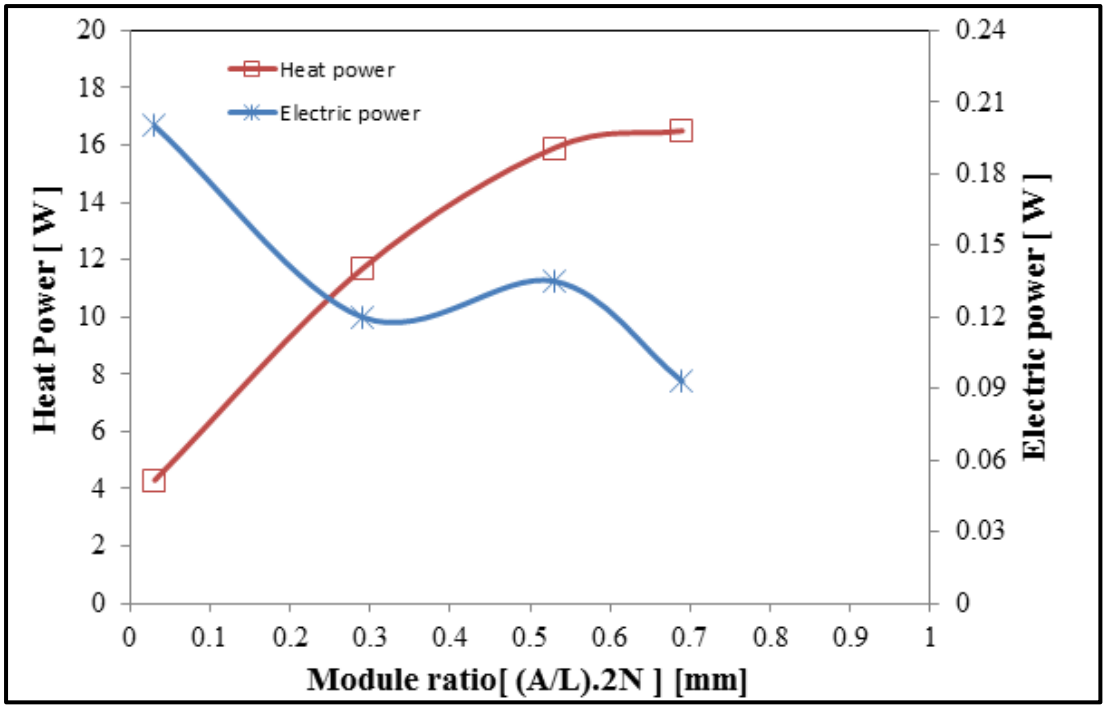

The optimum heat power and electrical power at steady state condition as a function of the module ratio under condition 5.